Glycopolymer Polyelectrolyte Multilayers Based on Maltose-Modified Hyperbranched Poly(ethyleneimine) For Future Drug Delivery Coatings and Biomedical Applications

D I S S E R T A T I O N

zur Erlangung des akademischen Grades

Doctor rerum naturalium

(Dr. rer. nat.)

vorgelegt

der Fakultät Mathematik und Naturwissenschaften

der Technischen Universität Dresden

verfasst von

M.Sc.

Samaa Ragab Ali Ragab Salem

geboren am 15.03.1981 in Kairo, Ägypten

Eingereicht am 24.04.2015

Die Dissertation wurde in der Zeit von April 2011 bis April 2015 im Leibniz-Institut für Polymerforschung Dresden e.V. angefertigt

Gutachter: Prof. Dr. Brigitte Voit (TU Dresden, IPF Dresden)

Prof. Dr. Regine v. Klitzing (TU Berlin)

Eingereicht am: 24.04.2015

Tag der Verteidigung: 01.07.2015

‚‘A person who never made a mistake
never tried anything new, ‘

Albert Einstein

ACKNOWLEDGEMENTS

There are so many people to thank for helping me during the last four years and in my Ph.D. project. So many have made my short stay in Germany away of all of my family and friends a lot easier than I thought it was going to be. I will try to cover all the bases without being my usual long winded self.

My greatest thanks are owned to my supervisors, Prof. Dr. Brigitte Voit and Dr. Dietmar Appelhans. I have the honor to work with an important character such Prof. Dr. Brigitte Voit, who will always be an example of intelligence, good-humored, confident, support, morals and a real role model for all of her students. She gave me a generous chance by choosing me for working in her research group in IPF Dresden. Without her care, wise advice and last not least, the financial support this work would not be even possible.

Secondly, I would like to thank Dr. Dietmar Appelhans for his guidance, encouragement, and patience over the whole four years. Thank you so much for forcing me, sometimes kicking to learn and look at science, research and work from different points of view , which in turn playing an important role to change a lot in my personality and opening my mind. Your support was essential to my success here.

A warm appreciation and special thanks for Dr. Martin Müller, Mr. Berhard Torger, David Vehlow, Mr. Bernd Keßler and Mrs. Birigt Urban. Their contribution to my work, advices and helping me a lot in ATR-FTIR measurements and related calculation cannot be underestimated and actually it is considered as a priceless learn of art and value that cannot be determined.

A great thankfulness for Dr. Klaus-Jochen Eichhorn and Mr. Roland Schulze, who helped me a lot in ellipsometry measurements, theoretical basics and related calculation. Without their advices nothing of what have been already done would be successful. Their contribution cannot be underestimated.

I would like to thank Mrs. Anja Caspari for thoroughly measuring several hundreds of my samples by DLS and zeta potential measurements. A special thanks to Mr. Andreas

Janke for the AFM measurements. Even if they were busy or it was late evening, they found a way to finish my measurements as fast as possible. I would like to thank Ms. Anne Richter for introducing and guiding me for working on ellipsometry. For the constant support and creating a nice working climate, my warm thanks to Dr. Doris Pospiech, Mrs. Carmen Krause, and the entire departments of Polymer Structures and Bioactive and Responsive Polymer.

Furthermore, I am indebted to people who surrounded me every day for their help and kind of support. Thank you, Sabina Z., Bettina M., Christin S., Maria R., Sandra T., Monika W., Nicole H., Nikita P., Franka E., Hirak S., Sourav C., Soumyadip C., Sumela B., Christiane E., Guping H., Jörg K., David S., David G., Emrah D., Francesco P., Frank D., Mohamed Y., Haiping Z., Jens G., Ulli G., Johannes F., Maria H., Markus F., Marta H., Robert P, Sonya M., Frank D., Elixana M., Roberto D. R., Beatriz R., and the whole IPF Dresden members. In fact they were not only faithful colleagues and friends but even more. I have lived with them a lot of unforgettable moments.

I would like to send my deep appreciation and thankfulness to German Academic Exchange Service (DAAD) and Egyptian Ministry for Higher Education for their helping to accommodate me in a foreign country and financial support for the whole Ph.D. project and in fact without their helping this work would not been even achieved.

Finally, I would like to express my thanks, deep feelings and loyalty to Germany and Germans, who proved always that they are elites in all domains, whether in practical work or even in personality and it was a great chance for me to know them in a closest way. Actually, I owe them a lot. Last and not least, I would like to thank and dedicate this work to my beloved family, my parents, my brother and sister, my husband and my little sweet son, Jwad K.

CONTENT

LIST OF ABBREVIATIONS

A

AFM	Atomic force microscopy
ATP	Adenosine 5'-triphosphate
ATR-FTIR	Attenuated total reflection Fourier-transform infrared spectroscopy
AMP	Adenosine 5'-monophosphate disodium salt
ATP	Adenosine 5'-triphosphate disodium salt
ALG	Sodium alginate

B

BH_3*Py	Borane pyridine complex (8M)
BA	Bronic acid
BPEI	Branched poly(ethyleneimine)

C

CHI	Chitosan
CS	Carrier system
CMP	Cytidine 5'-monophosphate disodium salt
CTP	Cytidine 5'-triphosphate disodium salt

D

D%	Percentage of dendritic groups
DB	Degree of branching
DF	Degree of functionalization
DP	Dendritic polymer
DMM	Double-monomer methodology
DLS	Dynamic light scattering
DS	Degree of substitution

E

EOF	Electro-osmotic flow

F

FA	Folic acid

G

Glc	D (+)- Glucose monohydrate
Ge-IRE	Germanium internal reflection element

H

HA	Hyaluronic acid
HA-Na^+	Hyaluronic acid sodium salt
HBP	Hyperbranched polymer
HB	Hyperbranched
HE	Heparin
HE-Na^+	Heparin sodium salt
HPEI	Hyperbranched poly(ethyleneimine)

L

L%	Percentage of linear groups
Lac	Lactose monohydrate
LPEI	Linear poly(ethyleneimine)

M

MADQUAT	Quaternary ammonium derivative poly(trimethylammonium ethyl methacrylate chloride)
Maltose	Mal
ML	Multilayer
MO	Methylene orange
M_n	Number average molecular weight

MWCO	Molecular weight cut off
M_w	Weight average molecular weight

N

NMR	Nuclear magnetic resonance

P

PA	Polyanion
PAA	Poly(acrylic acid)
PAH	Poly(allylamine hydrochloride)
PAZO	Poly-(1-[4-(3-carboxy-4-hydroxyphenylazo)benzenesulfonamido]- 1,2-ethanediyl)
PC	Polycation
PCD	Particle charge detector
PD	Polydispersity
PDADMA	Poly(diallyldimethylammonium chloride)
PDI	Polydispersity index
PE	Polyelectrolyte
PEC	Polyelectrolyte complexes
PEI-OS	Hyberbranched poly(ethyleneimine) modified with oligosaccharides
PEI-5k	Hyberbranched poly(ethyleneimine) with molecular weight 5 kDa
PEI-25k	Hyberbranched poly(ethyleneimine) with molecular weight 25 kDa
PEI-750k	Hyberbranched poly(ethyleneimine) with molecular weight 750 kDa
PES	Poly(ethylenesulfate)
PGA	Poly(L-glutamic acid)
pI	Isoelectric point
PPI	Poly(propylenimine)
PLL	Poly(L-lysine)
PPI-OS	Poly(propylenimine) dendrimer modified with oligosaccharides

PSS	Poly(sodium 4-styrenesulfate)
PTEBS	Hyperbranched polymer and poly[2- (3- thienyl) ethoxy 4-butylsulfonate]
PU	Polyurethane

Q

QCM	Quartz crystal microbalance

R

rms	Root mean square

S

SAXS	Small-angle X-ray scattering
Si-IRE	Silicon internal reflection element
STRP	Streptomycin
SD%	Degree of swelling

T

T%	Percentage of terminal groups
TDF	Total degree of functionalization

1. INTRODUCTION

People will always have a desire to explore. Sure there is a little bit of danger in the unknown, but human beings can't back away from something that is a challenge. We are born explorers, empty vessels, curious and fascinated by the world around us. It is the human nature. Economically, humans seek always and without stopping beyond their needs, e.g. physiological needs, safety needs, health needs etc., eager to learn and full of curiosity and creativity. On achieving one need, they will rush after the other and they will never and by any ways be satisfied.

Human beings start their life surrounded by surfaces: from their skin to faces, from skeleton to body internals, to the walls and streets of their homes and cities, to the images, books, and screens of our cultures and civilizations, to the natural world and what we imagine beyond. Nowadays, modern production processes require inherent state-of-the-art surface technologies. Furthermore, rising standards of technical products are creating the perception that surface technologies are often the central impetus needed for meeting product specifications. Design engineers thus face two essential tasks: On the one hand, part specifications need to be transformed into properties of materials and surfaces. On the other hand, selected materials technologies have to be integrated in the corresponding process chains. Apart from the required part specifications, production cost and ecological aspects and when it is related to the living organisms and people life then the biocompatibility are important issues. Controlling the bulk and surface properties of materials is a real challenge for bioengineers working in the field of biomaterials, tissue engineering and biophysics. In the field of implantable biomaterials, the bulk properties of materials are known to be important for the overall properties, especially for mechanical strength, but their surface properties have long been recognized as being highly important. The surface of the materials is an interface between the material and the host tissue, and it is able to trigger a wide variety of biological process.

Considerable efforts are thus devoted toward functionalization of the surfaces of materials used in biomedical applications, i.e. typically metals, polymers and ceramics, in order to render them bioactive, that is able to trigger a specific cell response. Polymeric coatings appear especially interesting because of the diversity of the chemical and physical

properties they offer. For instance, polymeric coatings have been employed for the coating of stents. Natural biopolymers appear promising as biomimetic coatings, as a result of their natural similarity to human tissues. A lot of effort is thus dedicated to engineering new forms of biomimetic surfaces. Tissue engineering has grown as a field in its own: its aim is to use a combination of cells, engineering and materials. These together with suitable biochemical and physicochemical factors, improve the biological functions of damaged tissues (bone, cartilage, blood vessels, skin, etc.) or replace them.

In the field of biomaterials, controlling the surface properties of the materials may be a means to influence cell behavior including recolonization, adhesion, migration or even differentiation. Therefore, various strategies have been developed to modify the materials' surface properties, such as by Langmuir-Blodgett deposition and self-assembled monolayers. For the past two decades, layer-by-layer (LbL), also called polyelectrolyte multilayer (PEM) coatings, has emerged to become a new and general way to modify and functionalize surfaces whose applications range from optical devices to biomaterial coatings. The technique is based on the alternate deposition of at least one polyanion and one polycation. On account of their biocompatibility and non-toxicity, these latter films constitute a rapidly expanding field with great potential applications: preparation of bioactive and biomimetic coatings, preparation of drug release vehicles, buildup of cell adhesive or anti-adhesive films. Consequently, the versatility of the LbL method makes it an attractive technique for a number of areas including electrooptics, sensors and catalysis. In addition, with LbL natural polymers that are already widely used for biomedical applications including hydrogel preparation, soft tissue repair and viscosupplementation can now be prepared in the form of thin films and deposited onto various types of substrates. *In vitro and in vivo* studies have shown that some polyelectrolyte multilayer nanofilms are biocompatible, and may enhance adhesion and growth of cells like osteoblasts, [2] chondrocytes, [3, 4] myoblasts, [5] chondrosarcomas, [6] and smooth muscle cells. [7] Although there are several forms of LbL films (films, capsules and membranes), this work will focus on LbL supported films on a planar solid substrate, which is carried out using a solution dipping method. However, to understand and to tailor such interactions, it is essential to know about the fundamental physicochemical properties of the multilayer films.

The present thesis will focus on studies dealing with stable LbL films made of weakly charged hyperbranched poly(ethyleneimine) modified with oligosaccharides (PEI-OS) in combination with natural polymers that can be used in the area of drug delivery. There is a need for low-cost ‘‘smart’’ coatings that balance the ability to release complex drug profiles with the flexibility of incorporation into a range of biomaterials. [8] Bioactive molecules that were effectively shown to have a biological effect and studies using model drug molecules will be mostly concerned. In this project PEMs with non-covalent affinities and with controlled tuning and targeting release properties for a modeling drug will be fabricated. By simply varying either the total number of layers deposited or the conditions used during the assembly process, the films can range from nanometers to few microns in thickness. In fact, it has been well documented that variation in such parameters as the concentration of polymers, their stoichiometric ratio, [9] their molecular weight, [10] the concentration of salt used in the adsorption and wash baths, [11, 12] and the time allowed for polymer adsorption, [9, 13] among other film properties, greatly influence the film thickness and stability. Depending on the type of PEs used the PEM growth regime in addition to PEM thickness with the number of LbL adsorption cycles are considered as one of the main factors in controlling multivalent probes load and release. In addition to number of cycles, in this study pH responsive weakly charged PEs will be also addressed. PEM’s assembly pH and immersion solutions with different pH values control the protonation degree of acidic or basic groups of weak PE, where they regulate charge density along the PE chains. Thus, these factors are influencing PEM conformations and mutual interactions.

2. THEORETICAL BACKGROUND

2.1. Dendritic polymers and their applications

2.1.1. Dendrimers and hyperbranched polymers topology: a promising class of materials

The architectural parameter of branching introduces new physical properties and levels of control not possible in strictly linear polymers.[14] Recently, much interest has been given to highly branched polymers such as perfectly branched dendrimers (**Scheme 2-1**), [15] and randomly branched hyperbranched polymers (HBPs) (**Scheme 2-2**). The term dendritic must be clarified: dendritic means highly branched tree-like structures and cover both, (**i**) dendrimers as well as (**ii**) HBPs but also other highly branched or fractal molecules. The well-defined dendrimers will be firstly presented. The term dendrimer was created by Tomalia *et al.* [16] in 1985 from the greek words dendros. It means tree, and meros, which means part.[16] Dendrimers are polymers, which are highly uniform, monodispers, three-dimensional and globular in shape and their outer scaffold possesses high numbers of reactive functional groups. They are perfectly branched molecules prepared in a step-wise manner with the potential to come close to structural and molar mass uniformity.

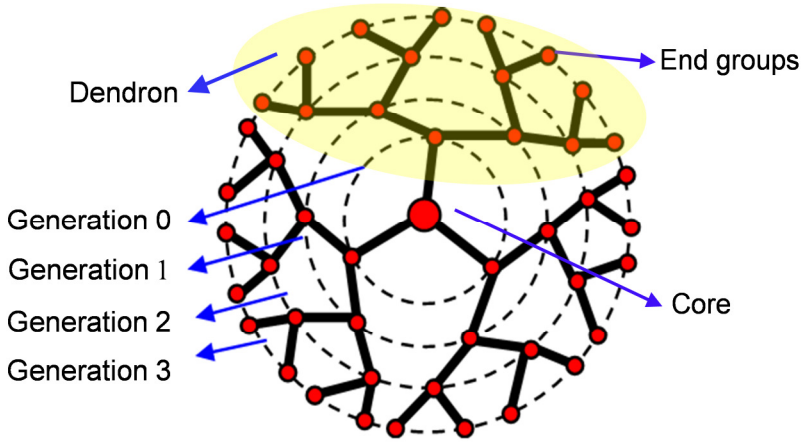

Figure 2-1. Schematic represents the configuration of tri-functional dendrimer of generation 3. Adapted from Reference [17]

Their molecules are composed of repeating units emanating from a central core. The core is characterized by its functionality, which is the number of chemical bonds

through which it can be connected to the external parts of the molecule. Through the bonds of the core, the layers are attached to the core and each of these arms is terminated with the multifunctional branched unit (**Scheme 2-1**). [18] They are so attractive because of their perfect structure , exact molar mass and all the possibilities to mimic very complex molecules as found in nature, but at the same time the synthesis of high generation dendrimers without any defects can be considered one of the major challenges in organic chemistry (**Scheme 2-1**). [19] Compared to well-defined dendrimers comes the HBPs, which possess highly random structures, imperfect branching but also globular shapes as dendrimers (**Scheme 2-2**).[20] HBPs are prepared in a random one-pot synthesis from monomers having branching potential, e.g. AB_2 based, but with low control over structure and molar mass (**Scheme 2-2**). Synthesis of HBPs might not be trivial but certainly feasible. [19]

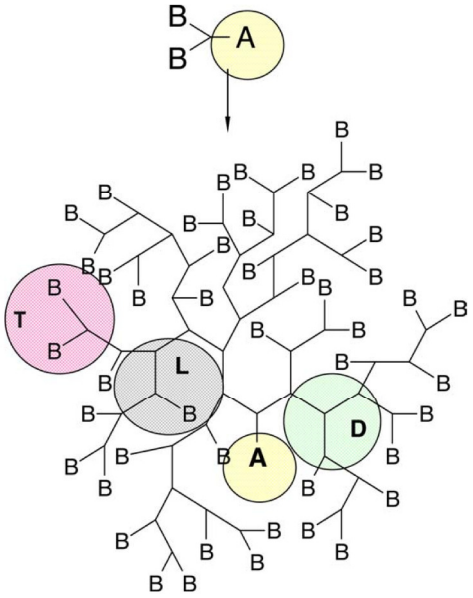

Scheme 2-1. Schematic representation of a HBP by AB_2 monomers exhibiting linear (**L**), dendritic (**D**) and terminal (**T**) units as well as one unreacted **A** functionality as focal unit. [19]

In experiments, due to the ‘’one-pot’’ synthesis technique, HBP are usually polydisperse systems with different topologies and molecular sizes. [21, 22] To distinguish perfectly branched dendrimers and randomly HBPs a common value is the so called degree of branching (DB). The DB was initially stated by Hawker *et al.* (**Eq. 2-1**), [18] and refined by Hölter *et al.* (**Eq. 2-2**).[23] The degree of branching represents the percentage of the three possible connectivities, dendritic (D), linear (L) and terminal monomers (T),

among the total monomers in the polymer; from an AB_2 random polymerization, it is defined as:

$$\mathrm{B}(AB_2) = \frac{T_{AB_2}+D_{AB_2}}{\mathrm{T}_{AB_2}+\mathrm{D}_{AB_2}+\mathrm{L}_{AB_2}} \qquad \textbf{Eq. 2-1}$$

If conversion of A is high, D ≈ T, the formula is reduced to the more widely used equation:

$$\mathrm{B}(AB_2) = \frac{2\mathrm{D}_{AB_2}}{(2\mathrm{D}_{AB_2}+\mathrm{L}_{AB_2})} \qquad \textbf{Eq. 2-2}$$

Where D is the number of fully branched units and L is the number of partially reacted units. [23] **Eq. 2-1** is only applicable to high molecular weight HBPs, **Eq. 2-2** represents an universally applicable formula for low and high molecular weight HBPs. [23] By definition, a linear polymer has no dendritic segments and DB equals zero. In contrast, dendrimers exhibiting perfect branching have no linear segments and therefore DB equals unity. Since HBPs have both linear and dendritic units, a reliable analytical method must be sought to measure the relative concentrations of these units to calculate their DB which falls in the architectural continuum between linear polymers and dendrimers. [24]

2.1.2. Hyperbranched polymers properties and applications

In this section, we would like to focus purely on HBPs. In this part we will navigate with the most famous properties and applications for HBPs. There are several advantages of HBPs over traditional linear polymers and we are going to illustrate some of them:

- They are highly reactive due to the large number of functional end-groups.
- Their viscosities are significantly lower than those of traditional polymers due to the lack of chain entanglement and higher degree of branching.
- Their polarities and solubility can be adjusted by their functional end groups and selective solvent.
- Their highly defined globular structure allows them to serve as branching scaffolds for other architectures. [25, 26]

Since HBPs possess high numbers of functional surface groups their properties with regard to, e.g. solubility, compatibility, reactivity, surface adhesion, self-assembly,

chemical recognition or luminescence properties can easily be adapted. Additionally their high thermal stability, low solution and melt viscosity allow efficient large scale production. This makes them suitable candidates for industrial applications such as dispersion agents, rheology modifiers or as cross linkers in elastomers, since here their broad molecular weight distribution does not harm their performance. [20] Due to their unique and easy synthesis, HBPs have a wide range of potential applications. HBPs and their substitutes can be used as nanomaterials for host guest encapsulation, [27] fabrication of organic-inorganic hybrids, [28, 29] and nanoreactors. [30, 31] Due to a large number of functional groups and interesting optical, electrochemical biology and mechanical properties of HB molecules, patterning of HBP films are receiving increased attention. [32-34] Due to their high solubility, low viscosity and abundant functional groups, HBPs have been used as the base for various coating resins, [30] including powder coatings, [35] flame retardant coatings, [36] and barrier coatings for flexible packaging. [37]

2.1.3. Hyperbranched poly(ethyleneimine) properties and applications

Hyperbranched polyethyleneimine (HPEI) is an amine-functional HBP with a globular, dendritic-like structure and branching degree of 66-75% (**Scheme 2-3**). It is a clear viscous liquid. [38] HPEI is a well-known functional polymer and its application fields are very wide. For example, HPEI has been used for a long time not only for various industrial purposes, e.g. flocculating agent, thickeners and dispersion stabilizer, but also in biomedicine application, such as gene transfer processes. [39] Furthermore, HPEIs have also been utilized in quantum dot nanocomposites, [40] as unimolecular inverted micelles for anionic dye encapsulation [41] and catalyst support. [42-44] HPEI adsorbs strongly on the silica surface and causes a reversal of the electroosmotic flow (EOF) due to its positively charged surface. It can modify the separation selectivity of small and large ions and can mask the silanole groups and as a consequence this can lower the EOF and eliminate analyte-wall interaction. [38]

Among the total non-viral gene vectors, HPEI with high transfection efficiency has bright prospects in application. [45, 46] However, HPEI is not fit for keeping on gene expression, [46, 47] due to its serious cytotoxicity. [48-50] Actually, the transfection efficiency and cytotoxicity are almost antagonistic. PEI with molecular weight including e.g. 25 kDa, 800 Da or less displays a low cytotoxicity and transfection efficiency.

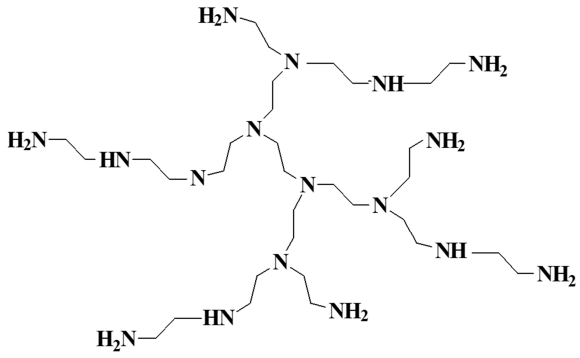

Scheme 2-2. Structures of hyperbranched poly(ethyleneimine) (HPEI). [38]

In contrary, PEI with higher molecular (up to 750 kDa) weight shows higher transfection efficiency and cytotoxicity. Investigators attempt to make some modification against PEI properties. Up to now, PEI has been modified with chloroquine, [51] cyclodextrin, [52] polyethylene glycol (PEG), [53] folic acid (FA), [54] heparin, [55] hyaluronic acid (HA) and oligosaccharide decoration …etc. [56] The broad scope of modification contains also carbohydrates like chitosan, [57-59] galactose, [60-62] or mannose, [63] and others. [64-66] Appelhans *et al.* [56] have presented a rapid method for the development of the HPEI decorated with different oligosaccharide architectures (PEI-OS) as carrier systems (CS) for drug and bioactive molecules for in-vitro and in-vivo experiments. [56]

2.1.4. Sugar modified dendritic polymers and their applications

Carbohydrates are the most abundant, easily accessible and cheap biomolecules in nature. Beside their potential uses as key chemical raw materials and energy source, they have been recognized to play a key role in a wide variety of complex biological processes. With functions similar to those of natural carbohydrates, synthetic glycopolymers are fabricated with specific pendant saccharide moieties, e.g. dendritic glycopolymers. [67] They are essential macromolecules that display many structural and functional features. A feasible and common strategy to overcome the cytotoxicity of cationic dendrimers or HBPs is surface modification. However, amidation, [68] pegylation, [69] or the derivatization [70] with fatty acids have proven to reduce the cytotoxicity. Another proper way to achieve biocompatibility is the decoration of their surface with mono- or oligosaccharides. The

latter, however, has not only shown to decrease cytotoxicity, but also to introduce further interesting features in these delivery systems.

Dendritic glycopolymers are considered to be the results of the attachment of different kinds of mono- or oligosaccharides to synthetic dendritic scaffolds by means of different diving forces and interactions. Dendritic glycopolymers have been developed as potential multivalent agents in the field of glycomics.[71] Some biological interaction studies and applications for glycopolymers, for example, in antivirus/bacteria, scaffolds for tissue engineering and gene/drug delivery are investigated. [60, 66, 72-74] Interfering as an anti-adhesion drug, like toward viruses to minimize infection diseases, is also numerously investigated. [75-79] There is a huge potential for glycopolymers as a multifunctional macromolecules nowadays in many other applications like in that of the optical biomarkers, [80] for the stabilization of metal clusters and nanoparticles , [81, 82] and their use as potential anti-prion agents.[80, 83] Thus, the results indicate that these dendritic glycopolymers are promising and attractive candidates for biomedical applications. In this study, HPEI decorated with different oligosaccharide architectures has been used. The high potential of HPEI as a gene carrier lays in the fact of possible protonation of every nitrogen atom in the polymer structure. Therefore, HPEI possesses a high cationic charge density and can easily interact with negatively charged nucleic acids forming complexes.

The biggest problem is, however, the cytotoxicity of HPEI polymer. In 2009, Dr. Appelhans' group, [56] (Leibniz-Institute für Polymerforschung Dresden e.V.) has intensively studied the introduction of various oligosaccharide architecture (of low and high molecular weight) in the outer sphere of PPI and HPEI. In contrary to PPI-OS dendrimers, the PEI-OS macromolecules possess imperfectly branched structure. For the generation of various oligosaccharide substitution degrees, they established an easy one-pot approach on the HPEI surface. Sugar moieties were covalently bonded to the primary and secondary amines of HPEI by reductive amination reaction. This is considered as a first step toward the development of novel dendritic core-shell architectures as nanocarriers which allows the formation of H-bonds, electrostatic interactions as well as hydrophobic-hydrophobic interactions. The HPEI offers primary amines (terminal units T) and secondary amines (linear units L) that can be transferred to the tertiary amines (dendritic

units D) (**Scheme 2-4**). Appelhans *et al.* [56] distinguished between the three different groups with regards to their structure and the degree of substitution.

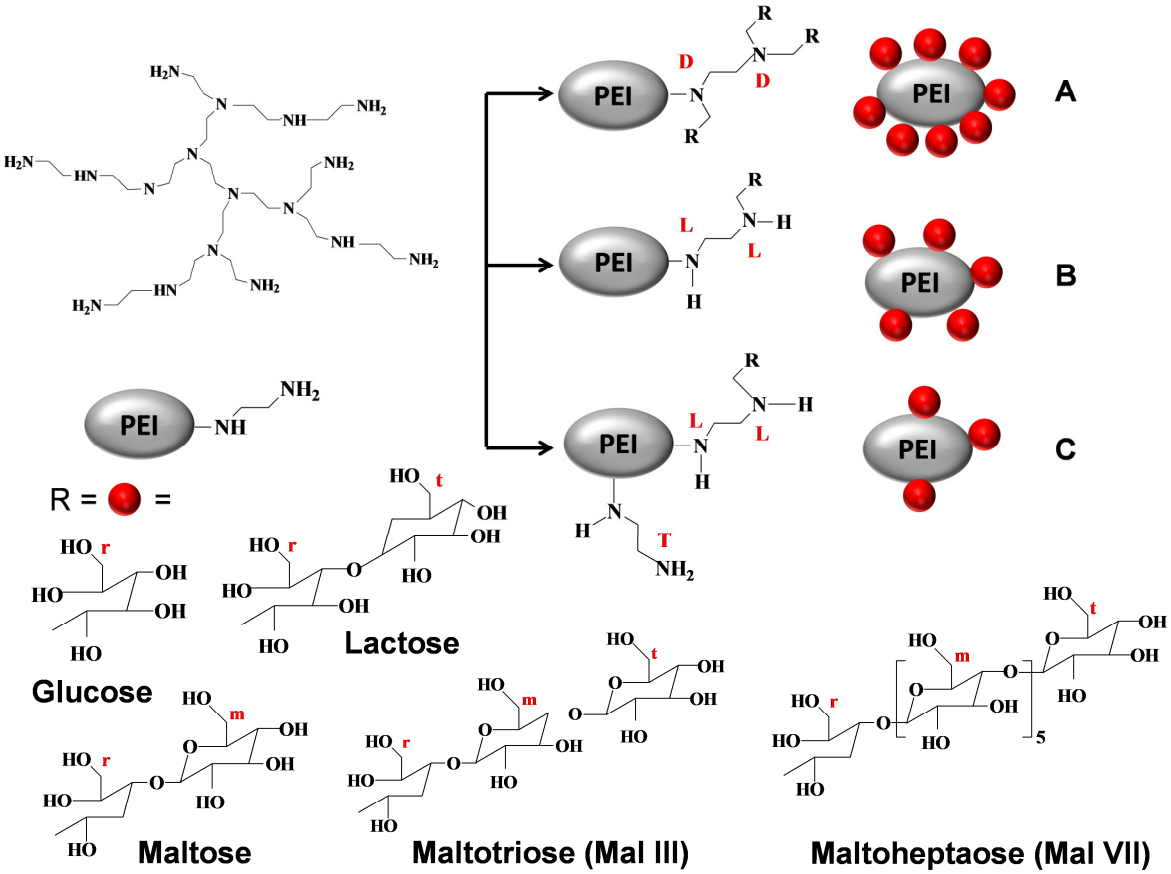

Scheme 2-3. Schematic presentation of PEI decorated with different oligosaccharide architectures forming different structures A-C. Adapted from reference [56]

Abbreviations: **Sugar units**: r = reductive unit; m= middle unit; t= terminal unit

Branching units: L= linear unit; T= terminal unit and D = dendritic unit.

Three different structures of PEI-OS have been fabricated as follows (**Scheme 2-4**):

(i) Structure A: It is characterized by its dense decorated and closed organized oligosaccharide shell with preferred D units.

(ii) Structure B: PEI surface with preferred L units in the outer shell. It has a lower degree of functionalization and less secondary amines converted to tertiary amines, and could be obtained by utilization of low PEI:sugar ratio (1:0.5).

(iii) Structure C: PEI surface with a combination of nonconverted T units and L units. It presents an open sugar shell with free primary amines in comparison to structure A and B where at least all primary amines were converted to secondary amines. It could be obtained by utilization of PEI:sugar ratio (1:0.2). [56]

Recently, several papers and reviews have addressed sugar modified polyethylene structures. In 2010, Richter *et al.* [84] used maltose-decorated HPEI (PEI-Mal) and already fabricated a stable crosslinked film. The film thickness was varied from 63 to158 nm (in dry state) and from 78 to 395 nm (in swollen state). A phosphate containing drug was assumed to act as model drugs (ATP, AMP, CTP, and CMP). The film thickness of the swollen film was directly reduced after the addition of the triphosphate containing drug (ATP and CTP) and increased in the presence of monophosphate containing drug (AMP). [84] These surprising results were attributed to the high electrostatic interaction between the triphosphate drug and the core/shell of the PEI-OS.

In 2012, Szulc *et al.* [85] have obtained physiological nucleotide-dendrimer complexes under different conditions (incubation time, salt concentration and pH). In this context, it has been shown that binding of sugar residues to a dendrimer/hyperbranched surface decreases dendrimer/hyperbranched toxicity. Thus, such a modification improves biocompatibility of PPI dendrimers and HPEI. They have examined the fourth and the fifth generations of cationic PPI as potential anticancer drug carriers. PPI dendrimers with 50% of primary amino surface has been fabricated after being modified with maltose sugar moieties. Physiological nucleotides (AMP, ADP and ATP), that are metabolites of nucleoside analogues, have been used as an anionic couterion and model molecules. Stability of complexes against enzymatic degradation and different medium conditions has been checked. Therefore, they claimed that the drug could be delivered to the cell in an active phosphorylated form without a need to be activated in vivo by kinases. Moreover, PPI-m dendrimers possessing many surface groups can serve as a platform for attaching cancer-specific targeting ligands which selectively bind to receptors that are expressed on the surface of cancer cells.[85]

In 2012, Polikarpov *et al.* [86] have fabricated a multicompartment hydrogel hosting dendritic glycopolymers as a potential multirelease system in which pH-dependent sequential release of drug and dendritic carrier molecules from the hydrogel can be induced. Alternatively, a simultaneous release of drug molecules and nanocarriers from the hydrogel was also possible by adjusting the pH and hydrogel structure. Essential for the success of this concept was the design of the dendritic nanocarrier which in this case was HPEI decorated to a different degree of modification by maltose units (PEI–Mal with structures A–C (**Scheme 2-4**)). They evaluated in detail the complexation capacities of

these structures towards ATP as the model drug. PEI–Mal macromolecules, themselves were incorporated in anionic hydrogel to host anionic ATP molecules governed by non-covalent interaction. The uptake and release for ATP was dependent on the dendritic glycostructure and was pH responsive. They investigated that the uptake of ATP has altered the properties of PEI–Mal, e.g. the surface charge changes and thus, in the case of structure C immediate precipitation occurs during ATP uptake. In addition, ATP aggregations have been investigated after being loaded to PEI-Mal compartments. They postulated two different types of interactions between ATP and PEI-Mal. (**i**) Firstly, a strong electrostatic interactions between the positively charged PEI core and the anionic ATP. (**ii**) Secondly, weaker hydrogen bonding through the maltose shells. It was found that selective pH-dependent release of ATP from the multicompartment release system was possible assuring that the nanocarrier macromolecules will not simultaneously escape with the drug molecules from the hydrogel. A selective release of ATP at pH 5.4-7.4 has been achieved when a boronic acid (BA) containing hydrogel was used. These results were due to the strong boronic acid–maltose complexes formed at pH 5.4 and 7.4 in the hydrogel and the presence of chemical binding between the maltose units from the dendritic glycopolymers and BA units in the hydrogel. Switching to pH 2, the borate bonds are hydrolyzed leading to simultaneous release of PEI–Mal carrier loaded with ATP. However, when using a hydrogel without being crosslinked with BA units, a simultaneous release of ATP and the dendritic glycopolymers scaffold out of the host hydrogel has been observed. [86]

In 2014, Tripp *et al.* [87] evaluated the general interactions of dendritic core-shell glycolarchitectures, using PEI-OS as the core component, with neutral, cationic and weakly anionic biologically active analyte molecules in aqueous solution and compared the complexation capability with the parent HPEI. Ultrafiltration experiments have been carried out by using an aqueous solution of the relevant PEI-OS and the different analyses in a molar ratio of 1:10. The uptake measurements were calculated after 3 hours and 20 hours. This study elucidates that independently on the size of the core used, whether PEI-5k or PEI-25k core; oligosaccharide architectures can increase the complexation capability for the analyte/drug molecules. The degree of complexation is greatly influenced by the density of the oligosaccharide shell. On the other hand in the presence of high ionic interaction the minor priority is to the oligosaccharide shell density. What was surprising in these results that parent HPEI exhibit weak interactions with all applied analyte

molecules. On the other hand, vitamins B1, B2 and B6 (neutral ionic state) also show weak interactions with most of PEI-OS (uptake capacity ≤ 20%). However, in case of vitamins B3 and B12, the estradiol derivative and the proteasome inhibitor pantoprazole showed strong and very strong interactions with PEI-OS (the uptake capacity ≥ 50-100%). It was concluded that in case of neutral or zwitter ionic state (B1, B2, and B6), weak interactions between the host molecule and the guest analyte were achieved. These results were attributed to the absence of the ionc/electrostatic interactions between host and guest molecules and the driving forces were only related to hydrogen bonds, Van der Waals forces or force of dispersion. In contrast, the anionic groups, i.e. carboxylate in B3, B12, the estradiol derivative and pantoprazole, allow for moderate or strong ionic interactions with the cationic amino groups of the dendritic PEI scaffold in PEI-25k and PEI-OS. Furthermore, the required electrostatic/ionic interactions with the PEI scaffold only become available with a suitable sugar shell, which leads to an expansion of the otherwise collapsed HPEI core. [87]

2.2. Polyelectrolytes: definition, properties and applications

Polyelectrolytes (PEs) are a particular case of charged polymers with acid or basic ionizable groups that in adequate solvents can be dissociated. This will lead to a polymer with a charged backbone plus its neutralizing counterions. When the dissociation is completed these PEs are called strong PEs while if the dissociation is only partial and pH-dependent they are called weak PEs. Due to their particular physicochemical properties, PE systems are commonly used in industry for different and variable applications, and they also serve as an important generic study case for biological systems, since most biopolymers are PEs. [88] Electrostatic interactions between charges lead to the rich behavior of PE solutions qualitatively different from those of uncharged polymers. For example:

(1) The crossover from dilute to semi-dilute solution regime occurs at much lower polymer concentrations than that in solutions of neutral chains.
(2) There is a well-pronounced peak in the scattering function of the homogenous PE solution. The magnitude of the wave vector corresponding to this peak increases with concentration as $c^{1/2}$. There is no such peak in solution of neutral polymers.

(3) The osmotic pressure of the PEs in salt-free solutions exceeds the osmotic pressure of neutral polymers at similar polymer concentrations by several orders of magnitude. It increases almost linearly with polymer concentration and is independent of the chain molecular weight in a wide range of polymer concentrations. This almost linear concentration dependence of the osmotic pressure together with its strong dependence on added salt demonstrates that osmotic pressure is mainly due to the counterion contribution.

(4) PE chains in semi-diluted regime follow untangled dynamics in a much wider concentration range and the crossover to the entangled dynamics occurs further away from the chain overlap concentration than in solution of uncharged polymers.[89]

PE chains at surfaces and interfaces represent an example of both two- and three dimensional PE solutions in which the local polymer concentration is controlled by interactions between adsorbing substrate and PE chains. As the surface charge density increases, the dilute solution of adsorbed chains transforms into a two-dimensional semi-diluted solution. If the surface charge density increases even more, The PEs adsorbed layers will also increase in thickness. The new and unusual phenomenon observed in the adsorbed layers is the surface overcharging (overcompensation of surface charge) by adsorbed PE chains. The amount of surface overcharging can be tuned by varying the solution ionic strength. The charge inversion plays a central role in the layer-by-layer (LbL) deposition technique (**Section 2.4.2**). This self-assembly method has been introduced for fabrication of the molecularly layered multi-composite films with a high degree of complexity. The film growth is achieved by alternating the deposition of polyanions and polycations from their aqueous solutions. The simplicity of the electrostatic assembly technique with practically no limitations on the shape of charge bearing species allows fabrication of multilayer film (ML) from synthetic PEs, DNA, proteins, inorganic platelets, nanoparticles and viruses.

2.2.1. Applications of polyelectrolytes (PE)

Polyelectrolytes have many applications, mostly related to modifying flow and stability properties of aqueous solution and gels. For instance, they can be used to either stabilize a colloid suspension, or to initiate flocculation (precipitation). PEs, like proteins, polypeptides and nucleic acids, play essential functions in human physiology and

metabolism. On the other hand, PEs have wide applications in chemical science and engineering, especially in colloids, surface, interface fields. For example PEs are used in the health and personal care industry as thickening reagents, [90] rheology modifiers, [91] and viscosity enhancers for shampoos, conditioners, deodorants and body lotions. [92] They are also used in water treatment, [93] waste treatment, [94] sludge dewatering. [95] PEs are widely employed to modify properties of surfaces or of colloidal particle suspensions. They are industrially used in papermaking, mineral separation, or to control flow properties of particle slurries. [96, 97] Others PEs are commonly used as additives to control colloidal stability and adhesive properties of surfaces. [98] Additionally, they are added to many foods. Some of the PEs that appears on food labels is pectin, carrageenan, alginates, polyvinylpyrrolidone derivatives and carboxymethyl cellulose derivatives. [99] They are also used in a variety of materials, including cement. [99] Finally, water soluble PEs are used in the biochemical and medical engineering field, such as: implant coating, drug delivery system etc.

2.3. Polyelectrolytes complex (PEC)

Polyanion and polycation can co-react in aqueous solution and form polysalts; [100, 101] in a complexation process closely linked to self-assembly processes. [102] The interaction usually involves a polymeric acid or its salt with a polymeric base or its salt. Depending on the variety of factors, it may cause the system to separate into a dilute phase and a concentrated complex coacervate phase, or it may result in a more or less compact precipitate or gel. The dense liquid phase, which is relatively concentrated in macromolecules, is called the coacervate. The definition of “coacervation” refers to the metastable suspension of macroion-rich droplets. Bungenberg de Jong and Kruyt coined the name “complex coacervation”.[103] Complex coacervation is the separation of a macromolecular solution composed of two oppositely charged macroions into two immiscible liquid phases.

The general conception is that the main driving force of complex formation is the gain in entropy caused by the release of low-molecular-weight counterions (**Scheme 2-5**). Then one can simply understand that electrostatic interactions are the main attractive forces, but hydrogen bonding, ion dipole forces, and hydrophobic interactions frequently play a significant role in determining the ultimate structures. The formation, properties and

applications of such PECs have been described in a large number of books and reviews. The properties of PECs are known to be influenced not only by the chemical composition of the polymers (molecular weight, stoichiometric ratio, charge densities …etc.), but also by secondary experimental conditions like the concentrations of the PEs prior to their mixing ratio, ionic strength of the solution, mixing order ….etc.

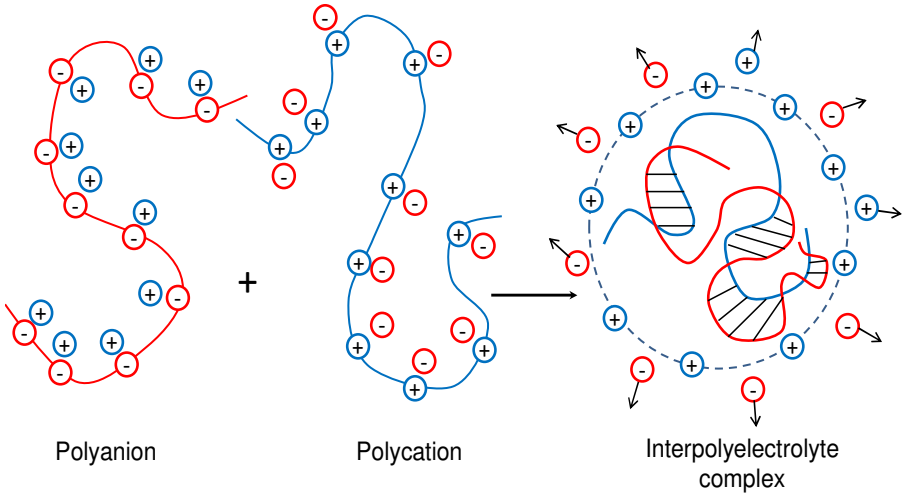

Scheme 2-4. Simplified sketch represents the release of counterions upon PEC formation, due to gain of entropy forces. [104]

The structure formation is mainly determined by the fast kinetics of the process (less than 5 µs, depending on , e.g. the concentrations of PEs and their molecular-mass), followed by a slower stage in which chains redistribute to a PEC conformation closer to equilibrium. [104]

2.4. Adsorption of polyelectrolytes (PE)

2.4.1. A brief historical overview of theoretical models of PE adsorption

Adsorption of charged polymers on charged surfaces and interfaces is a classical problem of polymer physics and has been addressed under extensive theoretical and experimental studies for the last four decades. [105-107] Interest in this problem is stimulated by its tremendous importance for different areas of natural sciences ranging from materials science to physics of disordered systems and biophysics. One of the first analytical calculations of the PE adsorption at a charged surface was performed by Wiegel. [108] He investigated for PE chain in the direction of Gaussian statistics. Thus, he calculated the threshold adsorption and the thickness of the adsorbed chain as a function of

salt concentration. The binding of flexible macromolecules to the oppositely charged cylinder was treated by Odijk in a similar way. [109] The interaction between the charged monomers on the chain was taken into account by Muthukumar, [110] who considered a general case of the adsorption of PE chain that can take any conformation between those of a self-avoiding walk and a rod-like structures, depending on the ionic strength of the solution. This theory was later extended to PE adsorption on charged patterned surfaces, [111] and validated by Monte Carlo simulations. [111-113] The scaling theory of the conformations of a weakly charged PE chain near a charged surface was proposed by Borisov *et al.* [114] There are different stages of adsorption of a polyion corresponding to the rearrangement of chain conformations on different length scales. The predictions of the theory were confirmed by computer simulations. [115] The detailed interfacial properties of a lattice model for adsorption of a single PE chain were studied by Beltran *et al.* [116] using Monte Carlo simulations. It was demonstrated that PE chains flatten out forming long trains of loops upon increase in the surface charge density or in the fraction of the charged monomers on the chain. The Hoeve's theory, [117, 118] for adsorption of uncharged polymers was generalized by Hesselink, [119] who incorporated the electrostatic contribution into Hoeve's partition function of an uncharged adsorbed polymer and considered the total free energy of a system as a sum of electrostatic and non-electrostatic terms. Assuming a step-like polymer density distribution in the adsorbed layer, Hesselink calculated the adsorption isotherm and polymer surface coverage as a function of salt concentration. The adsorbed amount rises very steeply and levels off at the saturation value in solutions with extremely low polymer concentrations. Hesselink's theory predicts an increase of adsorbed polymer amount with increasing salt concentration.

The significant fraction of theoretical works dealing with multi-chain PE adsorption on a charged surface was carried out within the framework of the self-consistent field (SCF) method. [120, 121] The polymer density distribution is coupled in these theories to the local electrostatic potential through the combination of the Poisson–Boltzmann equation and the Edwards equation describing polymer conformations in the effective external potential. This approach was first applied by van der Schee and Lyklema, [122] and Evers *et al.* [123] They have shown that strong repulsion between charged monomers leads to very thin adsorbed layers. The adsorbed amount increases and the adsorbed layers become thicker, if this repulsion is screened by adding salt. The extension of the Van der Schee and Lyklema theory to the case of weak PEs was done by Bohmer *et al.* [124] The

charge on adsorbed weak PE is determined by the pH and salt concentration in the local environment of ionizable groups. [124-127]

2.4.2. Polyelectrolyte multilayer self-assembly

Polyelectrolyte multilayers (PEM) can be assembled on charged surfaces by the so called LbL technology. As it was previously mentioned, the films known as PEM are made by alternating deposition of polyanions (negatively charged polymers) and polycations (positively charged polymers). The first report of the LbL technology dated back to 1966 when Iler prepared a ML structure by electrostatic interactions between colloidal anionic and cationic particles. [128] The technology was however not systematically established until 1990. Decher and Hong started to prepare MLs of oppositely charged PEs on charged substrates. [8, 129-131]

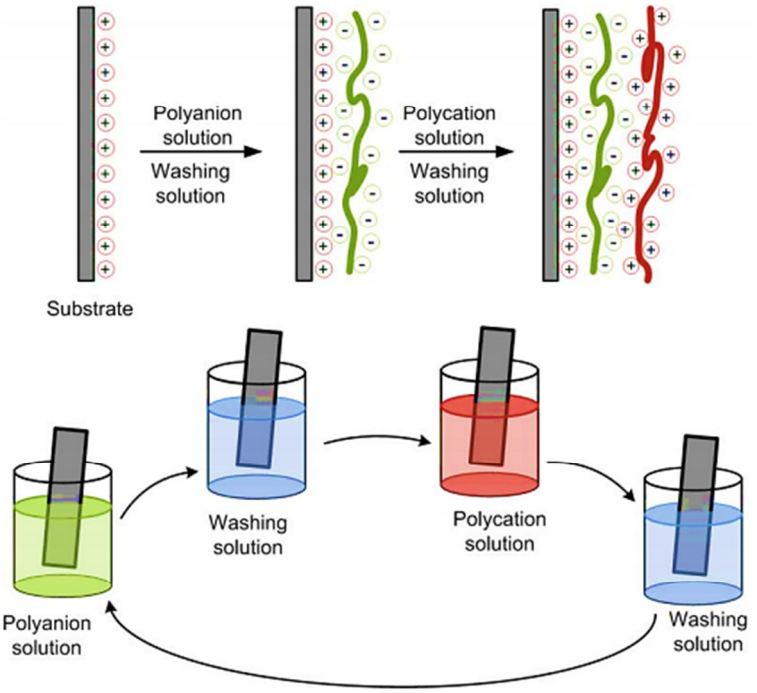

Scheme 2-5. Scheme of self-assembly of LbL film on a planar surface.[8]

It is shown in **Scheme 2-6** that when a substrate of a positive surface charge is immersed in an aqueous solution of anionic PE for several minutes, a thin layer of polyanions is adsorbed onto the substrate and the surface charge of the substrate is reversed to be negative. A polycation layer can be assembled onto this negatively charged surface in the same manner. When this cycle is repeated, PEM is formed. This process is

normally referred to as self-assembly of ML films based on electrostatic forces between oppositely charged PE. [132, 133] When a defined surface charge is achieved, no further polymers can be adsorbed. Hence, the self-limiting process leads to homogeneous and well reproducible layers of defined thickness on charged surfaces. Non-adsorbed PEs are removed in the rinsing step.

LbL technique possesses numerous advantages used for various purposes in academic researches, as well as industrial applications. Some of these advantages can be presented as follows:

(1) The process is relatively inexpensive and one simply needs to dip a substrate into alternating positively and negatively charged PEs containing solutions to form uniform and stable layers.

(2) The ML-assembly process employs a variety of water-soluble, charged polymers in an economical and environmentally benign aqueous process that produces finely-controlled thin-films, applicable to a virtually limitless number of surfaces.

(3) It is not specific to electrostatic forces. Thin film layers can also be held together by other types of non-covalent bonds, such as hydrogen bonds and hydrophobic interactions. [134] coordinate binding, [135], covalent binding,[136] charge transfer, [40] … etc. This means that there are a variety of polymers to choose from when using the LbL technique, and we can choose the most appropriate method and material according to the conditions that are present in the problem.

(4) Changing the pH of PEs will cause the charge of its solution to change, which is beneficial for some systems in which electrostatic interactions must be taken into account.

(5) Variation of substrates: any charged material, e.g. silicon, gold, platinum, plastic, glass, quartz, stainless steel, nanoparticles, blood cells, colloid particle…etc., can be used as the deposition substrate. Even uncharged materials, like PTFE, [137] were reported as substrates.

(6) Easy variation of the thickness: generally, the thickness of the monolayer is approximately 0.2 – 10 nm. Furthermore, the thickness of the monolayer can also be changed by varying the parameters of the solution, such as: pH, concentration, ionic strength and deposition time. Therefore, the thickness of ML thin film, which is composed of several monolayers using LbL technique, can be very precisely controlled by varying the deposited layer numbers and conditions. [130]

(7) There are other candidates that can be used besides PEs for the LbL film assembly such as proteins, [138] nucleic acids, [139] lipids, [140] viruses, [141] inorganic nanoparticles, [142] and organic dye molecules…etc. [143]

2.4.3. Effect of the image forces and short-range interactions on PE adsorption

The interaction of PEs and charged surfaces is an important phenomenon in industrial and biological processes. This section summarizes the current understanding of PEs adsorption to the oppositely charged solid substrates. To understand this phenomenon we have to discuss the influence of the substrates and their physical properties on the building up process. It is easily understandable that changing of the substrate for a given set of PE may have a strong influence onto the elaboration and the properties of the fabricated PEM. Since, differences in the very beginning of adsorption step, e.g. different substrate, may have significant repercussions in the further steps up to unknown growth levels .The first few bilayer depositions are influenced by short-range interactions between the substrate and the PEs. However the physical interactions between the substrate and the PEs can influence the ML morphology up to a thickness in the µm range. [144] Relative dielectric permittivity of the substrate and its surface charge are important factors that govern the surface morphology and must be identified.

It was formerly assumed that the dielectric constant of the solvent ε_1 and the substrate ε_2 are the same. However, in many experimental situations, such an adsorption of PE chains from water onto clay, polymer latex particles or at the water/air interface, the dielectric constant of the solvent ε_1 is larger than that of the surface ε_2. [145] The presence of a charge in a medium (with dielectric constant ε_1) near the surface (with dielectric constant ε_2) causes polarization for both media. The result of this is the appearance of the image charge at the symmetric positions with respect to the dielectric boundary with magnitude: [146]

$$q' = \left(\frac{\varepsilon_1 - \varepsilon_2}{\varepsilon_1 + \varepsilon_2}\right) q = \Delta_\varepsilon q \qquad \textbf{Eq. 2-3}$$

Where q is the valence charge, the image charge q' is located at the symmetric position with respect to the dielectric boundary. The magnitude of the image charge is defined by dielectric jump Δ_ε between the solvent and the substrate. [89, 147]

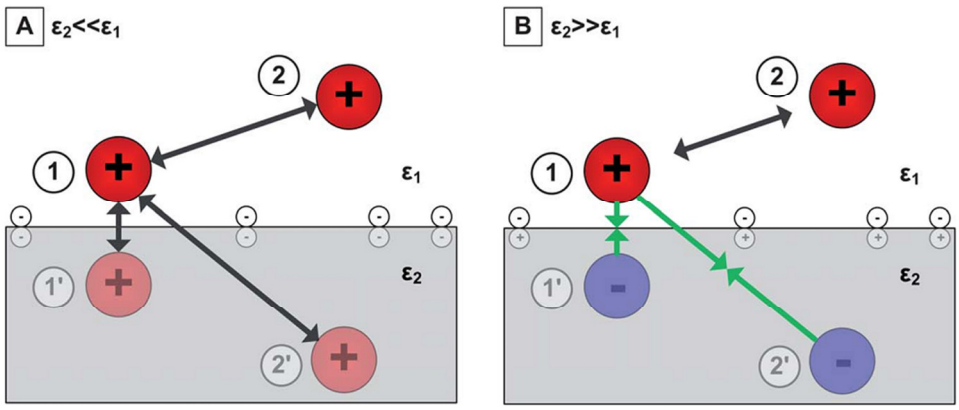

Scheme 2-6. Schematic diagram shows the electrostatic forces acting on a positive test charge (charge 1) in proximity to a second positive charge (charge 2) and a negatively charged surface. ε_2 is the dielectric permittivity of the surface material, while ε_1 is the dielectric permittivity of solvent. Charged surface exert short-ranged force on positive test charges (1 and 2), inducing image charges 1' and 2' on the surface of substrate. (**A**) For dielectric surfaces ($\varepsilon_2 << \varepsilon_1$), positive charges are induced on the substrate. (**B**) For metallic surfaces ($\varepsilon_1 << \varepsilon_2$), negative charges are induced on the substrate. [144]

If the dielectric constant of the substrate is much smaller than that of the solvent ($\varepsilon_2 << \varepsilon_1$) (**Scheme 2-7A**), which is usually the case for PEs adsorption from aqueous solution onto polymeric and dielectric substrates, the magnitude of the image charge q' is almost equal to the valence charge q. This leads to the effective repulsion of the test charge from the dielectric boundary. However, if the dielectric constant of the adsorbing substrate is larger than that of solvent ($\varepsilon_2 >> \varepsilon_1$) (**Scheme 2-7 B**), the valence of the image charge is opposite to the test charge creating an additional attraction to the adsorbing surface. In other words, if PEs are adsorbed from an aqueous solution ($\varepsilon_1 \sim 80$) on a dielectric surface ($\varepsilon_2 < 10$), the dielectric jump Δ_ε is close to 1 and thus q' has the same sign and nearly the same magnitude as q. Therefore, the probe charge experiences an electrostatic repulsion from the surface. However, for the adsorption to metallic surface ($\varepsilon = \infty$) the dielectric jump Δ_ε is equal to -1. The image charge q' has now the same magnitude but an opposite sign compared to q. One concluding point is that the repulsion between the charges is increased for dielectric surfaces (**Scheme 2-7 A**) and decreased for metallic ones (**Scheme 2-7 B**).

Besides electrostatic contributions, the forces between PE chains or between PE complexes are also influenced by Van der Waals-type interactions. These interactions are attractive, and usually described by a truncated-shifted Lennard-Jones potential. [148-150] Recent simulations on the buildup of PEMs show, that the strength of this is so-called monomer–monomer interactions. It is strongly influences the morphology of the PEM. [151, 152] For high values of the monomer- monomer interaction (in the range of the thermal energy) the simulations predict a dewetting of the PEs from the surface. For lower values of monomer-monomer interaction, dewetting process is expected to proceed by formation of small complexes. Such dewetting structures are usually described as islets, islands or droplets that cover the surface forming finally a non-continuous film.

This can be understood by recalling image charges induced on the substrate are effectively changes monomer–monomer interaction. For materials with low ε_2 this interaction is reduced by increasing the electrostatic repulsion between PE chains or PE complexes (**Scheme 2-7 A**). This leads to formation of small complexes that repel each other and thus tend to cover a large part of the surface (dielectric substrates). For materials with high ε_2 the electrostatic repulsion between the PE chains or PE complexes is reduced (**Scheme 2-7 B**) resulting in a dewetting process that resembles a collective dewetting process. Larger droplets with greater height cover less percentage of the surface (metallic substrates). Attraction to the negative image charges reduces the repulsion between two test charges, charge 1 and charge 2 (**Scheme 2-7**). It was investigated by Guillaume-Gentil *et al.* [144] that the nature of the used substrate has a strong influence on the morphology of the weakly interacted pairs (poly(L-lysine)/hyaluronic acid) (PLL/HA) MLs while it does not have an effect on the morphology of the strongly interacting polyelectrolyte couple (poly(allylamine hydrochloride/poly(sodium 4-styrenesulfate))(PAH/PSS) MLs. [144]

2.4.4. Effect of precoating on the adsorption of PEM

It is worth to mention that the good adhesion of the precoating to the base substrate depends on electrostatic interactions and ionic bonds. Therefore, the buildup of successive layers is mainly affected by type of substrate (**Section 2.4.3**), the precoating and type of the PEs themselves. [153, 154] Former investigation has been performed by Bosio *et al.* [154] , they investigated for ML regime with PEM pairing (PAH/PSS). They aimed to compare

silica surface force data by two different approaches. They studied the interactions between silica substrates coated with MLs both (**i**) with (Approach 1) and (**ii**) without (Approach 2) precoating layer of HPEI (M_w ~25 kDa). They compared also between Approach 1 (after first 3 layers) and Approach 2 after reaching 9 cycles deposition, where the surface properties lost "memory" for substrate and start the true ML step.

They observed that PEM with precoating layer yielded a bilayer of thickness 25Å (16 Å for PSS and 9 Å for PAH), this value was dramatically closer to the thickness of the first 5 bilayers fabricated without a precoating. AFM measurements also showed that PEI precoating approach is smoother and contains fewer irregularities and holes than the Approach 2 (without precoating). While for ML fabricated with Approach 2, AFM measurements showed holes of hundreds of nanometres in size. These holes disappeared as the number of coating cycles increased. Such defects were not observed when using PEI precoating. They finally concluded that the presence of the PEI precoating enhanced a lot PEM fabrication and reduce the effect of short range force exerted by charged solid substrate on the PEM surface and bulk structure, even it enhances polyions complexes assembly. In addition to the previously discussed points, precoating also enhanced the attraction force toward substrate. [154]

2.4.5. Basic law controlling the growth regime of LbL assembled PEM

When ML films are built up with polycations and polyanions, their mass or thickness grows mainly either linearly [155-159] or exponentially [153, 160, 161] with the number of bilayers. The linear build-up in PEMs is usually observed after the nonlinear initial build-up. [162, 163] The linear regime can be realized as a steady state where the deposition of a PE, with a finite interpenetration range, generates a constant mass and thickness increment to the developing film (**Scheme 2-8 a**). The exponential build-up regime in the PEM assembly is actually a relatively common feature (**Scheme 2-8 c**).

There are two mechanisms explaining the exponential buildup regime and may be explained as follows:

(i) Active surface: In this concept the nonlinear build-up is attributed to the continuous increase of surface roughness, isolated islands are formed at the beginning. The growth

rate is exponential because of the height and radius of the islands. Therefore this status leads to an increase in the physical surface area available for adsorption. [164, 165]

(ii) Active volume: This concept can be realized as a certain part of a film that is capable of adsorbing the depositing polymer. This active volume concept corresponds to zone III of the PE zone model (**Section 2.4.6**). [162] The height of the active volume can be characterized in terms of the charge penetration length, defined by the theory of Schlenoff and Dubas, [163] in which the diffusion of PE in and out of the film can be realized such that the whole film acts as an active volume in which at least one of the polyions can freely diffuse.

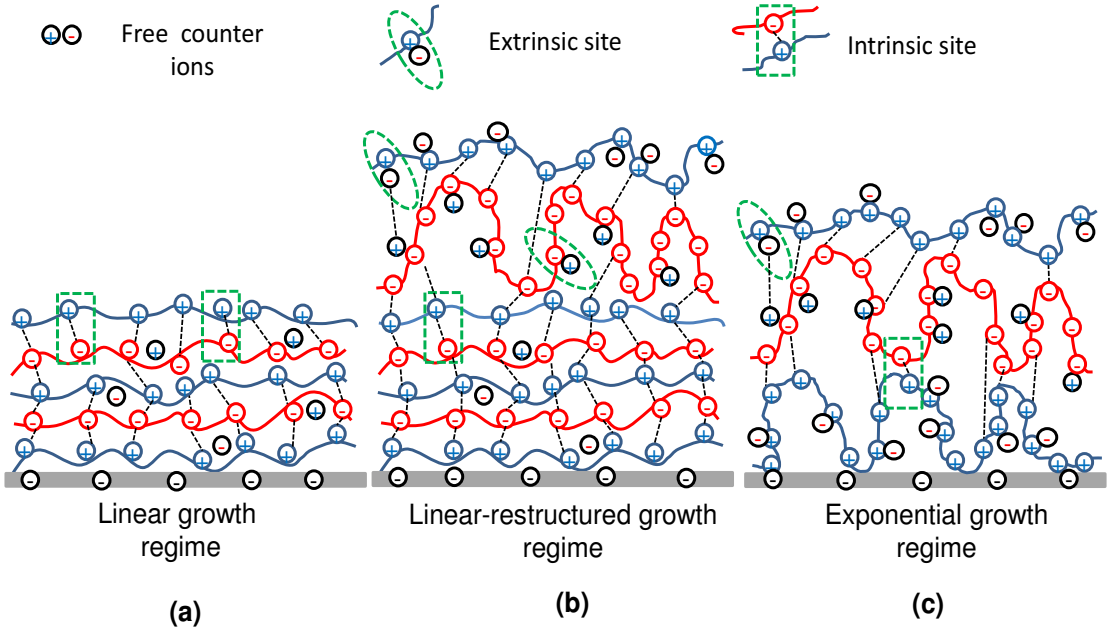

Scheme 2-7. Schematic presentation shows the internal PEM structure (**a**) linear PEM (**b**) linear-restructured (**c**) exponential PEM growth regime. Adapted from Reference [166]

The general assumption is that linearly growing MLs are composed of intrinsically charged and compensated PE complexes. However, exponentially growing MLs are composed of both intrinsically and extrinsically charged compensated ones. This gives a higher density of complexation sites in case of linearly growing MLs than for exponentially growing ones (**Scheme 2-8 a, c**). [167] Therefore for LbL films composed of strong PEs, as in case of the combination of PAH /PSS, the film grows linearly with the number of deposited layers. [159] In contrast, combinations of most biopolymers like PGA/PLL, PEM grows exponentially. [168] In this model the polyions are not being kinetically trapped in the position where they have been deposited but

diffusing inside the film and this has been proposed by Picart *et al*. for explaining the nonlinear growth behavior.[160]

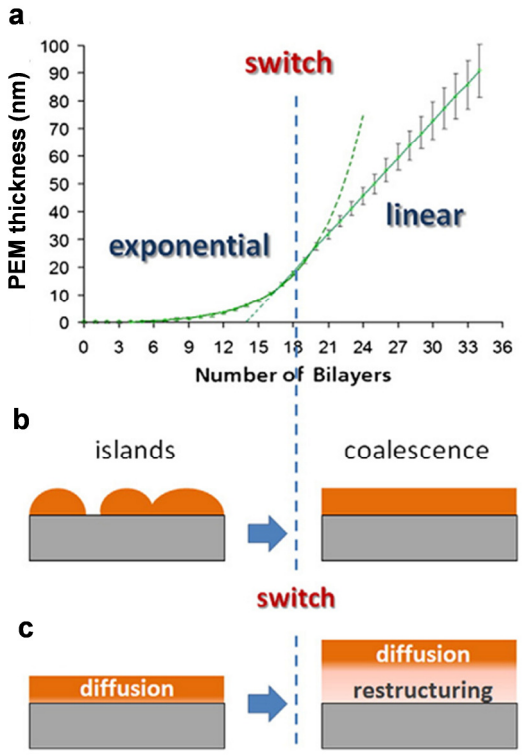

Scheme 2-8. Schematic diagram shows (**a**) Growth profile showing a switch from exponential to linear growth regime. (**b**) Scheme of roughness model representing a coalescence of initially formed islands at the switch point during the PEM buildup. (**c**) Scheme of 'diffusion'' model representing a formation of restructuring zone (polymer diffusion is restricted) underneath the diffusion zone at the switch point. Adapted from Reference [166]

Latter on there are a lot of other designed growing regime subtitled from the main growing regimes (**Scheme 2-8 b, 2-9**). In this part we will explain the growth profile, which consists of a mixture of the two parts, exponential and linear and how the transient/switching between both growth regimes occurs. The difference in the ML growth regime will be defined by the ratio between both parts. For linearly growing films the exponential part is short (switch is after a few layers or less) and sometimes cannot be well identified. In case of the exponentially growing films, the exponential part is larger and can be easy identified. But in some other cases the switching point from exponential to linear regime takes long (sometimes after the deposition of 18 bilayers). This switch might be due to two different models, either as mentioned above (**i**) the surface roughness model or

(**ii**) the diffusion model. (**i**) In the surface roughness model, surface is flattened after few deposition steps. This flattening is mainly presented due to the island's coagulation. Therefore, this model may easily explain what so-called ''substrate effects''. (**ii**) The second explanation is the diffusion model. According to this model the switching from exponential to linear regime is due to the inability of certain polymers to diffuse into the entire multilayer. [167]

It was found that the switch takes place sometimes, irrespective of contact time or molecular weight of the PE. [169] In order to explain this result, a new model has been constructed which assumes a 'restructuring'' inner compartment with restricted polymer diffusion (so –called 'forbidden zone) and a higher density (**Scheme 2-9 c**). This switching has been observed for PEM HA/PLL with PLL of high molecular weight (~ 360 kDa). In contrast, the lower molecular weight PLL can diffuse and should keep the exponential regime, since the amount of free PEs within the PEM increases with increasing PEM thickness. Obviously, this is not the case all the time: Also short chains show a transition from exponential to linear growth (according to the diffuse model). There is still a lack of understanding. One idea is that the short PLL can diffuse out of the whole ML and form complexes with the oppositely charged HA outside the ML. [170] Another explanation is that PE chains are still mobile within the ML, but they cannot reach the surface due to an electrostatic barrier formed at the surface. [171] That would lead to overcompensation for one species than the other. [172]

2.4.6. The three zone theory

When a ML film is composed of two simple PEs, a pair of oppositely charged homopolyelectrolyte, the film can be subdivided into three distinct zones (**Scheme 2-10**). Zone I is comprised of one or a few polymer layers that are close to the substrate. Zone III (active volume) is comprised of one or a few layers that are close to the solution or to the air. In this zone, the multilayer is highly influenced by the interface to the solution or to air. Zone II represents the film in a range that is not influenced by either interface. Simply, Zone II (core zone) is neutral with constant properties similar to its PEC. It is charge compensated and thus can behave like a polyzwitterion. However, Zone I and Zone III are charged with small gradients of excess charges and neutralized by small counterions. Therefore, the physicochemical

behavior of the neutral and charged zones is distinguishable different. It should be clear that the transitions between zones I and II and between zone II and III are gradual. The more layers are added, the more for zones I and III will preserve their respective thicknesses while zone II will grow in thickness. It should swell when exposed to salt or buffer solutions as the salt will break ionic bonds between polyions. In contrast, the layers in zone III should be charge compensated. This means that they should swell in pure water and collapse in salt solution owing to the screening of the electrostatic repulsion between charges of equal sign. [162]

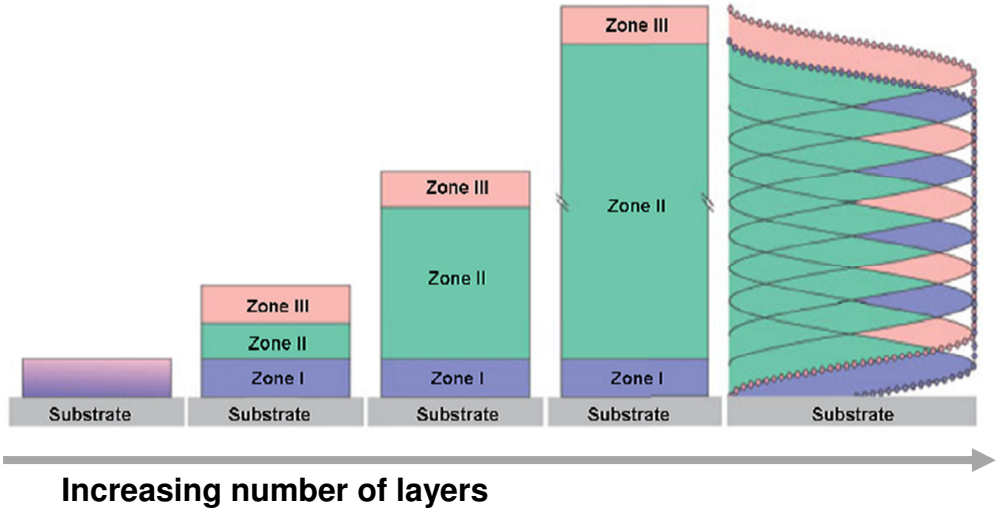

Scheme 2-9. The zone model of PEM films. [162]

Ladam *et al.* [162] also investigated that both the substrate's chemical influences and zone I are limited to a few nanometers (**Scheme 2-10**), after which their influence has totally disappeared and never been shown on PEM morphology and its physicochemical adsorption onto substrates. In contrary, it was also investigated by Guillaume-Gentil *et al.* [144] in 2011, that for PEM PLL/HA, the substrate has a strong influence on the morphology of PEMs. This influence is not limited to the first few bilayer depositions (nm range) as it has been expected from the three-zone model, but can be observed in PEM up to a thickness of 24 bilayers (µm range). [144]

2.5. Relation between turbidity of PEs complexes in solution and PEM build-up

The stoichiometry of water-soluble polyacids and polybases has an important role in the formation of PEM on the surface of the solid substrates. In a system containing two

oppositely charged polymers in solvent, exothermic interaction between the polymers results in phase separation. This produces diluted and concentrated phases, each containing both polymers.

The concentrated phase usually contains a fixed ratio of polymers (often 1:1) regardless of the mixing concentrations, and may be a viscous liquid or a precipitate in strongly interacting systems. However, it has been already investigated that it is possible to predict qualitatively the possibility to deposit multilayers films at a given pH and ionic strength by just mixing a polycation and a polyanion solution to reach a ratio of 1:1 stoichiometry of PE interactions. [173, 174] H. Mjahed *et al.* [175] have investigated that turbidity in PE solution is considered as a snapshot predictive process to building up PEMs. The prediction merely would require to mix polycation/polyanion solutions in different solution concentrations, pH or ionic strength and to follow if phase separation occurs. [175]

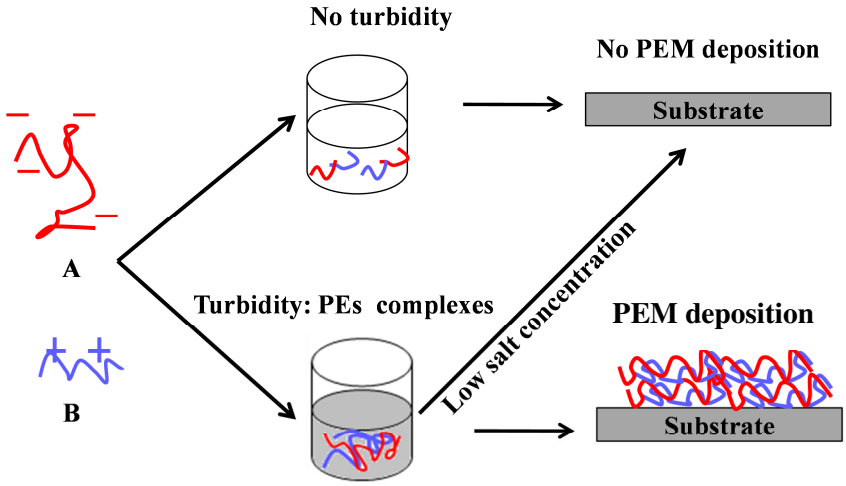

Scheme 2-10. Schematic diagram represents the relationship between turbidity of PEs complexes in solution and the buildup of PEM films. Adapted from Reference [175]

Simply one can understand that the formation of soluble complexes in solution is unfavorable to the deposition of PEMs. On the other hand the formation of insoluble complexes to a glassy state plays a critical role in the formation of PEM films. It is clearly obvious in **Scheme 2-11** that after complexation if the solution turns immediately to turbid, this is a strong indication that the build-up of PEM films is possible under these conditions. When the solution remains transparent, particularly at high ionic strength, it means that the formation of soluble inter-PECs and the absence of complexation are thermodynamically

favored, which plays against the build-up of PEM films. This turbidity absence may be due to either the too strong screening ionic strength of the solution or the too low surface charge density of the contributed PE. This leads finally to the solubilization of the complexes, or a disappearance of the coacervate phase .[175]

2.6. Kinetics of multilayer build-up

The adsorption of each layer takes place simultaneously with complexation of the PEs, due to charge interactions between previously deposited layers. The level of inter-digitation is determined during the adsorption process of each layer, assuming the internal chain in the ML to be immobile. Movement of chains to the surface and a quick mass adsorption is the first steps of kinetics. [9, 176] In this case the rate of adsorption is controlled by the diffusion of PE coils. Rearrangement of chain takes place at the surface and mass adsorption continues at a slower rate until reaching saturation. [176]

The second kinetic step involves chain rearrangement making the diffusion of chains into the areas of previously deposited layer possible. The irreversible complexation of charges is finally achieved by combining positive and negative PEs. [9, 177] The proof of the layer inter-digitation was experimentally concluded not only from the properties of the preformed MLs, but also is evident already during the formation process of the assembly. Kinetics and equilibrium properties influence the ML build-up. Rearrangement of slower chains allows for equilibration and adsorption of more chains. The flexibility of the final layers ensures the inter-digitation and thus the complexation. Finally, further adsorption is hindered by repulsive interaction, while the deposited amount in each layer is determined by the efficiency of the inter-digitation and complexation. In order to understand the fundamental physical properties of ML, leading to the strong response of PEMs to variation of external conditions, it is important to navigate in a short journey with the driving forces and key factors to control PEM internal structure.

2.6.1. Driving forces and key factors controlling the growth of PEM

The driving forces behind the deposition of MLs are the bonding between the incorporated polyions toward each other's and toward the substrate. The bonding forces

depend on the nature of the polymers and on the physicochemical parameters used for deposition. The multilayer formation and the final internal structure is a complex balance between different types of interaction mainly categorized into two different types of forces: (**i**) electrostatic and (**ii**) non-electrostatic interactions that will be presented as follows:

2.6.1.1. Electrostatic interactions

The formation of PEM architectures is based on alternating deposition of oppositely charged PEs (polycations and polyanions) from aqueous solution to a solid support. [131] In principle, the adsorption of molecules, carrying more than one equal charge (negative for anionic and positive for cationic PEs), allows the charge reversal on the surface (**Scheme 2-6**).

In many earlier papers the charge inversion after each deposition step is discussed as a precondition for PEM formation. This was the main reason for assuming that the electrostatic interactions are the main driving forces responsible for the formation and stability of PEMs. [178] This opinion was supported by the fact that mostly after each deposition steps the ψ_ζ potential (electrical potential in the interfacial double layer) changes its sign, resulting in a kind of zigzag curve. [179] This experimental result is supported by the theoretical explanation of charge overcompensation, calculated with classical self–consistent mean field theory.[180] The general idea is that during MLs formation complexes are formed between oppositely charged PEs leading to a release of small counterions. This would lead to what so-called ‘‘intrinsic’’ charge compensation connected with a very low counterion concentration within the film. In contrast to this, the charge compensation by small counterions is called ‘‘extrinsic’’ charge compensation (**Scheme 2-8**). [145]

On the other hand, the adsorption of oppositely charged PE layer leads to local charge neutralization. The apparent contradiction can be solved by the generation of an excess surface charge density used for the next adsorption step (so–called charge overcompensation). Thus, under the assumption that charge overcompensation is needed, effect of polymer charge density is crucial since a threshold charge density should be overcome for the formation of MLs. [181] However, recent measurements show that no

change in sign of the ψ_ζ potential is necessary to form PEM and therefore, the driving force for the LbL assembly needs not to be electrostatic interaction and strongly depends on the investigated system. [182]

2.6.1.2. Non-electrostatic interactions

For simulations, a non-electrostatic short-range interaction between the charged surface and the polyions was needed to establish MLs. [183] Without that interaction, the formation of complexes in the bulk strongly competed with the adsorption of the polyions onto the charged surface. MLs have been deposited using various types of bonding forces such as ionic, hydrogen, donor acceptor, covalent, double layer force, short range force, Van der Waal force, DLVO and non-DLVO forces and stereo-regularity based… etc. In the following the effect of these non-electrostatic interactions is described.

(**a**)***Type of polyelectrolyte***. The properties of PEs also affect the type of PEM growth regime and total thickness. The chain stiffness cannot be the only reason for the differences in ML thickness. It is assumed that the balance between hydrophobicity and hydrophilicity of the PEs plays an important role for the thickness. A certain degree of hydrophobicity seems to induce a stronger increase in MLs thickness. [184]

(**b**)***Type of counterions***. The type of counterions also plays an important role in ML formation. Usually, the ions are chosen according to ‘‘ Hofmeister series’’. Leontidis has summarized the properties of the ‘‘ Hofmeister ions’’ in a comprehensive way. [185] Hofmeister ions are considered as small ions have a relatively small polarizability, have high electric fields at short distances, have a well-ordered large hydration shell (cosmotroic ions, water structure makers) and prefer to keep their water of hydration. On the other hand there are large ions, so-called chaotropic ions. These ions are large with a significant polarizability, a weak electric field and their hydration water can be easily removed. A very complex interplay of different contributions caused by ion-water, surface-water, surface-ion, PE-water, PE-ion and surface –PE has to be taken into account. [186] In the case of MLs a stronger coiling leads to an increase in thickness and roughness, comparable to the effect of increasing ionic strength or decreasing charge density. The effect of anions is much larger than the effect of cations, since the anions have a much larger difference in polarizability than typical cations due to the larger variety of their diameters. [187]

(**c**) ***Solvent effects***. The interactions between PEs and solvent have a large effect on the conformation of the polymer both in solution and upon deposition onto the substrate. Solvation forces depend not only on the properties of the intervening liquid medium but also on the chemical and physical properties of the surfaces, e.g. hydrophilic or hydrophobic, smooth or rough, amorphous or crystalline (atomically structured), homogeneous or heterogeneous, natural or patterned, rigid or fluid-like. These factors affect the structure that confined liquids adopt between two surfaces, which in turn affects the solvation force. It is therefore often difficult to distinguish between a solvation force—that is, one that arises from the intrinsic properties of the solvent molecules—and a surface force that depends on the properties of the surfaces or solute molecules.[188]

An excellent example for a solvent is water, while water is a high polarity solvent, it will still dissolve many PE. Solvents with poorer solvating, e.g. ethanol, methanol, effect on the ions, lead to a stronger ion-PE association, i.e. a stronger coiling of the PE chains. This is the reason for increasing ML thickness with increasing ethanol concentration, [9, 189] and a decreasing conductivity of PE solutions (only free ions contribute to the conductivity). [190]

(**d**) ***Hydrogen bonded multilayers***. H-bonding interactions represent an alternative driving force for the LbL growth of ML. In H-bonding self-assembly, unlike electrostatic self-assembly, the polymers are ‘‘virtually uncharged’’. But, it is possible to adsorb PEs onto surface coated with PEs of the same charge.

2.6.1.3. Gain in entropy as main driving factor

Actually, it is assumed that the most important reason for the multilayer formation is the gain in entropy due to the release of counterions. No charge reversion is necessary and the complexation between polyions is favored against charge compensation by small counterions (**Scheme 2-5**). At high salt concentration, there is a large local counterion concentration around the PE chain. Meanwhile gain in entropy still exists even at high ionic strength. In addition the electrostatic energy for charge compensation is reduced at high ionic strengths, since polymer charges can come closer. Both let the adsorbed amount increase at high ionic strength up to a certain salt concentration. Beside the facts mentioned above, gain in entropy explains also the effect of degree of charge. However, at very low

degree of charge the gain in entropy is not large enough due to a small amount of released counterions. [145]

2.6.2. Effect of salt on PEM fabrication

In aqueous solution the individual properties of the PEs are assumed to be covered by long ranged intra– and intermolecular Coulomb interactions between the electrical charges of the chain. [191] These expectations are based on mean field theories, such as the Poisson-Boltzmann formalism, which are routinely used in colloid science and computational biology. [188] Assumptions of this theory are: water is homogeneous continuum with a certain dielectric constant, ions are point charges and do not interact with each other forming continuous charge distribution. Since for objects suspended in water dissolved ions are always present, the interaction of charged bodies with the free ions profoundly modifies the nature of the electrostatic interaction. [192] In particular, the ions in an electrolyte have a screening effect on the electric field from individual ions.

In pure water the charges on a linear PE chain repel each other due to Coulomb repulsion and therefore the chain has more expanded rigid–rod–like conformation. By adding salt, the polyelectrolyte chain intents to collapse to a more conventional conformation which is essentially identical to a neutral chain that is usually found to be in a random conformation in solution (**Scheme 2-12**). This results in a larger thickness and a stronger roughness of the adsorbed layers. [145]

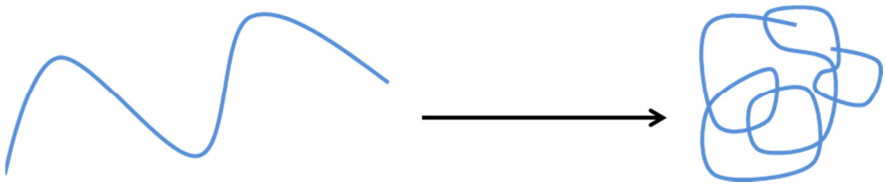

Scheme 2-11. Schematic representation presents the salt's effect on the shape of a PE in solution. Addition of salt makes PEs contract into random coils. [145]

Additional salt reduces the amplitude and the range of repulsive electrostatic force between equally charged chains or chain segments. The range of the electrostatic interaction is measured by the Debye length λ_D which is a function of the ionic strength.

For monovalent ions and water at 25 °C, the Debye length is given by the following formula, **Eq. 2-3** is represented in Reference [193]:

$$\lambda_D = \frac{0.3\ \text{nm}}{\sqrt{I}} \qquad \textbf{Eq. 2-3}$$

Thus even for relatively modest salt concentrations electrostatic effects are strongly screened. At physiological conditions ($I = 0.1$ mol L^{-1}) and for monovalent ions ($z = 1$) the Debye screening length $\lambda_D \approx 1$ nm. This means that although the Coulomb interactions are long–ranged, at physiological conditions they are strongly screened above length scales of a few nanometers, which results from multi–body correlations between ions in a salt solution. [193]

The Debye–Hückel approximation becomes progressively more accurate with increasing salt concentration and in the limit of zero salt; it is reduced to Coulomb interactions. When Debye screening length is less or equal to the diameter of water molecules surrounding the ion (0.3 nm), field theory is now not appropriate anymore, since it ignores molecular nature of the liquid and therefore Monte Carlo and molecular dynamics simulations become more meaningful. For more details see Reference. [194] Generally, the field theory breaks down at small distances, where it no longer faithfully describes the ionic distribution and forces between two surfaces. [188] Pure electrostatics predicts a flat PE adsorption onto an oppositely charged surface. [195] Experimental studies show that the film thickness for some PEM systems increases with increasing salt concentration despite the fact that addition of salt into solution screens electrostatic attraction between the PEs and oppositely charged surface. [8] The type of the conterions profoundly affects the thickness of multilayers. Leontidis has summarized the properties of the '' Hofmeister ions'' in a well comprehensible way. [196] Small ions like F^- and Li^+ have a relatively small polarizability, high electric field at short distances. They prefer to keep their water of hydration. In addition, they have a well ordered large hydration shell (cosmotropic ions, water structure makers). Chaotropic ions like I^- and Cs^+ are large with a significant polarizability, a weak electric field and their hydration water can be easily removed (water structure breakers). Therefore chaotropic ions can interact more strongly with the oppositely charged PE than cosmotropic ions, leading to a stronger screening of PE charges related to stronger coiling, thicker ML thickness and larger roughness. The thickness and roughness of PEM increases in the order of: $Li^+ < Na^+ < K^+$ and $F^- < Cl^- <$

Br^- (**Scheme 2-13**). Salomäke *et al.* have shown that the PEM (Poly (sodium 4-styrenesulfate)/Poly(diallyldimethylammonium chloride)) (PSS/PDADMAC), which are prepared in the presence of different types of salt, increases in thickness according to salt type. [189]

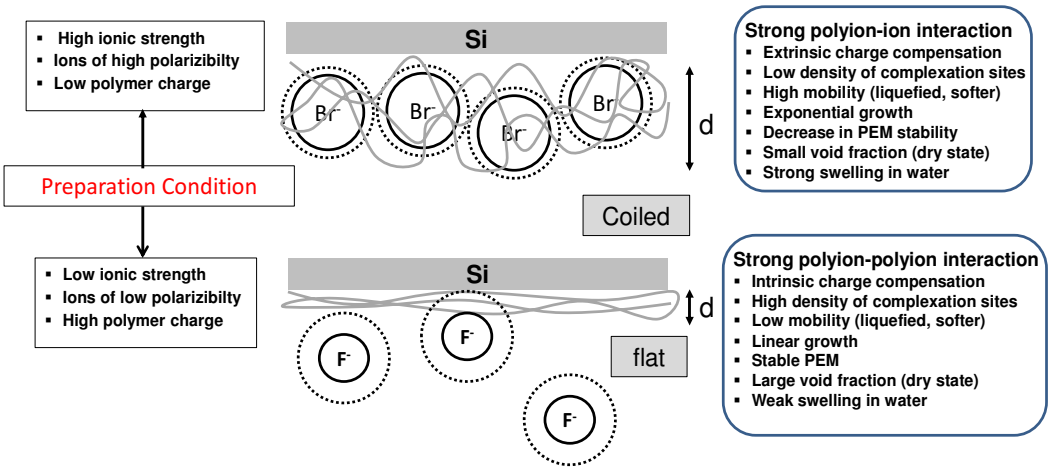

Scheme 2-12. Representative sketch illustrates the effect of different counterions on multilayers' thickness (*d*) (Hofmeister series). Adapted from Reference [145]

To understand the counterions effect on the formation of PEM then the behavior of PEM deposited on a solid substrate , which is governed by the same physics as that of the corresponding complexes formed in the bulk systems, must be assumed. If equilibrium can be established, the existence of complex coacervates depends essentially on the ratio between the amounts of cationic and anionic polymers and on the ionic strength. A schematic stability diagram of PEM was suggested in 2002 by Cohen Stuart [197] (**Scheme 2-14**) which considers the effect of the mole fraction of positively charged PE species, F^+, and the concentration of counterions (salt) (**Scheme 2-14**) (This stability diagram is essentially a cross section through the full (3-D) phase diagram, taken at constant total polymer concentration). It is totally obvious that as the ionic strength increases as the region L become narrower, where non soluble complexes will be found. This is due to the screening effect done by the side of the salt ions, which leads to the complex weakness as mentioned above. Soluble complexes exist in L' and L'', where small fractions of F^+ (region L') is found, this means that this region belongs to the negatively charged soluble electrolyte complexes, however, for high F^+ (region L'') contains positively charged soluble complexes. Above some critical salt concentration

(depends on polyanions and polycations concentration ratio), the PEM is no longer stable and decomposed (region S). [198]

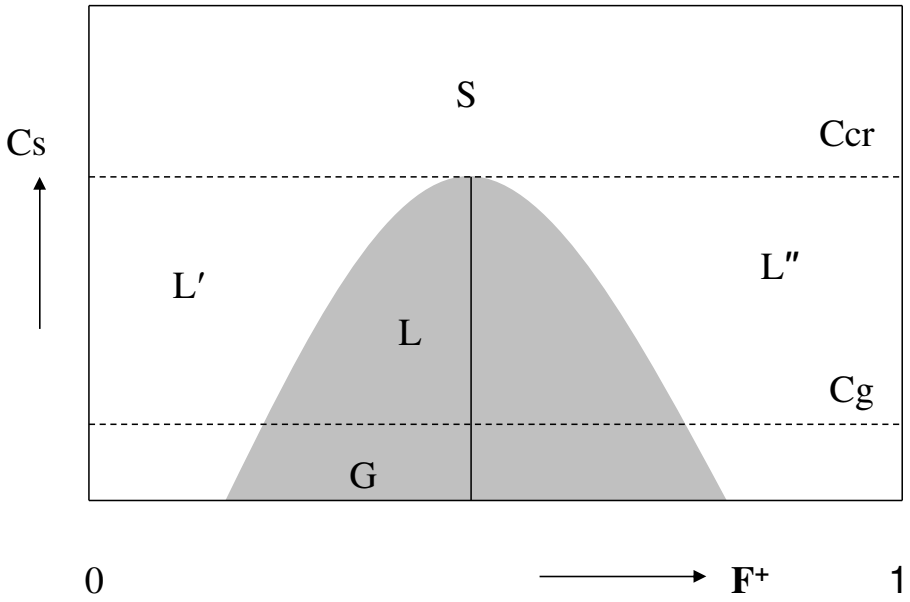

Scheme 2-13. Schematic diagram represents stability diagram of an adsorbed multilayer consisting of oppositely charged PEs. The dependent axis represents the composition of the mixture given as mole fraction of cationic species F^+. The independent axis represents the ionic strength or salt concentration Cs. L region (gray part) indicates the soluble complexes, G the glassy state, L‘and L’’ are the soluble PE complexes and in the S region no complexation occurs.[198]

2.6.3. Responsive polyelectrolyte films

One of the most important arguments is the pH responsive PEM that contain at least one PE respond to external pH. Formation of pores induced by pH has been experimentally demonstrated for both hollow weak PE capsules and weak PE films on a solid substrate. [199] For LbL films composed of at least one weak PE, reversible porosity can be created if the pH is shifted from the pH of preparation. [199] By that excess charges are created which increases the osmotic pressure in the film by adsorbed counterions. In consequence the water content increases, the film swells and the permeability increases. The switching of permeability has been utilized for binding and releasing low molecular weight compounds such as dyes and drugs, [200] encapsulations of water soluble polymers and proteins. [201]

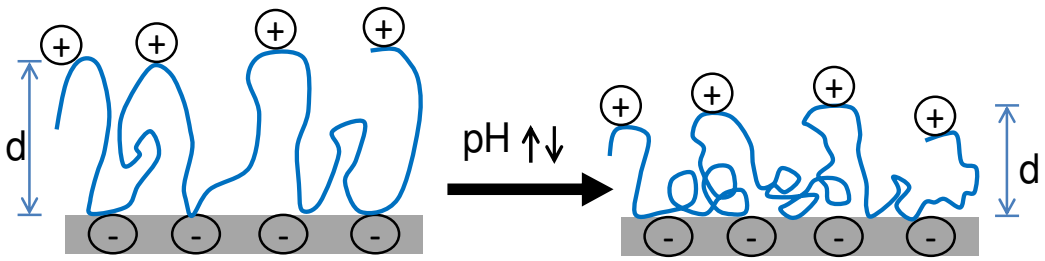

Scheme 2-14. Proposed model of pH responsive PE and a partial collapse in the interfacial phase transition of the weakly charged polycation on a negatively charged dielectric surface after being protonated. Adapted from Reference [202]

One other important point is the relation between PEM assembly pH values and its thickness. For weakly charged PEs, a sharp maximum in film thickness at intermediate charge density was observed. At pH 10 thick films can be build up and both towards lower and higher pH the film thickness decreases. A similar dependence on pH was predicted by theoretical models (**Scheme 2-15**). [202] A reason for the maximum could be that in the case of weak PEs, the polyanion is charged (fully ionized) in the basic regime and uncharged (partially ionized) in the acidic regime. For the polycation the opposite is true. [203] For instance, if the pH controlled charge density of the PE chains in the dipping solution is maximal, it is very low at the oppositely charged PE, which was adsorbed in the former deposition step. Moreover, changing in assembly pH could in a moment play the same role as counterion addition. [145] Thus, by varying the assembly pH for weak systems, the films can be prepared to be rich in the polycation, the polyanion, or to be relatively equivalent in both. This property is exclusive to weak systems because strong PEs tend to adsorb in flat conformations with very few unbound functional groups. [204] Notably, the rate of polymer adsorption is also found to be orders of magnitude faster when the charge density is low, which allows for efficient preparation of the films and more precise control over their composition, as well as their bulk and surface properties. [204, 205] Therefore, in case of weak PEs an intermediate charge density is favorable for the formation of a multilayer system otherwise destruction or destabilization would be the result. The nature of this unprecedented control that can be exercised over the composition of weak PEM films consequently influences the range of accessible film thicknesses. Shiratori *et al.* and Salem *et al.* showed that dramatic changes in thickness of adsorbed layers can be induced by very small changes in pH of the dipping solutions. [206, 207] When the polymers are highly charged, unfavorable segment–segment interactions lead to

extended chain conformations in solution and in the adsorbed state, hence the resulting films are relatively thin (**Scheme 2-15**). [205]

2.7. Controlling the physicochemical properties of weak PEM through acid/base equilibria

Multilayer thin films prepared from weak PEs can exhibit a rich suite of anomalous physicochemical properties. One of the major factors that influence the properties of such films is the acid/base chemistry of the weak functional groups for PEs. It is worth to mention that the benefits of working with weak PEs for ML film applications is their ability to prepare films from the same two polymers, but with dramatically different physicochemical properties. This is in fact not only because of the change in the charge density of the polymer chains in solution but also by the fact how they adsorb onto the planar substrate. These changes in turn dictate the overall properties of the films. [12] For weak PEs, the change density is a function of their acid/base equilibria. In case of polyacids and polybases, the dissociation behavior of each functional group along the chain is affected by the dissociation behavior of its neighbors. [208] Intuitively, the apparent acidity of the weak polyacid decreases with the progressive ionization of the polymer because of the difficulty to remove protons from polyions with increasing charge. [209] In 1947, it was shown by Katchalsky and Spitnik that the acid/base equilibrium of the chains is described by a modified version for the well-known equation of Henderson-Hasselbalch. [208]

$$\mathrm{pH} = \mathrm{pK_{a(app)}} - \mathrm{n}\log\left(\frac{1-\alpha}{\alpha}\right) \qquad \textbf{Eq. 2-4}$$

Where the $pK_{a(app)}$ is an apparent dissociation constant that reflects the overall acid base/equilibrium of the PE chains, and α is the degree of dissociation. The parameter n is related to the extension of polymer chains, which is related to their charge density. The inability to generalize the acid/base equilibria tends for PEMs is attributed intensively to the increased complexity in the PE systems, whose chains experience an increase in their degree of secondary conformational ordering when incorporated into ML films. [208]

One of the most important investigations, which were done by Rmaile and Schlenoff was the incorporation of both weak and strong polyacid (PAZO) and polybase (PDADMA) during the PEM formation. [210] They found that the adsorption of weak polyacid chains in the presence of strong polybase in the film results in an increase in the acid/base strength of the weak polyacid in comparison to its dilute solution behavior. However, when the films were exposed to NaCl solution the $pK_{a(app)}$ of the adsorbed weak polyion chains shifted more back toward the dilute solution $pK_{a(app)}$. They hypothesized that the more salt is added to the solution, the more segments are charge-compensated by salt counterions, resulting in the over population of PE ion pairs and subsequently a reduction in the acidity/basicity of the weak polyions. Burke and Barrett investigated for multilayer films composed of the simple PEs, PAA and PAH. [200] They evaluated the influence of the total number of polymer layers in the film, the assembly solution pH and the salt concentration in the polymer solution on the $pK_{a(app)}$ of each polymer. In all cases, the polyacid became a stronger acid and the same was for the polybase. It became a strong base upon incorporation into the PEM. They also observed that $pK_{a(app)}$ values shift by 1-4 pH units from their dilute solution values after being involved in the PEM formation.

2.8. Stability and swelling dynamics of PEM of weak PEs

Although much has been learned and debated regarding the main factors affecting the construction of polymer films using the LbL process, less attention has been given to their stability. One would expect the physicochemical parameters, e.g. pH and ionic strength...etc., affecting electrostatic interaction forces to alter both the binding of the film to the surface and the cohesion of the film. [133] The stability of single polymer layers remain unclear; that of multistep deposited films is even more ambiguous. Several papers have investigated the role of pH in PEM build-up, but few have addressed the effects of assembled pH in PEM stability. Dejeu *et al.* [133] have examined the stability of PEM fabricated with weak polybase PAH and strong polyacide PSS on silica interface. After construction at pH 9 in 10^{-2} M NaCl solution, PEM containing x bilayer depositions, where x was varying from 1-5 bilayers, was immersed in polymer-free solution at different pH values, between 4- 12. They subjected PEM to an immersion solution of the same conditions as assembly. All PEM with different number of layers were stable. They concluded for the stability of PEM (PAH/PSS), and more generally the stability of PEM consisting of at least one weak polyion, is strongly dependent on pH of assembly and

immersion surrounding. This is due to the determining influence of electrostatic bonds between the two polymers. There is a critical pH, above or below, PEM destabilization or destruction will be the result. They also concluded that there are two reasons for the two latter behaviors:

(i) When one of the polymer charge densities becomes too low, the binding strength of the molecular aggregates is no longer sufficient and the film breaks

(ii) When the charge of one polymer in the film decreases, the uncompensated charge of the other polymer creates a repulsive interaction between the molecules of that polymer, which induces a fast degradation of fabricated PEM. [133]

PEM stability challenge appears in a direct relation with swelling dynamics. In the swelling process especially in case of counterion-free solvents, solvent enters PEM structure through pre-existing voids or through spaces that are formed by local segmental motion in the polymer network, which is followed by local relaxation of polymer segments. The swelling mechanism is then characterized by diffusion and relaxation times of the polymer. This process can be described as 'void water'. [211] This case is identified when the rate of permeant diffusion is lower than the polymer segment mobility. In this process there is a continuous concentration profile in the film and a steady transport of the penetrant. [212, 213] In contrary, in case of physiological mediums, salt mediums…etc., true swelling will be created and leads to a highest increase in thickness. This process is so called 'swelling water'. [211] In this process the rate of diffusion is much faster than the swelling-induced polymer relaxation. This swelling is characterized by a sharp interface between the swollen polymer and unswollen polymer that moves at a constant rate.[213] The swelling water is also explained by a reduction in complexation sites and densities due to the transition from intrinsic to more extrinsic charge compensation. [211] This transition is also called doping; the term doping is used to describe the thermodynamically reversible addition of extrinsic charge (counterions) to PEC or PEM by adding salt to the solution. [214] For PEM morphology, doping is rapid and reversible. [215] Doping also impacts properties such as bulk modulus, volume, adhesion (e.g. cellular adhesion) and PEM stability. If one of the PEs is a weak acid/base, immersion solution and assembly pHs also control doping. [214]

Shen *et al.* [216] have investigated weak/weak system, where polyanion was HA and polycation was PLL. PEM was fabricated under pH-amplified conditions, that is, with PLL (1mg mL^{-1}) at high pH 9.5 and HA (3mg mL^{-1}) at low pH 2.9. Both polyions are partially ionized in such pH values. No salt was added to PE solution and having an intermediated drying step per layer formation. Different M_W of HA was investigated: 200, 400, 1300 kDa. They examined the swelling and stability of their fabricated PEM in different physiological mediums, e.g. PBS and 1.0 M NaCl. HA deposition has enhanced PLL diffusion especially at higher M_W of HA, and enhanced stability of the films was observed due to secondary interactions (hydrogen bonds) and intermolecular associations. Furthermore, the extent of film swelling in PBS was of the order of 400-600%, and notably, films ending by PLL were much more stable. They have observed that, PEM prepared with HA, M_W= 1300 kDa, has better stability conditions than those of lower M_W. PLL diffusion was found to be significantly faster in films made of higher M_W of HA. Overall, HA's M_W, HA's concentration and the nature of the outermost layer of the films are all important parameters contributing to film growth, internal cohesion, degree of swelling and stability in a physiological medium. [216]

2.9. Stable therapeutic agents load-release PEMs

Encapsulation of drugs or biomolecules and triggered release of the substance at desired time or location has high importance in biomedical applications. Due to its versatility and ease of use, the LbL assembly technique has been under intensive investigation for drug and gene delivery applications. [217] Especially the development of responsive LbL materials has advanced significantly in recent years. Responsiveness plays an important role in many delivery applications, either for loading of therapeutics or controlled and triggered release. The LbL fabrication process would allow for the control of drug upload and release, as well as the control of the material's mechanical properties caused by the thickness of the layers. [218] Due to the special properties of PEM, they have been intensively studied during the last 20 years for uploading of various materials and their sustained or controlled release by different triggers. PEM films that provide the sustained release of active biomolecules such as proteins, [219] peptides, drug molecules [220] or enzymes [221] from surfaces for local delivery have the potential to broaden the development of new delivery coatings for biomedical devices, regenerative tissue

scaffolds, and artificial organs. Substances of interest can be uploaded into PEMs by different strategies. [222] The most widely applied ones are: **1. Preloading:** cargo, analyte or drug model is one member of PEM components. Thus, the therapeutic agent is incorporated to PEM during PEM preparation. So far various substances such as drugs, proteins or nucleic acids have been successfully complexed or uploaded to PEM in this manner. [220, 223] **2. Postloading:** the examined PEMs were pre-swollen first by being stored in Millipore water or PBS till reaching the stability, and then followed by the addition of guest molecule. Finally, the latter step is followed by a number of successive rinsing steps till reaching equilibrium. [84, 224] However, there are many different methods that have been investigated for controlled release of the active therapeutic agents out of the PEM. The most famous techniques is through changing permeability of the stable PEMs, [225] or by thin films hydrolytic degradation. [226] In case of the hydrolytically degradation, one of the polyions undergoes a controlled degradation and erosion, thus will be the main tuning factor for PEM content releasing. [219, 227-229]

For stable PEMs as mentioned before, the main forces that stabilize LbL assembly systems are based on electrostatic interactions. [230] This makes such systems very sensitive to environmental conditions such as changes in the ionic strength of the medium, pH values or temperature, [221, 225, 231] and thus susceptible to disassembly. [230] The various parameters that can change the permeability of the PEM films are generally employed for controlled or triggered release of the uploaded materials at desired conditions. [232-235] Stable load-release PEM structures have not been widely discussed in literature. One of the most important checking experiments for stable load-release PEM is cyclic loading and release. Jian *et al.* [236] have fabricated PEM (Poly(allylamine hydrochloride)/Polyurethane)$_{10}$ (PAH/PU)$_{10}$ and (PAH/PU)$_{10.5}$. To evaluate PEM stability, the reversible property of fabricated PEMs towards loading and release of Methylene orange (MO) was investigated. Totally 14 cycles of loading in pH 4.0 and releasing in pH 9.0 were performed. They investigated that the absorbance fluctuated regularly with the successive loading and release of MO molecules in/out PEM (PAH/PU). They explained that PEM absorption efficiency to MO was almost unchanged after 14 times of loading and release. [236]

2.10. Applications for polyelectrolyte multilayers

The nanotechnology has brought revolution in the world by miniaturizing devices like computers, storage devices, displays, cellular phones etc. All these devices are based on the top – down fabrication techniques of the silicon industry. However, to further go down in the size scale of the devices, the bottom up type nanofabrication driven by self-assembly has recently gained interest. LbL deposition technique provides a simple and versatile means of the bottom up fabrication process. The applications of the LbL based systems can be divided into mainly two groups such as (**i**) physical and device applications and (**ii**) chemical and biological applications. [237]

LbL process offers a simple fabrication method along with great control over thickness which makes it attractive technique for modern device fabrication. Many applications such as solar cells, fuels cells, electrochromic devices, chemical sensors and semiconducting devices have been explored by LbL technique. Photoactive layer by layer films have been prepared by depositing semiconducting cadmium selenide (CdSe) nanoparticles onto polyelectrolyte multilayer films with the goal to develop devices with high light energy conversion efficiency, low cost and ease of preparation. [238] LbL method has also been used in preparing photovoltaic cells. A rhenium-containing PTEBS were deposited into thin films by LbL technique and their photocurrent responses were measured. Although the efficiency of the device was low, the layer by layer technique provided a simple versatile approach of preparing photovoltaic cells by solution process. [238] The LbL technique can prepare donor – acceptor films with precise molecular level control over the structure and energies of the active layers of photovoltaic cells. Fuel cells are another potential application which has been explored by LbL technique. [237] Optical chemical sensors have also been fabricated using layer by layer immobilization of a fluorescence indicator in the polymer. [239] Super-hydrophobic surfaces have been used for many applications like water repellency, contamination prevention, self-cleaning and antifouling. Biomimetic super-hydrophobic surfaces have been prepared by forming a rough surface on the smooth cellulose acetate nano-fibers using the layer by layer technique. [240] Antireflective and antifogging coatings have been prepared by assembling silica nanoparticles and a polycation by layer by layer technique. The surfaces formed were super-hydrophilic in nature. [241] The ability to design surfaces that can direct cell fate is

an important challenge in the field of tissue engineering and biomaterials. A PEM-based system is considered for a variety of applications, such as ion separation,[242, 243] drug delivery,[244, 245] encapsulation of enzymes, [246, 247] cell sheet engineering, [248, 249] antibacterial coatings,[250] and a support for lipid membrane. [251, 252]

2.11. Polyanions: their interactions, properties and sterical structures

In this section, it was important to scope more light on polyanions under investigation and how they profoundly affect PEM building up, PEM growing regime and morphology. In this work two different polyanions of two different charge densities have been used. The strong polyanion, which is so called heparin sodium salt and the weak polyanion which is hyaluronic acid sodium salt. In the following section their properties, their secondary conformational changes and their applications will be discussed in more details.

2.11.1. Heparin polyelectrolyte properties, conformational changes, and applications

Heparin is classified as glycosaminoglycan, which is considered as an important class of polysaccharides. It acts as a strong polyanion and linear chain biopolymer, which contains functional groups of sulfate ($-OSO_3^-$, $NHSO_3^-$) and carboxylate ($-COO^-$) (**Scheme 2-16 a**). It has an average charge of -75 and an average molecular mass of 15,000-20,000 Da. Heparin represents an attractive, but challenging target for scientific studies because of its structural complexity, including both microheterogeneity and dispersity. Heparin of antithrombotic and anticoagulant nature has been widely used to inhibit thrombosis for patients and prevent blood coagulation in medical treatments. [253] In addition heparin stimulates proliferation in some cell types and inhibits growth in others and also has the ability to increase stability or attract growth factor. [254] It also modulates several phases of wound healing. [255] Its biological activities results from the binding of various proteins to their anionic sites [256] Thus, a better understanding of the acidity of heparin's anionic sites is necessary to develop fully structure-activity relationships. Polyanionic heparin (HE) is one of the most acidic molecules found in nature. [257] It is categorized as a strong PE, following the PEs concept. Its charge density is not influenced by the ionic strength and pH of the environment. In turn, its rigidity, stiffness and the conformation structure of

its chains even its interaction with surrounding molecules are not influenced along a wide range of pH values. All determinations of the conformation of heparin (both in solution and in the solid state) have indicated similar, well-defined molecular structures in terms of overall chain conformation, with additional subtlety arising from the conformational versatility of the pyranose ring of iduronic acid (**Scheme 2-16 b**). [258, 259]

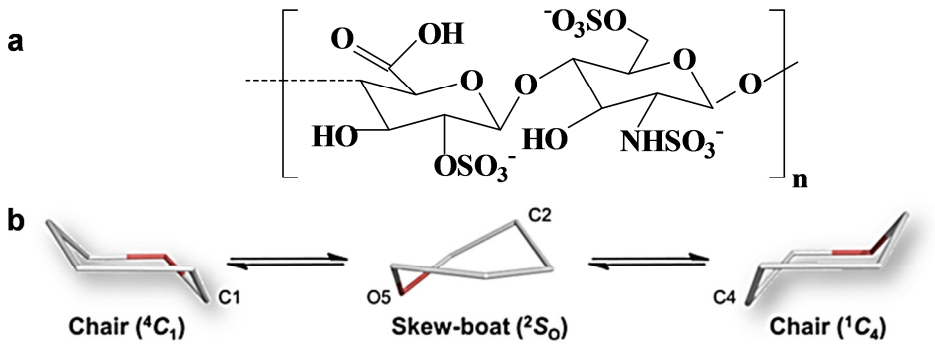

Scheme 2-15. Schematic diagram shows **(a)** chemical structure of heparin **(b)** stereographic representation presents the conformational itinerary of the pyranose ring as defined by Jeffery and Yates (1979). [260] The canonical rings presented in both sides are $^4C_1$ and $^1C_4$ chairs at opposite poles ($\theta = 0°$ and 180°, respectively) and boat skew-boat form around the equator (($\theta = 90°$) represented in the middle.

So far heparin has been presented as displaying both unusual mobility (in the iduronate ring) and unusual rigidity (in the glycosidic conformations) and hence the overall molecular shape. The question now is, is heparin more or less flexible than other polysaccharides? Perhaps the answer is ‘’differently flexible.’’ Heparin and its derivatives appear to reorient symmetrically in solution, implying a rod-like shape. The gycosidic linkages in heparin appear relatively stiff, but the iduronate pyranose rings can adopt at least two conformations. **Scheme 2-17** shows how ring form can change with only a model effect on the geometry of linkages to the two neighboring residues. However the flexibility of the iduranate pyranose ring regarding this conformational change indicates that it’s marginal and not so rapid compared to the overall molecular reorientation. [258, 259] Therefore the flexibility of the iduronate pyranose is not altering the shape of the heparin polysaccharide chain.

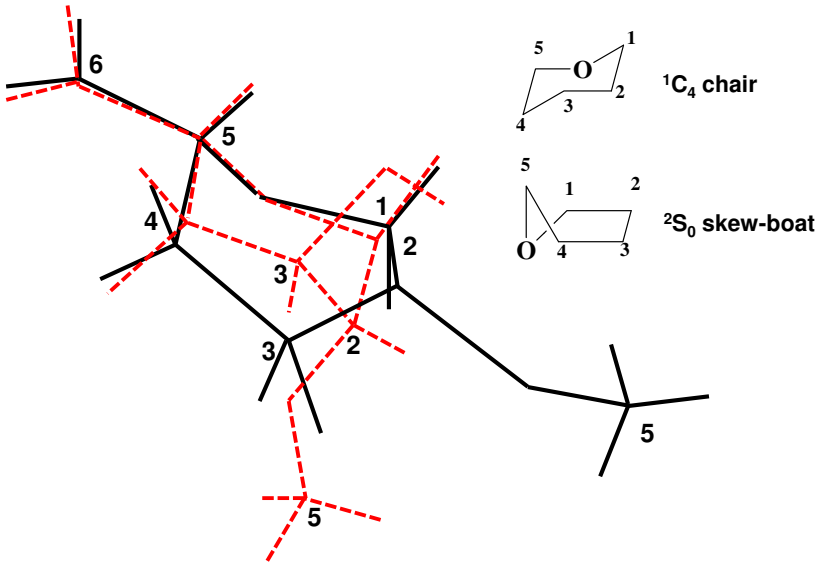

Scheme 2-16. Stick diagram of 2-*O*-sulfate iduronate, with two pyranose ring forms ($^2S_0$, solid lines, $^1C_4$ broken lines) which contribute to the conformation equilibrium of internal iduronate residues in heparin overlaid. The change between the two forms can be accommodated with relatively modest changes to the geometry of glycosidic linkages to adjacent residues, but there is a marked difference in the orientation of sulfate substituent. [261]

The anionic polysaccharide nature of the heparin also plays a profound role in presenting HE as a perfect candidate at specific conditions to be used in establishing PEM and complexes with cationic polymers. This complexation has a particular interest as scaffolds for a variety of engineered tissues and as coatings in the biomedical world. In 2009 , Niepel *et al.* [262] have reported that the adjustment of the pH of heparin solution to acidic, neutral or alkaline values (pH 5.0, 7.0 and 9.0) had an influence on PEM (HE/HPEI) morphology and on the surface topography regarding to the formation of domains. Further, heparin layers which have been assembled at pH 9.0 show larger structures or aggregates if compared to heparin layers formed at pH 5.0 or pH 7.0. They also investigated via quartz crystal microbalance (QCM) measurements that after changing the pH value of the heparin solution to the latter specific values, a distinct change in adsorption behavior was observed. In particular, heparin adsorption at pH 5.0 caused an increased negative change in QCM frequency and the heparin dissipation values (minimum of mass adsorption) was higher compared to heparin adsorption at pH 7.0 or pH 9.0. In turn this affects the following HPEI (polycation) adsorption. However, lower dissipation values are depicted compared to neutral or alkaline pH. Niepel *et al.* [262] used also static

water contact angle measurements to monitor the surface wettability of the self-assembled PEM fabricated on a glass slide. Heparin adsorption led to an increase in surface wettability dependent on the pH value on heparin. A change of heparin solution pH to acidic, neutral or alkaline values caused a distinct alteration in surface wettability. Heparin, as a strong PE, results in highly hydrophilic surface because of the presence of charged carboxylic and sulphate groups. However, the heparin solution that prepared at pH 9.0 was of less hydrophilic characteristics than that of pH 5.0 or pH 7.0 even all the prepared pH values shows a significant wettable characteristics. Conversely, HPEI as a weakly charged polycation possesses amino groups its adsorption should lead to less wettable surfaces with contact angles similar to self-assembled monolayers bearing identical groups. [262] This gives mostly a logic reason for keeping PEM outermost layer as heparin and not HPEI.

2.11.2. Hyaluronan polyelectrolyte properties, flexibility and applications

Another anionic polysaccharide of great biological interest is hyaluronic acid (HA). Hyaluronan (hyaluronic acid or hyaluronate) is a naturally occurring linear glycosaminoglucuronan consisting of a repetitive disaccharide β-(1 → 3) linked 2-acetamido-2-deoxy- D-glucopyranosyl-β-(1 → 4)-D glucopyranosyluronic acid sequence (**Scheme 2-18 a**). It mainly occurs in connective and skeletal tissue and periodontal ligaments of vertebrates. HA's synthesis takes place in the endoplasmic reticulum and Golgi bodies. [263] HA is found in the extracellular matrix of mammalian connective tissues as sodium hyaluronate (HA-Na^+). The physical properties and functions of HA-Na^+ are based on its ability to form viscoelastic aqueous solutions, the rheological behavior of which depends on the shear stress. It exerts lubrication functions in joints and is responsible for the viscoelasticity of the joint synovial fluid and eye vitreous humor, [264] thus making it an ideal candidate for use in optical surgery and as a viscosupplementation agent in joint diseases. [265] The moderate chain stiffness and the disordered elongated conformation adopted by HA in aqueous systems account for peculiar viscoelastic properties that are relevant to its performance in biological fluids. [266] HA-Na^+ plays an important role in many biological processes including tissue hydration, proteoglycan organization in the extracellular matrix, and tissue repair, and it has found application for several clinical purposes and for cosmetic use. [267] Recently a number of specific interactions between HA-Na^+ as a weakly charged polyanion and different polycations of different charge strength have been established, which have also a

pointed role towards a biomedical application and the role of hyaluronan in recognition and regulation of cellular activities.[153] HA-Na^+ rich suite of properties is indeed bringing a lot to the table; therefore it attracts the interest of a lot of scientist to investigate its biochemical and biophysical properties. Here in this part we will travel together with literature in a short journey to discuss about HA-Na^+ properties, interactions, conformational and sterical structures. Despite the very simple structure of the repeating disaccharide, there are about 60 years of intensive research on the properties of HA-Na^+ solutions. As described in a number of literatures, [268, 269] the conformation and the interactions of HA-Na^+ in solution are still controversial. Upon complete ionization of the carboxylic groups within D-glucuronic acid, the charges are about 1 nm from each other. These charges are influenced by ionic strength and pH of the environment and, in turn, influence the shape of the chains and their interactions with surrounding molecules.

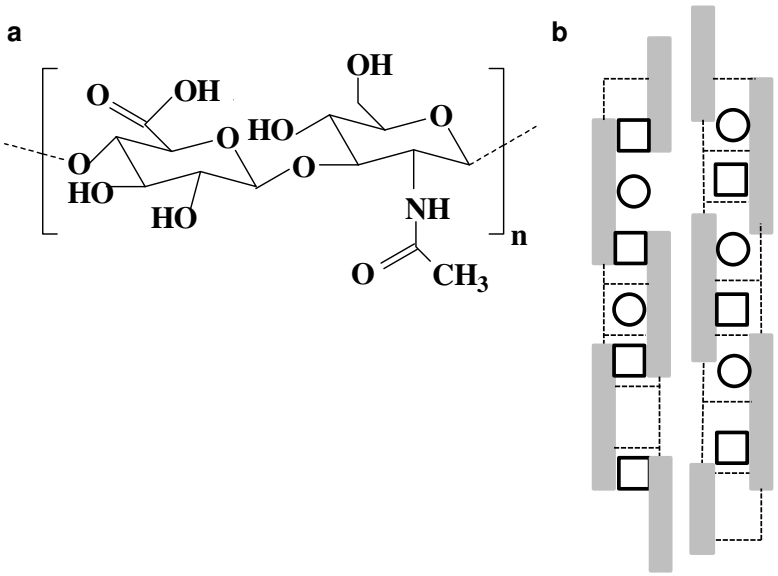

Scheme 2-17. Schematic diagram shows: (**a**) chemical structure of hyaluronic acid (**b**) a possible duplex formation between two HA chains. In addition it present the imaginary worm-like structure presented by Odijk's model. The two participating single HA helices are antiparallel to each other. The dotted lines delineate each sugar unit; the circles represent acetamido, and square represent carboxylate groups. The gray bars are the hydrophobic patches stretching along three sugar units on alternate side of the polymer chain. [268]

A typical PE pattern of viscosity was pointed out by Balazs and Laurent in the 1950s. [270] HA-Na^+ chain conformation changes respond to the solvent pH and ionic strength, which greatly influence its physicochemical properties in solution. [270, 271]

HA-Na^+ chains collapse as the charges become neutralized and contract with increasing ionic strength and decreasing pH, which indicates their PE behavior. [272] Also at higher pH there is an important question related to chemical change produced by such higher pH. It was investigated by Mathews and Decker that in alkaline medium there is a profound decrease in the solution viscosity. [273] They explained this dramatic reversible decrease in HA viscosity in alkaline medium, by the disruption of hydrogen bonds when protonated groups participate this in turn ionize HA's hydroxyl groups . This ionization leads to loss of H atoms and, in turn, results in the destabilization of the ordered structure. [273] Darke *et al.* also confirmed that the confirmation of the polymer is more random at high pH than at the neutral pH. [274] Fouissac *et al.* [275] explained that the electrostatic expansion of HA chains could be well described within the framework of Odijk's model, by assuming a wormlike chain (**Scheme 2-18 b**). For short enough chains, almost rodlike properties may then indeed be expected and the electrostatic interaction is viewed as only perturbing the wormlike shape of the macromolecule. However, Hayashi *et al.* [276] indicated that the electrostatic contribution to the persistence length at a lower salt concentration is much larger than what would be predicted from Odijk's model. [276, 277] HA chains in solution have expanded ''somewhat stiff'' random coil structure. The stiffness of the HA polymers promotes an extended random-coil configuration and their long chain ensures that they occupy enormous molecular domains. These begin to overlap and form an entangled network at level of 0.5-1.0 g L^{-1}, which may be stabilized by chain-chain interactions. [276] Cleland *et al.* showed that the size of HA varies with pH and salt concentration as would be expected for a flexible PE. [272]

By nuclear magnetic resonance (NMR) measurements on HA solutions, Darke *et al.* identified two types of residues in HA chains. [274] The relationship between the relaxation times and conformational mobility showed that there are two types of domains with different mobility. While one had the mobility of a flexible polymer, the other was so stiff that it had to contain cooperative structure. The stiff part represented 55-70% of the HA structure, and this proportion was not altered by changing the ionic strength, temperature or by moderate change in pH. Therefore they suggested that the stiff chain segments are different from the flexible chain segments by minor covalent features. Darke *et al.* [274] and Ghosh *et al.* [278] have observed that upon treating the 'stiff' segments with 1M NaOH convert most of the latter segments reversibly go to a more flexible form. [274, 278] Cowman *et al.* [279] reported that, for low HA molecular weight in water, it

was strongly indicated that the acetamide group was wrongly oriented to allow a hydrogen bond between the amide proton and the carboxyl group of the adjacent uronic acid subunit. [279] They found evidence for the replacement of the hydrogen bond between the amide proton and the carboxyl group by a single water molecule bridging both groups. Molecular models of HA secondary structures containing water bridges revealed that such bridges can join the acetamido and carboxylate groups in four ways which are sterically different. [279] Besides extended hydrogen-bonded arrays, Scott and colleagues also observed large hydrophobic regions, of about eight CH groups, on alternate sides of the single HA helices. [264] The hydrophobic patches were postulated not only to stabilize duplex formation but also to be a basis of the network-forming and laterally aggregating behavior of HA. [264]

In the world of PEM and PEC, HA-Na^+ plays an important role, due to its secondary conformational changes especially after being conjugated with weakly charged polycation. The plethora of recent papers and reviews discussing PEM fabrication in the presence of polyanionic HA-Na^+ have been published. [153, 166, 271] The counterpolyanion HA-Na^+ was chosen not only because it is biocompatible, but also because it offers the possibility of being easily conjugated with bioactive molecules. Most research groups in the world of PEM build-up PEMs using HA in corporation with weak polycations and less who deal with PEM (HPEI/HA). Lee *et al.* [280] developed mussel-inspired cytocompatible encapsulation method for achieving a 'cell-division control' with cross-linked LbL shell. They suggest a measuring unit for the relative timing of cell division with LbL-encapsulated yeast cell as a representative example (**Scheme 2-18**) Catechol-grafted PEI (PEI-C) and HA are chosen as PEs for the LbL process. PEI (Mw: 25 kDa, 500 mg), a cationic polymer used for LbL assembly on yeast, was conjugated with 3-(3,4-dihydroxyphenyl) propionic acid to yield PEI-C. For polyanion, HA (200 kDa, 300 mg) was modified to HA-C by reacting HA with dopamine in the presence of 1-ethyl- 3-(3-dimethylaminopropyl) carbodiimide. The oxidative cross-linking of catechol moieties was performed at slightly basic pH value (pH 8.5) for 12 hours after formation of PEM on individual yeast cells (**Scheme 2-18**). They measured the surface of native yeast cell to exhibit potential of -32.8 mV. The LbL process started with positively charged PEI-C, and the surface charge after each LbL step was measured by zetapotential. The zigzag potential figure indicated the successful PEM formation. They prepared three different LbL-encapsulated yeast cell with three different numbers of layers per deposition: 10 bilayers, 20 bilayers and 30 bilayers. The viability of yeast cells was investigated after encapsulation

by fluorescein diacetate (FDA) [281] and resazurin assays. [282] The cell viability was determined with at least 300 yeast cells and both assays showed high cytocompatibility for PEI-C and HA-C as counterpartners in LbL shell. They observed that the more the bilayer number the lower the cells viability. Lee *et al.* and lot of previous reports suggested that the cationic polymers damaged cells and their viability dramatically decreased as the number of bilayers increased. [280, 283-285] The viability reduction was further performed after PEM shell crosslinking. They assumed that that reduction may be due to the oxidized species generated during the cross-linking step. They also demonstrated a retarded cell division by formation of a nanometric shell. Cell division was quantitatively calculated and controlled by the number of PEMs nanolayers and the cross-linking reaction. The 'cell-division timing' was varied by the thickness of the LbL-encapsulated yeast cells, e.g. PEM with 20 bilayers deposition delayed the cell- division with about 12 hours [280]

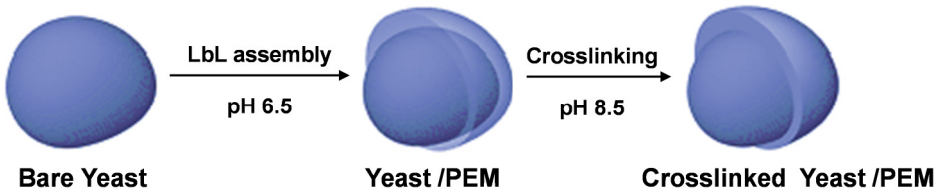

Scheme 2-18. Schematic representation for Lee *et al.* experimental procedures, PEI-C and HA-C were chosen as counterpartner for LbL construction, and cross-linking of PEs was performed at pH 8.5 for 12 hours. Adapted from Reference [280]

Also Burke and Barrett, [271] have built up PEM (PLL/HA) via LbL technique. They have observed significant shifts in the acid-base equilibria dissociation constants of PLL and HA upon incorporation into a ML film, from 1 to 3 pH units different from the accepted dilute solution values. [271] They explain this observation according the ability of the chains of these PEs to adopt secondary conformations and to increase the degree of conformational order upon adsorption. Hence, the trends in the shifts of acid-base equilibria are strongly dependent upon the types of PEs in the ML film. They have also found that the acid-base equilibria properties of the PEs in the film can be used to tailor the physicochemical properties of the film by varying the assembly solution pH and ionic strength environment. [271]

3. MOTIVATIONS AND GOALS

3.1. Motivation

Drug delivery is an important issue, especially for new generation of therapeutic agents. Efficacy is the most important characteristic for any drug or bioactive materials. However, efficacy of the drug may often be reduced because of the inability to deliver the drug to the specific cells or tissues. After administration, the drug may pass through different physiologic barriers and/or pathways, decreasing the actual amount of drug that reaches the desired site. Tissue specificity, product stability and solubility are all desirable characteristics of drug, but are not always attained. [286] Therefore, the need to develop a drug carrier system with such characteristics is of great importance and is always in progress. The drug delivery coatings can address some of the above issues. Moreover, these coatings for an implantable medical device can be used for several purposes including:

1. Prevention of harmful reactions and other negative responses from body to device and vice versa.
2. Prevention of microorganisms from causing infections on and around the device after implantation.
3. Delivery of therapeutic agents directly to the problematic cell for curing.
4. The direct transfer of therapeutic agent, e.g. anti-inflammation and anti-fibrosis, prevents cell necrosis (cell death) which is mainly due to the growing inflammations and fibrosis around both the living cell and the implant as a foreign subject. This in turn stops veins and venules proliferation and cell nourishing and leads finally to cell necrosis. Finally, two different probabilities will be expected: (**i**) formation of malignant tumor or (**ii**) the implant detachment.

In searching for an ideal carrier system, hyperbranched polymers (HBP) may have significant potential. HBPs are highly branched macromolecules with a large number of functional groups on the surface of the polymer. The versatile and tunable properties of HBPs together with the ease of synthesis make them as promising materials in drug delivery applications. The delivery systems are not only capable of providing sustained and

controlled release of encapsulated bioactive compound, but also protect the non-released bioactive material from degradation and physiological clearance. However, a lot of previous reports suggest that the cationic polymers, e.g. hyperbranched poly(ethyleneimine) (HPEI) damaged cells and their viability (**Section 2.1.3**). [280, 283-285] According to previously stated it was dramatically important to search for a polycation that carries both properties: (**i**) the biocompatibility and (**ii**) the dendritic globular shape which gives the advantage regard to the bioactive molecules uptake and controlled release. These properties arise the question whether poly(ethyleneimine) modified oligosaccharides (PEI-OS), which shows a strongly enhanced biocompatibility, is suitable for guest molecule entrapment or not. Appelhans *et al.* [56] modified HPEI by a reductive amination reaction with various oligosaccharides. It was shown that the obtained core-shell polymers were able to complex anionic molecules such as adenosine 5'-triphosphate disodium salt (ATP). Complexation capacities of the polymers were dependent on the size of the core, the length of the oligosaccharide, and the density of the sugar shell. Thus, polymer with the lowest DS% (~16 %) has entrapped ~ 60 molecules of ATPs. However, the one with the highest DS% (~77 %) encapsulated only 40 ATPs. The observed difference in the complexation capabilities was attributed to the different penetration abilities of ATP molecules through the open and dense oligosaccharide shells (characterized by the DS% = ~16 and ~77 %, respectively) of polymer macromolecules. It was supposed that ATP molecules could not penetrate through the dense maltose shell of the polymer macromolecules with the DS% = ~77 % for interacting strongly with the HPEI core. On the contrary, the loose shell of the polymer macromolecules with the DS% = ~16% enabled penetration of ATP molecules to the core. Lower complexation capacity of the HBP with the dense shell can be also attributed to the fact that additional modification of HPEI chains led to a decrease in their flexibility and create larger spaces filled with guest molecules. [56] What have been successfully done by Appelhans *et al.* [56] that they opened a new future in the field of drug delivery systems and built the first building block in this work. This study will be the first that directly applies the polycationic maltose modified hyperbranched poly(ethyleneimine) counterparts with different polyanions for building up novel drug delivery carriers.

Polyelectrolyte multilayers (PEM) have revealed themselves as a promising avenue towards biomedical applications and drug delivery coatings in today´s life sciences. In this study, new vision for multilayer concept and its relation with materials will be presented. It

will open new chances and challenges to build up PEM with newly innovated polycations and polyanions of different charge densities affinities and different stoichiometric ratio. LbL technique as a cheap method with numerous advantages (**Section 2.4.2**) is widely used for PEM construction. Most of the published reports present an equal (1:1) polyions stoichiometric ratio. [166, 236, 248, 287] Limitation of LbL technique was recognized when no inter-polyelectrolyte binding occurred. This may be in the case of polymers with lower charge densities than critical and/or when there is a large mismatch between polyions charge densities. In this study, new investigations will be established to find the optimum stoichiometric ratio which may be not the 1:1 ratio but it is possible to vary such ratio in order to obtain PEM growth on the surface of interfaces and to optimize PEM building-up with polyions of different kinetic affinities toward each other. The final structure of the multilayer film is assumed to consist mostly of 1:1 complexes of polyelectrolytes [9, 288, 289] although there are also reported exceptions.[12, 290]

In spite of the successful PEM construction which is frequently reported [137-141, 164, 181] there are only few reports that investigate PEM stability. [236] In LbL technique a defined number of monolayers, each with a thickness in the nm range are adsorbed, such that ultrathin films are obtained with a defined thickness in the nm to μm range, where electrostatic interaction between PEs ensures chemical and mechanical stability of PEM. Variation of the PEs and variation of preparation parameters like pH, salt concentration, temperature and ionic strength can tune the physical and chemical properties of PEM. The same parameters can act as external stimuli for post preparative changes of film properties. The flexibility of PEM with respect to such wide physical and chemical stimuli/variables promotes their application potential in several fields. Current issues of great interest are the swelling and permeability of these multilayers and their response to external stimuli. When multilayers are brought into contact with a solution of different pH and ionic strength, typically swelling of the film is observed that might be accompanied by chain rearrangement and uptake of water, solvent or electrolyte. There is plenty of literature on pH-driven properties of PEM prepared from weak PEs. [212, 291-295] pH-sensitive and ionic strength induced swelling of linearly and exponentially growing multilayers made from biopolymers is also well studied by various groups. [211, 296-298] Furthermore, the dependence of salt induced swelling on the internal structure of PEM has been examined. [299] Even a successful permeation or diffusion of various ions through readily prepared PEM is observed.[300-304]

After choosing suitable PEM components and controlling its stability, it is the task for the therapeutic agent to be efficiently loaded and released. By one way or another, the system equilibrium state to the surrounding media will affect PEM's loading efficiency and release profiles. The more the PEM is in equilibrium; the higher is loading efficiency and vice versa. For essence, the therapeutic agent can be loaded and released by finely tuning the PEM interior after exposing PEM system to different biological factors, pH, ionic strength…etc. Controlled drug release from PEM is essential to ensure enough therapeutic agents to reach the damaged cell; and sufficient drug content in the carriers could lead to efficient therapeutic agent uptake by cells. Therefore, controlled therapeutic agent release and high drug loading are vital in PEM preparation. However, both have often posed a number of technical challenges to scientists. Drugs can be incorporated into PEM or any drug carrier system by either preloading [220, 223] or postloading [84, 224] method. According to the former reports, when the drug is loaded during PEM formation and is considered as one of PEM counterpart, this is the so called drug preloading. However in postloading method, drugs are loaded in the prepared PEM by disturbing PEM internal kinetics and driving forces, where drug is adsorbed on the surface of PEM. In addition to loading strategies, there are also several efforts dedicated to control drug release in PEM system , e.g. light, [305] magnetism, [306] pH, [307-309] ionic strength,[310] glucose,[311] and redox, [312] having emerged recently. Such drug delivery systems, which release their payload in responding to internal or external triggers, offer great advantages. However, the development of stimuli-responsive PEM, especially those made of biopolymers, is still in the early stage. Because of the short development history of PEM technology, great potential for biomedical applications, and the almost infinite possibility of varying parameters in the preparation process, further studies are needed to advance the development of stable sustained drug delivery systems.

3.2. Goals

The goals of this work are focused on the fundamental understanding of HPEI decorated with maltose moieties (PEI-Mal) of two different saccharide shell densities (PEI-Mal-B and PEI-Mal-C) within a polyelectrolyte multilayer (PEM) system. Both PEI-Mal structures will be enrolled in establishing highly sophisticated PEM as a model for drug delivery coatings suitable for bioanalytical or biomedical tasks. Polycationic PEI-Mal of

both structures as weakly charged polycations will be used to build-up a stable PEM in counterpart with biocompatible polyanions using LbL technique. For that, a strongly charged heparin sodium salt (HE-Na^+) and a weakly charged hyaluronic acid sodium salt (HA-Na^+) will be chosen as biocompatible anionic counterparts. The most important and challenging point in this work is to form a highly equilibrated system against different biological factors, e.g. pH, ionic strength, etc. Parent PEI is considered as a weak polycation and the challenge in this study is directly related to the low charge density of PEI-Mal. To overcome PEM stability problems, it was important to adjust the charge densities for both polycations and polyanions via polyions stoichiometric ratio and to examine their complexes (PEC). These adjustments will be established by carrying out different pretests for their PEC formation using different characterization methods, e.g. particle charge detector (PCD), and dynamic light scattering (DLS) and zeta potential (ζ) measurements. After building up a stable PEM, such PEM will be loaded with adenosine 5' tri-phosphate disodium salt (ATP) molecules as a drug model.

The whole work will be categorized into two main tasks:

- PEI-Mal of both structures, PEI-Mal-B and PEI-Mal-C, as weakly charged polycations will be used to build-up a highly stable PEM using LbL technique. The polyanions are also chosen to be biocompatible negatively charged PEs with different charge densities, e.g. the strongly charged HE-Na^+ and the weakly charged HA-Na^+. Herein, two different systems weak/weak system (PEI-Mal/HA-Na^+) (equal stoichiometric ratio of 1:1) and weak/strong system (PEI-Mal/HE-Na^+) (different stoichiometric ratio) will be built-up. PEM formation, thickness, swelling behavior and physiological stability of such highly biocompatible PEM for both established weak/strong and weak/weak systems will be intensively studied. Three different Approaches A, B and C will be established which differ in the precoating and assembly pH to achieve stable PEMs. PEM swelling and stability will be investigated after PEM being subjected to different biological factors.

- After the formation of highly stable PEMs it will be the task to check the ability for drug loading. The biological guest molecule in this study will be the anionic aromatic physiological nucleotide ATP. The loading process will be performed with two different strategies (**a**) post-loading (**b**) pre-loading techniques.

(a) Drug preloading: In this step, PEI-Mal/ATP complex and polyanion/ATP mixture will be prepared with different molar ratio. The latter complex/mixture will be used for the layering up process.

The following investigation will be achieved:

(i) Varying the mixing ratio of guest molecules in order to achieve the most kinetically stable PEM, the highest loading efficiency and a retarded release.

(ii) Drug release profiles for stable PEM structures will be studied in dependence of various conditions, e.g. pH, different ionic strength, buffer mediums…etc.

(b) Cyclic upload and release (drug postloading):

This strategy is a cheap and an easy way for drug uploading and release out of PEM. It will be one important challenge that PEM will keep its stability for a long duration.

This investigation will be created to:

(i) Emphasize PEM high stability conditions versus time.

(ii) Check the release depending on the different physiological conditions

4. RESULTS AND DISCUSSION

4.1. Properties of glycopolymers (PEI-Mal)

Hyperbranched poly(ethyleneimine) (HPEI) modified with maltose moieties (PEI-Mal) refers to a class of core-shell polymers with a dendritic core. HPEI structure enables complexation of anionic molecules, e.g. deoxyribonucleic acid (DNA) or small interfering ribonucleic acid (siRNA) or any other kinds of polyanions, whether synthetic or natural, e.g. HE, HA , PAA, PSS… etc.

4.1.1. Synthesis of PEI-Mal

PEI-Mal was obtained by reductive amination of HPEI (M_w = 25,000 g mol^{-1}, Mn= 9,600 g mol^{-1}, PDI= 2.6, DB= 70.6%) with maltose in the presence of strong reductive agent (borane-pyridine complex) in borate buffer at 50°C for 7 days as it was described by Appelhans *et al.* [56] The degree of substitution (DS%) depends on the ratio between the parent PEI and the oligosaccharide results in the formation of three different structures PEI-Mal-A, PEI-Mal-B and PEI-Mal-C, of different outer shell architectures presented in (**Scheme 2-4**). As it has been previously discussed in **Section 2.1.4**, structure A is characterized as HBP backbone densely decorated with sugar moieties. This in turn forms a densely organized oligosaccharide as a closed shell with preferred D units. Structure A is out of the scope of this work due to its very low charge density property and its closed maltose shell, therefore the discussion will be focused on the properties of structure B and structure C.

Table 4-1. DF%, TDF% and degree of T, L and D units of modified PEI obtained from elemental analysis for different PEI-Mal. [56]

	PEI-25k	**PEI-Mal-B**	**PEI-Mal-C**
Ratio PEI:OS	-	1:0.5	1:0.2
Mw of the PEI core (g.mol^{-1})	25,000	25,000	25,000
DF%	-	35	16
TDF%	-	27	14
D%	30.7	36	30
L%	36.7	64	56
T%	32.6	-	14

Table 4-2. pI for parent PEI-25k and PEI-Mal-B and -C determined by zeta potential measurements. DF% for PEI-Mal-B and PEI-Mal-C are also represented. [86]

Polymer	pI	DF%
PEI-25k	10.7	-
PEI-Mal-C	9.4 ± 0.05	16
PEI-Mal-B	9.0 ± 0.1	35

According to Appelhans *et al.,* [56] DF%, TDF, D%, L% and T% groups were calculated and are presented in **Table 4-1.** The calculations were based on the data obtained from the elemental analysis for the synthesized polymers and the data previously obtained for pure HPEI from ^{13}CNMR. [56] The parent PEI structure contains primary amino functions as terminal units and secondary amino functions as linear units. The dendritic units consist of tertiary amines. Polymers with different DF% of amino groups were obtained by varying the ratio between PEI and maltose (Experimental, **Section 6.1.1.1**). Thus, structure B is characterized by the presence of mostly secondary amino groups in the PEI structure, and structure C is characterized by a mixture of primary and secondary amino groups. It is worth to mention that with the increase of DF%; isoelectric point (pI) of PEI-Mal gradually decreased from 10.7 to 9.0 (**Table 4-2**). Data in **Table 4-2** were calculated from **Figure 4-1.** [86]

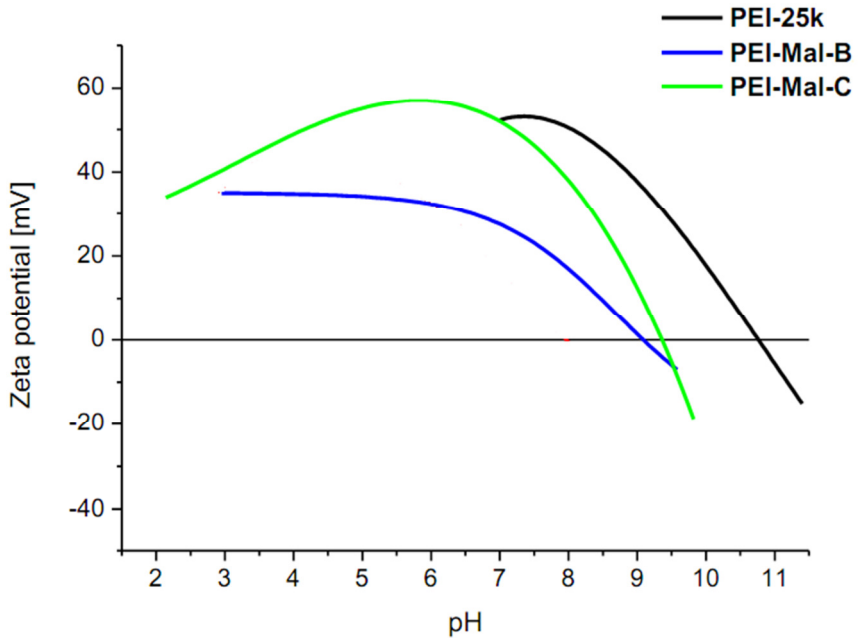

Figure 4-1. pH-dependency of zeta potential for PEI-25k, PEI-Mal-A, PEI-Mal-B and PEI-Mal-C (concentration of polymers solution is 0.5 mg mL^{-1}) (Polikarpov *et al.* - Supporting information). [86]

4.1.2. PEI-Mal characterization and its solution properties

Appelhans *et al.* [56] have already studied PEI-Mal polymers and solutions. PEI-Mal polymers were characterized by a number of methods to receive information about their physicochemical properties. PEI-Mal structures were defined by means of elemental analysis and NMR. They have also investigated for solution properties by means of zeta potential, DLS, PE titration and SAXS measurements. This section will represent some of the important results, related to this working project, investigated by both Appelhans *et al.* [56] and Polikarpov *et al.* [86]

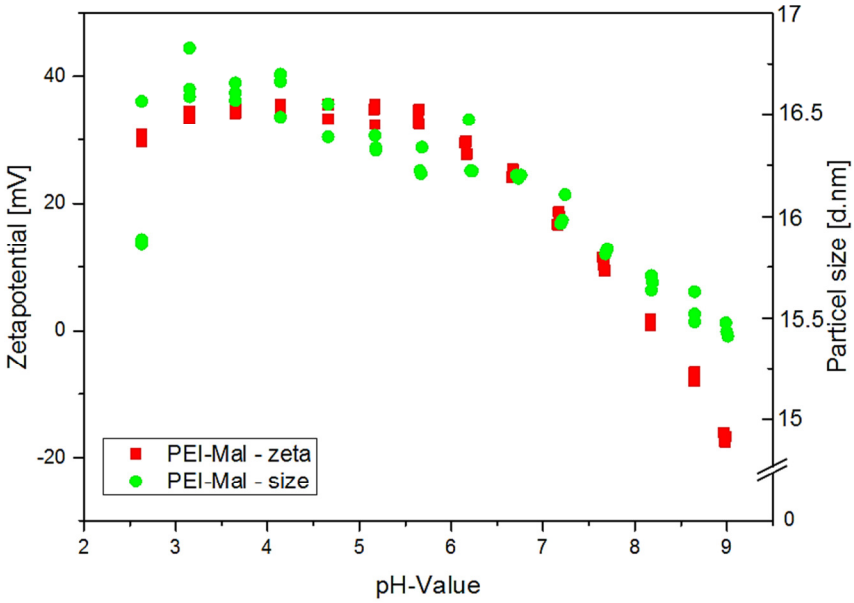

Figure 4-2. DLS measurements for streaming zeta potential and particle size of PEI-Mal-B depending on different pH value (polymer concentration 0.5 mg mL^{-1})

Polikarpov *et al.* [86] have studied the solution stability for PEI-Mal-B and -C. They investigated the PEI-25k core by SAXS and DLS measurements. Thus, at various pH values PEI-Mal exists mostly in the form of single molecules with diameter of 11-16 nm and these results almost fit this work results. [86] pH dependency of zeta potential for parent PEI-25k, PEI-Mal-B and -C was determined in **Figure 4-1**. [86] Zeta potential measurements were only applied for the determination of the pI, qualitative investigations of its charge properties, and estimation of solution stability. However, for PEI-Mal-B it is shown that PEI-Mal macromolecules do not aggregate over a broad range of pH values

(**Figure 4-2**). This can be due to the presence of a high amount of surface hydroxyl groups in structure of PEI-Mal that favor dissolution of PEI-Mal macromolecules.

Since zeta potential measurements are not entirely enough for polymeric charge density investigation and evaluation, thus Polikarpov *et al.* [313] have calculated the charge density of PEI-Mal via PE titration. The particle charge detector (PCD) was used to calculate the polymeric charge density (Experimental part, **Section 6.3.1**). [313] They emphasized that the PEI-Mal charge density is pH-dependent and is gradually increased with the decrease of DF% and pH. The number of average molecular mass (M_n) for PEI-Mal-B and PEI-Mal-C has been calculated via elemental analysis. M_n for PEI-Mal-B and PEI-Mal-C were analyzed to be 39,1 and 29,6 g mol^{-1} , respectively. [313] It was investigated that at pH 2.0, almost all amino groups of PEI-Mal, without paying attention to the shell density are protonated. However at pH 9.2 and 11.2, PEI-Mal-B outlines a low anionic charge density per macromolecules similar to PEI-Mal-C and the values for both PEI-Mal were of negative values. These results were explained by Appelhans *et al.* [56] , that at pH>pI, PEI-Mal macromolecules are negatively charged (**Figure 4-1**). [313] It can be postulated that this may be a result from their interaction to boric acid during the synthesis. Borate can interact with the molecules containing hydroxyl groups in sugar molecules via covalent bond. At pH 7.4, 5.4 and 2.0, PEI-Mal-B possesses lower cationic charge density per macromolecule compared to that of PEI-Mal-C. [313] The determined charge properties of the larger dendritic glycopolymers PEI-Mal-B and -C completely resemble previously published charge properties of smaller dendritic polymers PEI-Mal, consisting of PEI-core with molecular weight 5,000 g mol^{-1}, [56, 66] due to shielding effect of wrapping maltose units against PEI-core and different compositions of terminal, linear and dendritic units in PEI-Mal. This kind of shielding effect of oligosaccharide units was also proven by PE titration experiments, streaming potential titration experiments and theoretical molecular modeling for PPI glycodendendrimers showing that anionic PEs cannot or only partly compensate the cationic charge of the dendritic PPI scaffold in the core-shell architecture of PPI glycodendrimers. [83, 314, 315] A similar situation is given by PEI-Mal macromolecules used here in this study, that they possess a lower cationic surface charge and charged density than the parental PEI-25k that is considered as a weakly charged cationic PE.

4.1.3. Polyelectrolyte titration experiments for determining charge density of PEI-Mal, charge neutrality between cationic PEI-Mal macromolecules and polyanions HE-Na^+ and HA-Na^+

Limitation of LbL technique was recognized in case when no inter-PE binding occurred. Firstly, this may be in case of polymers whose charge density is lower than critical and when there is a large mismatch between the charge density of polyions under investigation. Secondly, it is often found when combinations of a strong polyacid at neutral/basic pH values and a positively charged proteins or synthetic HB polycation with ammonium groups are used for PEM deposition. [287] This kind of PEM erosion/dissolution gives us the inspiration to conclude that the strong intermolecular association between a pair of PE chains is not the only prerequisite for successful film deposition.

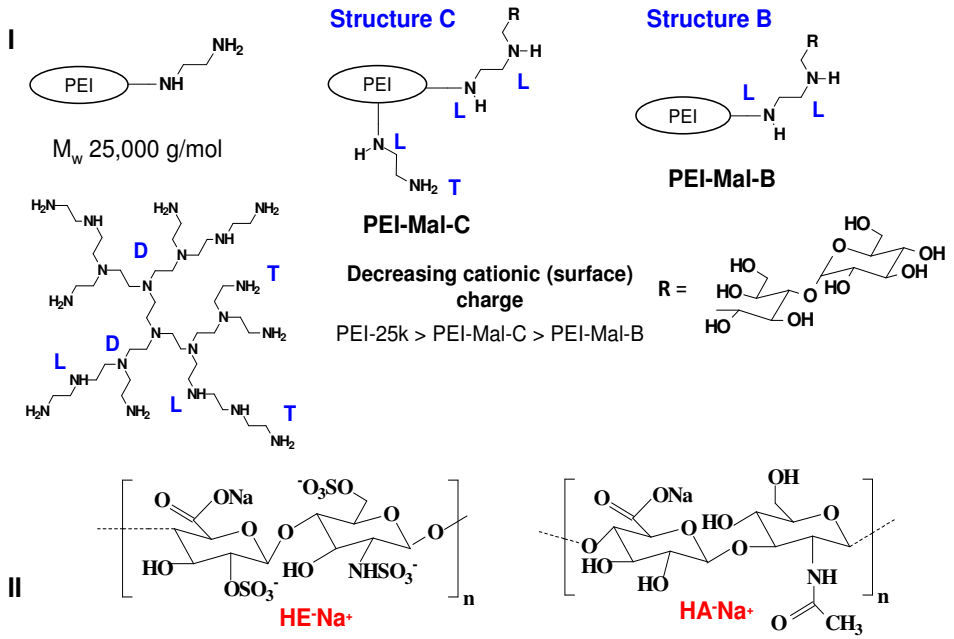

Scheme 4-1. I. Molecular architectures of dendritic glycopolymers, PEI-Mal-B and PEI-Mal-C. Dendritic glycopolymers differ in the degree of maltose substitution. PEI-25k acts as the molecular platform of dendritic glycopolymers. **II.** Chemical structure of heparin (HE-Na^+) and hyaluronic acid (HA-Na^+).

It was important to find a possible way to investigate such polyions and to expect the most probable stoichiometric ratio, which might be not the 1:1 ratio, in order to reach the final structure of a multilayer film which is assumed to consist mostly of 1:1 complexes

of PEs. Therefore, pretesting experiments were carried out by means of particle charge detector (PCD) were emphasized by using DLS, zetasizer and ATR-FTIR. **Scheme 4-1** presented the polycations, PEI-Mal-B and PEI-Mal-C and polyanions, HE-Na^+ and HA-Na^+ under investigations.

Table 4-3. Average charge density [q (C g^{-1})] of PEI-Mal determined by PE titration; the concentration of PEs is 1mg mL^{-1} (the values were calculated using **Eq. 6-1**)

pH	Polyions	q (C g^{-1})
7.5	HE-Na^+	-200
7.5	HA-Na^+	-99
3.2	ATP	-13
7.5-8	PEI-Mal-B	+55
7.5-8	PEI-Mal-C	+90
5.5	PEI-Mal-B	+69
5.5	PEI-Mal-C	+139

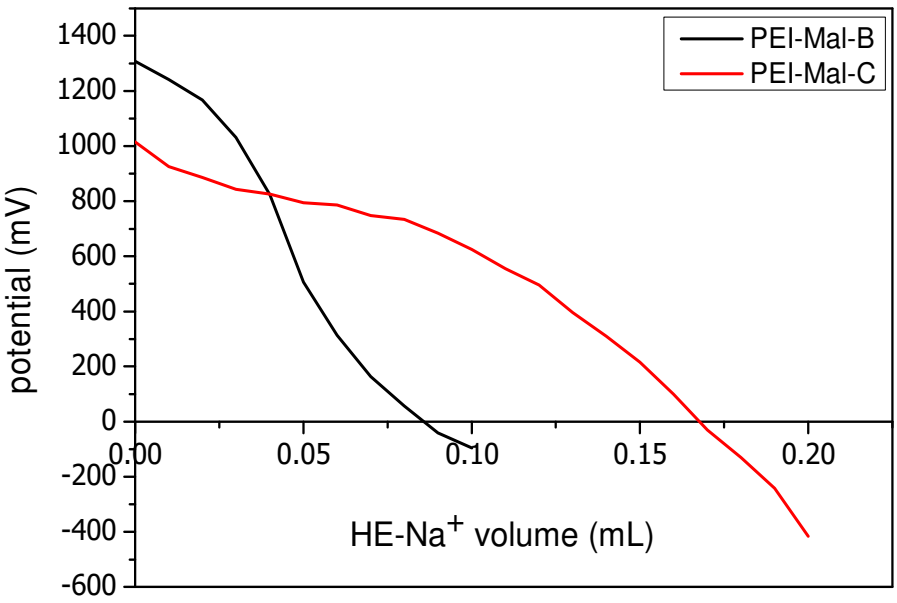

Figure 4-3. Charge compensation of weakly charged cationic dendritic glycopolymers by strongly anionic polysaccharide HE-Na^+ using PCD method. Titration curve of polycations PEI-Mal-B (black line; 1mg mL^{-1}) and PEI-Mal-C (red line; 1mg mL^{-1}) against polyanion HE-Na^+ (1mg mL^{-1})

It is worth to mention that the behavior of PEMs is governed by the same physics as that of corresponding PECs in solution. This likelihood between the behavior of PEs in solution and PEM growth onto a substrate's surfaces in addition to the relation between the PEM growth and the phase behavior of PECs in solution, force investigators to examine PEC. Therefore it was important to know more information about the particle size and the resultant charges for the used PEs in the form of PEC, which is considered to be the first step for being able to achieve stable PEMs. In addition, these pretesting experiments will give more information about the expected mass ratios which will be expected to form stable PEMs. In order to find the right mass ratio between both PEI-Mal and other polyanions for stable PEM fabrication, additional PE titration experiments were carried out using PCD.

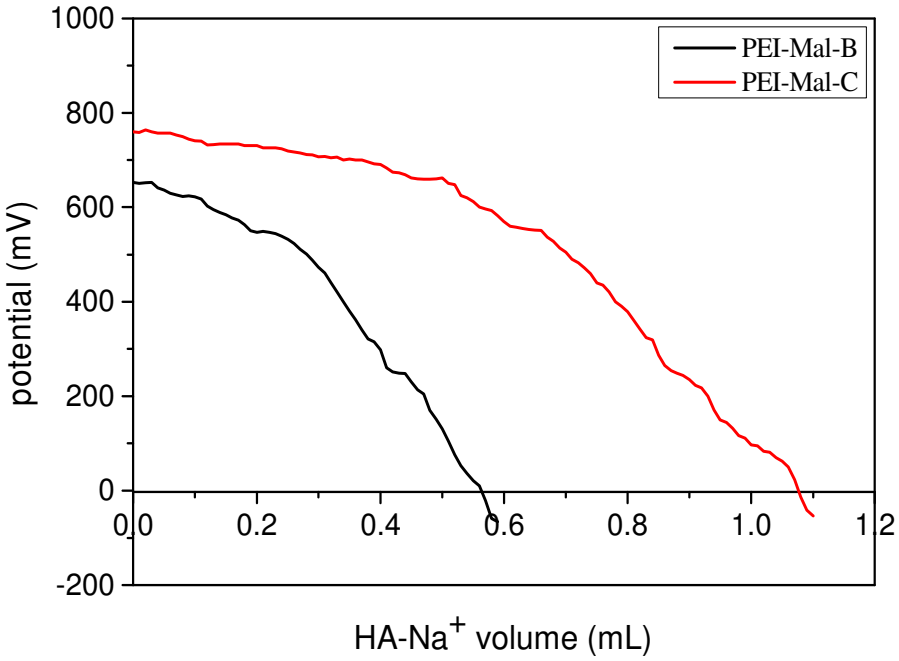

Figure 4-4. PCD titration diagram for charge compensation between PEI-Mal (PEI-Mal-B and PEI-Mal-C) against HA-Na^+. Titration curve of polycations PEI-Mal-B (black line; 1mg mL^{-1}) and PEI-Mal-C (red line; 1mg mL^{-1}) against polyanion HE-Na^+ (1mg mL^{-1})

The charge densities for polycation PEI-Mal macromolecules (PEI-Mal-B and PEI-Mal-C) at pH values 7.5 and 5.5, and polyanions (HE-Na^+ and HA-Na^+) were calculated by means of PCD and is presented in **Table 4-3**. Two different methods have been performed. The first method is based on titration of the PEs with low molecular-weight PES (negatively charged) (0.001M) and PDADMAC (positively charged) (0.001M), respectively (Experimental part, **Section 6.3.1**) (**Table 4-3**). The second method is based

on the titration of polycations with the polyanions for PEM preparation. A stream of potential is reaching the isoelectric point (zero mV) in case of charge neutrality. One milliliter of the polycation (1mg mL^{-1}) added to 9mL Millipore water was titrated against polyanion (1mg mL^{-1}) (**Figure 4-3, 4-4**). On reaching the isoelectric point, the mass ratio between the polyions according to the volume of the polyanion used to neutralize the polycation can be calculated. The calculated ratio in case of weak/strong (PEI-Mal/HE-Na^+) system for both PEI-Mal-B and C are shown in **Figure 4-3**. The calculated value of the expected mass ratio for PEC (PEI-Mal-B/HE-Na^+) was 12:1, while it was 7:1 for PEC (PEI-Mal-C/HE-Na^+). However in case of weak/weak system, PEC (PEI-Mal/HA-Na^+), the calculated mass ratio for PEC (PEI-Mal-B/HA-Na^+) was 2:1 and for PEC (PEI-Mal-C /HA-Na^+) was 1:1 (**Figure 4-4**). These mass ratios were used to the fabrication of the first PEM.

In order to emphasis those previously calculations by means of PCD, DLS and zetapotential were used. The advantage of DLS and zetapotential in this study is to find the most appropriate PEC mass ratio, where the higher particle size and the lowest potential to isoelectric point are proposed. Appendix, **Figure 8-2** shows that the particle size for PEC (PEI-Mal-B/HE-Na^+) with mass ratio 20:1 is the most appropriate ratio for PEM formation. In addition, for PEC (PEI-Mal-C/HE-Na^+) (Appendix, **Figure 8-3**) the mass ratio of value 7:1 is the right one with appropriate particle size and potential. The mass ratio for PEC (PEI-Mal-C/HE-Na^+) was in agreement with that of PCD titration experiment. However, in case of PEC (PEI-Mal/HA-Na^+), it is shown in Appendix, **Figure 8-4**, that the higher PEC particle size and lowest PEC potential is of mass ratio 2:1, while for PEC (PEI-Mal-C/HA-Na^+) it was 1:1 (Appendix, **Figure 8-5**). These results may be relied on the average charge densities of polycations, PEI-Mal-B and PEI-Mal-C against polyanions, HE-Na^+ and HA-Na^+. For both systems, weak/strong and weak/weak, the mass ratio for PEI-Mal-B was higher than that of PEI-Mal-C. These results were in agreement to the average charge densities calculated with PCD (**Table 4-3**). Whereas, it is shown in **Table 4-3** that q (C g^{-1}) at pH 7.5-8 for both PEI-Mal-C and PEI-Mal-B is + 55 and +90, respectively. The same calculations have been performed for the polyanions, HE-Na^+ and HA-Na^+ (**Table 4-3**). The average charge density for HA-Na^+ was much lower than that of HE-Na^+. The q (C g^{-1}) for HA-Na^+ and HE-Na^+ has been calculated with values -99 and -200, respectively. This gives a clear reason for the mass ratio increment for PEC with HA-Na^+ against its consort with HE-Na^+.

4.1.3.1. ATR-FTIR investigation for PEC (PEI-Mal-B/HE-Na^+)

After the examination of PEC (PEI-Mal-B/HE-Na^+), two different mass ratios have been determined by means of PCD, DLS and zetapotential. At this moment it was important to confirm our data by using another module. A comparison with turbidity studies and PEM formation showed that complexes close to charge compensation point are not water soluble and give rather thick PEM. On the other hand the highly charged complexes (high stoichiometric coefficient) are water soluble and unsuitable for PEM formation. The relation between solubility of complexes and the ability to form PEMs becomes very comprehensible (**Section 2.5**). A minimum charge density is required for the formation of PEM. [316] Below this threshold charge the number of complexation sites may not be high enough to form stable complexes.

Often the thickest PEMs are obtained for a charge density between this threshold and the nominal 100% charge density level. The reason is an increase in solubility of the PE with increasing degree of charges, which counteracts the ability for adsorption. Not only the average charge density, but also the distribution of the charges along the chains plays an important role in building up PEMs. ATR-FTIR has been used to confirm the mass ratio for PEI-Mal-B and HE-Na^+ (Appendix, **Figure 8-6**). In these experiments the right mass ratio through the ATR-FTIR measurements has been investigated. Loading amount, stability and PE release in Millipore water have been determined for different PECs of different mass ratios. PECs of mass ratios 1:1, 12:1 and 20:1 were molded onto Ge-IREs and a prepared PEM (PEI/(HE-Na^+/PEI-Mal-B)$_{20}$) of mass ratio (PEI-Mal-B:HE-Na^+) (20:1) have been examined and their ATR-FTIR spectra is shown in Appendix, **Figure 8-6**. Series of release in Millipore-water for 0, 5, 60 and 1440 min have been measured. ATR-FTIR spectra show that the most stable PEC for (PEI-Mal-B/HE-Na^+) is that of mass ratio 20:1. This PEC was totally stable in Millipore water and suffered no PE release for 1 day (Appendix, **Figure 8-6**). Whereas PEC with mass ratio 1:1 was the most unstable, since it is well known from charge density and PEI-Mal preparation condition that the stoichiometry for both HE-Na^+ and PEI-Mal is not equal.

4.2. Precoating preparation and characterization

4.2.1. pH-dependent adsorption properties of a PEI-25k on silica wafers

PEI-based PEs are widely used as adhesives, dispersion stabilizers, thickeners… etc. The adsorption of weak PEs on oppositely charged surfaces depends on various parameters including pH and ionic strength, which can significantly change the charge density of the polymer as well the surface. However, the non-electrostatic surface affinity and the solvent quality also play an important role. The actual balance of the interactions between the different constituents of the bulk solution and the surface layer (polymer segments, solvent molecules, surface groups…etc.) determines the equilibrium properties of the system.

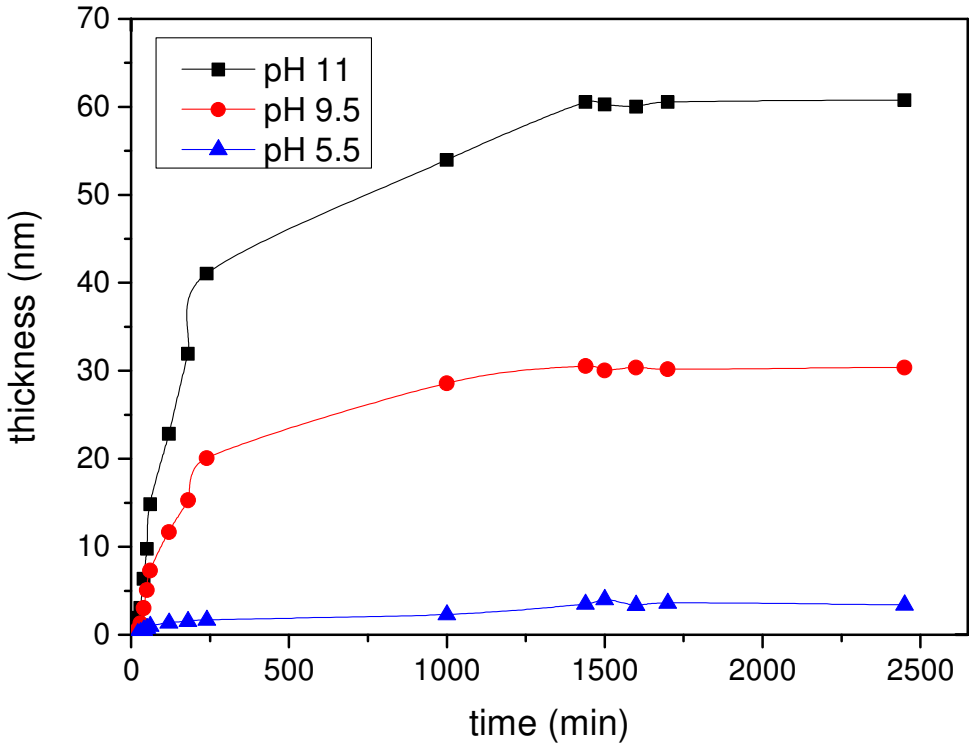

Figure 4-5. Ellipsometric measurements showing thickness of PEI-25k of different pH value as a function of time. Freshly prepared PEI-25k of 2mg mL^{-1} dissolved in ultraclean Millipore-water, acidic pH was adjusted with HCl (0.5M).

An additional feature of the adsorbed weak PEs is that their charge density is adjusted in the adsorbed layer due to the local electrostatic potential profile near the surface. As a consequence to this fact, it was concluded from different literatures [317] that this kind of adsorption possesses are considered as a very sophisticated assumption. In case

of branched or starlike PE the problem is even more complicated since the adsorption of these structures is less understandable than that of the linear ones.[318] The mechanism of PE adsorption can generally be viewed as a three-step process: (**i**) transport from the bulk to the surface, (**ii**) attachment to surface and (**iii**) the rearrangement in the adsorbed layer till reaching the equilibrium profile. However, the adsorption step and the whole precoating kinetics are mainly determined by the balance of the first two steps, which without doubt will affect the equilibrium of the whole PEM growing up later on. In this work, a comprehensive study of the pH-dependent adsorption properties of a PEI-25k on silica wafers will be presented (**Figure 4-5**). Some problems in PEM building up which is related to the different charge densities for the weakly charged polycations (PEI-Mal) and the used polyanions, especially strongly charged HE-Na^+, in case of weak/strong system (PEI-Mal/HE-Na^+), has been observed. At this moment it was very critical to find a way in order to increase the charge density of the substrate (e.g. silicon wafers) to avoid its great influence on the first adsorbed layers. The strong affinity of PEI toward silica surfaces as compared to polyamines has profoundly directed us toward that choice (**Figure 4-5**). [319] HPEI was selected as polycation to form pre-coatings which acting as uniform anchoring networks for consecutive layers formation featured with a homogeneous and smooth PEM surface and high number of bilayer.

The observed data will be compared with that of Mészáros *et. al.* [319] for the adsorption of HPEI of molecular weight (750,000 g mol^{-1}) (PEI-750k) , their supporting electrolyte was NaCl. An attempt will be made to explain the differences between results of this work and theirs. It is important to mention that PEI-25k is practically neutral at pH ≥ 10.5 whereas it possesses considerable charge density in the acidic pH range. The determination of the charge density of PEI-25k was based on the standard potentiometric titration method observed in Reference. [320] Mészáros *et al.* [319] investigated the adsorption amount of PEI-750k on the surface of thermal oxidized silicon wafers as a function of time at various pH values (pH 10.5, 9.2, 7, and 4.3) for 100 minutes. However in this work, freshly activated thermal oxidized silicon wafers were used (Experimental, **Section 6.1.2**). The additional silicon oxide layer was of thickness of 27 nm measured by ellipsometry, and the wafers were immersed in aqueous PEI-25k solution (2mg mL^{-1}) for ca. 2 days. PEI-25k solution was investigated in different pH values 10.5-11, 9.5 and 5.5 (**Figure 4-5**). The latter pH values gave three different precoatings, PEI-11, PEI-9.5 and PEI-5.5, respectively. Thickness for the three created precoatings has been traced as a

function of time for different pH values (11, 9.5, 5.5) for 2 day. Precoatings thicknesses were monitored by means of ellipsometry (**Figure 4-5**). **Figure 4-5** shows that PEI-11 (neutral pH) resulted in the formation of thick PEI precoating with film thickness of about ~ 60 nm. The precoating thickness was decreased as acidity was increased. In case of PEI-9.5, the created precoating was of thickness ~ 30 nm. PEI-5.5 was of much lower thickness and was monitored of maximum value of ~ 4nm after the duration of ca. 2 days. In all cases the precoating thickness started to increase with time (~1day), this period is followed by a plateau period with no more obvious increase in thickness has been observed (**Figure 4-5**).

PEI-25k precoating monitored thickness is considered as the mirror reflection of the adsorbed amount of PEs at different pH values on the surface of silicon wafer. Mészáros *et al.* [319] demonstrated that the mechanism of adsorption can be split into at least two distinct parts: (**i**) At the onset of the adsorption the adsorbed amount linearly increases with time. (**ii**)Then the rate of adsorption tends to have a constant value and the surface compensation was formed. They proved that the lower the pH the greater the faster the plateau value of the PEs adsorption to be attained. The reversibility of PE adsorption is also an essential question. For example, there is strong evidence that the adsorption of some weak PE shows significant hysteresis in a pH cycle experiment. However, this was the exact situation in case of pH 9.5 and pH 5.5. The thickness was dramatically affected by the acidic pH, thus in case of pH 5.5 the thinnest thickness has been achieved (≥4nm) (**Figure 4-5**). These results have a great agreement with that of Mészáros observations. The higher the pH value, the larger the adsorbed amount of HPEI and the thicker the film thickness. [319] This variation in PEs adsorbed amount and the layer thickness may be due to the pronounced role of the electrostatic segment/segment repulsion. i.e., by increasing degree of the protonation of PEI, two different repercussions will be achieved:

(i) The deviation from the initial adsorption rate becomes steeper.

(ii) The adsorption decreases monotonically with the increase of pH value at a fixed ionic strength.

In other word it is possible to say that as pH value deviated from neutral the possible role of an electrostatic barrier in the kinetic theories become brightly observed. These results flow **Eq. 2-3** where in neutral pH value, the non-electrostatic affinity of the

PEI-25k chains toward the silica surface (dielectric surfaces) starts to be dominate. This will switch the wetting process and will increase the amount of PEs adsorption. Respectively, most of the PEI-25k solution is going to spread homogenously on the surface of the silica substrate. This can be understood by recalling that image charges induced on the substrate which effectively changes the monomer–monomer interaction (**Section 2.4.3**). For materials with low dielectric constant this interaction is reduced by the increased of electrostatic repulsion between the PE chains (**Scheme 2-7 A**). The latter aspect leads to formation of small complexes that repel each other and thus tend to cover a large part of the surface (dielectric substrates). At this moment the whole substrate's surface area has a high affinity for adsorbing more amount of PEs on its surface and this logically followed by thickness increase.

The only restriction for thickness increase is the screening effect. The higher the protonation degree of the PEI, the lower the ionic strength, the higher the electrostatic barrier developed and the slower the adsorption process. However, by increasing surface coverage a barrier against further adsorption is developed. Therefore, the attachment process slows down till reaching the equilibrium and eventually the plateau formation. This was well agreed with our observations, where PEI-11, PEI-9.5 and PEI-5.5 yield a mean thickness of about 60nm, 30nm and 4nm, respectively after 20 hours (**Figure 4-5**). No increase in any of films thickness was observed after one more day of investigation. The only striking deviation with Mészáros *et al.* [319] observations from these results was within the time achieved for reaching equilibrium . Mészáros *et al.* [319] used NaCl (0.001, 0.01 and 0.1 M) as a main supporting electrolyte in all of their prepared PE solutions. They reach the total compensation break point in < 50 seconds. Herein, equilibrium has been reached after 20 hours (**Figure 4-6**). Schneider *et al.* [318] point out at the very end of their paper: The outcome of an adsorption experiment must depend on (**i**) the relative rates of surface impingement on the one hand and (**ii**) surface spreading on the other hand. When spreading occurs relatively fast, more molecules will lay flat so that the adsorbed mass will be low.

4.2.2. AFM surface measurements for precoatings: PEI-11 and PEI-9.5

The master aim of this study is the highest surface coverage, the highest surface charge density and the highest thickness in order to diminish the influence of the substrate

upon the following layering steps. However, it was very important, especially in the case of weak/strong system, to relieve/diminish the low affinities between PEI-Mal and HE-Na^+. Therefore, the thick layers PEI-11 (~ 60 nm) and PEI-9.5 (~ 30 nm) were only chosen for further experiments. Thus, it was important to check the topology and morphology for both chosen precoatings for later on PEM building up.

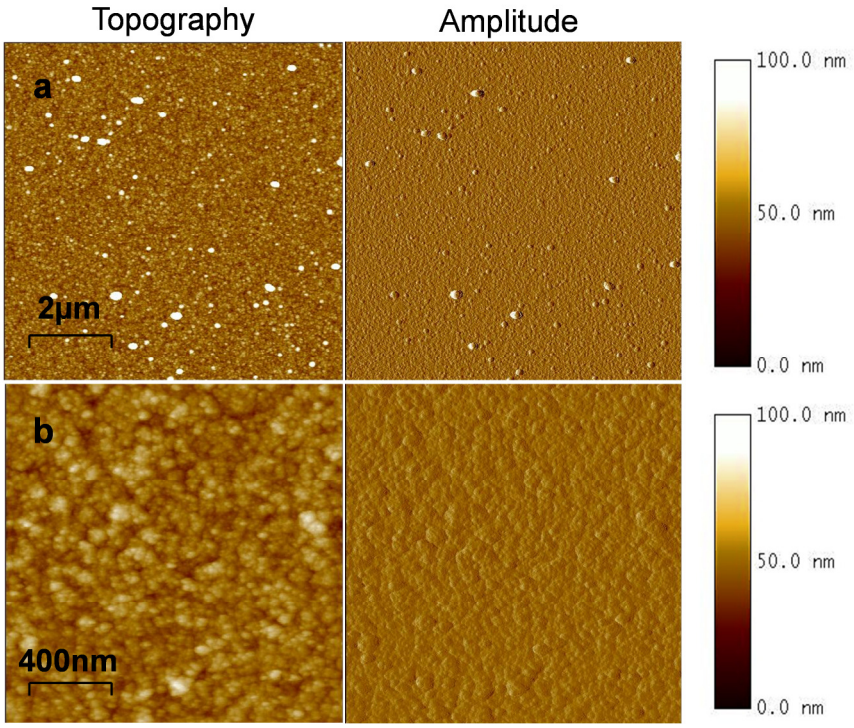

Figure 4-6. AFM measurements for the topographic and amplitude images, with different lateral dimensions 2 and 10 μm^2 for the pre-coatings (PEI-25k). (**a**) and (**b**): PEI-25k adsorbed on Si wafer at pH 11 after 20 hours; film thickness measured by ellipsometry is ~ 60 nm. PEI-25k pre-coating is only possible when using Si wafer with additional SiO_2 layer of ~28 nm.

By considering the AFM topography measurements of such PEI-25k precoatings, **Figure 4-6** and **Figure 4-7** show the surface topology for both precoatings PEI-11 and PEI-9.5, respectively. PEI-11 provides smooth precoating surface with rms value of about 10 nm calculated for lateral dimensions of $10\mu m^2$ (**Figure 4-6**). Blob-like structure did not appear in the AFM images (**Figure 4-6**). It should be noted that because of weak PE nature of the PEI-25k, the charge density is adjusted in the adsorbed layer. [123] This means that the amino units in contact to the negatively charged silica are more charged than the amino

groups lay further from the silica. This effect further increases the weight of the attractive segment/surface interactions at the expense of the repulsive segment/segment interactions by increasing pH. This means at certain pH value the adsorption does not depend on the PEs concentration, and this was exactly found in case of pH 10.5-11. In this case the adsorbed amount of PEI-25k increased, attached strongly to the substrate, and showed a smooth, continuous and well defined layer (**Figure 4-6**). In case of the protonated version, PEI-9.5 (**Figure 4-7**); the AFM measurements show that the rms of the precoating is increased till reaching 28nm calculated for lateral dimension of 10µm^2. This indicates that the PEI-25k precoating formation is attributed to the formation of island on the top of PEI precoating. In addition to what has been discussed above, the screening effect restricts both the adsorbed amount of PEs and precoating morphology as well (**Figure 4-7**).

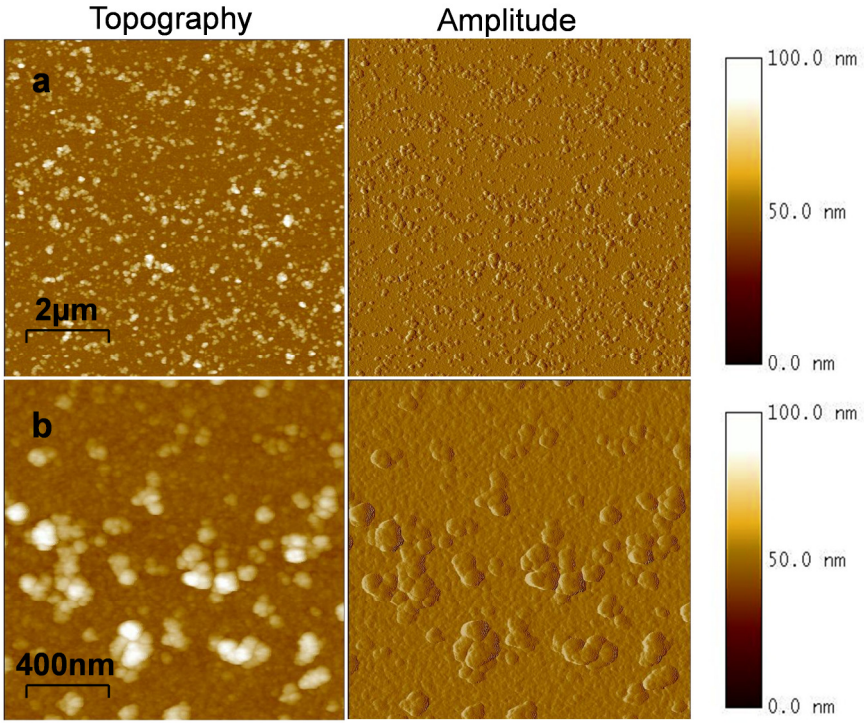

Figure 4-7. AFM measurements for the topographic and amplitude images, with different lateral dimensions 2 and 10 µm^2 for the pre-coatings (PEI-25k). (**a**) and (**b**): PEI 25k adsorbed on Si wafer at pH 9.5 adjusted by HCl (0.5M) after 20 hours; film thickness measured by ellipsometry is ~ 30 nm. PEI-25k pre-coating is only possible when using Si wafer with additional SiO_2 layer of ~28 nm.

In addition to the thickness determined by the optical ellipsometric module, for further confirmation film thickness was also determined by means of AFM. Thus, the

AFM measurement can be used as a direct and accurate method to detect the layer thickness because a direct AFM tip contact with the substrate and the coated surface is given.[165] Three PEI precoatings were scratched by hand with a razor blade to remove all the PEM film from a specific area to re-measure the film thickness of the PEI precoating. The three different scratches have been done on the same PEM and the mean value has been taken. The resulted thickness was not totally away from that was detected by ellipsometry. Thickness of mean value of ~58 nm was detected for PEI-11 (Appendix, **Figure 8-7**), whereas about ~31 nm for PEI-9.5 (Appendix, **Figure 8-8**) was measured. The additional AFM results confirm that the PEI-precoating is a homogeneous layer with heterogeneous surface especially for the protonated layer (PEI-9.5). One final remarkable point is that precoating formation is only possible on Si wafer surface, which possesses an additional SiO_2 layer of about 25–30 nm. This SiO_2 layer is needed for the deposition of PEI-25k as precoating while Si wafer surface with native SiO_2 layer with 1–2 nm of thickness is not suited for any precoating formation. This experimental requirement is not well understandable in the course of our study at the moment and needs additional experiments to clarify this point. From here on, the PEM characteristics will be interpreted on the basis of the adsorption properties of PEI-11 and PEI-9.5.

4.3. Polyelectrolyte multilayer formation (PEM)

Along the lines on what happened to the precoating PEI-25k on the surface of silica substrate, PEI-25k dynamic and static adsorption features on silica are significantly depending on the subtle balance of the attractive segment/surface and repulsive segment/segment interactions. This balance determines the extent of the electrostatic barrier in the adsorption mechanism, PEI-25k adsorbed amount and its depends on assembly pH, and the presence of strong non-Coulombic interaction between PEI-25k and the silica substrate. Thus, this study is trying to follow up the precoating by a number of bilayers, which will eventually follow the same mechanism but with additional sophisticated processing steps. The multilayer concept (**Section 2.4.2)** is based on the sequential adsorption of at least two polymer species having high affinities to each other.

The first experiments on PEMs made of oppositely charged PEs (polycation and polyanion) were created by Decher *et al.* using LbL technique (**Scheme 2-6**). [131] This

way of PEM processing is now one of the most versatile and efficient ways to build up films with required properties and well-controlled thickness. Although the basic idea of the PEM is fairly simple, the theoretical description is quite complex because of the long range of the Coulombic interaction attaching layers to each other and the conformational changes of both polyions during interactions. In this work, it was tried to prepare stable biocompatible PEMs, which are composed of the very weakly charged polycation PEI-Mal of the two different structures PEI-Mal-B and PEI-Mal-C and two different polyanions have been used, HE-Na^+ and HA-Na^+ (**Scheme 4-1**). Two different systems have been fabricated: (**i**) the first system is weak/strong system, where PEI-Mal was assembled with the strongly charged HE-Na^+. (**ii**) The second system was weak/weak system, where PEI-Mal-C was assembled with the weakly charged HA-Na^+. Three different approaches, Approach A, B and C (**Scheme 4-2**) have been used in the preparation of these PEMs. Approach A, B and C fabrication strategies are shown in Experimental, **Section 6.1.5.2**.

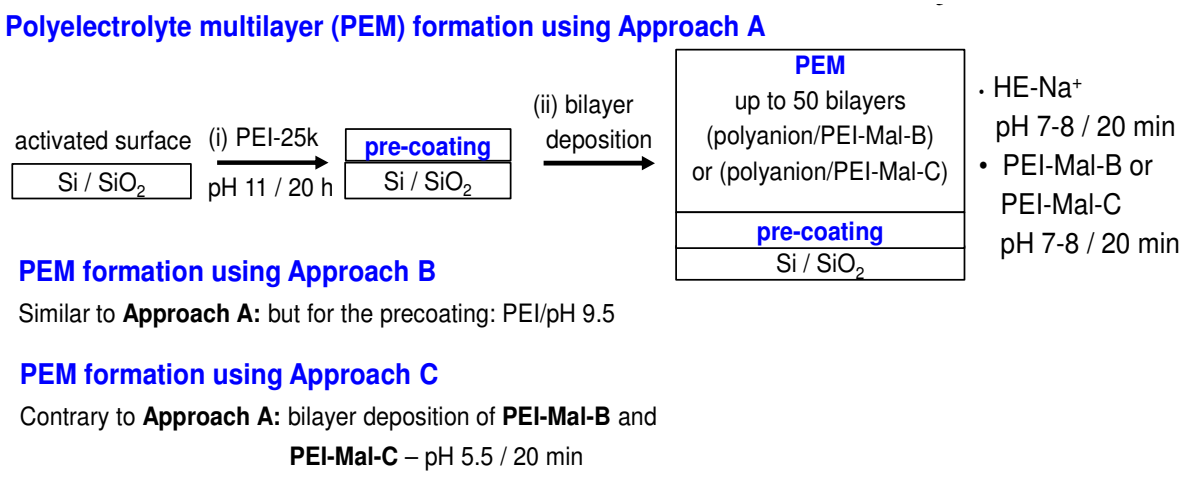

Scheme 4-2. Schematic diagram represents PEM approaches: Approaches A, B and C used in PEMs fabrication.

4.3.1. PEM deposition mechanism

The successive growth progression has been investigated in a plenty of published papers. [162, 321] They illustrated that the self-assembly ML films does not grow as a successive superposition of interacting polymer layer, such as puff pastry but they exert a kind of inter-diffusion processing. The principal findings in this section can be helpful in attempting to rationalize the observed data later on. **Scheme 4-3** represents the successive

PEM deposition. **Scheme 4-3** represents that even after coating silicon substrate with the positively charged PEI-25k, parts of silica surface remain free of polymers. However, precoating diminishes the free uncompensated parts of substrate and reduces the force exerted by the substrate on true PEM. This coating strongly raises surface charge density and reverses its charge from negative to positive, which is totally ready to welcome the contrary charge and the first layer (negative charge). In the second step, the deposition of PEI-Mal took place exclusively through electrostatic interaction with the predeposited polyanion molecules forming aggregates.

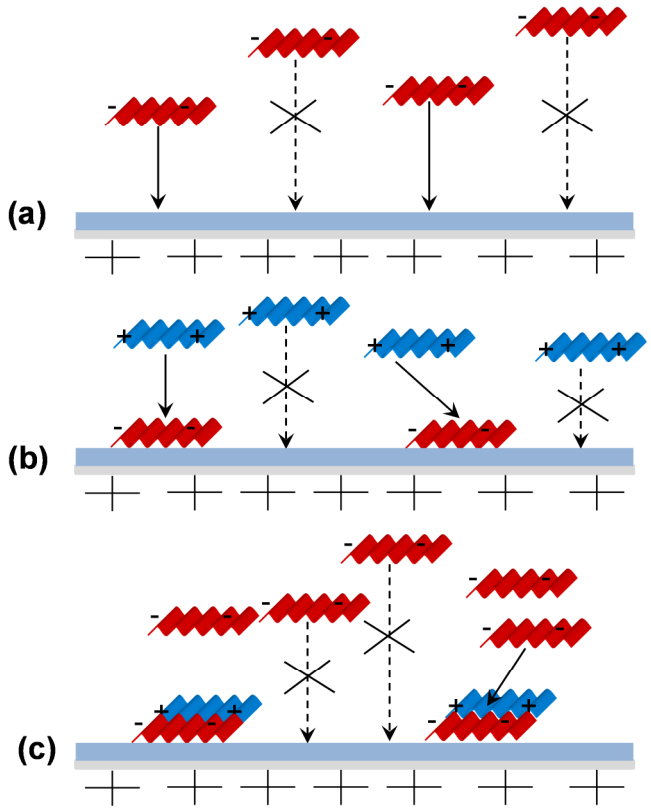

Scheme 4-3. Scheme shows PEM step deposition mechanism on precoated positively charged substrate. First layer (**a**), second layer (**b**), third layer (**c**). Substrate is Si-wafer with additional thermal oxide (SiO_2) layer coated with PEI-25k. Adapted from Reference [321]

For further deposition, when the polyanion is introduced for the second time, the molecules could adsorb both on the bare of the coated substrate and on the charged aggregates. This kind of complexation which might be found due to the interaction between polycations and polyanions form what is the so called bloblike structure. The more the order of bloblike structure increased, the more the formation of the valleys and islands are possible. On addition of new PEs and as layering up continued on and on, these

islands start to coalescence and mutually merge setting a continuous film. After each deposition step it could be logically understandable that the reversal charge to the last layer is managed. Dejeu *et al.* have been investigated that the surface always takes the charge sign of the last deposited polymer. [321]

4.4. Weak/strong system PEM (PEI(HE-Na^+/PEI-Mal)$_n$)

4.4.1. PEM (PEI(HE-Na^+/PEI-Mal)$_n$) fabrication

For further understanding the weak/strong system, PEM is fabricated by using PEI-Mal as a weak polycation counterpart, while the polyanion in this system is HE-Na^+. There are three types of acidic functional groups in the HE-Na^+ polymer. The sulfate monoesters and the sulphamido groups (SO_3^-) are both highly acidic, having pK_a value ranging from 0.5 to 1.5. Less acidic are the carboxylate groups (COO^-) of various unsulphated and mono-sulphated uronic acid residues, having pK_a values of between 2 and 4. [322] Dukhin *et al.* have shown that the surface potential of PEM is dependent on its bulk composition and that the surface charge is lower than the intrinsic charge of the respective PEs in solution.[323] In addition, the isoelectric point (point of zero charge) could be an indicator for layer interpenetration as it is located between the pK_a of HE-Na^+ (pK_a~ 3) [262] and that of both the positively charged groups (ammonium groups) for PEI-Mal-B (pK_a ~6.8) and for PEI-Mal-C (pK_a~ 8.3). [313] Around this pH value, the charge density of the polymer decreases and the backbone becomes almost neutral in more basic solutions. On the other hand, the appearance of negative potential of PEI-Mal-B and PEI-Mal-C in the basic solution (pH =7.5 from there on) give the inspiration that acidic HE-Na^+ are not efficiently screened by the large PEI-Mal molecule. It must be taken in account that the negative potential in basic solution for PEI-Mal-B is higher than that of PEI-Mal-C.

4.4.2. Results for weak/strong system: growth regime and thickness

As shown in **Section 4.1.3**, in case of PEM (PEI(HE-Na^+/ PEI-Mal-B)$_n$), PEM optimized assembly mass ratio for PEI-Mal-B: HE-Na^+ was 20:1. However, in case of PEM (PEI(HE-Na^+/ PEI-Mal-C)$_n$), the PEM optimized assembly mass ratio for PEI-Mal-C: HE-Na^+ was 7:1. These concentration ratios have represented the right charges affinities

for PEI-Mals and HE-Na^+ at which PEM (PEI(HE-Na^+/ PEI-Mal)$_n$) has been already fabricated.

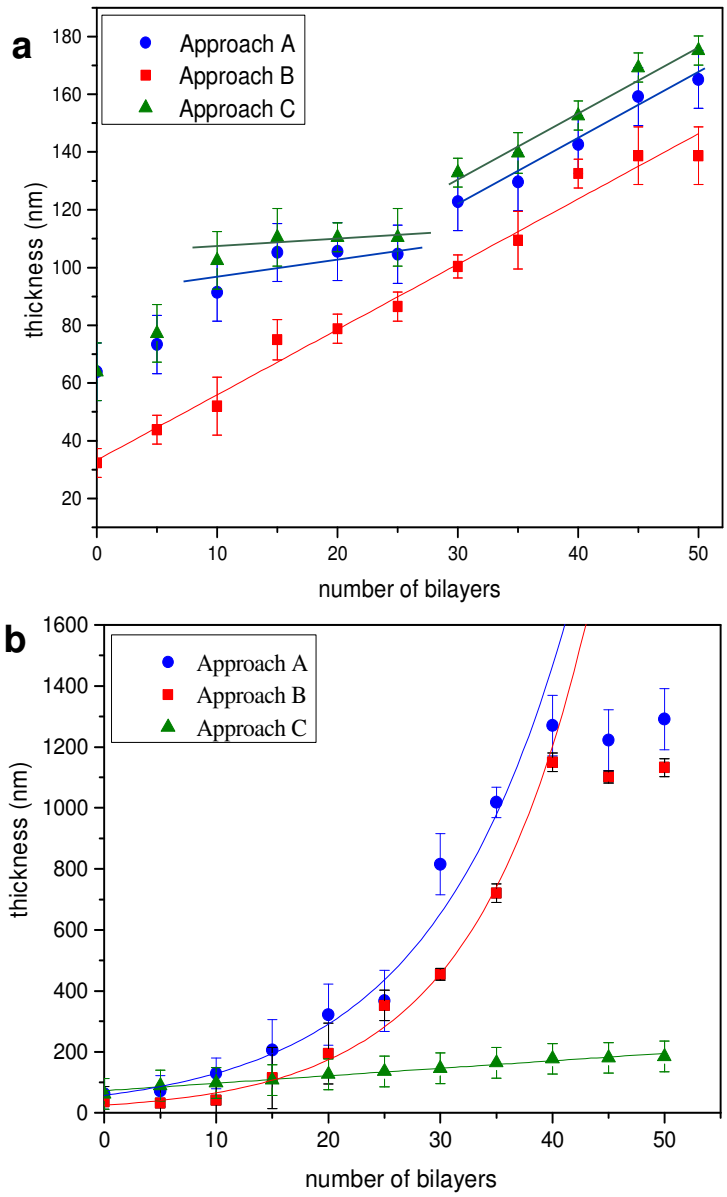

Figure 4-8. Progression of film thickness versus number of adsorbed bilayers during the fabrication of final PEM (PEI(HE-Na^+/PEI-Mal)$_{50}$) with 50 bilayers: (**a**) bilayers with PEI-Mal-B and (**b**) bilayers with PEI-Mal-C fabricated by Approach A, B and C (**Scheme 4-2**). Ellipsometric measurements were performed in dry state. Solid lines are fits of theoretical bases related to the growth regime.

After each 5 bilayer depositions, on precoated positively charged Si wafer, ellipsometric measurements were carried out to evaluate PEM growth regime and PEM

thickness (**Figure 4-8 a**) for PEI-Mal-B and (**Figure 4-8 b**) for PEI-Mal-C. PEM growth mechanism was followed by using Cauchy model on a surface of thermal oxidized silicon wafer of thickness 27-30 nm measured by ellipsometry. A well-defined and reproducible PEM ($PEI(HE\text{-}Na^{+}/PEI\text{-}Mal\text{-}C)_{10}$) is shown in Appendix, **Figure 8-9**. These latter successive depositions have been measured via in-situ ATR-FTIR measurements (Appendix, **Figure 8-9**). In the case of PEI-Mal-B, the thickness of the PEM increases from 5 to 50 bilayer depositions for the Approach A, B and C (**Figure 4-8 a)**. Surprisingly, there was nearly similar PEM thickness for all proposed approaches starting from about ~70 up to ~175 nm for all the three approaches. For a closer look to PEM ($PEI(HE\text{-}Na^{+}/PEI\text{-}Mal\text{-}B)_{50}$) fabricated by Approach A and C, a "pseudo-linear" PEM's growth with a thickness revealed to a plateau-like occurred between 10 to 25 bilayer deposition followed up by linear thickness growth from 30 to 50 bilayer depositions. This means that the linear PEM growth for the whole 50 bilayer deposition was partly suppressed due to plateau-like growth thickness in the middle of bilayer formation for Approach A and C (**Figure 4-8 a**). In contrary for Approach B, linear growth is shown in (**Figure 4-8 a**). The thickest PEM was that fabricated by Approach C with bilayers thickness increased from ~77 nm for 5 bilayers till ~175 nm for 50 bilayers. There were no great thickness differences between Approach A and Approach C. Both approaches were built-up on the same precoating conditions (PEI-11). In case of Approach A, bilayers were measured by ellipsometry to give thickness of about ~73 nm and ~165 nm for 5 and 50 bilayers, respectively. In contrary, in case of Approach B, bilayers were ellipsometrically recorded in the range of ~44 nm and ~139 nm for 5 and 50 bilayer depositions, respectively (**Figure 4-8 a**).

On considering the PEM's growth and thickness for PEI-Mal-C illustrated by ellipsometric measurements, a remarkably different 50 bilayer deposition for the Approaches A-C (**Figure 4-8 b**) was provided in comparison to those fabricated by PEI-Mal-B (**Figure 4-8 a**). It was roughly estimated from **Figure 4-8 b** that upon using approaches A, B for PEI-Mal-C, a kind of exponential PEM growth was observable. From 5 till up-to 40 bilayer, PEM thickness increased exponentially. In case of Approach A, 5 bilayers was measured by ellipsometry to give ~73 nm, PEM was reproducibly increased till 50 bilayers of thickness ~1.29 µm. PEM fabricated by Approach B gave lower thickness compared to Approach A. In case of Approach B, 5 bilayers were recorded in

thickness of 32 nm and then PEM was increased till reaching 50 bilayers of thickness ~1.13 µm. There was a transition in PEM growth regime from exponential, in case of Approaches A and B, to linear, in case of Approach C. Thickness for Approach C was suppressed and returned back to the nano-range. PEM thickness fabricated by Approach C for 5 bilayers and 50 bilayers deposition was ~90 nm and ~185 nm, respectively (**Figure 4-8 b**). One of the most interesting results, that when PEI-Mal was slightly more protonated to pH 4, no PE mass deposition and PEM fabrication have been observed on the surface of the planar substrate. The theoretical solid lines (**Figure 4-8**) were considered as fit lines. In **Figure 4-8 a**, for Approach A and B and when describing PEM formation of PEI-Mal-B, the solid straight lines from 30 to 50 bilayers follow linear equation (y = a+ b* x) with slop value 1.94. The point standard error is of value 3.3 nm. However, the slop value and the point standard error for Approach C was 2.10 and 3.9 nm, respectively. In **Figure 4-8 b**, when applying PEI-Mal-C for PEM formation, the theoretical line for Approach A, B followed the exponential equation y= a*exp.(b* X), in contrary the compacted Approach C followed the straight line equation with slop value 2.4 and point standard error 3.6 nm.

4.4.3. Discussion for weak/strong system: growth regime and thickness

In discussing the PEM behavior in case of PEI-Mal-B, it is difficult to say that this plateau-like growth, for PEMs fabricated by Approach A and C, was only due to substrates effect. However, the most reliable reason for such ''pseudo-linear'' growth may be due to the mismatch and lower charge affinities between PEI-Mal-B and HE-Na^+. HE-Na^+ charge density is considered to be three times that of PEI-Mal-B (**Table 4-3**). To overcome this mismatch, HE-Na^+ concentration (0.05 mg mL^{-1}) was lowered toward that of PEI-Mal-B (1mg mL^{-1}) with stoichiometric ratio of 20:1. According to the fact that PEM films self-assemble is thanked to interactions between the negative and positive groups and to the entropic gain associated with these associations. In addition to latter, HE-Na^+ is considered as a strong polyanion, whose charge density is fixed on variable ranges of pH values. Moreover, PEI-Mal is considered as a weak polycation, its charge density varies with the acidity of the aqueous solution. This preparation procedure give the inspiration about the internal structure of PEM (PEI(HE-Na^+/ PEI-Mal-B)$_n$). One can imagine that PEI-Mal-B chains were more flexible than that of HE-Na^+ (rigid scaffold) and can partially diffuse in and out the system. However, the HB properties and the ellipsoid shape of PEI-Mal-B have

to be taken in account. In case of Approach C, PEI-Mal-B was higher protonated than in case of Approach A and B. Thus, PEM thickness fabricated with Approach C was affected and appeared to be thicker than Approach A and B. The marginal thickness increase for PEM fabricated by Approach C (≤ 10nm) and the lower MSE values measured by ellipsometry may give the inspiration that the increase in PEM thickness is due to active volume concept and not to active surface concept (**Section 2.4.5**). In summary, for the protonated PEI-Mal-B at low assembly pH (pH 5.5), a higher charge density can be supposed which in turn should foster the adsorption of HE-Na^+ (**Scheme 4-4**) . In contrary , in Approach A and B, PEI-Mal-B (higher assembly pH 7.5) should possess a lower positive surface charge, which provides less electrostatic attraction resulting in the reduction of HE-Na^+ adsorption. These findings explain indeed the increase in PEM thickness for Approach C compared to A and B. However, the marginal thickness differences possessed by Approach C against the other two approaches are not enough to assume for PEM inner structure. In addition, it was expected for the approach C to switch in its growth regime to a regular fully linear mechanism, but this was not the case here (**Figure 4-8 a**). On the basis of these results, suggestion for further more experiments and investigations should be under consideration. Moreover, the difference between the growth behavior of Approach A and C (pseudo-linear) to that of Approach B (linear) also needs more investigation

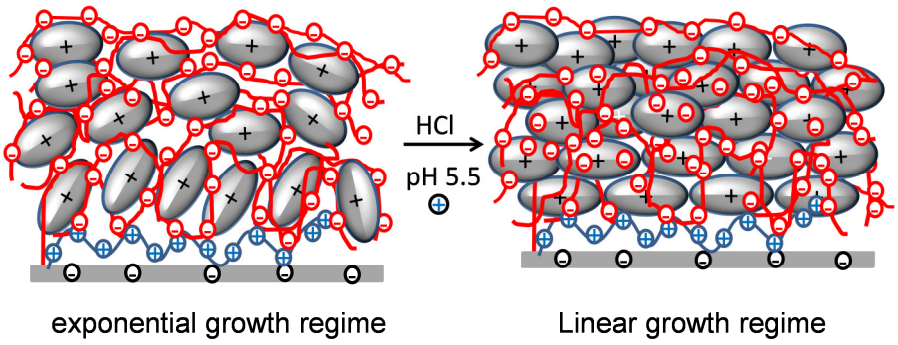

Scheme 4-4. Simplified schematic diagram shows an imaginary assumption for PEM switching from the exponential to linear in case of Approach C.

Growth regime transition and materials conformational changes were more obvious in case of PEM with PEI-Mal-C than that of PEI-Mal-B. A typical exponential growing regime in case of Approaches A and B has been observed **Figure 4-8 b**. As a consequence, many charges in PEM (PEI(HE-Na^+ /PEI-Mal-C)$_{50}$) for Approach A and B

are not compensated and an excess of negative charges from HE-Na^+ are existed. This without doubt affects the growth regimes for both approaches due to the folding mechanism for the linear highly charged HE-Na^+ toward the large molecular sized hyperbranched PEI-Mal. Taking in account that there is still a degree of flexibility exerted by PEI-Mal-C (pH=7.5-8). From 5 till up-to 40 bilayer, deposition is exponentially performed. This irregular deposition and increasing of PEs mass adsorption are suddenly followed by a stopping in the PEM growth from 45 to 50 bilayer depositions (**Figure 4-8 b**). This may imply that the charge density of one PE, probably of the cationic PEI-Mal-C, plays a deciding role after 40 bilayer deposition. From this point it is assumed that, the outermost cationic surface charge of the PEM is too small to allow a further (continuous) thickness growth for PEMs. In this context, several previous investigations have shown that there is a critical minimum charge density, below which no multilayer growth is possible. [9, 159]

This exponential growing regime for Approaches A and B was converted to linear one once changing the fabricating approach to Approach C. In case of Approach C, PEI-Mal-C was protonated and exerted higher cationic charge than before which in turn increase the charge affinities between PEI-Mal-C and HE-Na^+. Moreover, most of the uncompensated negative charges for HE-Na^+ were partially compensated which directly lower the flexibility condition of PEI-Mal-C and the folding behavior of HE-Na^+. In turn, PEM growth regime was converted from the exponential micrometer regime to linear nanometer growth regime (**Figure 4-8 b**). As a result it can be concluded that by simply controlling the assembly pH and the charge density, it is possible to control PEM thickness. However in some cases, the complete destruction of PEM is processed. One of the most interesting results is that when PEI-Mal was more protonated (pH 4.5), the charge affinities between PEI-Mal and HE-Na^+ were totally disturbed due to the presence of high electrostatic screening effect. Namely it can be presumed that screening of electrostatic interaction enhances the charge affinities between the polyions, but this can be predicted only till reaching a critical value, above which the whole PEM dissociation is expected.

For Approaches A and B to fabricate PEM (PEI(HE-Na^+/PEI-Mal)$_{50}$), the only illustrated difference between these two approaches is in the precoatings zone. In case of approach A, the precoating was PEI-11 which yielded a mean thickness of ~ 60 nm, while for approach B, the precoating was PEI-9.5 which yielded a mean thickness of ~ 30 nm

(Experimental, **Section 6.1.5.2**). In case of PEM (PEI(HE-Na^+ /PEI-Mal-B)$_{50}$) and if we ignore such plateau-like growing, PEM fabricated by Approach A has thickness pronounced by order of ~30 nm at the first 5 bilayers than that of Approach B. This thickness difference decreased gradually during the layering up till reaching ~10 nm after 50 bilayer depositions. These results can be relied on to two different reasons: (**i**) The first and the easiest explanation is related to the starting thickness at 0 time (precoating thickness), where the difference between two precoatings was of value ~30nm and this difference in precoating thickness lasted with error value till reaching the 50 bilayers. (**ii**) The second explanation and the more reliable reason is that in case of PEI-9.5 there are still some free uncompensated spaces on the surface of substrate as that has been discussed in (**Scheme 4-3**). However, substrate compensation via PEM counterparts (PEI-Mal-B and HE-Na^+) affects negatively the final PEM thickness. This starting difference gradually decreased with the further layering up, which gives an impression that the short forces induced by charged substrate disappeared gradually as layering up goes on further.

Another interesting feature for Approach A and B for PEM (PEI(HE-Na^+ / PEI-Mal-C)$_{50}$) is the exponential PEM growth. **Figure 4-8 b** emphasizes PEM fabricated by Approach A and B are with difference in thickness value of ~40 nm in case of the first 5 bilayers. This difference value was gradually increased till reaching 50 bilayers with thickness difference of order ~ 158 nm. These findings are in agreement with our second explanation for the case of PEI-Mal-B, that the forces induced by the substrate affected the final PEM thickness. This may be due to the mismatch between charge affinities of PEM counterpart. A similar situation has been discussed by Bosio *et al.* [324] when they prepared PEM (PAH/PSS) of 8 layers. On investigation, they compared between PEM with PEI-25k precoation and another without precoating. In principle, they found that the silica influence is present for the first few deposited layers (5 layers), however this influence is diminished as they go further away from the substrate. [324] In our case the situation was more complicated due to the differences in the polyanion and the polycation charge affinities for the both case PEI-Mal-B and PEI-Mal-C. Thus not only the substrate decides the growth regime of the first layers, but also different other parameters, e.g. charge densities, polymer segment, pH, molecular weight, solvent molecules, non-electrostatic affinities, processing…etc.

4.4.4. Topology and homogeneity of weak/strong system characterized by AFM

In order to understand the qualitative differences between Approaches A-C, the topography of the surfaces was investigated by means of AFM. Tapping Mode™ AFM images have been taken in dry state for lateral dimensions of 2 and 10 μm^2. All approaches were investigated for 10 and 50 bilayers. AFM images (Appendix, **Figure 8-10- 8-16**) have shown that the surface coverage of PEM increased continuously with every adsorption cycle. AFM imaging of PEM (PEI(HE-Na^+/PEI-Mal-B)$_n$) fabricated by Approach A has shown holes in case of 10 bilayers (**Figure 8-10**). These holes were of sizes around 30-50 nm. It was very surprising that in the case of Approach A for PEI-Mal-B, the formation of holes was observable in the early stage of low number of bilayer deposition (Appendix, **Figure 8-10 a, b**). However, they were progressively filled with increasing the number of bilayer cycles (Appendix, **Figure 8-10 c, d**). These holes for PEM (PEI(HE-Na^+/PEI-Mal-B)$_{10}$) fabricated by Approach A disappeared when PEM build-up proceeded on the surface of Si-IRE (Appendix, **Figure 8-11**). Although, one cannot completely exclude that hole formations which also may be exist in all other PEM approaches (Appendix, **Figure 8-12 - 8-16**), but AFM study gave no obvious indication to this point. Such defects were more pronounced in case of PEI-Mal-B than PEI-Mal-C. This may be relied on the lower charge affinities of PEI-Mal to HE-Na^+, whereas in case of PEI-Mal-C this kind of affinities were more enhanced than that of PEI-Mal-B (**Table 4-3**)**.** The data discussed in **Table 4-4** give more information about precoatings and PEM roughness (rms). It was shown that PEI-9.5 is significantly rougher than PEI-11 layer (**Figure 4-6, 4-7**).

All approaches share similar features in PEM roughness and homogeneity. Thus, in case of PEM of 10 bilayers, although the prepared films were uniform macroscopically, they were not homogenous on the micrometer scale. Generally, PEMs with 50 bilayers were more homogeneous and smoother compared to those of PEMs consisting of 10 bilayers. In case of 10 bilayers, there was eventually no great difference in the surface roughness by means of root mean square (rms) values whether for PEI-Mal-B or PEI-Mal-C (**Table 4-4**). It is worth to mention that PEMs with 50 bilayer for PEM (PEI(HE-Na^+/PEI-Mal-B)$_n$) were slightly rougher (rms of ~15 nm for Approach A) than PEM (PEI(HE-Na^+/PEI-Mal-C)$_n$) (rms of ~2 nm for Approach A). In all cases, the demonstrated roughness for approach C was the highest. These findings may be due to the PEI-Mal

protonation and the presence of the free counter ions compared to Approach A, whereas both Approach A and C are built-up on the same precoating conditions (PEI-11).

Table 4-4. Root mean square (rms) for PEMs PEM (PEI(HE-Na^+/PEI-Mal)$_n$) of 10 and 50 bilayers calculated by means of AFM. The rms was calculated for the lateral dimension of 10μm^2.

			rms [nm]	
Approaches	**PEI-25k**	**Thickness [nm]**	**Precoating**	
A,C	PEI-11	58	11.0	
B	PEI-9.5	31	28.1	
			Bilayers	
Approaches	**PEI-Mal**		**10**	**50**
A	PEI-Mal-B		27.4	14.6
B	PEI-Mal-B		25.9	16.6
C	PEI-Mal-B		36.4	19.3
A	PEI-Mal-C		20.0	2.0
B	PEI-Mal-C		18.5	1.2
C	PEI-Mal-C		27.9	10.7

4.4.5. Conclusion for weak/strong system: thickness, growth regime and topography

In summary, PEMs formation in respect to different charge density between PEI-Mal-B, PEI-Mal-C against that of HE-Na^+ which built up on precoated surfaces. Precoating (PEI-25k) application enhanced thickness, uniformity and smoothness of the prepared PEMs surfaces as it has been proved by means of AFM. On the other hand, both PEI-Mal structures were suited to form PEMs with HE-Na^+ attributed to PEM reproducible thickness although different stoichiometric mass ratios were used. Due to the higher cationic charge density of PEI-Mal-C than that of PEI-Mal-B, the film thickness of PEMs was much higher than that of PEMs consisting of PEI Mal-B when applying Approach A, B (**Figure 4-8**). In case of Approach C, where the assembled pH for PEI-Mal was 5.5 (**Scheme 4-2**), at this pH value PEI-Mal was strongly charged, while for PEI-Mal at physiological pH 7.5-8, the charge density was lower. It was roughly estimated that PEM

fabricated by Approach C for both PEM (PEI(HE-Na^+/PEI-Mal-B) and PEM (PEI(HE-Na^+/PEI-Mal-C) gives similar PEM thickness , although different charge densities between both cationic counterpart (**Figure 4-8)**. In this study, the most surprising finding in the PEM characterized by ellipsometric measurements was certainly the occurrence of sharply defined regimes of different bilayer growth after changing the polycationic partner from PEI-Mal-B (**Figure 4-8 a**) to PEI-Mal-C (**Figure 4-8 b**). Moreover, it has to be mentioned that highly reproducible PEMs were given by Approach A, B and C (**Figure 4-8**), average data of three experiment series have been shown (**Figure 4-8**). For PEM (PEI(HE-Na^+/PEI-Mal-B)$_{50}$), fabricated with Approaches A and C, shows pseudo-linear growth with plateau-like growing up for bilayers between 10 to 25. PEM (PEI(HE-Na^+/PEI-Mal-B)$_{50}$) fabricated by Approach B shows linear growth regim. PEM (PEI(HE-Na^+/PEI-Mal-B)$_{50}$) fabricated by Approaches C has shown a marginal increase in PEM thickness (≤10nm) than that of Approach A.

Obvious growing transition has been established in case of PEM (PEI(HE-Na^+/PEI-Mal-C)$_{50}$) (**Figure 4-8 b**) . Approach A and B for PEM (PEI(HE-Na^+/PEI-Mal-C)$_{50}$) have grown exponentially. Only when applying Approach C for PEM (PEI(HE-Na^+/PEI-Mal-C)$_{50}$) , a real constant adsorption of PE can be recognized and thus a constant increase for PEM growth was in principle achieved till 50 bilayer depositions (green straight line - **Figure 4-8 b**). In other word, the molecular flexibility of the PEI-Mal-C macromolecules was partially destroyed at pH 5.5 due to the higher charging and thus the formation of thicker PEMs was not supported as it has been observed in the case of Approaches A and B. Intriguingly, in case of PEM(PEI(HE-Na^+/PEI-Mal-C)$_{50}$) fabricated with Approaches A and B, another interaction and organization characteristics between the anionic and cationic PE macromolecules to generate extremely thick PEMs can be assumed. Thus, the combination of different key issues, e.g. more rigid HE-Na^+ scaffold, higher charge of PEI-Mal-C than PEI-Mal-B at pH 7.5–8, and assumed higher molecular flexibility for PEI-Mal-C than PEI-Mal-B at pH 7.5–8, was responsible for the extraordinary thick PEM formation.

The presented data have indicated a clear difference in the behavior of the deposited PEMs for both PEI-Mal-B and PEI-Mal-C. Since the charge of strong polyanion HE-Na^+ is not pH dependent, it was suggested that the differences in film thickness and structure originates from pH effect on charge density and conformation of PEI-Mal

molecules. Overall, we can conclude that the pH of the PEI-Mal-C solution and its rigidity were preferentially governing higher film thickness of PEMs consisting of PEI-Mal-C and HE–Na^+. In contrary, the formation of PEMs consisting of PEI-Mal-B and HE-Na^+ was not dominated by one PE as it has been observed in PEM (PEI(HE-Na^+/ PEI-Mal-C). Similar explanation for this specific PEM formation may be applied to other kinds of PE complex especially whose are tailored with counterpart polyions of different molecular shapes and charge affinities. Overall, from the results of these characterizations based on ellipsometry and AFM study it is difficult to conclude which fabrication approach (**Scheme 4-2**) can be the most efficient for achieving stable PEMs under physiological conditions. More stability and swelling investigation in different charged-free and charged buffer will be presented later on (**Section 4.6.1**)

4.5. Weak/weak System PEM (PEI (HA-Na^+/PEI-Mal)$_n$)

In order to present polyelectrolyte multilayer fabricated with equal stoichiometric ratio, weak/weak system has been investigated. PEI-Mal-C and HA-Na^+ represent polycationic and polyanionic counterparts, respectively, in week/week system. A mechanism was outlined where biopolymer thin films can be electrostatically adsorbed under highly charged "sticky" conditions and then quickly transformed into stable well controlled films simply by altering the pH environment. HA-Na^+ and PEI-Mal-C are both classified as weak PEs, only partially charged at moderate pH near their pK_a. The pK_a of HA-Na^+ carboxyl groups is 2.9–3.5 of total mass concentration of 0.5mg mL^{-1} and pH 7. [325, 326] The pH and ionic strength environments greatly influence the physicochemical properties of these polymers in solution. Thus, in turn it is believed that such changes will impact the properties of PEM (PEI(HA-Na^+/PEI-Mal-C)$_n$), where n is bilayers number.

4.5.1. Results for weak/weak system: growth regime and thickness

In exact similar conditions as in weak/strong system (**Section 4.4)**, weak/weak system was built up via the well-known Approaches A-C (**Scheme 4-2**). To elaborate on the relationship between the film assembly pH and PEs inter-diffusion induced surface mobility of PEI-Mal and HA-Na^+, PEM (PEI(HA-Na^+/PEI-Mal-C)$_n$) growth thickness has to be measured by stepwise ellipsometric measurements. PEM growth mechanism was

followed by using Cauchy model on the surface of thermal oxidized silicon wafer of thickness 27-30 nm measured by ellipsometry (**Figure 4-9**). The thickness of PEM was strongly influenced by the degree of polymer charge and assembly pH of the PE solution during preparation. In case of weak PEs both PEM charge surface and the charge of the adsorbing chain were modified simultaneously by changing the pH of the dipping solution. Well-defined PEMs have been fabricated by the introduction of the multilayer concept based on the sequential adsorption of the two polymer species PEI-Mal-C and HA-Na^+, where it was previously proved that both have high charge affinities to each other (**Figure 4-4** and Appendix**, Figure 8-5**). Therefore the preparation concentration ratio for polyanion: polycation was 1:1 using 0.5 mg mL^{-1}. The thickness of the PEM increases from 1 to 25 bilayer depositions for the Approaches A -C (**Figure 4-9**).

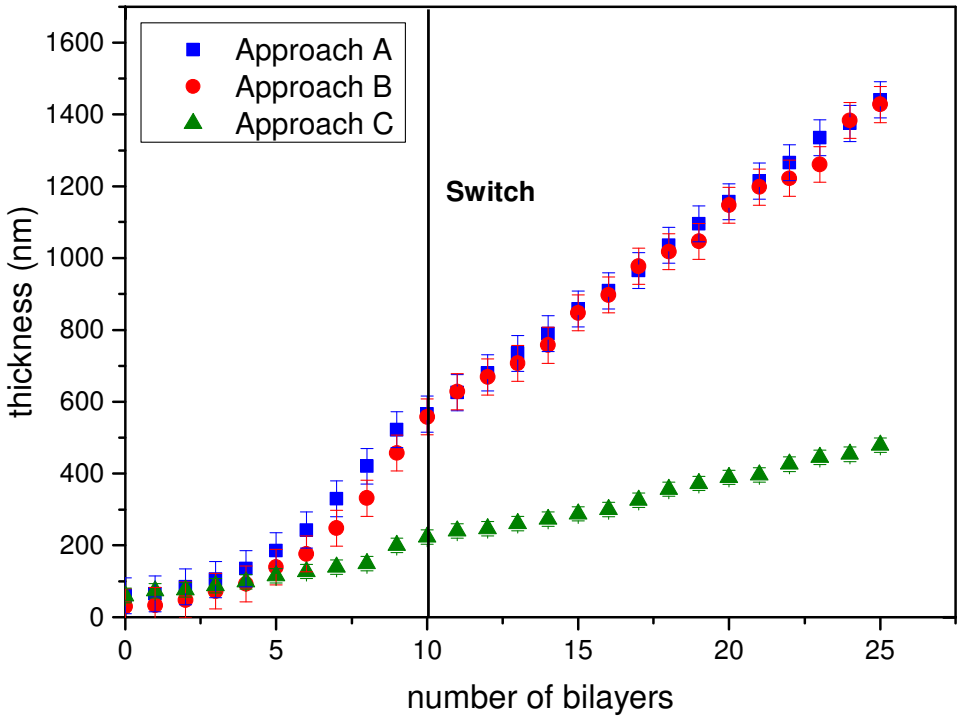

Figure 4-9. Progression of film thickness versus number of adsorbed bilayers during the fabrication of final PEM (PEI(HA-Na^+/PEI-Mal-C)$_{25}$) with 25 bilayers fabricated by approaches A-C.

Figure 4-9 shows PEM (PEI(PEI-Mal-C/HA-Na^+)$_{25}$) fabricated by Approaches A-C. In case of Approach A: the first bilayer was detected to be ~65 nm, while 25 bilayers were 1.44µm. similarly for Approach B, for the first bilayers and 25 bilayers, the thickness

was ~74nm and 1.43µm, respectively. The measured thickness for PEM (PEI(PEI-Mal-C/HA-Na^+)$_{25}$) fabricated by Approach C, were of values ~74 and ~479 for the first bilayer and 25 bilayers, respectively. Thick films have been obtained for all the usable approaches A-C, with a rather well-controlled thickness. However, the lowest thickness was encountered for Approach C with about ~479 nm for 25 bilayer depositions. It was difficult in case of Approach A and B to follow the building up of PEM (PEI(HE-Na^+/PEI-Mal-C)$_n$) for more than 25 bilayers using ellipsometry, because further PEM was totally opaque and lost its shinny surface. It was obviously observed from **Figure 4-9** that PEM (PEI(HA-Na^+/PEI-Mal-C)$_{25}$) converted from one growth regime to another and in between there was a switching point. According to this observation it was important to investigate such PEM by calculating differences between the measured bilayers thickness and investigate the area before PEM growth transition (1st bilayers to 9th bilayers) for Approaches A-C (Appendix, **Figure 8-20 a**). It was observed that PEM has grown in anomalous phase and this was followed by a switching point at the 10th bilayer, which in turn was followed by approximately constant growing regime (Appendix, **Figure 8-20 a**). For the area exist before the switching point (Appendix, **Figure 8-20 a**), the growing regime for bilayers 1st to 9th was irregular with fast increase in PEM thickness for Approaches A, B and C (Appendix, **Figure 8-20 a**). Appendix, **Figure 8-20 b** shows the area before growth transition which shows an agreement what previously stated.

4.5.2. Discussion for weak/weak system: growth regime and thickness

Weak/weak system with counterpart of equal stoichiometric ratio (1:1) has been built up in the same way as in weak/strong system (**Section 4.4**). Hyaluronic acid is considered as weak polyanion, its charge density varied according to its pH. Light scattering analysis has shown that HA solutions in acidic media degrade randomly. [278] Also at an alkaline pH random chain scission occurs. [325] As it has been explained in **Section 2.11.2**, at alkaline pH, hydrogen bonds which take part in the structural organization of HA chains are destroyed, which results in a large loss of the intrinsic stiffness and the formation of a more compact, flexible random coils. [278] These observations gave more interesting features for more investigations. In other word, on varying assembly pH value of HA-Na^+, it can adopt complex secondary conformational ordering. The ability to change the conformation of the adsorbing HA-Na^+ chains with

different pH values strongly affects the bulk properties of the films. PEM (PEI(HA-Na^+/ PEI-Mal-C)$_{25}$) was built-up via changing assembly pH values of HA-Na^+ opponent to that of PEI-Mal-C (pH 7.5 and 5.5). Firstly, HA-Na^+ solution was adjusted to pH 5.5 (acidic medium) and secondly HA-Na^+ pH was adjusted to pH 8.5 (alkaline medium). It was investigated that in both assembly pH for HA-Na^+ (acidic or alkaline) no PEM was observed onto the surface of substrate. In case of HA-Na^+ acidic assembly pH, it was expected that no layers will be created since in this case the charge density of polyanion is lower than that its neutral pH value. In case of alkaline HA-Na^+, it was expected that stable PEM will be established when alkaline polyanionic HA-Na^+ countered the protonated polycationic PEI-Mal-C at pH 5.5. Since, both of polyions have the highest charge density, the highest charge affinities toward each other and the same stoichiometric ratio toward. Unfortunately, the whole PEM was also destroyed. These observations may help in emphasizing the previous observations related to HA-Na^+ responds toward different pH values. Destroying HA-Na^+ backbone and losing it steric nature and conformational changes are higher than it has been expected (**Section 2.11.2**). But to answer the question: Why PEMs of acidic and alkaline HA-Na^+ pH assembly did not reproduce on surface of the charged substrate? More investigations have to be performed in this direction. The successful PEM build-up was achieved only when HA-Na^+ was assembled at its physiological pH value (pH 7.5) with PEI-Mal-C (pH 7.5 and 5.5). Therefore, HA-Na^+ prefers to keep its nature than its charge density being adjusted against the PEI-Mal-C to build up PEM (PEI(HA-Na^+/PEI-Mal)$_{25}$) fabricated by Approach A, B and C.

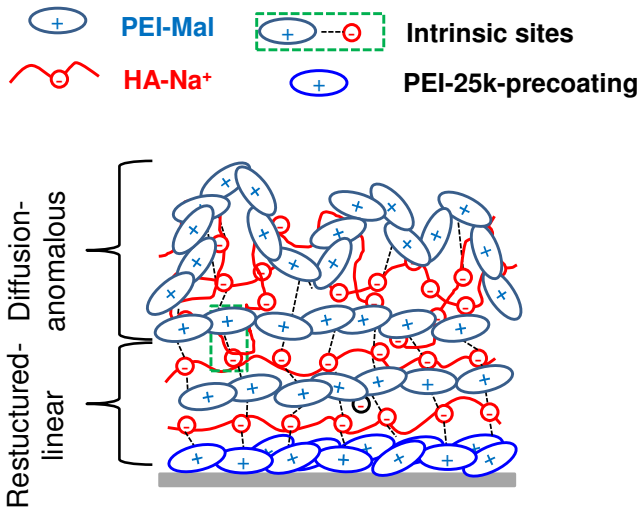

Scheme 4-5. Simplified represents the internal structure of PEM (PEI(HA-Na^+/PEI-Mal-C)$_n$) for approaches A-C, where two different growth mechanisms are quietly exist in the same system, i.e. n represented the number of bilayers.

As it has been discussed previously, both PEI-Mal-C and HA-Na^+ in their neutral pH have a certain degree of flexibility. This segments flexibility affects in turn the PEM growth mechanism and the reproducibility. **Figure 4-9** gave a rough estimation about the growth regime of PEM (PEI(HA-Na^+/PEI-Mal-C)$_{25}$).The construction of PEM (PEI(HA-Na^+/ PEI-Mal)$_{25}$) took place over two buildup regimes. The first one is characterized by the formation of anomalous layer thickness increase, **Figure 4-9** was zoomed-in in **Figure 8-20 b**, showing only the first stage of the building up till 9th pair deposition. The second regime has started once reaching the 10th pair deposition. The PEM regime was switched to linear growing up regime, where the bilayers increased monotonically in thickness (**Figure 4-9**)**.** The only logical explanation for this phenomenon is due to the segment flexibility for both counterparts, that both HA-Na^+ and PEI-Mal-C were diffusing in-and-out of PEM structure. This kinetic transition helps to produce PEM that contains two diffusing species simultaneously in the same structure (**Scheme 4-5**). This also has implications for the dynamics: while the inner layers are very stable and rigid due to the motional restriction of the multiple electrostatic interactions, however the outer layers part is less dense and much more mobile (**Scheme 4-5**). This growing up regime has been shown for the three approaches but it was less pronounced in case of Approach C (**Figure 4-9**). These results can remarkably explain that there was a kind of combination between outer interdiffusion-anomalous and inner restructured-linear growing layers in one PEM by alternating deposition of PEI-Mal-C/HA-Na^+ (**Scheme 4-5**). As it has been discussed previously that PEM transition from one growing regime to another happened when one or both PEM's PEs are diffusing in and out of PEM structure. In case of Approach C: protonated PEI-Mal-C gain some stiffness portions, which in turn are restricted its flexibility and interdiffusion to the inner bulk of PEM structure. Meanwhile HA-Na^+ was still in its worm-like shape at pH 7.5 and did not hinter its in and out diffusion feature. This help to compensate the excess cationic charges, not only for the outermost layer but also the entire PEM structure. In contrary for Approach C: total transition to kinetically blocked regime has been observed, where PEI-Mal-C lost part its flexibility (**Figure 4-8 b**). As it has been discussed in **Section 2.11.1**, HE-Na^+ is characterized with its rod-like structure. However in weak/weak system, Approach C is still enjoying two different growing up regimes (Appendix, **Figure 8-20 a**). In the discussion of weak/strong system it was proven that the growing regime was greatly depending on the pH of the polycation PEI-Mal, while in case of weak/weak system, both polyions are weakly charged, their charged densities changed according to their solution pH and this in turn affects PEM growing behavior. The higher

thickness which was demonstrated in case of Approaches A and B was greatly diminished by factor 3.5 comparing to that PEM fabricated with Approach C.

It is important to attract reader attention to Approaches A and B and to have a small comparison between weak/weak and weak/strong systems. The situation in case of weak/weak system was totally different than that of weak/strong system. In case of weak/weak system, the effect of the precoatings PEI-11 and PEI-9.5 were not clearly shown in (**Figure 4-9**)**,** especially after transition, in contradiction to what have been already discussed for weak/strong system (**Figure 4-8**)**.** These results may imply that the growth regime and the PEM thickness are greatly influenced by the coated substrate when PEM counterpart charge affinity to each other is weak and there is a large mismatch between both used polyions. However in case of weak/weak system, PEI-Mal-C charge density is slightly increased than that of HA-Na^+ (**Table 4-3**). This affected both the stoichiometric ratios and PEM growth mechanism; in addition it neglected the effect of precoatings on the true fabricated PEM. Therefore both Approach A and B were similar despite the different beginnings.

As has been well reported in literature, the inter-diffusion of PEs can be found specifically in the superlinearly or exponentially growing films of LbL deposition. This work results were been also observed by Madaboosi *et al.* in 2012, [166, 327] although they have used PEM of weak/weak system using PLL and HA (PLL/HA)n , n = 12- 96 pair deposition. The PEM was built by using the dipping method. Both polyions were of linear chain structure. They measured PEM $(PLL/HA)_n$ thickness, in order to better understand their growth behavior. Two methods were used to determine the thickness. The first one was the scratch-and-scan method. It was comprised by the removal of a small part of the film and subsequent imaging the surface with a scanning probe AFM. The second method was the full-indentation method. The total penetration depth in a force measurement has already been used to determine the thickness of nanometer-scale coatings. They compared both methods together in order to confirm their results. Their PEM was highly reproducible. The film thickness increased with a quiet high rate from about 0.4 to 7µm for n= 12 and n= 96 bilayers deposition, respectively. They explained this high reproduction and increase in PEM thickness, that PEMs $(PLL/HA)_n$ are known to be highly hydrated and less ordered. It has been previously suggested that they grow exponentially up to a certain bilayer number and thereafter the growth regime switched to linear one. For the dry

state, a transition from exponential to linear growth was observed for n= 10 -18 depending on the PE molecular weight. [153, 169, 328]

In 2008, Yoo *et al.* [329] also studied the phenomenon of the inter-diffusion and the mobility of PEs during the electrostatic LbL assembly and that the inter-diffusion can particularly affect the final morphology and structure of the desired PEM. They investigate a self-assembled PEM of LPEI and PAA by adsorbing charged virus onto the surface of PEM. They reported that the high mobility of LPEI may be attributed to its relatively low pK_a (100% secondary amines with pK_a ~ 5.5, [330] compared to the higher pK_a of primary amines (pK_a ~ 9.0-10.0) in polycation such as poly(allylamine) or other primary amine containing polymers). [207] They also mentioned that one of the most advantages of using a weakly charged PE such as PEI is that its ionic interactions with other charged groups can be readily tuned by the manipulation of assembly pH. They focused on the pH range between 3 and 5.5 where LPEI exhibit notable changes in the degree of ionization and the structure stability of thin PEM LPEI/PAA was maintained. The inter-diffusion behavior of PEM LPEI/PAA during assembly led to very thick top layers (200-800nm, for 11 to 15 bilayers, respectively) of PE on the ML surface once a certain bilayer thickness has been achieved. The top LPEI layer led to greater mobility because there was (**i**) a decreased effective ionic cross-link density between polymer chain segments in such films, enabling greater overall chain mobility within the film surface layer, and (**ii**) this thicker layer of more weakly associated LPEI chains in the top layer also led to more swollen, hydrated (i.e., plasticized) films. These two effects resulted in a surface on which mobility is greatly enhanced, compared to the surfaces of more compact thin films assembled under linear growth conditions. [329]

Yoo *et al.* [329] investigated that the low roughness of PEM LPEI/PAA was likely due to the surface annealing effects of the mobile LPEI top layer under hydrated conditions, and that improved with increasing pH (decrease in rms roughness from 1.5 to 0.3 nm with increasing the assembly pH 3 to 5 was obtained for the LPEI outermost layer in LPEI/PAA ML films deposited at this pH values). Intriguingly, film growth exhibited two different characteristics depending on the pH condition of film deposition: a linear growth profile under pH 3.5 (degree of ionization of LPEI 70% to 80%, pK_a of LPEI 5.5),[331] and a superlinear (exponential) growth above pH 4.0 (degree of ionization of LPEI was 60%). As the film deposition pH is increased, the PEM LPEI/PAA exhibited a

more prominent tendency toward exponential growth in thickness, which indicates the enhanced magnitude of LPEI interdiffusion for virus ordering. Under this condition, an increase in the number of bilayer deposition led to an increasingly thicker layer of top LPEI and greater mobility of the film at the top surface. On the other hand, at a lower assembly pH condition: the highly charged LPEI lacks the ability to inter-diffuse and is kinetically locked to the oppositely charged surface upon adsorption, much as a strongly charged PE rendered a linearly growing film. They also demonstrated that even the exponential growing films after reaching a thickness above 300-400nm, exhibit a linear growth characteristic. [329]

4.5.3. Topology and homogeneity of PEM characterized by AFM

The weak/weak PEM topology prepared by Approach A, B and C was investigated using AFM spectroscopy. Namely, film morphology and surface roughness are important parameters in determining the surface friction of fabricated PEM. PEM surface morphology was investigated with the AFM for 10 and 25 bilayers for all the three approaches (Appendix, **Figure 8-17- 8-19**). One of the most important characteristics of the images obtained by scanning AFM is 3D geometry of the objects which allows a detailed analysis of their morphology along the drawn profiles and performing morphometry (Appendix, **Figure 8-17 - 8-19**). It was deduced from AFM images that multilayers maintain a homogeneous structure and no cracks or pores have been observed on the PEM surface (Appendix, **Figure 8-17 - 8-19**), even for the lower number of bilayers (10 bilayers). Interestingly, rms calculated by AFM for all approaches was lower than in case of weak/strong system. The rms for PEM (PEI(HA-Na^+/PEI-Mal-C)$_{10}$) was of values 18, 20 and 30 for Approach A, B and C, respectively. However for 25 bilayers, the rms values were 1, 5 and 10 for Approach A, B and C, respectively, where PEM has become really homogenous and flat.

The represented PEM with highly smooth surface and lower rms values for all the fabricated approaches will be discussed according to similar published results. In this part, plenty of published data have discussed the role of polyions charge affinities and their properties on the smoothness of PEM surface. Picart *et al.* [153] fabricate PEM of 8 bilayers from PLL and HA. They reported that after an appropriate number of layering up depending on the kind of polyions and their charge affinities to each other, neither

individual islands nor islets were visible any more. All these structures seem to have coalesced, leading to the formation of an almost uniform film.[153] They also scratched the smooth surface of PEM $(PLL/HA)_8$ and they found that underneath the ML does not behave as a hard but rather a viscoelastic gellike material. [153]

The properties of the outermost layer of the films are also dependent on the conformation of the absorbed chains. Such behavior is in accordance to the viscoelastic properties and the gel-like structure of HA-Na^+. [332] The outermost layer for the PEM (PEI(HA-Na^+/PEI-Mal-C)$_{25}$) was HA-Na^+, this profoundly affected PEM rms value. It was also reported by Zinoviev *et al.* [333] that the morphological structure of HA-Na^+ was mainly represented by globular formations forming a branched 3D structure with complexes from tens to hundreds of nanometres in diameter. [333] The surface morphology of the films with different ratios of HA-Na^+ was investigated by AFM. Xu *et al.* [334] fabricate a hybrid film of chitosan (CHI) and HA-Na^+ on a glass substrate. The film of pure CHI shows a relatively smooth surface morphology. Along with the incorporation of HA-Na^+, the resulting films become rougher and aggregates can be observed on the surfaces. The size of these aggregates enlarged with the increase of the HA amount. [334] Also, Picart *et al.* [153] addressed that HA-Na^+ deposited directly on a bare silica surface exhibit small globular structures of one hundred nanometers. [153] In addition, the surface chemistry of weak PEM films was sensitive to the PEM assembly pH value. AFM microscopy studies revealed that the surface friction of a PEM (PEI(HA-Na^+/PEI-Mal-C)$_{25}$) can be varied by as much as an order of magnitude depending on the assembly pH conditions. From Figures (Appendix, **Figure 8-17 – 8-19**) it can be observed that rms of Approach C > Approach B > Approach A.

4.5.4. Conclusion for weak/weak system PEM progression

In summary, it is important to know that the growing regime for PEMs mainly depends on: (**i**) kinetic interaction affinities between polyions (**ii**) conformational changes of polyions (**iii**) pH responsive effect that also affects weak polyions. In studying weak/weak system, linear restructured growing regime was observed where mixture of inner kinetically blocked restructured-linear and terminally anomalous top layers mixed together in the same built-up system. Weak/weak system fabricated by Approaches A-C showed a transition after the 10^{th} layer deposition. However in case of Approach C, PEM

thickness was much lower than in Approach A and B and its transition was less pronounced. This was assumed to rely on the fact that PEM fabricated by Approach C, where PEI-Mal-C was protonated (pH 5.5) and gained more stiffness portion. Meanwhile, HA-Na^+ (wormlike structure) was still in its neutral pH (pH 7.5), keeping its dynamic nature and mobility.

With respect to functionalization, the anomalous growing parts of the constructed PEM can be used as containers for different biomolecules, allows cascades-like reactions and in particular seems to have a great potential for exchange processes. PEM/ATP loading and release will be shown later on (**Section 4.7**)

4.6. Influence on swelling in Millipore water, NaCl and buffer solution

The high stability of PEMs is attributed to the large number of electrostatic and non-electrostatic interactions formed between PEM counterparts in subsequent layers. However, if the strength of these single interactions is decreased, the probability of desorption of a full polyion chain increases and the overall layer stability is affected. In fact, in case of reduced polycation–polyanion interactions instable layers are found. One example is the swelling and reduction of the interaction strength in salt solution, which can eventually lead to layer deconstruction.[335, 336] Kovacevic *et al.* [198] have explained stability issues in terms of a phase diagram, which describes PEMs as a glassy state at low ion concentration C_{ion}, 'liquid-like' at higher C_{ion}, and uncomplexed at very high C_{ion}, making the assumption of thermodynamic equilibrium (**Section 2.6.2**). The addition of polyions or salt to the 'liquidlike' phase leads to a shift into the phase of soluble complexes, and thus causes layer dissolution. Such a model picture shows the sensitivity of PEM stability on the strength of the interactions between single segments. The correlation of local interactions with overall ML properties is certainly a direction towards further descriptions of PEMs. [198] It is also worth to mention that equilibrium degree of PEM depends on the degree to which polymer network swell which is in turn governed by the elastic attractive force of the polymer chain, the thermodynamic compatibility of polymer and the swelling solutions features.[337]

One question that arises from **Figure 4-8** and **4-9** was: what is the possible relationship between the growth regime of the PEM and its stability? To answer this question, it was important to test PEM stability for both weak/strong and weak/weak systems toward different pH values and ionic strengths buffer solutions. To elaborate on the relationship between the film growing regime and coherent surface stability of PEMs, the swelling behavior of all discussed systems was examined by stepwise ellipsometric measurements under the effect of NaCl (0.1M), PBS buffer and Millipore-water, for four successive days.

4.6.1. Weak/strong system and swelling behavior investigated by ellipsometry

4.6.1.1. Results: swelling and stability of PEMs in Millipore water and NaCl buffer solution

In addition to study the dependence of the surface properties and PEM growth mechanism of PEM (PEI(PEI-Mal/HE-Na^+)$_{50}$) on different assembly pH values (Approaches A-C), bulk swelling behavior of these fabricated PEMs using immersion solutions of different pH and ionic strength must be investigated. Usually the degree of swelling was measured by the swelling ratio between dry and swollen conditions using ellipsometry. Degree of swelling %= 100 ($d_{swollen\ state} - d_{dry\ state}$)/($d_{dry\ state}$) (Experimental, **Eq. 6-6**). [338] The strictly focused point is to determine the swelling and stability of different PEMs composed of 50 bilayers deposition prepared by the Approach A, B and C. The level of swelling of PEMs in an aqueous or physiological environment is a critically important parameter, when intending to use PEM as a functional biomaterial coating for controlled drug delivery. PEMs (PEI(HE−Na^+/PEI-Mal-B)$_{50}$) prepared from salt-free solutions were soaked in salt-free immersion solution, e.g. Millipore water (**Figure 4-10**). Both PEMs (PEI(HE−Na^+/PEI-Mal-B)$_{50}$) and (PEI(HE−Na^+/PEI-Mal-C)$_{50}$) were also examined in salt solution, e.g. NaCl solution (0.1 M) (**Figure 4-11**) and in physiological PBS buffer (**Figure 4-12**). PEM (PEI(HE−Na^+/PEI-Mal-B)$_{50}$) fabricated by Approach A, B and C have been scanned for their swelling behavior in Millipore water for 4 days (**Figure 4-10).** These scanned figures directly presented the degree of stability over time. In case of Approach A, B and C the swollen thickness at zero time were ~375 nm, ~400 nm and ~465 nm, respectively. PEM fabricated by Approach C exhibited the highest degree of swelling. Burst PEs release has been associated for all fabricated approaches for

the first ~15 min seen by PEM thickness reduction. PEM thickness for Approach A, B and C was reduced till reaching ~260 nm, ~310 nm and ~450 nm, respectively. All approaches have shown after ~15min a kind of high stability conditions in Millipore water (**Figure 4-10**).

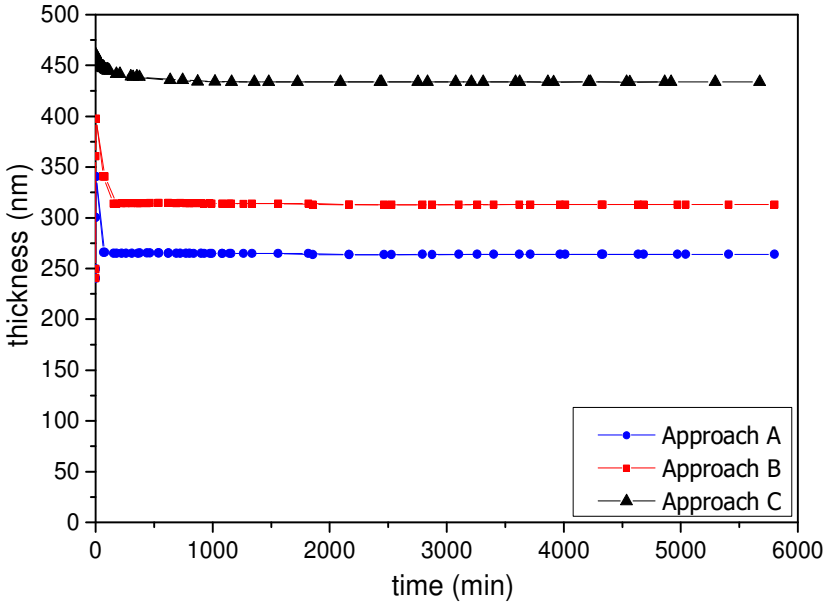

Figure 4-10. In-situ ellipsometric measurements of PEM (PEI(HE–Na^+/PEI-Mal-B)$_{50}$), fabricated by Approaches A-C, which represented time (min) versus film thickness (nm) for 50 bilayers deposition, soaked in Millipore water

The stability which has been shown in charged-free medium was followed by another investigation. It was important to check swelling and stability in a charged medium. PEM (PEI(HE-Na^+/PEI-Mal-B)$_{50}$) and PEM (PEI(HE-Na^+/PEI-Mal-C)$_{50}$) have been immersed in NaCl (0.1M) for one day (**Figure 4-11**). In case of Approaches A and B, PEM (PEI(HE-Na^+/PEI-Mal-B)$_{50}$) has swollen to thickness of ~500nm then degraded suddenly within no time (**Figure 4-11a**). However, in case of Approaches A and B for PEM (PEI (HE-Na^+/PEI-Mal-C)$_{50}$) , it has shown better stability than PEM (PEI (HE-Na^+/PEI-Mal-B)$_{50}$) in NaCl solution (0.1M). PEM (PEI(HE-Na^+/PEI-Mal-C)$_{50}$) has swollen to thickness ~ 4000 nm, they stood steady over about 250 min and this was directly followed by a sudden PEM degradation (**Figure 4-11 b**). For (PEI(HE-Na^+/PEI-Mal-B)$_{50}$) and (PEI(HE-Na^+/PEI-Mal-C)$_{50}$) fabricated by Approach C, They have shown a higher stability with no kind of degradation over the whole examined time (1 day). In case of PEI-Mal-B and –C, both PEMs have swollen to thickness ~500 and ~530, respectively. PEMs

have shown no kind of burst degradation, they swollen form zero time and stood steady (stable) for 24 hours.

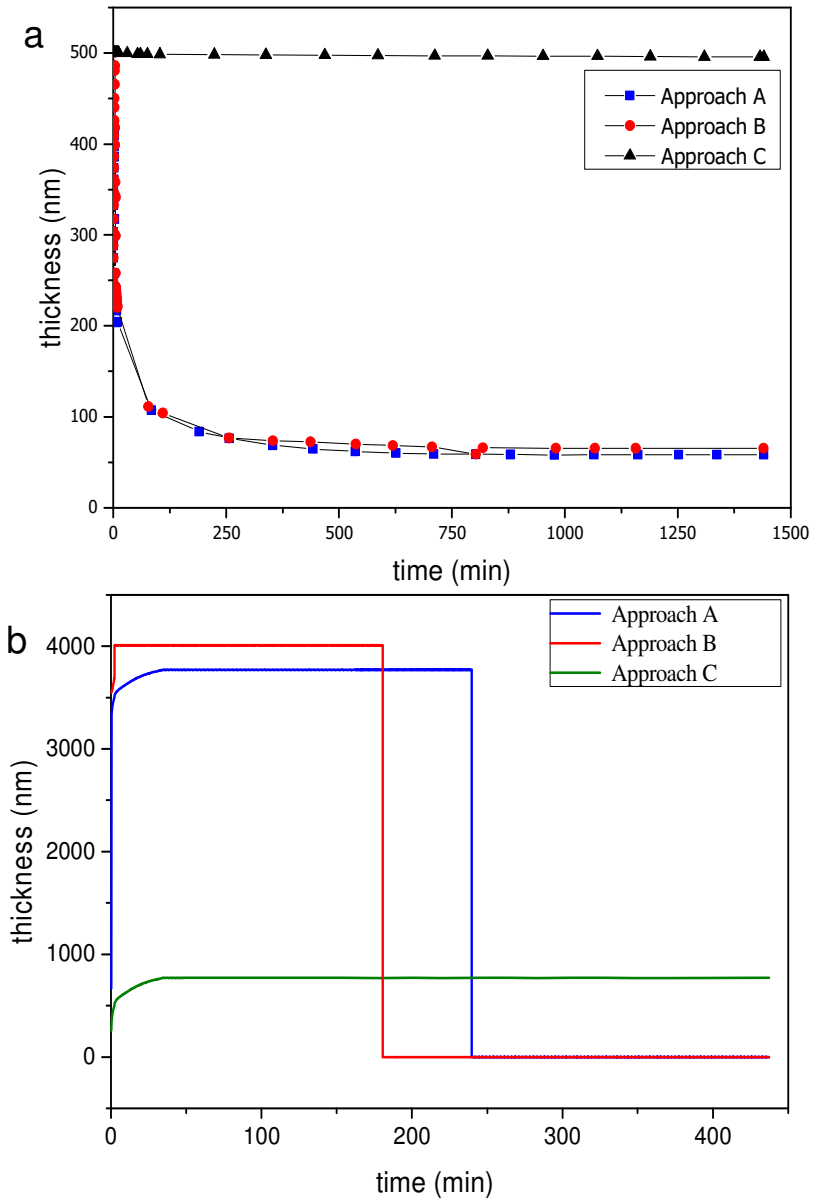

Figure 4-11. Swelling and stability properties of PEM $(PEI(PEI\text{-}Mal/HE\text{-}Na^{+}))_{50}$ for 50 pair deposition. PEMs have been fabricated by Approaches A-C and immersed in NaCl (0.1M) at pH 6.4 for 1 day. In situ ellipsometric measurements in respect to time (min) versus film thickness (nm) for PEM: a) PEI-Mal-B and b) PEI-Mal-C.

4.6.1.2. Results: swelling and stability of PEMs in PBS buffer at pH 7 .4

The most promising results can be observed for the PEM stability and swelling under physiological PBS solution at pH 7.4 and concentration, 137 $\times 10^{-3}$ M NaCl, 2.7

$\times 10^{-3}$ M KCl and 0.01 M phosphate (**Figure 4-12**). Degree of swelling was calculated via equation shown in **Table 4-5** and **4-6** (Experimental, **Eq. 6-6**). For example, the stability of PEMs in physiological PBS buffer was determined by the comparison of dry film thickness before and after swelling experiments (**Table 4-5**) and further indications of PEM stability can be obtained by analyzing the run of constant and/or inconstant refractive indices within this experiment series (**Figure 4-12**). In case of Approach A, PEM (PEI (HE-Na^+/PEI-Mal-B)$_{50}$) started with dry thickness of ca. 165 nm. This thickness was raised to reach ~341 nm at zero time and then the swollen thickness was reduced after 96 hours to reach ~146 nm (**Table 4-6**). Degree of swelling (SD%) was calculated (Experimental, **Eq. 6-6**) to give value of about 107 % at zero time (**Table 4-6**). After 96 hours of immersion the dry thickness was re-measured by ellipsometry and it was reduced to record ~60 nm with Δd value of about 105 nm (**Table 4-5**).

Table 4-5. Ellipsometry's study for 50 bilayers (PEI(HE-Na^+/PEL-Mal)$_{50}$) fabricated by approaches A-C; including film thickness *d* in dry state before and after being swollen in PBS buffer of pH 7.4, refractive index *n*, root mean squared error (*MSE*) and Δd = dry state thickness value (before swelling) - the dry state thickness value (after swelling). The average data of the three experiments for *d* were taken.

		Dry state before swelling			Dry state after swelling			
Approach	**PEI-Mal**	***d* [nm]**	***n***	**MSE**	***d* [nm]**	***n***	**MSE**	**Δd [nm]**
A	PEI-Mal-B	165	1.535	11.859	60	1.353	23.56	105
B	PEI-Mal-B	139	1.548	13.968	70	1.378	25.56	69
C	PEI-Mal-B	175	1.506	15.563	170	1.483	20.43	5
A	PEI-Mal-C	1291	1.533	27.103	849	1.411	25.24	442
B	PEI-Mal-C	1149	1.529	9.954	991	1.452	30.38	158
C	PEI-Mal-C	185	1.515	16.708	180	1.508	20.87	5

For Approach B, PEM (PEI (HE-Na^+/PEI-Mal-B)$_{50}$) , the situation was not so far from that of Approach A. Ellipsometry measured starting thickness in dry of ~ 139 nm which re-measured after being immersed in PBS for 96 hours to give value of 70 nm and with Δd of ~69 nm. These results have shown that both Approach A and B for PEM

(PEI(HE-Na^+/PEI-Mal-B) $_{50}$) were not stable in PBS solution and PEMs thickness was reduced with time. Refractive indices were directly proportional to thickness reduction. In dry state, refractive index was recorded for PEM (PEI(HE-Na^+/PEI-Mal-B)$_{50}$) fabricated by Approach A and B, in values 1.535 and 1.548 in dry state, respectively. These refractive indices for the same PEMs after being immersed in PBS for 96 hours gave values of 1.353 and 1.378, respectively (**Table 4-5**).

Table 4-6. Ellipsometry's study for 50 bilayers (PEI(HE-Na^+/PEI-Mal)$_{50}$) fabricated by approaches A-C; including film thickness *d* in dry state before being swollen and the swollen state in PBS buffer [b] of pH 7.4, refractive index *n*, root mean squared error (MSE) and [a] degree of swelling (SD%) [a] . The average data of the three experiments for *d* were taken.

Approach	PEI-Mal	Dry state before swelling	Swollen state 0h			Swollen state 96h			SD%	
		d [nm]	*d* [nm]	*n*	MSE	*d* [nm]	*n*	MSE	0h [%]	96h [%]
A	PEI-Mal-B	165	341	1.363	6.236	146	1.364	9.062	107	-
B	PEI-Mal-B	139	398	1.371	6.210	237	1.373	4.241	186	70
C	PEI-Mal-B	175	400	1.371	4.401	327	1.371	6.051	130	105
A	PEI-Mal-C	1291	3501	1.391	30.853	2655	1.385	44.021	171	106
B	PEI-Mal-C	1149	4002	1.378	15.243	2702	1.379	35.650	248	135
C	PEI-Mal-C	185	309	1.384	20.310	310	1.379	4.486	67	68

[a] Degree of swelling % = 100× ($d_{swollen\ state} - d_{dry\ state}$)/ ($d_{dry\ state}$)

[b] PBS buffer of 137 mM NaCl, 2.7 mM KCl, 0.01M phosphate at pH 7.4

For PEM (PEI(HE-Na^+/PEI-Mal-C)$_{50}$) fabricated by Approach A and B, it has been shown (**Table 4-5** and **4-6**) that those PEMs were unstable. PEM (PEI(HE-Na^+/PEI-Mal-C)$_{50}$) fabricated by Approach A gave starting dry thickness of value ~1.29 µm. This thickness was remeasured after PEM being immersed in PBS for 96 hours, the resultant thickness and Δd was ~849 nm and ~442 nm, respectively. For PEM (PEI(HE-Na^+/PEI-Mal-C)$_{50}$) fabricated by Approaches B: the starting dry thickness was ~1.49 µm and reduced after being immersed in PBS for 96 hours to reach ~991 nm with Δd ~158 nm. It is worth to mention that the refractive indices have shown direct reduction with PEMs

thickness after being immersed in PBS buffer for 4 days. For PEM (PEI(HE-Na^+/PEI-Mal-C)$_{50}$) by Approach A, the refractive index for dry state was 1.533, it was reduced to 1.411 after being immersed in PBS for 96 hours (**Table 4-6**). It was shown that all PEM fabricated by Approach A and B were degradable (**Table 4-6**).

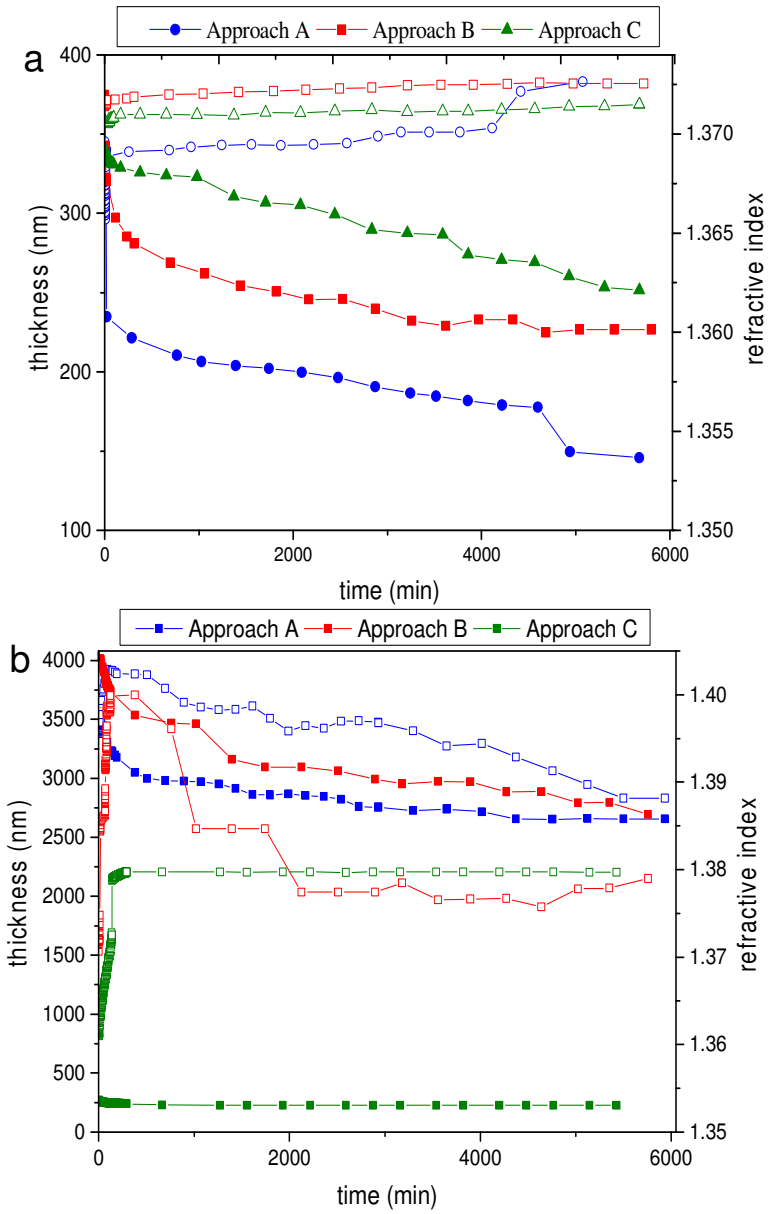

Figure 4-12. Swelling and stability properties of PEM (PEI (PEI-Mal/HE-Na^+)$_{50}$) for 50 pair deposition. PEMs have been fabricated by Approaches A-C and immersed in PBS buffer at pH 7.4 for 4 days. In situ ellipsometric measurements in respect to time (min) versus film thickness (nm) (closed symbol) and refractive index (open symbol) for PEM: (**a**) PEI-Mal-B and (**b**) PEI-Mal-C.

Although PEMs for PEI-Mal-B and PEI-Mal-C bilayers fabricated by Approach A and B outlined the greatest PEM degradation under physiological PBS buffer (**Table 4-5**), it can be obtained from results that Approach A and B for PEM (PEI(HE-Na^+/PEI-Mal-C)$_{50}$) suffered lower degradation than for PEM (PEI(HE-Na^+/PEI-Mal-B)$_{50}$) (**Figure 4-12**, **Table 4-5** and **Table 4-6**). About 50% of PEM (PEI(HE-Na^+/PEI-Mal-B)$_{50}$) bilayers were detached; however only 14% of PEM (PEI(HE-Na^+/PEI-Mal-C)$_{50}$) bilayers suffered degradation. When considering the results presented in **Table 4-5**, **4-6** and **Figure 4-12**, it was possible to notice that within the series of PEMs with PEI-Mal-B as well as PEI-Mal-C, the highest stability for the PEMs was exhibit by PEMs fabricated by Approach C. For PEM (PEI(HE-Na^+/PEI-Mal-B)$_{50}$) and PEM (PEI(HE-Na^+/PEI-Mal-C)$_{50}$), the starting dry thickness was 175 and 185 nm, respectively. In both cases, degradation of PEM thickness was only with Δd of range of ~5 nm (**Table 4-5**). For refractive indices, the dry starting state has shown refractive index of value 1.506 and 1.515 for PEMs (PEI(HE-Na^+/PEI-Mal-B)$_{50}$) and (PEI(HE-Na^+/PEI-Mal-C)$_{50}$), respectively (**Table 4-5**). After PEM (PEI(HE-Na^+/PEI-Mal-B)$_{50}$) and (PEI(HE-Na^+/PEI-Mal-C)$_{50}$) being subjected to PBS for 96 hours , re-dried and re-measured, the refractive indices have shown values of 1.483 and 1.508 for PEMs (PEI(HE-Na^+/PEI-Mal-B)$_{50}$) and (PEI(HE-Na^+/PEI-Mal-C)$_{50}$), respectively.

4.6.1.3. Discussion: swelling and stability of weak/strong system

For discussing the presented swelling and stability results for PEMs fabricated by Approach A, B and C, it was important to give a brief introduction on the differences between PEMs swelling and stability in charged-free and charged immersion solutions. Dodoo *et al.* [211] created two different expressions for explaining water swelling inside the well-fabricated PEM. [211] The two created expressions were ‘void water’ and ‘swelling water’. The differences between the two expressions hanged mainly on the fact that PEM created by formation of island, islets and blob-like structures in the very beginning. These structures later on will coalescence and mutually merge setting a continuous films by the results of layering up (**Scheme 4-3**). In other words when the samples are measured with an optical modulus, e.g. ellipsometry, the change in scattering length density and refractive index of the PEM is reduced with respect to the one of the pure PEs. Dodoo *et al.* [211] explained that when PEM is exposed to charged-free medium, e.g. Millipore water, certain amount of the incoming water permeated and hydrated PEM under investigation changing the data for PEMs thickness and their

refractive index. They called this behavior 'void water' or water hydration uptake, which means that the increase in thickness is only due to water squeezing in between layers and through coalescence sites. In addition it has been already identified that, when layers are totally stable, this water squeezing will not rupture or damage the MLs. [211] In contrary, Dodoo *et al.* [211] also explained that the true swelling led to a highest increase in thickness, and they called this behavior 'swelling-water'. They explained that, 'swelling-water' happened when PEM is exposed to salt or buffer solutions. This is explained by a reduction in complexation sites and densities between opposite polyions related to a transition from intrinsic to more extrinsic charge compensation (**Scheme 4-6**). In turn this transition leads to higher chain mobility, higher degree of flexibility and stronger ability for the system to swell. In addition the solution uptake is controlled by the internal interactions between polymer segments versus those between polymer and solution molecules.[339]

In this study and in case of charged-free immersion medium, e.g. Millipore water (**Figure 4-10**), PEM (PEI(HE-Na^+/PEI-Mal-B)$_{50}$) after being immersed in Millipore water, it started to swell till reaching equilibrium. All fabricated approaches have shown swelling of about two times their thickness in dry state. Millipore permeated and invaded coalescence sites and in-between layers, this led PEM to swell. In case of unstable Approaches A and B, they lost about ~30% and ~22% of their thickness in the swollen state, respectively after being immersed in Millipore water for ~15 min. In case of Approach C, about 3% of PEM thickness in swollen state was lost within the first 15 min of subjection. The results which have been shown in **Figure 4-10**, show that PEM fabricated by Approach C swell in a more pronounced way than PEM fabricated by Approaches A and B. Thickness reduction is mainly due to osmotic pressure exerted by Millipore water molecules on MLs, which lead to PEM rupture and thickness reduction. After 15 min and till the end of investigation (4 days), all PEM structures kept their stability and suffered no more loss in thickness.

In discussing results for PEM (PEI(HE-Na^+/PEI-Mal)$_{50}$) swelling in charged immersion solutions, a typical swelling for weak/strong system has been scanned in NaCl (0.1M) (**Figure 4-11**) and PBS buffer (**Figure 4-12**) over time. All approaches have possessed variable degrees of swelling, thickness reduction and stability behavior for 4 days. When comparing the film thickness before and after swelling (**Table 4-5**, **4-6**) ,

PEMs fabricated by Approach C for PEI-Mal-B and PEI-Mal-C possessed the highest PEM stability for all investigated PEMs under NaCl (0.1M) and PBS buffer conditions. However, the swelling behavior of PEM cannot be only considered to make conclusions about the final PEM stability. Thus, it is important to compare the film thickness and the associated refractive indices before and after swelling experiments.

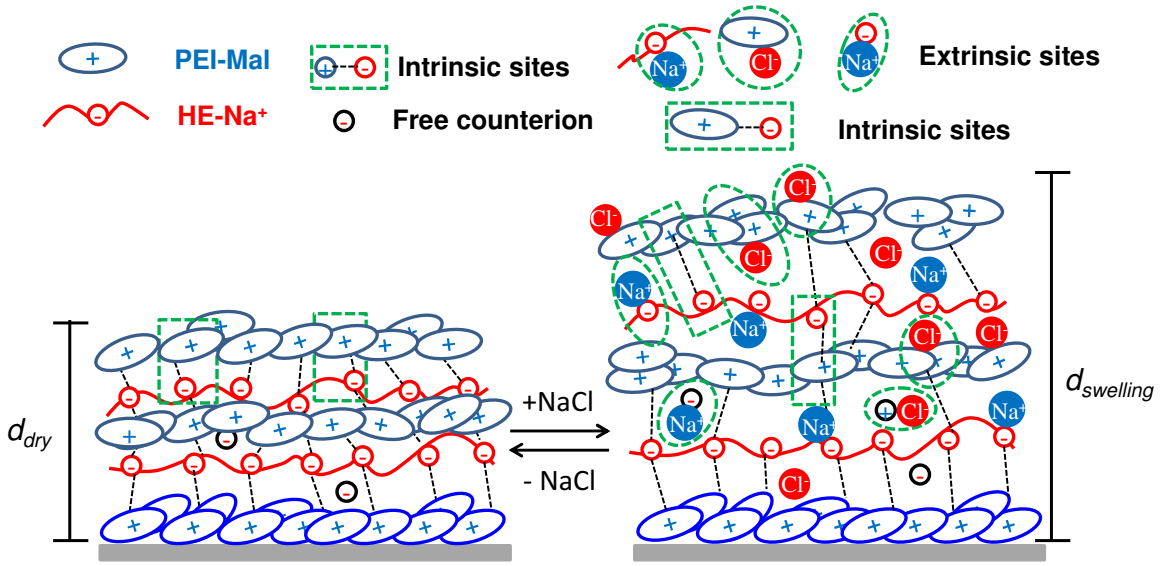

Scheme 4-6. Simplified model explains water swelling expression. However PEM exhibit a pronounced swelling behavior in dependence on the salt concentration for layers immersed in aqueous solution.

In case of NaCl (**Figure 4-11**), MLs swell in NaCl solution (0.1M) due to polymer chain repellence toward each other. This was not only due to the electrostatic repulsion between negative charges, but also due to local increase in the osmotic pressure created by the attraction of counterions in case of non-compensated HE-Na+. Small salt ions penetrated into the layers and competed with the polyion charges for binding sites (**Scheme 4-6**), so that they can release polyion bonds and the degree of complexation will be decreased. Such a release of a fraction of the polyion bonds lead to a more flexible layer arrangement. This intrinsic-extrinsic transition (**Scheme 4-6**) is assumed to be temporary in case of stable PEMs. Once the exerting forces are removed, polyion-polyion complexations return back to their positions. For more specifications, PEMs fabricated by Approach A and B for both PEI-Mal-B and PEI-Mal-C have degraded in NaCl solution (0.1M) in 6 hours (**Figure 4-11**), due to charge distribution in the bulk and near the polymeric surfaces. It is worth to mention that once PEM fabricated by approach A and B were exposed to NaCl (0.1M) a dramatic swelling has been observed and finally this led to

their destruction. However, the swollen state has been stabilized after the protonation of PEI-Mal-B and PEI-Mal-C (Approach C). Approach C was a kinetically blocked structure, where well-structured polyion-polyion complexation was created. Small excess of uncompensated negatively charged sites existed. These conditions created a well-equilibrated system which stood stable for 1 day in NaCl (0.1M). However, in the case of Millipore water as an immersion solution (**Figure 4- 10**), the films prepared by the three approaches A-C have shown a stable feature after a burst degradation (ca. 15 min) for 4 days and this is rational due to the electroneutral condition. Again, using Approach C both cationic PEs fabricate stable PEMs triggered by the presence of high cationic charge of PEI-Mal-B and PEI-Mal-C at pH 5.5 when cationic PEs were adsorbed on the anionic surface of the PEM during layering up. Thus, more stable PECs were formed in the case of Approach C than in the case of Approach A and B. Generally, it can be recognized that large osmotic pressure and screening effects initiated by NaCl solution resulted in a complete degradation in cases of Approach A and B and stable PEM in case of Approach C.

Furthermore, the SD% of PEMs in physiological PBS buffer pH 7.4 was summarized in (**Table 4-6** and **Figure 4-12**) for PEI-Mal-B or PEI-Mal-C. In this case the situation was more complicated than the other two cases, Millipore water and NaCl. The immersion medium was rich with different ions of different ionic strengths and sizes, K^+, $Na2^+$, Cl^-, PO_4^{3-}. In case of Approach A and B, for PEM (PEI(HE-Na+/PEI-Mal-B)$_{50}$) (Figure 4-12 a) and PEM (PEI (HE-Na^+/PEI-Mal-C)$_{50}$) (**Figure 4-12 b**), their performance in PBS was unstable. This was also concluded from the behavior of the observed refractive indices (Table 4-6, **Figure 4-12)**, especially in case of PEM (PEI (HE-Na^+/PEI-Mal-B) $_{50}$). Refractive indices, for Approach A and B for PEMs (PEI(HE-Na^+/PEI-Mal-B)$_{50}$) and (PEI(HE-Na^+/PEI-Mal-C)$_{50}$), fluctuated and showed a kind of unstable reduction (**Figure 4-12 b**). In case of PEM (PEI(HE-Na^+/PEI-Mal)$_{50}$) for both PEI-Mal-B and PEI-Mal-C, the most stable PEM over the whole time of investigation was the one that fabricated by Approach C. The differences between initial dry thickness and the end dry thickness (Δd) has been calculated in value of 5 nm for both PEM with PEI-Mal-B and PEI-Mal-C (Approach C) (**Table 4-5**). PEM (PEI(HE-Na^+/PEI-Mal-C)$_{50}$) fabricated by Approach A, B and C exhibited higher stability than PEM (PEI(HE-Na^+/PEI-Mal-B)$_{50}$) and the highest stability was for PEM fabricated by Approach C (**Figure 4-12**). It can be postulate that the highest stability of PEM (PEI(HE-Na^+/PEI-Mal-C)$_{50}$) compared to PEM (PEI(HE-Na+/PEI-Mal-B)50) fabricated by Approach C was partly reasonable due to the

larger cationic charge density of PEI-Mal-C than PEI-Mal-B structures at assembly pH 5.5 (Approach C) (Table 4-3). Thus in the swollen state, cationic repulsive forces in PEMs were larger than PEMs fabricated by Approach A and B. As it was previously investigate, changing in pH could play the same role as counterion's addition. [204]

4.6.2. Swelling and stability of for weak/strong system investigated by ATR-IR

In order to further support the results from PEM growth and their stability observed by ellipsometry, in-situ ATR-FTIR spectroscopy was used to characterize both the degree of swelling and the degree of stability for all fabricated PEMs. Approaches A and C were used for PEMs (PEI(HE-Na^+/PEI-Mal-B)$_{20}$) and (PEI(HE-Na^+/PEI-Mal-C)$_{20}$), respectively (Appendix, Figure 8-21). PEMs have been built up on an oxidized Si-IRE that was used for the in-situ ATR-FTIR investigation, the experiment was repeated for three times for the same sample. Generally, the ATR-FTIR spectra of PEM (PEI(HE-Na^+/PEI-Mal)$_{20}$) (Appendix, Figure 8-21: after 20 bilayer fabrication in dry state) showed typical absorbance bands at 892, 1028, and 1229 cm^{-1} for HE-Na^+, but also for PEI-Mal at 812, 1459, and 2839 cm^{-1} (Appendix, **Figure 8-21**).

In Appendix, **Figure 8-21 a**, ATR-FTIR spectra of PEMs (PEI(HE–Na^+/PEI-Mal-B)$_{20}$) (upper panel) and (PEI(HE–Na^+/PEI-Mal-C)$_{20}$) (lower panel) in the initial dry state (black spectrum) and in contact to PBS (blue spectrum) are shown. Interestingly, for PEMs (PEI(HE–Na^+/PEI-Mal-B)$_{20}$) (lower panel), the spectrum of the wet state show a higher intensity of the n(SO_2) band (1109 cm^{-1}) due to HE–Na^+ compared to the dry state, whereas for PEM (PEI(HE–Na^+/PEI-Mal-C)$_{20}$) (upper panel), the spectrum of the wet state was lower than that of the dry state. Generally, ATR-FTIR senses swelling processes as a decrease of intensity, since the polymer segments are more diluted in the swollen or wet state. This was the case for PEM (PEI(HE–Na^+/PEI-Mal-C)$_{20}$) in contrast to the PEM (PEI(HE–Na^+/PEI-Mal-B)$_{20}$) . That for the latter case even the wet-state spectrum is higher and can be explained by the increase of the refractive index of the environment increases from n =1.0 (air) to n =1.33 (water). Further analysis of the ATR swelling data (Appendix, **Figure 8-21 a**) resulted in a concentration loss of 29% for PEM (PEI(HE–Na^+/PEI-Mal-B)$_{20}$) and 58% for PEM (PEI(HE–Na^+/PEI-Mal-C)$_{20}$) of polymer segments upon swelling in PBS due to their dilution by the taken up water. Thus, in-situ ATR-FTIR study impressively confirmed the similar swelling and stability features of PEMs fabricated by

Approach A as found under the experimental conditions of in situ-ellipsometric measurements (**Table 4-5**, **4-6**). Thus similar reasons are responsible for the lower and higher degradation of PEM after swelling experiments in PBS buffer at pH 7.4 during ATR-IR experiments: (**i**) lower cationic charge density of both PEI-Mal structures at pH 7.5-8 (**Table 4-6**) tailored the formation of weaker PECs and (**ii**) these PECs in PEMs were not stable enough to withstand the osmotic pressure originated from PBS buffer. Moreover, phosphate ions will also interfere/destroy PECs in PEMs. Furthermore, PEM stability in Millipore water investigated by ATR-FTIR was as high as under the experimental condition of in situ ellipsometry study when fabrication of PEMs based on Approach A. Despite the differently used number of bilayers in PEMs, results of reproducible swelling experiments investigated by in situ ellipsometry and ATR-IR study clearly imply that PEMs fabricated by Approach A are not completely stable under physiological conditions. Moreover, ATR-FTIR spectra of PEMs (PEI(HE–Na^+/PEI-Mal-C)$_{20}$) fabricated by Approach C are shown in Appendix, **Figure 8.20 b**, and were exposed to PBS buffer for 1 day. Analysis of ATR-FTIR swelling data (Appendix, **Figure 8-21 b**) provides a concentration loss of ≤5% for PEMs. Thus, PEMs show a high stability, confirming the ellipsometric results (**Table 4-5** and **4-8**). In contrary to Approach A, Approach C exhibits a high degree of stability for (PEI(HE–Na^+/PEI-Mal-C)$_{20}$), where again strong PECs in the PEMs were presented and resisted the osmotic pressure induced by PBS solution. Finally, this implied the use of pre-swollen PEMs with at least 20 bilayers in future uptake and release of drug to/from PEMs under a physiological environment.

4.6.3. Weak/weak system PEM (PEI(HA-Na^+/PEI-Mal)$_n$) swelling behavior investigated by ellipsometry

4.6.3.1. Results: Swelling and stability of PEMs in Millipore water and NaCl buffer solution

By replacing the strongly charged rod-like PE 'HE-Na^+' by the weakly charged worm-like polyanion 'HA-Na^+' in combination with PEI-Mal-C, new PEMs have been created following the mechanism involved in PEM (PEI(HE-Na^+/PEI-Mal-C)$_{50}$) preparation. It has been previously proved from weak/strong system that the equilibrium SD% of PEM was greatly influenced by film assembly pH as well as the pH of the immersion solution and its ionic strength. It will be shown in this part the differences

between weak/weak system and weak/strong system in the direction of equilibrium swelling.

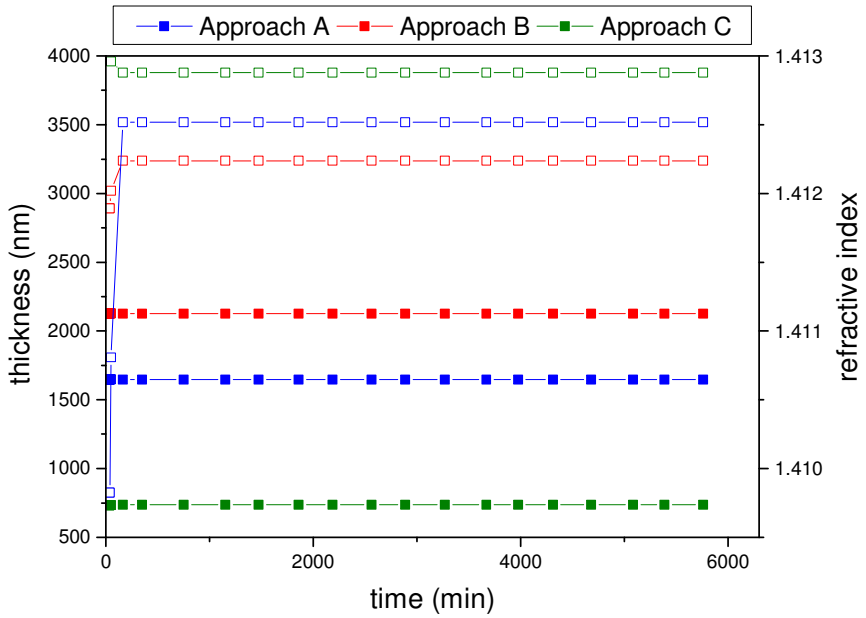

Figure 4-13. In-situ ellipsometric measurements of PEM (PEI(HA-Na^+/PEI-Mal-C)$_{25}$) show corresponding plots of PEM thickness (nm) (closed symbol) and the refractive index (open symbol) of the swollen PEM fabricated by Approaches A-C as a function of time (min) for 25 bilayers deposition soaked in Millipore water

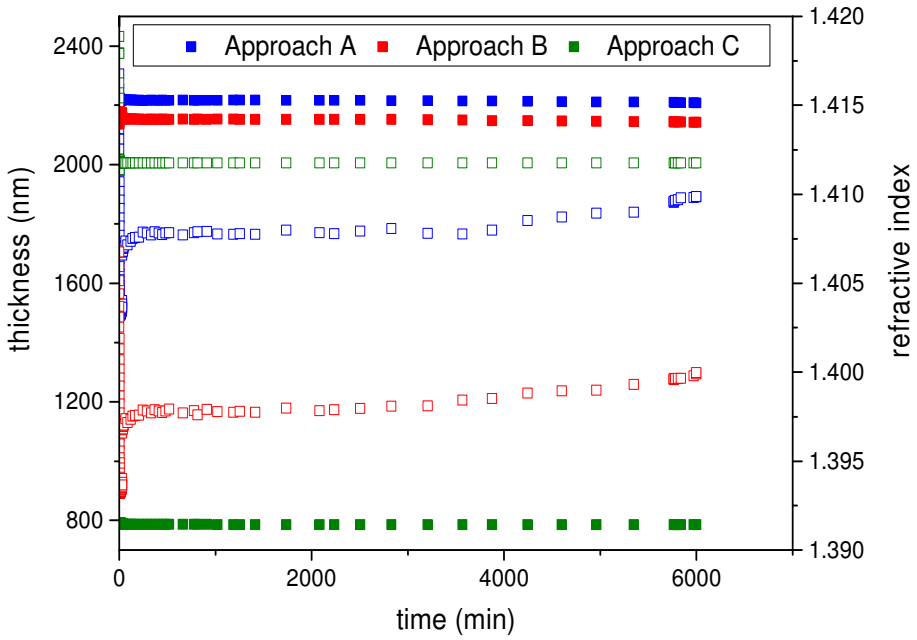

Figure 4-14. In-situ ellipsometric measurements of PEM (PEI(HA-Na^+/PEI-Mal-C)$_{25}$) shows corresponding plots of PEM thickness (nm) (closed symbol) and the refractive index (open symbol) of the swollen PEM fabricated by Approaches A-C as a function of time (min) for 25 bilayers deposition soaked in NaCl solution (0.1M).

In **Figure 4-13**, all of the Approaches A-C for PEM (PEI(HA-Na^+/PEI-Mal-C)$_{25}$) were exposed to Millipore-water for 4 days. The three approaches have shown stable PEMs over the whole exposed period with different degree of swelling. Approaches A and B behaved exactly like in case of weak/strong system. For Approach A (dry thickness: 1.44 µm, immediate swollen thickness: 1.8 µm) and for Approach B (dry thickness: 1.42 µm, immediate swollen thickness: 2.1 µm). Dry thickness of PEM fabricated by Approach C was in the range of nanometer and its swelling behavior was also lower than that of Approaches A and B. Approach C (dry thickness: 479 nm, immediate swollen thickness: 750 nm) (**Figure 4-13**).

Table 4-7. Ellipsometry's study for 25 bilayers (PEI(HA-Na^+/PEI-Mal-C)$_{25}$) fabricated by approaches A-C; including film thickness *d* in dry before being swollen and the swollen state in NaCl (0.1M), refractive index *n*. The average data of the three experiments for *d* were taken.

Approaches	Dry thickness (before swelling) [nm]		Swollen thickness (0 hour) [nm]		Swollen thickness (96 hour) [nm]		Dry thickness (after swelling) [nm]		Dry thickness [nm]
	d	*n*	*d*	*n*	*d*	*n*	*d*	*n*	Δd
A	1440	1.551	2220	1.416	2207	1.409	1415	1.531	25
B	1428	1.545	2216	1.393	2182	1.301	1388	1.525	40
C	479	1.535	790	1.413	785	1.413	478	1.541	-

After showing high stability conditions for all fabricated approaches in charged-free immersion medium, Millipore water, it was important to switch to charged medium. **Figure 4-14** shows the behavior of Approach A, B and C in NaCl (0.1M). It has shown that the most stable approach was Approach C, even the performance of the other two Approaches A and B was not totally unstable in NaCl (0.1M) medium compared to weak/strong system fabricated by Approach A and B. However, PEM degradation for Approach A and B was more obvious in the trend of the refractive indices than in their observed thickness (**Figure 4-14**). Refractive indices trend for Approach A and B was not following that of PEM thickness for the same approaches and this may be due to PEM irregular degradation. [340] The whole PEM (PEI(HA-Na^+/PEI-Mal-C)$_{25}$) behaviors, thickness before and after swelling and refractive indices, fabricated by Approach A, B and C are shown in **Table 4-7**. Data show that compared to weak/strong system, all presented PEMs approaches were not strongly affected by NaCl (0.1M). After four days, differences

in thickness were in range of nanometer and Δ d was calculated in values 25 and 40 nm for Approaches A and B, respectively. In case of Approach C no degradation has been calculated after 4 days.

4.6.3.2. Results: Swelling and stability of weak/weak system in PBS

The most important results observed for PEM stability and swelling under physiological PBS solution at pH 7.4 of conc. 137 $\times 10^{-3}$ M NaCl, 2.7 $\times 10^{-3}$ M KCl, and 0.01 M phosphate are presented in **Table 4-8, 4-9** and **Figure 4-15**.

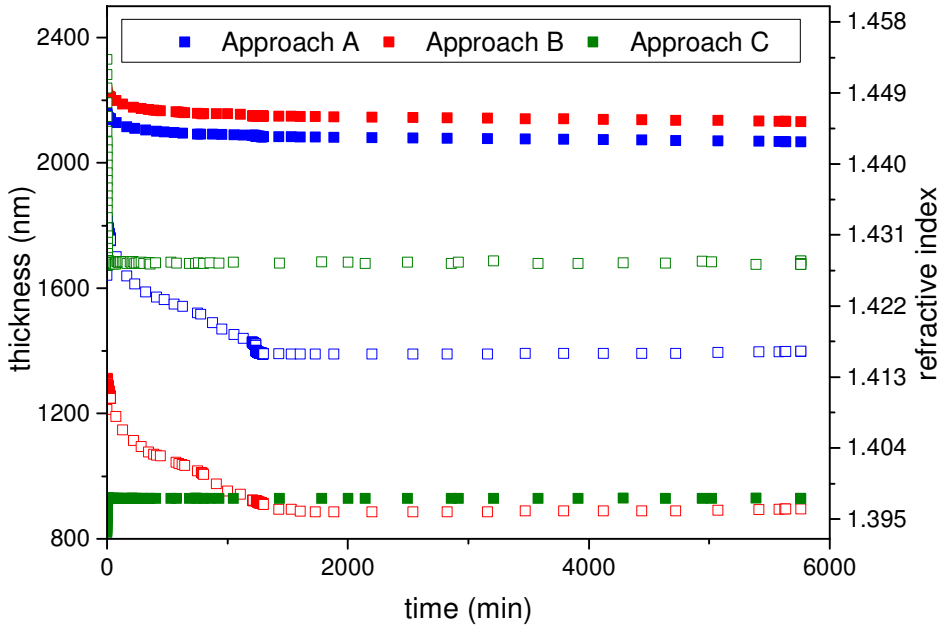

Figure 4-15. In-situ ellipsometric measurements of PEM (PEI(HA-Na^+/PEI-Mal-C)$_{25}$) shows corresponding plots of PEM thickness (nm) (closed symbol) and the refractive index (opened symbol) of the swollen PEM fabricated by Approaches A-C as a function of time (min) for 25 bilayers deposition soaked in PBS buffer.

The swelling behavior in PBS solution has been examined for series of PEMs (PEI(HA-Na^+/ PEI-Mal-C)$_{25}$) and the highest stability for the PEMs was exhibited by PEMs (PEI(HA-Na^+/ PEI-Mal-C)$_{25}$) fabricated by Approach C. Surprisingly, no degradation of PEM thickness has been observed in the dry states, after/before being immersed in PBS buffer solution. The thickness results are shown in **Table 4-8 and 4-9.** In contrary to Approach C, PEMs (PEI(HA-Na^+/PEI-Mal-C)$_{25}$) fabricated by Approach A and B outlined the greatest PEM degradation under physiological PBS buffer with obvious

reduction in refractive indices for both Approach A and B (**Figure 4-15**, **Table 4-8**) where ~ 11% of PEM pair deposition were degraded in case of Approach A, while about 12% of PEMs (PEI(HA-Na^+/PEI-Mal-C)$_{25}$) thickness was degraded in case of Approach B was observed (**Table 4-8**, **4-9**).

Table 4-8. Ellipsometry's study for 25 bilayers (PEI (HA-Na^+/PEI-Mal-C)$_{25}$) fabricated by Approaches A-C; including film thickness *d* in dry before and after being swollen in PBS buffer of pH 7.4, refractive index *n*, root mean squared error (*MSE*) and Δd = dry state thickness value (before swelling) - the dry state thickness value (after swelling). The average data of the three experiments for *d* were taken.

Approach	PEI-Mal	Dry state before swelling for 0hour			Dry state after swelling for 96 hours			Δd
		d [nm]	*n*	MSE	*d* [nm]	*n*	MSE	[nm]
A	**PEI-Mal-C**	1440	1.552	10.859	1282	1.353	23.56	158
B	**PEI-Mal-C**	1427	1.560	15.968	1256	1.378	25.56	171
C	**PEI-Mal-C**	479	1.561	6.563	480	1.523	10.43	-

Table 4-9. Ellipsometry's study for 25 bilayers (PEI(HA-Na^+/PEI-Mal-C)$_{25}$) fabricated by Approaches A-C; including film thickness *d* in dry before being swollen and the swollen state in PBS buffer [b] of pH 7.4, refractive index *n*, root mean squared error (*MSE*) and [a] degree of swelling (SD%) [a] . The average data of the three experiments for *d* were taken.

Approach	PEI-Mal	Initial dry state	Swollen state for 0 hour			Swollen state for 96 hours			Degree of swelling	
		d [nm]	*d* [nm]	*n*	MSE	*d* [nm]	*n*	MSE	SD_{0hr} %	SD_{96hrs} %
A	**PEI-Mal-C**	1440	2160	1.425	11.853	2067	1.416	20.021	50	44
B	**PEI-Mal-C**	1427	2146	1.408	15.243	2053	1.396	25.650	50	44
C	**PEI-Mal-C**	479	720	1.453	9.310	730	1.427	13.486	50	52

[a] Degree of swelling % = 100× ($d_{\text{swollen state}} - d_{\text{Dry state}}$)/ ($d_{\text{Dry state}}$)

[b] PBS buffer of 137 mM NaCl, 2.7 mM KCl, 0.01M phosphate at pH 7.4

In cases of Approach A and B the refractive indices also showed a higher reduction (**Figure 4-15**), where PEM refractive index in dry state measured by ellipsometry was 1.55 and was reduced to value 1.35 for the dry PEM after being subjected to PBS for 4 days (**Table 4-8**). PEMs thickness reduced with Δd with value 158 nm and 171 for Approach A and B, respectively. Degree of swelling (SD%) was also calculated (Experimental, **Eq. 6-6**). The SD% for the three fabricating Approaches A-C was similar for the immediate swelling (0 hour) and gave about 50%. After spending 96 hour in PBS solution, SD% was decreased for Approaches A and B and about only 44% has been calculated. In case of Approach C SD% was constant all over the submersion period.

4.6.3.3. Discussion: Swelling and stability of weak/weak system in different immersion solutions

In this part two different points will be under discussion: (**a**) PEM lower degree of swelling compared to weak/strong system and (**b**) higher degree of stability and its reason in comparison to weak/strong system. Then let's start with the first point of discussion. By replacing rod-like structure HE-Na^+ with worm-like structure HA-Na^+, it is assumed that the variability in the conformational arrangement of polymer chains in weak/weak PEM not only has profound effects on their overall thickness in the dry state and the growth regime, but also it is primarily responsible for the lower SD% that these films experienced when exposed to buffer solutions has ionic strength affinity. [341-343] Moreover, when a film is assembled under highly charged conditions, the layers are stitched together tightly with many ionic cross-links. [341-343] Thus, when exposed to a solution environment, these films experience a partially limited degree of swelling. This assumption has been documented by Mendelsohn *et al.* [199] who reported that only ~10 % increase for PEM (PAA/PAH) thickness, i.e. weak/weak system, has been detected when exposed to an ionic immersion solution. PEM (PAA/PAH) has assembled under pH conditions where both polymers were highly charged in solution. [199] In this study and especially in case of weak/weak system upon exposure to NaCl(0.1M) (**Figure 4-14**) and PBS solution (**Figure 4-15**), PEMs can undergo a SD% of about ~ 50% (1 time) of their original dry thickness (**Table 4-9**). It was proved that the three fabricated Approaches A-C have shown approximately the same swelling percentage behavior although different fabrication conditions were used and different PEM thickness (**Table 4-9**). An example of this retarded ability of weak/weak PEM films to swell compared to linearly growing up

weak/strong system is shown in (Appendix**, Table 8-1).** In case of weak/strong system the kinetic affinities between contained PEs were weaker and the extrinsic-intrinsic replacement was more advanced than in weak/weak system. Therefore, it was postulated that the SD% in case of weak/strong system was higher than that of weak/weak system.

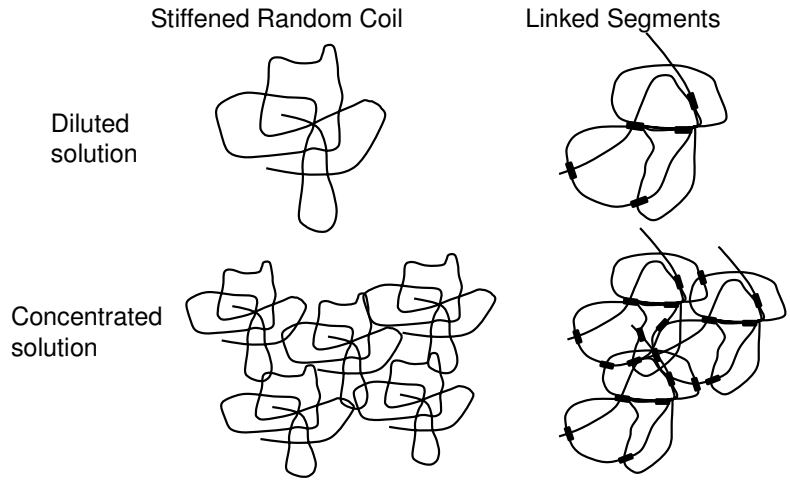

Scheme 4-7. Models of HA-Na^+ behavior in dilute solution. HA-Na^+ behaves as a stiffened random coil. The presence of linked segments would act in opposition to chain stiffening in determining the hydrated domain. In concentrated solution, stiffened random coils show entanglement; they form viscoelastic solutions and retain flow and do not become gels. The presence of linked segments would create a network and lead to gel formation. [344]

In addition, it has been hypothesized that the restructured-linear growth of PEM (PEI(HA-Na^+/PEI-Mal-C)$_{25}$) results from inter-diffusion of PEI-Mal-C in coherency with HA-Na^+ in its gel-like structure (0.5 mg mL^{-1}) in and out of PEM structure (**Scheme 4-7**). It has been discussed in **Section 2.11.2** that HA-Na^+ at its physiological conditions and in concentration starting from 0.5 mg mL^{-1} behave as a stiffened random coil with a range of flexibility in solution (**Scheme 4-7**). In case of Approach A and B, PEM thickness was higher than that of Approach C (Appendix, **Table 8-1** and **Table 4-8**). For Approach C, it was previously assumed that such range of flexibility was only rely on HA-Na^+. This provided a rational basis for understanding the unusual hydrodynamic and rheological behavior of HA-Na^+. [344] The stiffening was proposed to be at least in part due to hydrogen bonding between adjacent saccharides, combined with some effect from the mutual electrostatic repulsion between carboxyl groups. [345] This restricts rotation and flexion at the glycosidic bonds and creates a stiffened yet mobile polymer chain (**Scheme 2-18**). The flexibility and permeability properties of HA-Na^+ network can then be

accounted for in terms of inter-chain hydrodynamics interactions of this extended structure, with entanglement being especially important at elevated concentrations (**Scheme 4-7**). However, even at high concentrations, under physiological conditions, individual HA-Na^+ chain remain mobile and at no stage do HA-Na^+ solution undergo transition to a gel-like state (**Scheme 4-7**). [344] In addition to what previously mentioned, PE hydrogels, e.g. HA-Na^+, typically experience a decrease in swelling as the salt concentration is increased because of electrostatic screening. [346-348] However, it must be noted that hydrogels are covalently cross-linked, which, unlike ionic cross-links, are unaffected by changes in the local ionic strength environment. In the case of PEMs, the ionic bonds that hold the layers together are known to break upon increase in the local ionic strength. [199] These observations may give a reason for this higher stability and lower degree of swelling. This hypothesis is totally obvious in case of the swelling behavior in comparison to what has been observed in case of weak/strong system. The degree of swelling for all fabricated approaches was similar and did not exceed the 50% although different fabricated approaches.

In discussing SD% in case of non-ionic immersion solution, Millipore-water (**Figure 4-13**), the SD% was also retarded in comparison to what has been demonstrated for weak/strong system (Appendix, **Table 8-1**). For weak/weak system fabricated by Approach C, when exposed to Millipore water (**Figure 4-13**), PEM SD% calculated with value did not exceed 57%. Even in the other two Approaches A and B the calculated SD% did not exceed 50% (**Figure 4-13**). It has been discussed before that the main reason causing PEMs swelling in Millipore-water was the forces of hydrophobic interactions (also termed 'bonding') which are generated when multiple nonpolar solutes, or fragments of molecules, associate to maximize contact of outside-water with inside-water, maintaining the structure and hydrogen bonds network. This inside water comes from the PEM preparation itself as by alternating adsorption of polyanions and polycations from aqueous solution are assumed to contain hydration water in their dry state. This hydrogen bond network is temporary removed once the re-drying step is achieved, without changing in PEM primary structure. [349] Evidence was reported by Schwarz and Schoenhoff who applied ^1H NMR transverse relaxation to monitor the hydration water in PEMs. [349] Schlenoff *et al.* [349] also reported hydration contributions to association in PEMs. Dodoo *et al.* [211] analysis was based on neutron reflectivity and indicates no structural change in the dry PEM, assembled in H_2O, dried and subsequently exposed to both H_2O and D_2O for

8 hours and then dried. [211] It is assumed in case of weak/weak system PEM (PEI(HA-Na^+/PEI-Mal-C)$_{25}$), that PEM was more hydrated because the presence of HA-Na^+ in contrary the case of weak/strong system. Also retarded degree of swelling in Millipore water may also due to the higher compensation for the anionic charges (HA-Na^+) in PEM with cationic charges (PEI-Mal-C) (**Table 4-3**).

Secondly, PEM higher stability for weak/weak system especially for Approach C has to be discussed. By comparing this part to the latter (**Section 4.6.1**), both weak/strong and weak/weak system fabricated by Approach A and B, they have shown unstable conditions in case of PBS at physiological pH (Appendix, **Table 8-1**), emphasizing the hypothesis that PEM equilibrium are profoundly influenced and disturbed with both basic/acidic pH and ionic strength of the exposed environment. In contrary, Approach C for both systems has shown very stable conditions in charged-free and charged solution. It has been already discussed that PEI-Mal-C in weak/weak system for Approach A and B was weakly charged and has a portion of flexibility. At this moment an inter-diffusion condition was held between PEI-Mal-C and HA-Na^+ in a way to randomly compensate each other. However for Approach C, PEI-Mal-C was highly protonated in solution and partially lost its flexibility. It was previously assumed that the strongly charged polymers have more rigid structure in solution, and adsorb to surfaces in a fairly flat conformation with a high population of ionic cross-links to the surface. On the other hand, weakly charged polymers tend to be adsorbed on surfaces in a conformation rich in flexibility with much fewer ionic links to the surface per chain. [350] Thus at this moment, the warm like HA-Na^+ at its physiological pH value has the ability to inter-diffuse and polycationic charges, PEI-Mal-C, were successively compensated with successive polyanion, HA-Na^+, deposition. Therefore, PEM (PEI(HA-Na^+/PEI-Mal-C)$_{25}$) assembled at pH 7.5-8 (Approaches A, B) can undergo a great degree of chain extension and segment mobility. Moreover, those PEMs fabricated by Approach A and B adopt a larger thickness and lower swelling equilibrium. In contrary the intrinsic sites of interaction in case of Approach C was strongly created and segment-segments extension was created within a lower limits. This speculation was the most acceptable one to explain the higher stability for PEM prepared by Approach C.

In most cases, the swelling behavior for PEM films is destructive by nature, since exposure to extreme solution conditions, such as high salt concentration can lead PEM to

swell to the point of deconstruction due to breaking of the ionic cross-links that hold the layers together. [351] This condition fits for Approaches A and B in PBS buffer, However, what was surprisingly that the deconstruction point was after 40 hours (**Figure 4-15**). This delay in the PEM deconstruction may be due to the flexibility and the secondary conformational changes which have been created by both PEI-Mal-C and HA-Na^+ and their high kinetic affinities. The deconstruction in Approaches A and B was clear and more obvious in the trend of the refractive index curves which do not mismatch that of PEM thickness curves neither in case of Approach A or B (**Figure 4-14, 4-15**). This may be due to that the degradation way was not homogenous and involved with removing different patches from different positions in PEM. Thus, it was difficult for ellipsometry to follow such heterogeneous structure. The calculated Δd which are shown in **Table 4-8**, emphasize that ca. 158 and 171 nm for Approaches A and B, respectively have been degraded from PEM after being exposed to PBS solution for 4 days. This may be due to unfavorable interactions causing an increase in the extension of the unadsorbed segments in conjunction with the increase in hydration of the chains. [341, 343]

4.6.4. ATR-FTIR investigation for swelling and stability for weak/weak system

The technique of FTIR spectroscopy, including methods of sample presentation such as the attenuated total reflectance (ATR), has been successfully used to examine structures , conformational features, swelling and stability of PEM (PEI(HA-Na^+/PEI-Mal-C)$_{20}$) fabricated by Approach C (Appendix, **Figure 8-22**). The ATR-FTIR spectrum for this system is too complicated and full of overlapped bands due to the complicated network of inter- and intra-molecular hydrogen bonds occurring in HA-Na^+ itself and its own connection toward PEI-Mal-C. Appendix, **Figure 8-23** shows a comparable figure for overlapped spectra of both free casting model of HA-Na^+, PEI-Mal-C and PEM (PEI (HA-Na^+/PEI-Mal-C)$_{20}$). Appendix, **Figure 8-23 c** shows HA-Na^+ bands; at 3600-2800 cm^{-1} is the region of CH, NH, and OH stretching vibrations. A broad band at 3390 cm^{-1} is observed. This band can be assigned to hydrogen-bonded OH groups. However, it was very difficult to find a correlation between these intense OH stretching modes and vibrational states, due to the complicated network of inter-and intra-molecular hydrogen bonds occurring in polysaccharides. [351] At 1500-1200 cm^{-1} is the local symmetry region because it mainly included the deformational vibrations of groups having a local symmetry, i.e., the (HCH) and the (CH_2OH) groups. [351] At 1200-950 cm^{-1} is a region

which includes the highly coupled ν(C-O), ν(C-C), and δ(COH) vibrational modes. This region is sensitive to the conformational freedom of the polymer chains.[352] In addition this region is characterized by four bands centered at 1152, 1078, 1046 and 946 cm^{-1} which are typical for carbohydrates.[353] '' Amide bands'': The three signals centered at 1615, 1560 and 1314 cm^{-1} are assigned to amide I, II and III respectively. [354] ''Carboxyl bands'' : The bands at 1616 and 1413 cm^{-1} are assigned to the asymmetric and symmetric stretching modes of the planar carboxyl groups in sodium hyaluronate, respectively. ATR-IR spectra of PEMs (PEI(HA−Na^+/PEI-Mal-C)$_{20}$) shown in Appendix **Figure 8-22**, were fabricated by Approach C and exposed to PBS buffer for 1 day, the experiment was repeated for three times. Analysis of ATR-FTIR swelling data (Appendix, **Figure 8-22**) provided a concentration loss of about ≤ 60% for PEM (PEI(HA−Na^+/PEI-Mal-C)$_{20}$) fabricated by Approach C . As it has been discussed in **Section 4.6.3** these results may related to (**i**) the growth regime itself and stoichiometric ratios for contained PEs and their kinetic affinities. (**ii**) In case of weak/weak system the nature of the gel-like structure of HA-Na^+ was profoundly influenced the PEMs SD%. It was assumed that HA-Na^+ formed a complicated network structure, which increase with the increase of the layering up. Even it was discussed later that Approach C showed the highest stability when compared to other approaches. ATR-FTIR results confirmed that of ellipsometry (**Table 4-8 and 4-9**). In essence, as it has been discussed previously, this stability is due to the high attractive affinities between both polyions. In particular, increasing the degree of charge of the polycation can hinder the flexibility, as a direct consequence of the increasing number of binding sites due to the high degree of ionic crosslinks and complexation are achieved. Also important are the intrinsic backbone stiffness, that polymer depresses interpenetration and flexibility, in addition to the hydrophilicity, which promotes film swelling and softening in water.

4.6.5. Conclusion for weak/strong and weak/weak systems swelling and stability

One important factor promoting PEM swelling and thus increased mobility is the increase in salt concentration in the external medium exerting ionic strength force on PEM structure. The internal layering and inter-diffusion of PEs within MLs may be further disordered by the influence of external ionic strength. On the basis of these attributes, it was important to check PEMs stability and degree of swelling for both weak/strong and weak/weak systems. All the prepared PEM for all approaches A, B and C were stable in

Millipore water, where no kind of kinetic disturbance actions have been exerted on the surface and the inner bulk of PEMs under investigations.

For both weak/weak and weak/strong systems, Approach C was the most promising way to establish stable PEMs under physiological PBS for future application as drug release system. A possible explanation was that at assembly pH 5.5 both PEI-Mal possessed a high cationic charge density to undergo the desired fabrication of homogeneous and stable PEMs (**Figure 4-12** and **Figure 4-15**). In case of weak/strong and weak/weak systems fabricated by Approach C, PECs formation between the relatively weak cationic PEI-Mal in combination with strong anionic HE-Na^+ or weak anionic HA-Na^+ will not be destroyed in the presence of different ions of different ionic strengths and sizes in PBS buffer that induce osmotic pressure within the PEM. However, PEMs fabricated by Approach A, B are completely or partially degraded in different solutions due to the low cationic charge density of both PEI-Mal at pH 7.5–8.0. In case of weak/strong system HE-Na^+ remains in its fully charged state, therefore the interactions between the different layers were reduced and the excess of negative carboxylic and sulfonate group in the MLs leads to such destabilization. In case of weak/weak system the degradation for Approaches A and B was delayed and was not so high compared to that of weak/strong system. This study provides a proof-of-principle that counterions permeation through the PEM structure may lead to the whole PEM destruction due to the increment of counterion screening effect and intrinsic sites cleavage.

4.7. Stable PEM for drug loading and release

After controlling the stability of the fabricated PEM (**Section 4.6**), it was the task to study the drug efficient loading and release. The most stable PEM was the one fabricated by Approach C for both weak/strong and weak/weak systems. For essence, the model drug can be loaded and released by finely tuning the PEM interior after exposing the PEM system to different ionic strength and pH environment, keeping in mind the initial drug concentration at the very beginning during preparation. The focus in this part is to control the drug loading inside a stable PEM as well improving PEM stability. PEM charge equilibrium must be taken in account during fabrication and drug loading. For drug loading, two different methods have been constructed: The first one was termed as drug

adsorption or 'drug postloading' (**Scheme 4-8**). In this method the model drug, anionic adenosine 5' triphosphate (ATP), was loaded into the porous PEM through adsorption.

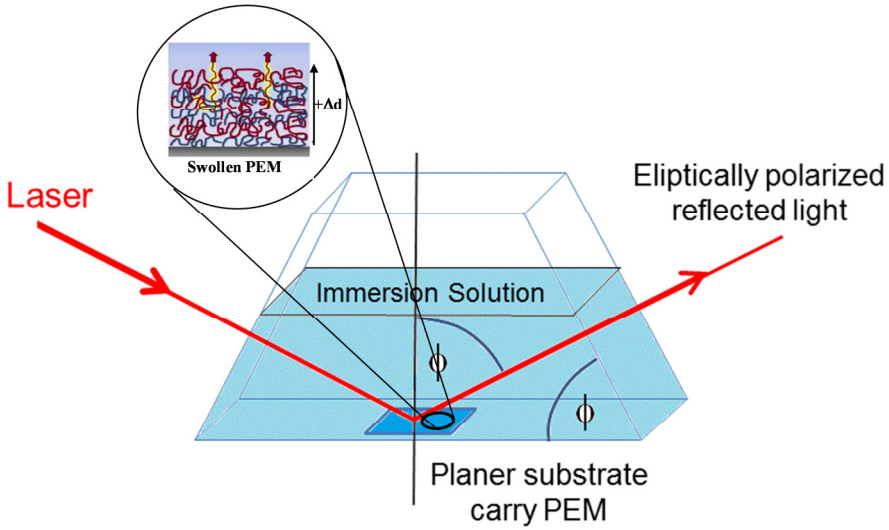

Scheme 4-8. Simplified sketch describes the in-situ ellipsometric procedure for drug postloading mechanism. The immersion solution is changed over PEM and ellipsometry monitor PEM in all steps, swelling, drug uploading and releasing. i.e. ϕ considered as the ellipsometric angle from which the refractive index and thickness of PEM can be calculated.

The second method is so called drug polyions complexation or 'preloading'. In this method PEM deposited was adjusted by preparing equal charge strength of the anionic drug (ATP) and the used polyanion. ATP was mixed/complexed with both polyanions and polycation (**Scheme 4-9**). The chosen concentration was depending on the molecular weight of the respective monomer units of the used polyanion. In order to seek for the most equilibrated system for achieving the highest uptake efficiency, different molar ratios of polyanion:ATP (PA: ATP), 3:1, 1:1, 1:2 and 1:3, were prepared. According to these ratios, polycation: ATP (PC: ATP) ratios were also calculated according to their molar masses. The calculated PC: ATP values in descending arrangement were 1: 35, 1:29, 1:23 1:18, 1:12 and 1:5, for ATP mass values with descending arrangement 0.6, 0.5, 0.4, 0.3, 0.2 and 0.08 mg mL^{-1}. A fixed mixing ratio PE: ATP of 5:1 was used for both polyanion and polycation.

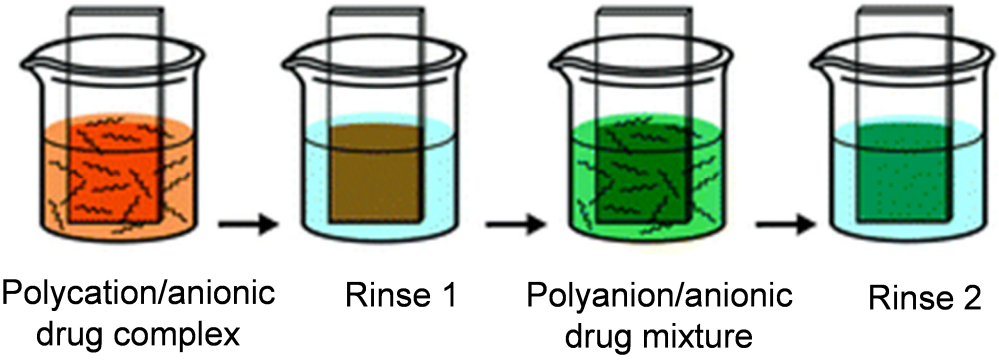

Scheme 4-9. Simplified sketch describes the PEM building-up in combination with model drug. Model drug is mixed with both polyanion and polycation solutions. Each deposition is followed by a rinsing step in Millipore solution.

Releasing step was performed by applying several rinsing steps to the PEM, where all samples were submerged in different physiological pH values and salt concentrations, e.g. Millipore-water, HEPES buffer (0.05M), PBS (0.01M) and NaCl (0.1M). The release of drug was monitored using in-situ ATR-FTIR and in-situ ellipsometry. In-situ ATR-FTIR, release measurements were performed by flowing 20 mL of release solution in a closed-loop mode at a flow rate of 5mL/min. In ellipsometric measurements, all measurements were in-situ measurements in quartz cuvette (**Scheme 4-8**). For ellipsometry the swelling solution was removed followed by the step of ATP addition and later several rinsing steps were established. It must be taken in account that PEM surface must be all the time stored under wet condition and in swollen state.

4.7.1. Main properties of Adenosine 5'- triphosphate (ATP)

Adenosine is a chemical presents in all human cells. It is difficult to speak about adenosine role in human body as it needs a lot of discussion to explain how it plays importantly in , out and in-between the human cells, i.e. in controlling nervous system, muscles contraction …etc. ATP is considered as an important drug model, which applied for different diseases. ATP (**Figure 4-16)** is sometimes used as emulsion to increase physical energy. It is also given intravenously for treating acute kidney failure, multiple organ failure, high blood pressure in lung arteries (pulmonary hypertension), cystic fibrosis, lung cancer, weight loss associated with cancer, and controlling blood pressure during anesthesia and surgery. [355, 356] Healthcare providers give adenosine

intravenously for treating surgical pain and nerve pain, pulmonary hypertension, and certain types of irregular heartbeat. [357] It is also given for controlling blood pressure during anesthesia and surgery.[357] Intriguingly, ATP is also considered as an anionic charged molecule. Therefore after being inserted into and PEM structure, it may be typically treated as a negatively charged couterions that affect PEM system morphology, stability, growth regime and equilibrium. Therefore, two types of interactions between ATP and PEI-Mal can be considered in the complex formation: electrostatic and H-bonding (**Scheme 4-10**). Electrostatic interactions exist between the cationic PEI scaffold of PEI-Mal and phosphate groups of ATP. This type of interaction is widely discussed in literature.[56, 358] The latter type of interactions is H-bonds between hydroxyl and amine groups of ATP and the maltose shell of PEI-Mal. The ability of ATP to form H-bonds with various sugars, [359] and liposomes,[360] was previously discussed. Therefore, the parameters and conditions that define uptake and release of ATP to PEM system have to be determined.

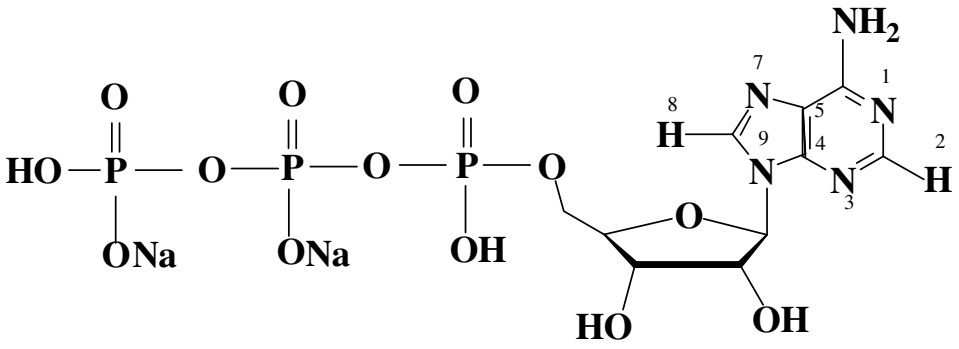

Figure 4-16. Structure of ATP dinatrium salt

ATP of concentration 0.5 mg mL^{-1} has been casted on the surface of Ge-IRE then followed by being scanned via single beam ATR-FTIR , i.e. Ge-IRE was placed in an opened ceramic ATR-FTIR holder (Appendix, **Figure 8-24 a**). ATR-FTIR analysis presented in Appendix, **Figure 8-24 a** (black spectrum) shows several strong bands appear in the range 1280-900 cm^{-1}. The major sugar interaction is observed with α-, β- , and γ-PO_2^- groups of ATP triphosphate chain, while base binding is not significant. [359] Evidence for this comes from major spectral alterations of the triphosphate chain vibration at 1248, 1126, 1081,1020 and 900cm^{-1} (Appendix, **Figure 8-24 a**),[361] while the adenine base vibrations can be found at 1700-1480cm^{-1}. [362, 363] PEM (PEI(HE-Na^+/PEI-Mal-C)$_{20}$) was preloaded with ATP molecule of concentration 0.5 mg mL^{-1} (Appendix, **Figure 8-24 b**). The broad and strong positive derivative features centered at 1250 – 900

cm^{-1} are due to a major increase in intensity of the phosphate vibration upon sugar-PO_2 interaction (Appendix, **Figure 8-24 b**). [361] An increase in the intensity of the adenine band at 1700-1650 cm^{-1} is due to the interaction of sugar with the pyrimidine NH_2 group (Appendix, **Figure 8-24 b**). [361] These observations will be used later on when discussing ATP loading and release (**Section 4.7.2 and 4.7.3**)

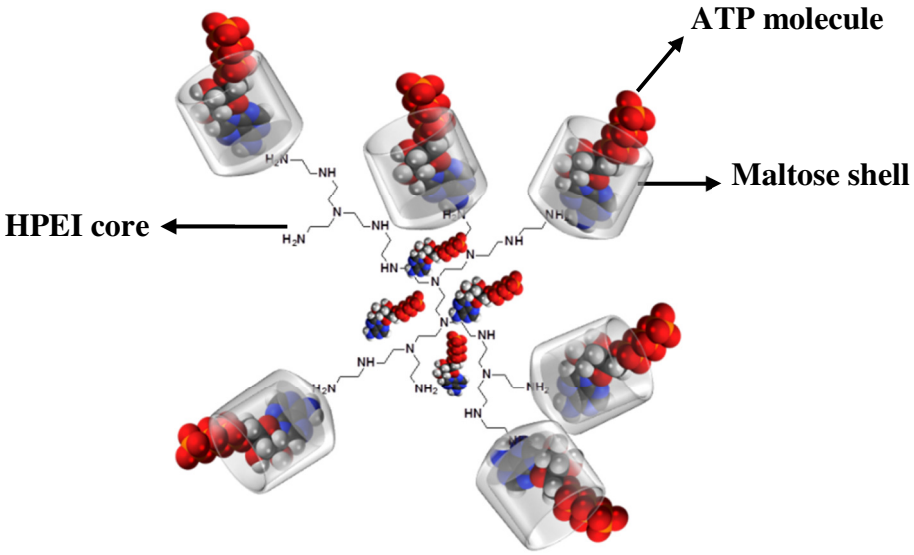

Scheme 4-10. Cartoon demonstrates the images of interactions of ATP molecules (**i**) electrostatically to the cationic scaffold of PEI-Mal (**ii**) and interacts via H-bond to the maltose shell

4.7.2. Drug adsorption (drug postloading)

4.7.2.1. Drug adsorbing pretesting for weak/strong system

Stability of PEM is the most important criteria for the scope of this work. Unfortunately, ATP/PEM ATR-FTIR spectrum showed only one isolated band for ATP at 900 cm^{-1} and no isolated band for PEM (PEI(HE-Na^+/PEI-Mal-C)$_{20}$) has been shown (**Figure 4-17**). Namely, it was important to prove that ATP release in not associated with PEM degradation and the whole ATP/PEM system will be stable even after changing PEM internal structure to increase its validity for drug loading and to create potential sites of interaction. In this part in-situ multi-beam ATR-FTIR spectroscopy has been used. PEM (PEI(HE-Na^+/PEI-Mal-C)$_{20}$) has been prepared via Approach C.

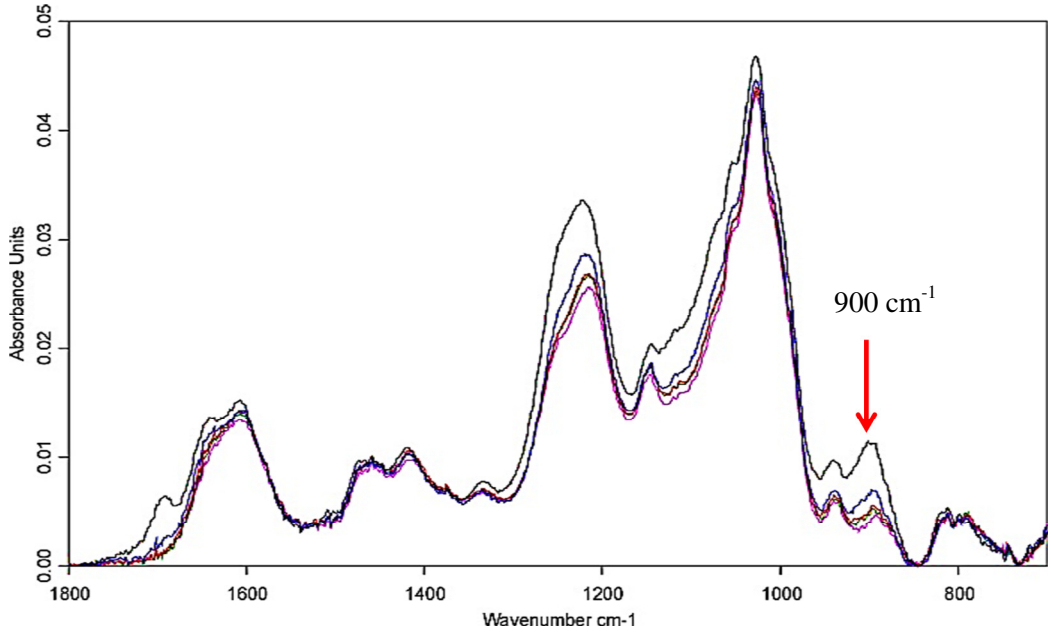

Figure 4-17. ATR-FTIR in-situ measurements trace dry PEM (PEI(HE-Na^+/PEI-Mal-C)$_{20}$) load and release. PEM was injected with ATP (0.5 mg mL^{-1}), and then this was followed by a rinsing step with Millipore-water. PEM was built-up on Ge-IRE and the spectra were taken between wavelengths 1800-800 cm^{-1}.

The outermost layer in all fabricated PEMs was composed of polyanion species (HE-Na^+). Ge-IRE-PEM has been built in the flow in-situ ATR-FTIR cell. While PEM (PEI (HE-Na^+/PEI-Mal-C)$_{20}$) was being in dry state, ATP (0.5mg mL^{-1}) was injected on the surface of PEM. The latter step was followed by rinsing steps using Millipore-water and pure HEPES buffer (0.01M). It is shown in **Figure 4-17**, that the whole PEM spectrum is compatible with ATP finger prints except one isolated band at 900 cm^{-1}. During ATP releasing with both rinsing mediums, Millipore-water and HEPES buffer, the intensity of the band at 900 cm^{-1} was reduced which is considered as ATP release. ATP rinsing with charged-free solution was not instantly and takes about 1200 min to remove the whole adsorbed ATP. As it is shown in **Figure 4-18** that the adsorbed ATP was eluted out of PEM (PEI (HE-Na^+/PEI-Mal-C)$_{20}$) in case of Millipore-water and pure HEPES buffer (0.01M).

It was also shown that the effect of HEPES buffer for the adsorbed ATP rinsing step was higher than that of Millipore-water (**Figure 4-18**). PEM was subjected to HEPES buffer and Millipore water for 1200 minutes. About 52% and 32% of ATP was released out of PEM after 1200 min via HEPES and Millipore-water, respectively. ATP was not

instantly released in case of Millipore water and this delay in ATP elution may estimate a kind of physical interaction between ATP and the polysaccharide HE-Na^+, e.g. hydrogen bonds. In addition, it is also assumed that there were some electrostatic interactions toward PEI-Mal-C in which it was difficult for charged-free solutions to disturb such electrostatic interactions. These findings give us evidence that ATP has been not only superficially adsorbed onto PEM outermost layer but also somehow permeated to the inner PEM, although adsorption took place on dry PEM (PEI (HE-Na^+/PEI-Mal-C)$_{20}$). Since, ATP adsorption on PEM in dry state was not highly efficient to permeate ATP molecules to PEM inner bulk structure. It was possible to remove ATP by rinsing the adsorbed PEM by Millipore-water or pure buffer solution without any further efforts in tuning ATP release using different values of ionic strength or pH values.

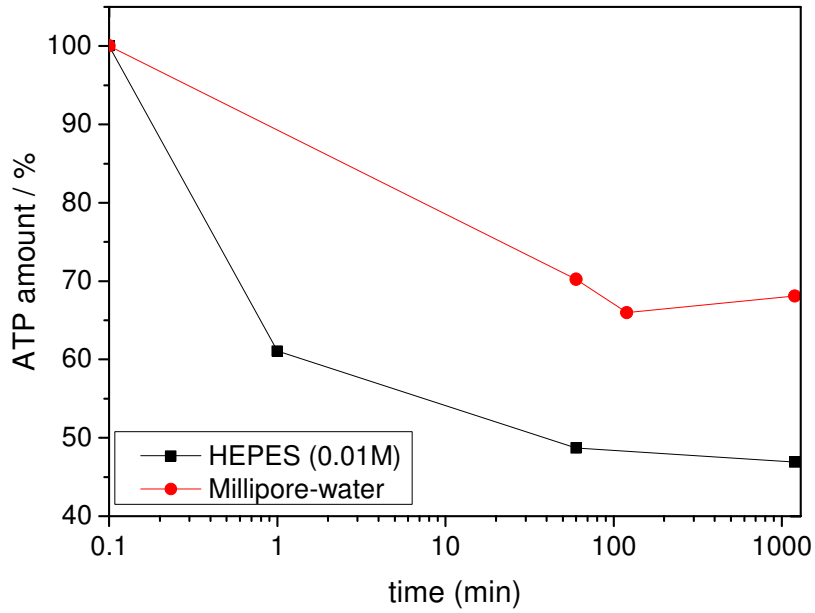

Figure 4-18. ATR-FTIR in-situ measurements trace ATP percentage amount versus ATP rinsing time. ATP (0.5 mg mL^{-1}) was injected and adsorbed onto dry PEM (PEI (HE-Na^+/PEI-Mal-C)$_{20}$) surface, then followed by a rinsing step with Millipore-water and HEPES buffer (0.01M) for 1200 min. PEM was built-up on Ge-IRE and the spectra were taken from 1800-800 cm^{-1}. For ATP amount calculation, area under the ATP isolated band (900 cm^{-1}) was calculated.

4.7.3. Drug postloading for weak/strong system

The linear LbL growth mode of PEMs, though widely appreciated and exploited, is an inherently non-equilibrium process, yielding non-equilibrium amorphous structure.

[178, 232, 336] In the adsorption process itself, individual molecules of polyions attach to the surface of a growing PEM via many ion pairing contacts.[9] Because the thickness increment ("layer" thickness) quickly becomes independent of total thickness, it is reasonably assumed that the adsorbing PE becomes locked in place, although some short-range of inter-diffusion still exist. This was the exact situation in case of PEM (PEI(HE-Na^+/PEI-Mal-C)$_{20}$) fabricated by Approach C. PEI-Mal-C was protonated, it lost its flexible chain and tilted to the rigid side (**Scheme 4-4**), which in turn affects the growing regime and the transition from exponential to linear growing up system. In this part we will focus for simplicity on the most stable system examined previously, which was PEM (PEI(HE-Na^+/PEI-Mal-C)$_{20}$) fabricated by Approach C and this was loaded with ATP as a guest molecule.

4.7.3.1. Results: Drug postloading for weak/strong system

Here the anionic drug model (ATP) was introduced to the well prepared PEM of 20 bilayers deposition. It has been described (**Section 4.7)** that in post-loading method ATP was introduced after being in direct contact to the readily prepared swollen PEM of 20 bilayers deposition (**Scheme 4-8**). Loading and release profiles have been measured via both ellipsometry and ATR-FTIR spectroscopy (**Figure 4-19**). Unfortunately, ATR-FTIR measurements have shown only one non-overlapped band, identified to the ATP molecules at wavelength 900 cm^{-1} (Appendix, **Figure 8-24, 8-25**), while all the other bands and finger prints were overlapped with PEM bands themselves. Then, it was difficult to confirm whether the drug release was accompanied with PEM degradation or it was stable after being loaded with and eluted out of ATP molecules. Thus, it was important to re-examine the PEM (PEI(HE-Na^+/PEI-Mal-C)$_{20}$) stability after ATP has been introduced. The experiments have been done via in-situ ATR-FTIR closed system by using a peristaltic pump at a flow rate of 5mL min^{-1} (**Section 6.2.1**). Readily fabricated PEM was subjected to Millipore-water, as a swelling medium, till reaching the maximum swelling equilibrium. The latter step was followed by the ATP (0.5 mg mL^{-1}) addition with keeping in mind that the PEM system must be in a wet swollen state all over the experiment. ATP subjection lasted around 40 minutes and then followed by 5 cycles of fresh Millipore-water rinsing steps. The final rinsing step was established by NaCl solution (0.1M) (**Figure 4-19**). The band of ATP that appeared at 900 cm^{-1} (**Figure 8-25**) has been integrated after PEM

swelling, ATP addition and during the rinsing steps for both Millipore water and NaCl solution.

The ATR-FTIR measurements are shown in **Figure 4-19 a.** They emphasized that PEM (PEI(HE-Na^+/PEI-Mal-C)$_{20}$) fabricated via Approach C (**Figure 4-19 a**) is stable after both ATP addition and elution. Interestingly, anionic ATP postloading inside the well prepared PEM has shown a cyclic upload and release of drug molecules (ATP) for more than 20 cycles in PEM (PEI(HE-Na^+/PEI-Mal-C)$_{20}$). It can be seen in **Figure 4-19 a** that the absorbance fluctuated regularly with the successive loading and elution of ATP molecules out of PEM (PEI(HE-Na^+/ PEI-Mal-C)$_{20}$) fabricated by Approach C. After the loading step it was difficult to elute ATP molecules out of the PEM system via Millipore-water, only in case of a highly concentrated salt solution NaCl (0.1M) the whole loaded ATP amount was released out of PEM. At this moment the PEM returned back to its initial swollen position (**Figure 4-19 a**).

Cyclic upload and release experiments have been repeated via ellipsometric measurements (**Figure 4-19 b**). Ellipsometric investigations were also very important in giving information about PEM inner structure and PEM/ATP potential sites of interaction. The examined PEMs (PEI(HE-Na^+/PEI-Mal-C)$_{20}$) were pre-swollen firstly by being stored in Millipore water till reaching its equilibrium state, and then followed by the addition of ATP and 5 cycles for rinsing steps (Experimental, **Section 6.2.1**). Rinsing steps were constructed of 5 rinsing cycles, every step takes around 20 min and after every 20 min about 2mL of the old solution was squeezed out and renewed. **Figure 4-19 b** investigates PEM/ATP interactions and shows PEM (PEI(HE-Na^+/PEI-Mal-C)$_{20}$) intra-structure. Ellipsometric data have been calculated for three cycles and are shown in **Table 4-10.** The calculated data in **Table 4-10** show that the initial thickness for 20 bilayers deposition in dry state was ~206 nm. After PEM swelling in Millipore- water, the PEM thickness was doubled to ~406 nm. The initial swollen step was created to pronounce the amorphous PEM behavior which in turn will increase the probability of ATP loading. Intriguingly, once the ATP has interacted with PEM (PEI(HE-Na^+/PEI-Mal-C)$_{20}$), PEM has shown a higher swelling (~526nm) (**Figure 4-19 , Table 4-10**), which was followed by a slight decrease in thickness and then returned back to the equilibrium state after rinsing. PEM was subjected to ATP for 40 min. ATP addition was followed by 4 rinsing cycles under

Millipore water. On subjecting PEM (PEI(HE-Na^+/PEI-Mal-C)$_{20}$) to the 4 cycle rinsing steps of Millipore water there were a sustained release of ATP and about 8% have been released after about 80min. The final rinsing step was established by NaCl (0.1M). In subjecting the uploaded PEM to NaCl (0.1M) the whole ATP content was instantly released returning the thickness to its initial swollen state ~401nm (**Figure 4-19,Table 4-10).** Dynamic scan of the experimental ellipsometric parameters are also shown in Appendix, **Figure 8-26**. Ellipsometric phase difference (Δ) (Appendix, **Figure 8-26 a**) and amplitude ratio (ψ) (Appendix, **Figure 8-26 b**) for cyclic upload and release of PEM (PEI(HE-Na^+/PEI-Mal-C)$_{20}$), swollen and rinsed with Millipore-water at λ = 632.8 nm are shown. Ellipsometric parameters followed directly thickness behavior.

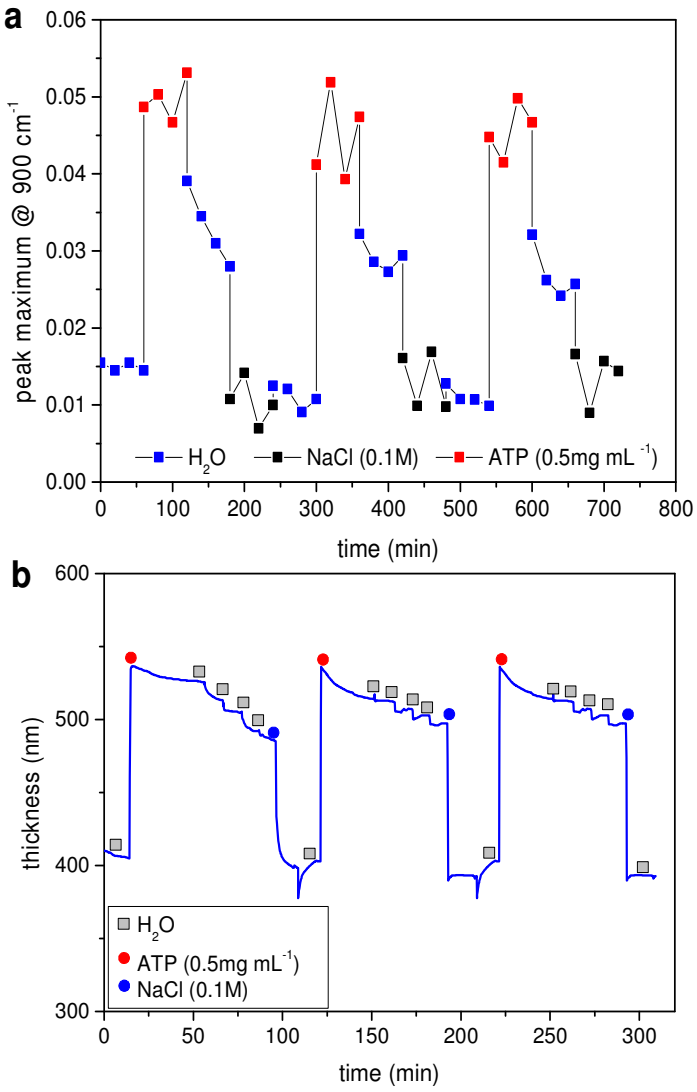

Figure 4-19. Cyclic loading and release traced via (**a**) ATR-FTIR (**b**) ellipsometry, for PEM (PEI(HE-Na^+/PEI-Mal-C)$_{20}$) , ATP of 0.5mg mL^{-1} . The cycle was measured for two hours.

Table 4-10. Table describes PEM thickness changes in ATP cyclic upload and release. Only three cycles for the same sample are presented. PEM (PEI(HE-Na^+/PEI-Mal-C)$_{20}$), thickness after the addition of ATP; thickness *d* (nm) and refractive index n at λ= 632.8 nm from ellipsometry, PEM was swollen and rinsed in Millipore-water these are followed by final rinsing step using NaCl 0.1M.

Conditions	PEM(1st cycle)		PEM (2nd cycle)		PEM (3rd cycle)	
	d (nm)	*n*	*d (nm)*	*n*	*d (nm)*	*n*
Dry state	206	1.537	206	1.537	206	1.537
Swelling [a]	406	1.455	409	1.452	410	1.461
ATP [b]	526	1.465	515	1.448	515	1.452
Rinse 1 [c]	514	1.467	513	1.450	512	1.449
Rinse 2 [c]	505	1.469	507	1.451	513	1.453
Rinse 3 [c]	492	1.470	502	1.452	507	1.453
Rinse 4 [c]	486	1.471	497	1.452	503	1.454
Rinse 5 [d]	401	1.467	400	1.443	410	1.443
Dry $_{swelling}$ [e]	208	1.536	208	1.536	208	1.536

[a, c] Swelling and rinsing in Millipore, respectively

[b] ATP addition, [d] NaCl 0.1M (pH6.5)

[e] dry state after being swollen

Another further experiment have been done to investigate ATP adsorption in the presence of different swelling media, charged-free and charged physiological media. Three different PEMs have been investigated under different swelling media, Millipore water and PBS. Thickness data for PEM (PEI(HE-Na^+/PEI-Mal-C)$_{20}$) subjected to Millipore water and PBS are shown in Appendix, **Table 8-2, 8-3,** respectively. On subjecting PEM (PEI(HE-Na^+/PEI-Mal-C)$_{20}$) to Millipore water as swelling and rinsing medium (Appendix, **Table 8-2**), its initial thickness ~206 nm has swollen to thickness ~434 nm. On reaching stable swollen state ATP was added. After ATP addition, thickness has swollen to reach ~472 nm. ATP addition has been followed by three cycles of rinsing. Rinsing steps have taken a total rinsing time of 100 min, 30min/cycle. After three rinsing steps thickness decreased to values ~478, ~459 and ~454, respectively. After 100 min only 4% for adsorbed ATP has been released in Millipore water. On subjecting PEM to PBS (Appendix, **Table 8-3**) as a swelling and rinsing medium, its thickness has been increased from its initial dry thickness ~220nm to swollen thickness of value ~400nm. After ATP addition PEM became more swollen and reached 541 nm. The latter step was followed by

five PBS rinsing steps lasted for 100 min, with rate of 20 min/cycle. The thickness after the five rinsing steps in ascending order was 527, 525, 529, 429 and 410 nm, respectively. After 100 min about ~24% of ATP was released. It was proved form previous experiments that ATP was released faster in the presence of PBS than in case of Millipore water. Appendix, **Figure 8-27 and 8-28** show the dynamic scan of the experimental ellipsometric parameters, phase difference (Δ) and amplitude ratio (ψ), at wavelength λ= 632.8 nm submersed in Millipore water and PBS as swelling and rinsing solution, respectively and ATP solution was of concentration equal to value 0.5 mg mL^{-1}. Both parameters, Δ and ψ followed PEM different thickness in all subjected solutions steps.

4.7.3.2. Discussion: Drug postloading for weak/strong system

One of the key results of this work has been presented in this part. PEM (PEI(HE-Na^+/PEI-Mal-C)$_{20}$) was investigated via both ATR-FTIR and ellipsometry. ATP was loaded and released for ≥ 20 cycles in case of ATR-FTIR and 5 cycles in case of ellipsometry investigations. Intriguingly, the absorbance fluctuated regularly with the successive loading and elution of ATP molecules out of PEM (PEI(HE-Na^+/ PEI-Mal-C)$_{20}$) fabricated by Approach C (**Figure 4-19**). ATP has shown a sustained release out of the PEM in case of Millipore water and showed the instant-full release in case of NaCl (0.1M). One can now make different assumptions. Firstly, it can be concluded that ATP molecules adsorbed to the PEM bulk and were not only superficially adsorbed. This in turn means that ATP exerted different potential sites of interaction with the prepared PEM. Secondly, the release profile was only tuned after subjecting PEM to higher ionic strength medium (NaCl, 0.1M).

Namely it can be presumed that PEM/ATP interaction is due to different reasons:

(i) Physical inclusion of ATP into the growing PEM, where LbL process is nothing else than "consecutive precipitation" of polycation/polyanion and the resulting PEM is considered to be a porous film in the micro- and nanoscale (**Scheme 4-3**).

(ii) Hydrogen bonding between polysaccharide HE-Na^+ in addition to the assumed hydrogen bonds created between ATP and the maltose shell of PEI-Mal-C.

(iii) Strong electrostatic counterion (ATP is the anioinic counterion) interactions to hyperbranched polycation systems (PEI-Mal-C).

(iv) The presence of the entropic effect, since one trivalent ATP disodium salt ion (ATP-Na) when interacts with protonated PEI-Mal-C liberates three monovalent chloride anions. The contained Cl^- ions in PEM (PEI(HE-Na^+/PEI-Mal-C)$_{20}$) were due to protonation of PEI-Mal-C using HCl (0.5M) (**Eq. 4-1**).

$$NH_3^+ + HCl \rightarrow NH_4Cl \qquad \textbf{Eq. 4-1}$$

ATP contains so called phosphoanhydride bond (**Figure 4-16**), which are formed by splitting out water between two phosphoric acids or between a carboxylic acid and a phosphoric acid. [364] This high energy bond tends to have a large negative Gibbs free energy (Δ G) which combines enthalpy and entropy portions in one value. [365] adenosine diphosphate (ADP) and orthophosphate (P_i) are resulted. ADP can be further hydrolyzed (**Eq. 4-2**). [365]

$$ATP + H_2O \underset{-\Delta G}{\longrightarrow} ADP + P_i \qquad \textbf{Eq. 4-2}$$

From equations **Eq. 4-1** and **4-2**, the following reaction is assumed (**Eq. 4-3**):

$$NH_4Cl + ATP - Na + H_2O \underset{-\Delta G}{\longrightarrow} NH_3^+ + Na\,Cl + ADP^{-2} + HOPO_3^{-2}$$

Eq.4-3

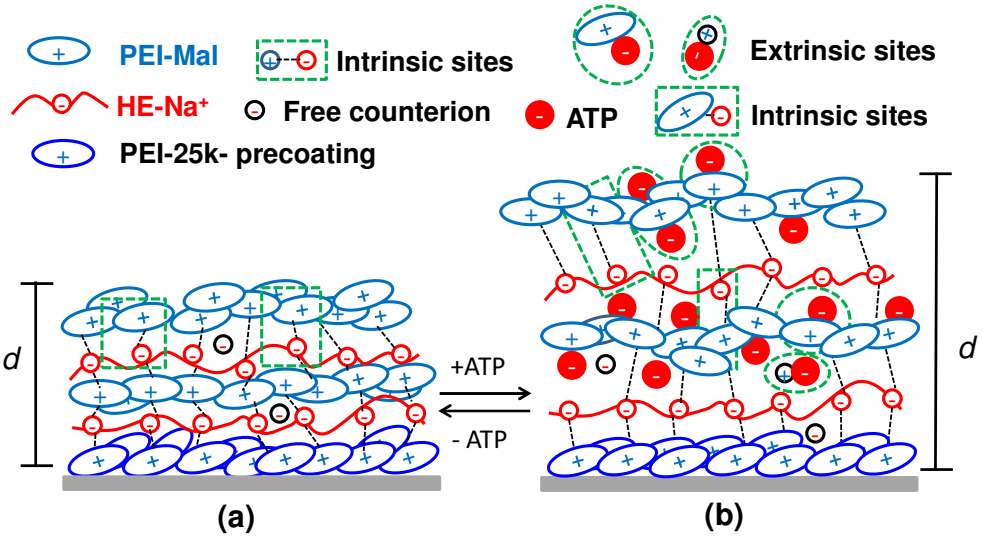

Scheme 4-11. Model showing PEM (PEI(HE-Na^+/PEI-Mal-C)$_{20}$) swollen in (**a**) Millipore water (**b**) addition of ATP (0.5 mg mL^{-1}), the PEM thickness has been swollen after ATP molecules addition.

It is very important to know that introducing of an anionic molecule to readily prepared PEM does not have a much different than the effect of swelling PEM in salt or buffer solution (**Section 4.6.1**). As it has been previously discussed, during the layering up the internal charge is mostly balanced by matching numbers of positive and negative polymer repeat units. This is the so called 'intrinsic compensation'. In introducing an additional counterion to the PEM system another kind of interaction is created which is so called 'extrinsic compensation' (**Scheme 4-11**). At the intrinsic limit, movement of part of or all PE molecules is difficult. A representation of negatively charged counter ion inter-diffusion into bilayer deposition is shown in **Scheme 4-11**. Assuming two stiffed chains of oppositely charged PEs, e.g. protonated PEI-Mal-C and HE-Na^+, all ion pairs would have to be disengaged simultaneously in order to move a polymer chain. A group of adjacent intrinsic ion pairs has to be sequentially dissociated, moved and reassociated (**Scheme 4-12**). The probability of such dissociation as shown in **Scheme 4-11** is very lower. If extrinsic charge (anionic ATP molecule) enters the picture, one of the positive PE charges is extrinsically compensated by the ATP molecule. ATP facilitates the local rearrangement of the PE by hopping with PE segment as it moves. [366, 367]

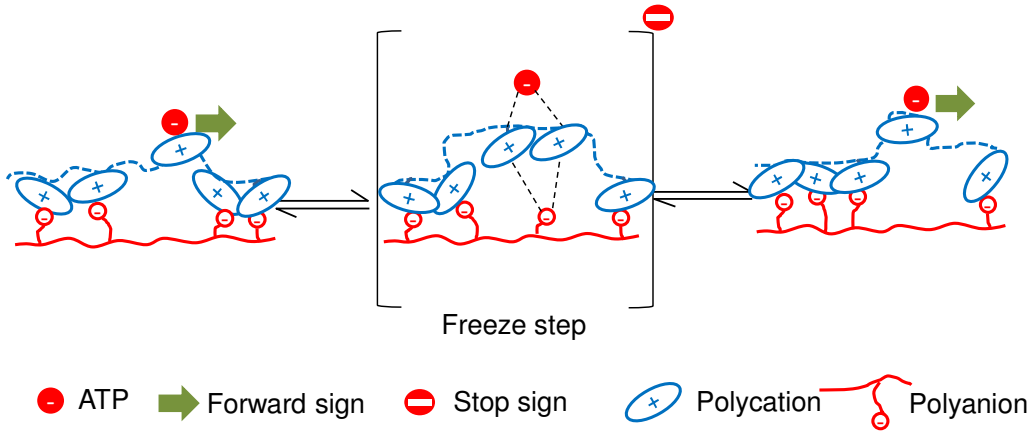

Scheme 4-12. Simplified model describing the participation of an extrinsic charge (solid dot): a negative counterion (ATP)) allows localized place-exchange of individual repeat units, or a small group of them. Adapted from Reference [366]

The transition state drawn in **Scheme 4-12** is merely suggested as a way to minimize the energy barrier for hopping by concerted participation of four charged species connected intrinsically (dotted lines in **Scheme 4-12**). Because of bond restrictions and connectivity, motions of PE segments are coupled. It is likely that several adjacent repeat units on a chain with the participation of several counterions undergo a quasi-concerted

localized reshuffling to end up with net polymer motion. It is worth to mention that extrinsic charge introduction can be considered as potential short circuits that facilitate mass transfer. [367] Thus, the presence of this extrinsic charge can significantly enhance transport of the bioactive ions, e.g. ATP, from the outside to the inside of PEM bulk structure. Farhat *et al.* described an approximate scaling of inter-diffusion with extrinsic ion content, where the introduced counterions hopping is promoted by extrinsic charges forming random clusters with charge equal to or greater than that of the introduced counterion itself. [367] Also, it has been discussed by Dai *et al.* that the tendency for PE ion pairing is strong and any newly created bulk extrinsic charge may well be extruded to the surface, reestablishing bulk intrinsic compensation and reluctant exchanger behavior. This behavior is keeping the PEM system all the time in equilibrium. [368]

In addition to the inter-diffusion and the role of the created extrinsic interaction, also performed osmotic pressure is determined mainly by the concentration of the counterions. A theoretical model was developed by Geo *et al.*, [369] which describes the dependence of the critical osmotic pressure on the elasticity modulus of the ML. They created ML hollow capsule with thin wall thickness of nanometer range. They demonstrated that capsule wall thickness and its dimensions could be varied in a defined way. This variation led in turn to elasticity moduli, which have been determined in values between 500 and 700 Mpa, depending on the system. These values were comparable to results obtained with macroscopic plastic materials and reflect a high degree of local interactions between the polyanion and the polycation. [369] Thus, in conclusion the presence of both osmotic pressure in combination with counterion inter-diffusion and presence of extrinsic/intrinsic alternation behavior help in raising the PEM permeability and thus PEM loading with the bioactive material , e.g. ATP. However, this extrinsic/intrinsic alternation especially in case of kinetically blocked linear growing regime results in PEM high degree of swelling (**Scheme 4-11**). For more specification, ATP interact extrinsically with PEM (PEI(HE-Na^+/PEI-Mal-C)$_{20}$), led to the dissociation of polyion-polyion intrinsic interaction and pronounced polyion-counterion extrinsic interaction led to PEM swollen (PEI(HE-Na^+/PEI-Mal-C)$_{20}$) (**Table 4-10**). For rinsing step with Millipore water no kinetic disturbance has been established and the release for ATP molecules out of PEM was sustained. On introducing NaCl (0.1M) to PEM/ATP system, anionic ATP preferred to ionically interact with Na^+ rather PEI-Mal-C. This in turn has

disturbed temporary extrinsic PEM/ATP interactions and then was followed by ATP release. Instantly PEM returned back to its original swollen thickness and switch back to polyion-polyion intrinsic interactions (**Table 4-10**, Appendix, **Table 8-2, 8-3**). Surprisingly, PEM was ready to repeat this procedure for several times without observable degradation.

4.7.4. Drug postloading for weak/weak system

4.7.4.1. Results: Drug postloading for weak/strong system

In contrary to weak/strong system the growing up regime for weak/weak system was a linearly-reconstructed growth regime. It has been already assumed that this system has an interesting feature in mixing both kinetically locked and labile growing regimes simultaneously in the same PEM system (**Section 4.5.1**). This kind of kinetically labile system in addition to the ionic gel structure of the polyanion (HA-Na^+) would influence the whole drug upload mechanism and the inner bulk structure of the PEM system. In this part, these kinds of influences are going to be shown in details.

The loading findings were in high agreements with the previous assumption for PEM progression mechanism. To compare ATP loading to weak/strong system, the same uploading method for 20 bilayers deposition for PEM (PEI(HA-Na^+/PEI-Mal-C)$_{20}$) has been used. ATP loading and release have been traced using in-situ ATR-FTIR and ellipsometry (**Figure 4-20**). For both in-situ results via ATR-FTIR and ellipsometric measurements (**Figure 4-20**), PEM (PEI(HA-Na^+/PEI-Mal-C)$_{20}$) has been stored in PBS buffer (PO_4^{3-} (0.01M) + NaCl (137 mM)+ KCl (2.7 mM)) for ~30 minutes followed by ATP loading step which took about 40 min (**Figure 4-20**). After ATP loading different rinsing steps took place, in Millipore water, NaCl (0.1M) pH 6.4 and finally in HEPES (0.05M) mixed with NaCl (0.1M) with 1:1 ratio and the mixture pH has been adjusted by NaOH (0.1M) to reach pH 9. This mixture will be abbreviated with the term 'HEPES+NaCl'. The total rinsing steps took place in 100 min. The rinsing time was divided into 30, 45, 25 min for Millipore water, NaCl (0.1M) and HEPES+NaCl, respectively. Intriguingly, this experiment was repeated for ≥20 cycles; emphasizing PEM stability and both, scaffold cyclic loading and release. Weak/weak system fluctuated constantly with ATP loading and release and the final ATP release has been performed in

HEPES+NaCl of pH 9 (**Figure 4-20**). In-situ ATR-FTIR spectra are shown in (Appendix, **Figure 8-29)** emphasizing that PEM/ATP interacted through postloading method.

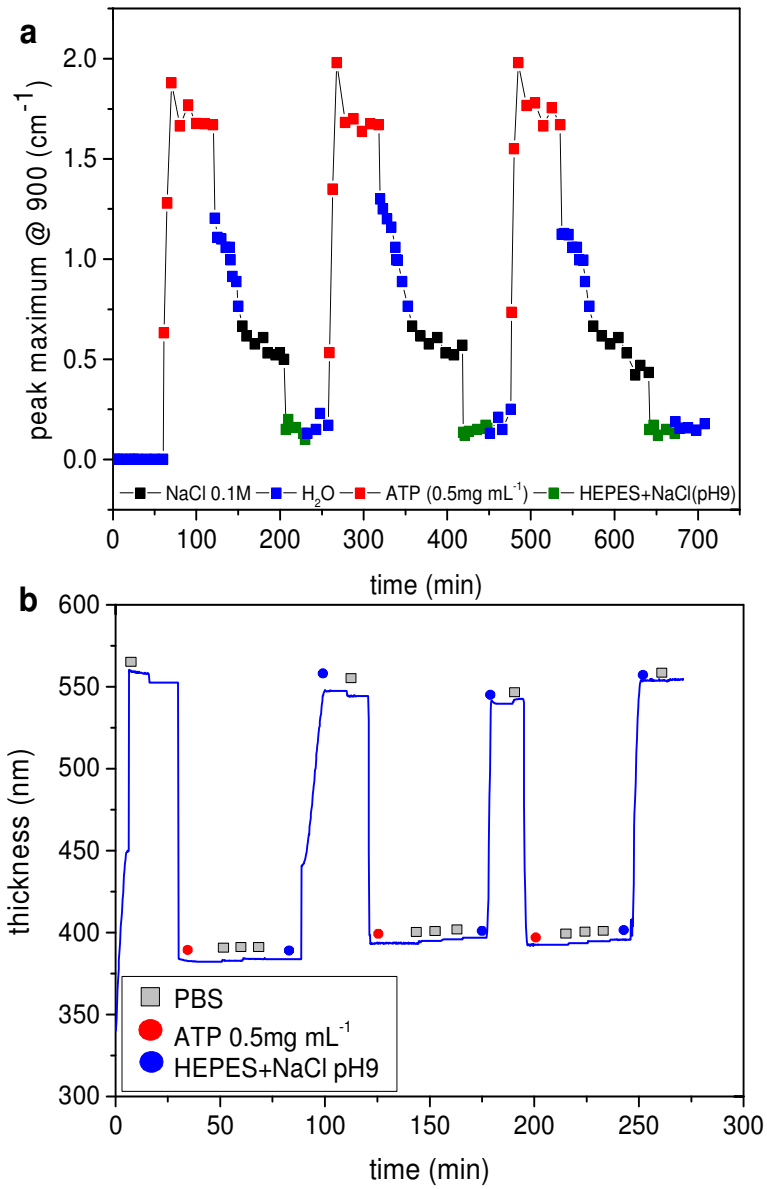

Figure 4-20. Cyclic loading and release traced via (**a**) ATR-FTIR and (**b**) ellipsometry, for PEM (PEI(HE-Na^+/PEI-Mal-C)$_{20}$). ATP was of concentration 0.5mg mL^{-1}.The cycle was measured for 4 hours.

An isolated ATP band at 900 cm^{-1} has been created (Appendix, **Figure 8-29)**. It has been integrated and the results are shown in **Figure 4-20 a**. Unfortunately, ATR-FTIR was only useful in emphasizing PEM (PEI(HA-Na^+/PEI-Mal-C)$_{20}$)/ATP postloading and its stability during upload and release (**Figure 4-20 a**). However, it gave no speculations about PEM inner structure during loading and release. For more investigations, PEM

(PEI(HA-Na^+/PEI-Mal-C)$_{20}$) cyclic loading and release experiment was repeated via in situ ellipsometry (**Figure 4-20 b**). In-situ ellipsometric measurements have been done in in-situ cuvette (**Scheme 4-8**). Thickness for PEM (PEI(HA-Na^+/PEI-Mal-C)$_{20}$) was measured in value of ~300nm (**Figure 4-20 b**,). It has been previously discussed for weak/weak system that it was stored in PBS solution for 30min (**Section 4.7.3**). Ellipsometry measured initial swelling behavior in PBS solution resulted in thickness value of ~558 nm (**Table 4-11**). The latter step was directly followed by pushing ATP to the swollen PEM (PEI(HA-Na^+/PEI-Mal-C)$_{20}$), the recorded thickness shrank to value of ~382 nm (**Table 4-11**). ATP addition was followed by 3 rinsing steps, ~15min/rinsing step, in PBS buffer. Ellipsometry monitored thickness of values ~382, ~383 and ~384 nm resulted after the three rinsing steps, respectively (**Table 4-11**).

Table 4-11. Table describes PEM thickness changes in ATP cyclic upload and release. Only three cycles for the same sample are presented. PEM of (PEI(HA-Na^+/PEI-Mal-C)$_{20}$), thickness after the addition of ATP[b]; thickness *d* (nm) and refractive index *n* at λ = 632.8 nm from ellipsometry, PEM was swollen and rinsed in PBS followed by final rinsing step using HEPES buffer in addition to NaCl at pH 9. The experiment has been repeated for three times for the same sample. i.e. PBS concentrations: PBS: PO_4^{3-} (0.01M) + NaCl (137 mM)+ KCl (2.7 mM).

Conditions	PEM(1st cycle)		PEM (2nd cycle)		PEM (3rd cycle)	
	d (nm)	*n*	*d (nm)*	*n*	*d (nm)*	*n*
Dry state	300	1.560	300	1.560	300	1.560
Swelling [a]	558	1.443	545	1.446	544	1.447
ATP [b]	382	1.465	393	1.468	398	1.464
Rinse1 [c]	382	1.463	394	1.463	398	1.464
Rinse2 [c]	383	1.464	394	1.465	399	1.463
Rinse3 [c]	384	1.465	395	1.461	399	1.460
Rinse4 [d]	547	1.440	543	1.443	545	1.441
Dry $_{swelling}$ [e]	298	1.541	298	1.541	298	1.541

[a, c] Swelling and rinsing in PBS, respectively

[b] ATP addition, [d] HEPES 0.05M +NaCl 0.1M (pH9)

[e] dry state after being swollen

For the illustrated results approximately no changes in thickness has been demonstrated, although each rinsing step has been performed with fresh PBS solution. ATP was instantly eluted after being subjected to the mixture of HEPES+NaCl pH 9. Thus, after the release of ATP molecules, PEM was returned back to its initial swollen position of monitored thickness of ~547 nm (**Table 4-11**). Three different repeating cycles have been investigated for three different PEMs. The re-dry thickness, after the three investigated experiments, has been measured by ellipsometry to give thickness of value ~298 nm (**Table 4-11**). By essence, the most surprised result in this part was the shrinking of PEM structure after ATP loading. This result was totally the opposite to what has been already investigated for weak/strong system.

Dynamic ellipsometric parameters, phase difference (Δ) and amplitude ratio (ψ) at λ = 632.8 nm, of ATP (0.5 mg mL^{-1}), of cyclic upload and release of PEM (PEI(HA-Na^+/PEI-Mal-C)$_{20}$) swollen and rinsed via PBS, are shown in (Appendix, **Figure 8-30)** . Dynamic ellipsometric parameters followed directly the cyclic swelling and shrinking behavior associated with the loading and release of ATP. As it has been done previously in weak/strong system, different media were used to check swelling and rinsing behavior. Both charged-free and physiologically charged medium, Millipore and PBS, respectively, have been investigated for PEM (PEI (HA-Na^+/PEI-Mal-C)$_{20}$). In case of Millipore water as a swelling and rinsing medium (Appendix, **Figure 8-31**), PEM (PEI (HA-Na^+/PEI-Mal-C)$_{20}$) of dry thickness ~300 nm has shown initial swollen thickness of value ~558 nm (Appendix, **Table 8-4)**. Upon ATP addition the PEM has been shrank to reach thickness of ~410 nm. About ~27% of the original PEM thickness was shrank after being subjected to ATP (0.5mg mL^{-1}). On following the ATP loading step with three different rinsing steps in Millipore water of total rinsing time of 40 min, PEM shrank thickness has not returned back the it original swollen state. It has been also shown that the refractive indices values directly followed PEM thickness behavior (Appendix, **Table 8-4**). The dry thickness started with refractive index of value 1.55, this value was reduced upon PEM subjection to Millipore water to value of 1.43. On subjecting PEM to ATP the thickness collapsed while the refractive index rose to value 1.443. By subjecting PEM to three rinsing step of total time of 45 min, refractive index didn't change so much (n= 1.442).

In case of PBS pH 7.4, as rinsing and swelling solution, the situation was not very different from that of Millipore water (Appendix, **Table 8-5**). The dry PEM of ~300 nm was stored in PBS and its thickness has swollen to value ~568 nm. Instantly, once subjected to ATP solution, PEM thickness was reduced to ~382 nm. PEM thickness collapsed with percentage of ~ 33% compared to the initial swollen thickness, and this was about 6% higher compared to that in case of Millipore water. Addition of anionic ATP molecules was followed by three rinsing steps in PBS solution for total rinsing time of 45 min. Reduced thickness was stable and didn't return back to its initial swollen thickness. It has been observed that when PEM (PEI (HA-Na^+/PEI-Mal-C)$_{20}$) was immersed in Millipore, the same collapsing PEM feature has been observed, but with lower attractive force than that of PBS (Appendix, **Table 8-4, 8-5**). The refractive indices showed the same behavior as illustrated thickness; where refractive index was monitored by ellipsometry for dry PEM to give 1.504. This value was as usual reduced in case of swollen state to reach 1.443 and thus it was re-increased after ATP addition to reach 1.465 (Appendix, **Table 8-5**). Similarly to the case of Millipore water, no change in refractive indices values for the three rinsing steps have been demonstrated. Dynamic ellipsometric parameters for Millipore water and PBS solutions have shown the same behavior for swollen and collapsed PEM (Appendix, **Figure 8-32, 8-33**)

4.7.4.2. Discussion: Drug postloading for weak/weak system

Surprisingly and unlike to the swelling behavior for weak/strong system after ATP addition, the swollen PEM (PEI(HA-Na^+/PEI-Mal-C)$_{20}$) showed a shrinkage on addition of the anionic ATP molecules (**Figure 4-20 b**). The weak/weak system was investigated for ≥ 5 times via in-situ ellipsometric and ≤ 20 times via in-situ ATR-FTIR measurements. The shrinkage was difficult to be investigated via in-situ ATR-FTIR (**Figure 4-20 a**), because all the integration calculations were based on the ATP band at 900 cm^{-1} (Appendix, **Figure 8-29**). This unexpected PEM thickness reduction (30% from the initial swollen thickness) supports the first assumption for weak/weak system restructure-linear growth regime (**Scheme 4-5**) (**Section 4.5**) and give the inspiration about PEM (PEI(HA-Na^+/PEI-Mal-C)$_{20}$) inner structure, PEM/ATP interaction and HA-Na^+ conformations and gel structure. Again, as it has been previously discussed, this restructure system has a switching point at 10th bilayer deposition (**Figure 4-9**), at which PEM structure has been

assumed to change the growing up regimes. It was assumed that this PEM has outermost kinetically labile MLs and innermost kinetically blocked MLs (**Scheme 4-5**). These anomalous inter-diffusion MLs properties dictate how the system will interact with biological structures. Firstly it is important to start the discussion with the top structure and the kinetically labile layers, which mainly assumed that it helps a lot in the appearance of the shrinkage feature (**Figure 4-20 b**). Upon subjecting PEM (PEI(HA-Na^+/PEI-Mal-C)$_{20}$) to ATP molecule, the anionic counterions are assumed to move with high probability directly to the uncompensated site for positive ions on the top of PEM (kinetically labile outermost MLs) (**Scheme 4-13**) and interact extrinsically with PEI-Mal-C. Moreover, it is also hypothesized that counterions will extrinsically interact with different cationic charges on different fabricated layers. The creation of the strong extrinsic interactions between the ATP molecules and polycation PEI-Mal-C chain will logically bring the anomalous features down and will reconstruct the kinetically labile growing up layers, arrange them systematically to be connected together and will collapse them in a dense structure (**Scheme 4-13**). This assumption may explain the obvious increment in refractive indices values, e.g. ~1.465 and 1.443 in PBS and Millipore water, respectively after ATP's addition (**Table 4-11** and Appendix**, Table 8-4, 8-5**). These refractive indices values returned back to its normal values, e.g. ~1.443 and 1.438 for PBS and Millipore water, respectively after ATP final release step.

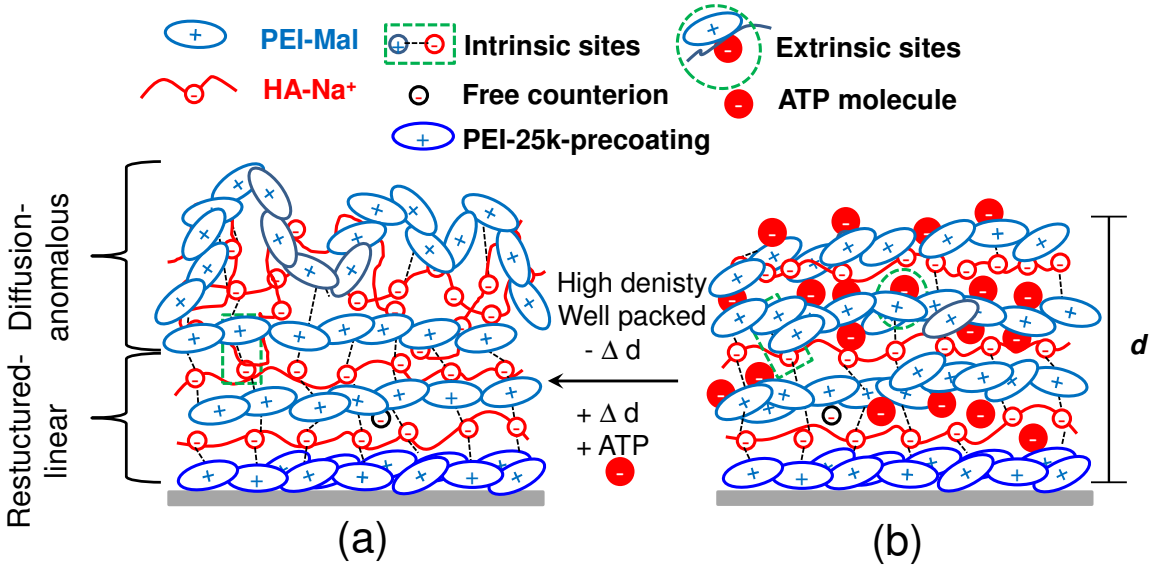

Scheme 4-13. Sketch demonstrating PEM (PEI(HA-Na^+/PEI-Mal-C)$_{20}$) swollen in (**a**) Millipore water (**b**) addition of ATP (0.5 mg mL^{-1}), the PEM thickness has been shrunk after ATP molecules addition.

The lower SD% behavior of PEM (PEI(HA-Na^+/PEI-Mal-C)$_{20}$) after being subjected to NaCl (0.1M) and PBS pH 7.4 (**Section 4.6.3**). It is shown in **Table 4-9**, that the SD% didn't exceed 50% which was a lower percentage compared to that of weak/strong system (**Table 4-6**) (**Section 4.6.1**). This may help in understanding the shrinkage feature which has been appeared after ATP addition (**Figure 4-20 b**). Where, after compensating all uncompensated positive charges, the rest of counterions will move with lower probability to breakdown the strong intrinsic sites in the internal bulk structure of PEM (kinetically blocked linear structure) (**Scheme 4-13**). The second reason for PEM (PEI(HA-Na^+/PEI-Mal-C)$_{20}$) collapse represented for weak/weak system may be due to the presence of the polyanion HA-Na^+ and its well-known ionic gel properties. Previously PE gel behavior and the conformational changes for HA-Na^+ have been discussed (**Section 2.11.2**). [370] There is a controversial discussion going on over the years about HA-Na^+ and its PE gel features. [348, 370-372] The swelling behavior of charged gels has been described in the seminal work by Katchalsky *et al.*, [373, 374] and both Flory and Rehner. [375-377] They observed that swelling resulted from a balance between the elastic energy of the network created by HA-Na^+ and the osmotic pressure of the ions. In salt-free gels this osmotic pressure is due to the counterions that are confined inside the volume of the gel in contact with water reservoir. In the presence of salt the osmotic pressure is associated with the establishment of Donnan equilibrium. [372] Katchalsky *et al.* considered also the effect of electrostatic interactions of the fixed charges on polymer chains. [373, 374] At low salt concentrations, it is conceivable that the flux of ions into the film from the bulk solution is too low to cause significant electrostatic screening of the charged groups on PE chains and significant ionic bond breaking. As the salt concentration is increased, it is believed that the equilibrium swelling behavior of these films results from a balance between electrostatic screening and ionic crosslink breaking in the film. Notably, the swelling process was found to be completely reversible and a shrinking film was observed. Moreover, there is no detectable loss of PE chains from the film was investigated. In fact, it has been shown that when much higher ionic strength conditions are applied, a complete film destruction resulted.[199, 378] These investigations emphasize the present observations about the retarded swelling behavior in the weak/weak system when subjected to PBS buffer and NaCl (**Section 4.6.3**, **Table 4-9**).

On basis of thermodynamics, when the gel is immersed in pure water, it will swell to a volume V which depends on the excess pressure P of the gel phase over the water. At

P=0 the gel is said to be in 'equilibrium swelling'. [348] Barret and Joanny have pointed out, 'equilibrium swelling 'is due to the fact that the osmotic forces of the polymer and the sodium ions in the gel are balanced by the contractility of the network. [379] In any case, thermodynamics is not a relevant issue in the present study, since it does not aim at comparing quantitatively measured values and theoretical predictions for the thermodynamic parameters. In essence, the polymer gel is at equilibrium with a reservoir of solvent if the osmotic pressure in the gel is equal to the osmotic pressure of the salt in the reservoir. That is, if the swelling osmotic pressure due to the entropy of the counterions is balanced by the pressure due to the elasticity of the polymer chains. [379] Whereas, the swelling equilibrium of networks, according to the basic Flory-Rehner idea, [377] results from a balance between the osmotic pressure acting to swell the network and the elastic pressure due to the stretching of the chains. However in the strong screening limit in the presence of an excess of salt, the gels are expected to behave as neutral gels with an effective excluded volume (collapsed or deswelling behavior) controlled by the ratio Debye-Hückel screening length and polyanion degree of ionization. [375-377]

4.7.5. Conclusion for drug postloading for both weak/weak and weak/strong systems

In this part we are summarizing the drug adsorption/release behavior for weak/strong and weak/weak systems. PEMs of 20 bilayers depositions using polycation PEI-Mal-C have been prepared via Approach C for both systems. ATP adsorption has been performed during the swelling state of PEMs whether in charged-free or charged media. For both PEM systems, it has been proved via ellipsometric and ATR-FTIR investigations that the anionic ATP molecules have penetrated PEM inner structure. It was assumed from the previous data that ATP molecules were stable and interacted with PEM mainly through strong electrostatic interactions. Therefore, it was difficult for ATP to be released in the presence of charged-free immersion solutions and without PEM kinetic disturbance. The complete ATP release has been done through NaCl (0.1M) pH 6.5 in case of weak/strong system (**Table 4-10**) and through HEPES + NaCl pH 9 (**Table 4-11**). Thus, the release properties of stable PEM/drug system can be sequentially controlled using two different film disassembly kinetics based on the rapid or gradual dissociation of electrostatic interactions between PEM structure and ATP molecules upon changes in pH and/or ionic strength of the submersion solution. Interestingly, in this part it was possible to reverse load and release for ATP to and out of the prepared PEMs for both systems under

investigation. This kind of swelling/deswelling property strongly supports PEMs stability toward loading and release. It can be seen from **Figure 4-19** and **4-20** that the absorbance fluctuated regularly with the successive loading and release of ATP molecules in both weak/strong and weak/weak systems, which means that the adsorption efficiency of the PEM film was almost unchanged after ≥ 20 times of loading and release.

The second interesting result was due to different swelling and shrinking behaviors for weak/strong and weak/weak systems, respectively, after ATP's addition. The swelling behavior of the weak/strong system (**Figure 4-19**), was assumed to be due to the extrinsic/intrinsic transition. Since, in case of weak/strong system, the system was kinetically blocked and mostly all polycationic charges have been compensated with polyanions contributions, when system was subjected to ATP molecule, ATP contribution was through extrinsic/intrinsic transition. Therefore, PEM has been swollen once subjected to anionic counterions ATP (**Scheme 4-11**). In contrary, in case of weak/weak system, swollen PEM has been shrunk once it was subjected to ATP molecules (0.5mg mL^{-1}). This shrinking behavior was assumed to be due to two different reasons. The first was due to the presence of uncompensated polycations. In this situation the uncompensated ones were recompensated by anionic ATP molecules. These strong extrinsic potential sites of interactions led to collapsing of PEM structure (**Figure 4-20**). Secondly this collapsing PEM behavior may be also due to the PE gel behavior for HA-Na^+, since it was discussed previously that in the presence of high salt concentration PE gel behaves as natural gel. [375-377]

4.8. PEM/Drug complexation or drug preloading

Controlled drug release materials have potential for utilization in biomedical implants, tissue engineering, and targeted drug delivery devices. The advantages of controlled release include greater drug effectiveness, better balanced drug concentrations in the body, and more convenience to the patient. [380] In this part we try to upload the drug molecules in the HB polycation decorated with maltose moieties (PEI-Mal-C). As described in Experimental, **Section 6.2.2** (Experimental , **Scheme 6-4**), ATP was added to both polyions with a mixing ratio of 1:5 and a series of molar ratios for the drug concentration was prepared depending on the molar concentration of the polyanion, HE-

Na^+ and HA-Na^+ (Experimental, **Section 6.2.2**). The uptake results show intriguing behaviors, which will later on affect PEM releasing profiles

4.8.1. Drug preloading to weak/strong system

4.8.1.1. Results : Drug preloading and release for weak/strong system

ATP is considered as a strong negatively charged counterion. It was assumed that after mixing the polycationic 'PEI-Mal-C' and the anionic 'ATP', well prepared PEC will be achieved, in which both PEI-Mal-C and ATP molecules strongly connected together via electrostatic interaction and hydrogen bonding. The complexation for both PEI-Mal-C and ATP molecules was optically observed, when the transparent PEI-Mal-C 1mg mL^{-1} was suddenly transferred to a cloudy colored solution after ATP injection for all presented concentrations. This color transition is due to the formation of PEI-Mal-C/ATP complex coacervates. PEM loading and release characterization have been followed as usual by the two well-known methods, single beam ATR-FTIR spectroscopy (**Figure 4-22**) and ellipsometry (**Figure 4-23**). For ATR-FTIR investigations, different ATP concentrations, 0.08-0.6 mg mL^{-1}, have been used in the preparation of PEM (PEI(HE-Na^+/PEI-Mal-C/ATP)$_{20}$). The loading process has been created through the layering-up via dip-coating (**Scheme 4-9**). ATP loading to PEM (PEI(HE-Na^+/PEI-Mal-C)$_{20}$) forms (PEM/ATP) complex, this PEM/ATP complexation is shown in **Figure 4-21** that gives a proof about ATP molecules incorporation and its effect on PEM equilibrium. Thus, the more ATP loading concentration, the more loading efficiency has achieved. The loading efficiency started to increment as ATP concentration was increased with values form 0.08-0.5 mg mL^{-1}, at which the critical concentration and most equilibrated point has been investigated. After this critical drug concentration, the loading efficiency started to decrease one more time (**Figure 4-21**). However, when the ATP concentration increased more than 0.6 mg mL^{-1}, PEM was no longer stable and decomposed.

As it has been described in Experimental, **Section 6.2.2** , ATP release was initiated by rinsing PEM (PEI(HE-Na^+/PEI-Mal-C/ATP)$_{20}$) by soaking the whole substrate/PEM/ATP in a releasing medium (50mL) and after each rinsing step PEM was subjected to N_2 steam for drying. The latter step was carried out for PEM of 20 bilayers built in an open holder and observed by single beam ATR-FTIR spectroscopy. Substrate/PEM was built-in ATR-FTIR open holder in the same position for every

measuring step. Re-hydration and swelling under aqueous medium did not affect the PEM release. ATP molecules release has been achieved only in a medium of HEPES (0.01M) mixed to NaCl solution (0.1M) in ratio 1:1 and pH7.4 adjusted by NaOH (0.1M) (**Figure 4-22**).

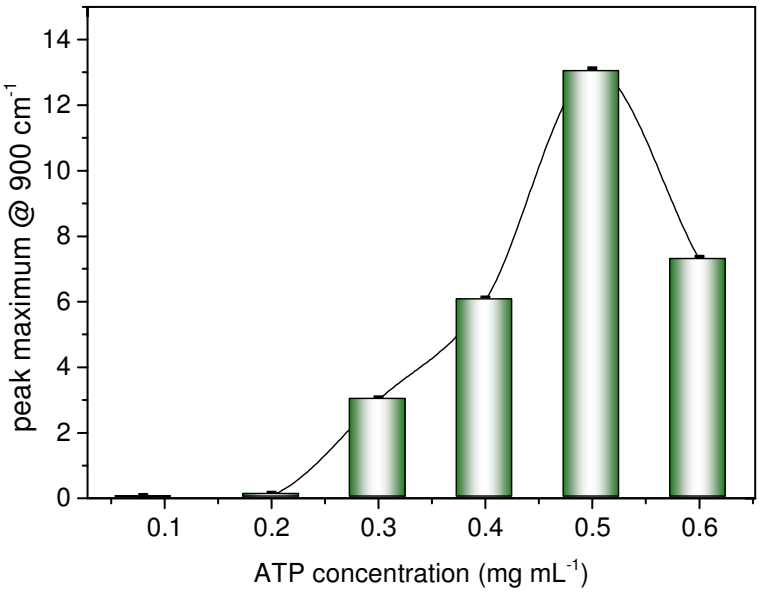

Figure 4-21. ATR-FTIR study for ATP of different concentration in PEM (PEI(HE-Na^+/PEI-Mal-C/ATP)$_{20}$). The integration calculation has been done on ATP isolated band at wavelength 900 cm^{-1}.

In order to calculate the ATP release versus time, ATP non overlapped band at 900 cm^{-1} has been integrated versus time and then plotted as it is shown in **Figure 4-22**. The release for all PEMs with different ATP concentrations has been followed up for about 1000 min (**Figure 4-22**). Release for ATP molecules of lower concentrations, e.g. 0.08 and 0.2 mg mL^{-1} was slower than that of the higher ATP mass concentrations (**Figure 4-22**). After 1000 min about 53% and 35% of ATP uptaken amount has been eluted for concentrations 0.08 and 0.2 mg mL^{-1}, respectively. ATR-FTIR spectra for the prepared PEM/ATP complex with different ATP concentrations 0.3, 0.5 and 0.6 mg mL^{-1}, respectively did not show any changes and PEM/ATP was stable for 1 day in Millipore water or pure HEPES buffer (Appendix, **Figure 8-34 – 8-36**). However, ATR-FTIR investigations (Appendix, **Figure 8-37**, **8-38)** have also shown that the release can be initiated for different ATP concentrations, 0.3, 0.5, 0.6 mg mL^{-1}, in HEPES (0.01 M) mixed with NaCl (0.1M) of pH value 7.4 adjusted with NaOH (0.1M). After 1000 minutes, about 87%, 80% and 90% of ATP of concentrations 0.3, 0.5, 0.6 mg mL^{-1}, respectively,

have been already released (**Figure 4-22**). It was previously investigated (**Figure 4-21**) that the higher absolute uptake of ATP was for the ratios PA/ATP and PC/ATP of ratio 1:2 and 1:29, respectively , which referred to ATP of mass value of 0.5 mg mL^{-1}. This concentration was the critical one, where after and before this ATP's concentration, PEM uptake efficiency was lower (**Figure 4-21**). ATP molecules uptake findings agreed to its release out of PEM. It was shown that the release versus time was affected by the loading efficiency and PEM stability (Appendix, **Figure 8-37**, **8-38**).

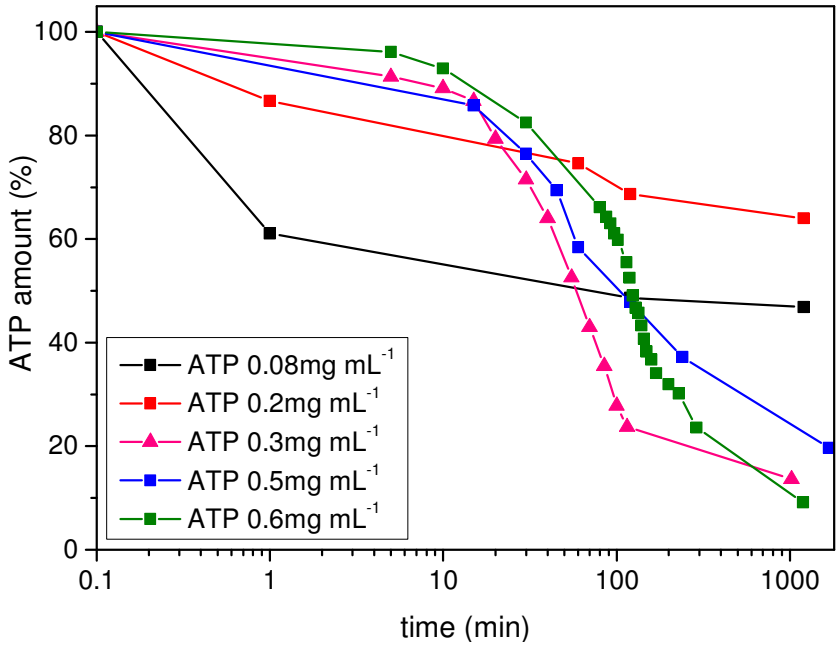

Figure 4-22. ATR-FTIR release study for PEI($HE^{-}Na^{+}$/PEI-Mal-C/ATP)$_{20}$) prepared via approach C for different concentration of ATP , the release study was done in HEPES buffer (0.01M) + NaCl (0.1M) mixed with ratio 1:1 at pH 7.4, pH was adjusted using NaOH 0.1M

The critical ATP ratio has been re-investigated via ellipsometric measurements. There were great agreements between the results via ATR-FTIR and that of ellipsometry (**Figure 4-23**). The data obtained by ellipsometry demonstrated that all PEM/ATP complexes have high swelling behavior to ≥6 times above their original thickness instantly following submersion (**Figure 4-23**). No film thickness decrease has been observed under submersion in pure HEPES and Millipore water (**Figure 4-23**). Also in case of PBS (PO_4^{3-} (0.01M) + NaCl (137 mM)+ KCl (2.7 mM)) pH 7.4, no obvious release has been observed. PEM started with dry thickness of 206 nm (0 hour) and the end dry thickness after 1day in PBS was 195 nm (Appendix, **Table 8-6**). Accordingly, film thickness readily decreased

after PEM (PEI(HE-Na^+/PEI-Mal-C/ATP)$_{20}$) being immersed in HEPES (0.01M)+NaCl (0.1M) pH 7.4. PEM thickness has been decreased with rate of ~ 7 nm/min for ATP 0.5 mg mL^{-1} (**Figure 4-23**). The film dry thickness for PEM (PEI(HE-Na^+/PEI-Mal-C/ATP)$_{20}$) was ~ 206 nm, while the end dry thickness for after 1 day in HEPES (0.01M)+NaCl (0.1M) pH 7.4 was 150 nm for ATP value of 0.5 mg mL^{-1}.

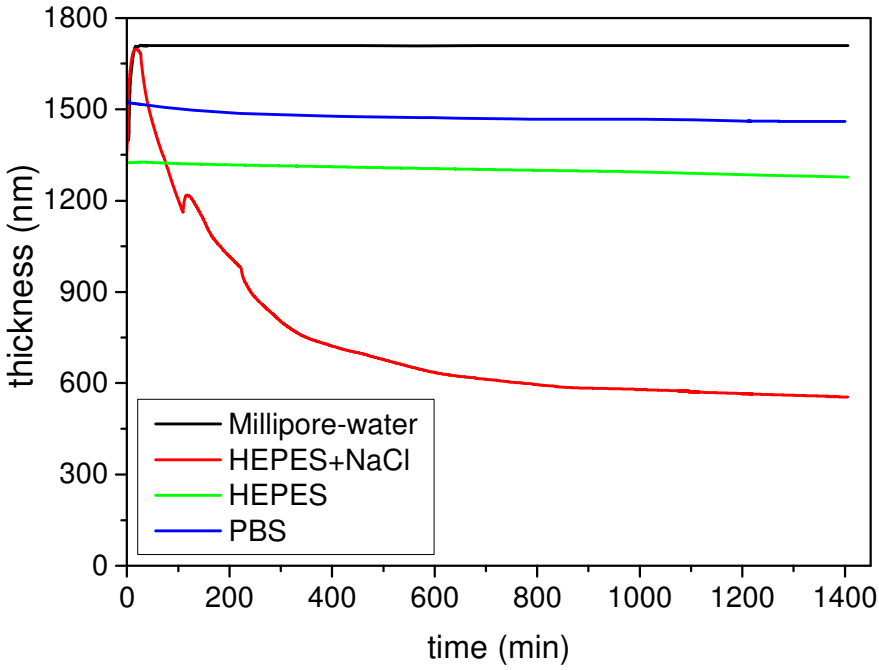

Figure 4-23. Drug preloading process for PEM (PEI(HE-Na^+/ PEI-Mal-C/ATP)$_{20}$) traced by ellipsometric measurements – for ATP 0.5mg mL^{-1}. ATP release was checked in water, HEPES (0.01M), PBS (PO_4^{3-} (0.01M) + NaCl (137 mM)+ KCl (2.7 mM)) and HEPES+ NaCl (0.1M) mixed with ratio 1:1

4.8.1.2. Discussion: Drug preloading and release for weak/strong system

ATP uptake findings (**Figure 4-21**) were in agreement with the stability diagram (**Scheme 2-14**), which was previously suggested by Chohen Stuart. [197] These results may be due to the increase of the screening effect exhibited by ATP molecules toward the polycation (PEI-Mal-C). This increasing in screening effect created by ATP anions of high concentrations may lead to the formation of soluble complexes, which in turn weakened polyion-polyion potential sites of interaction and strengthened polyion-ion sites of interaction. These complex coacervates depend essentially on the ratio between the amounts of cationic and anionic polymer and on the ionic strength. According to these results, it was assumed that ATP of higher concentration, >0.6 mg mL^{-1}, affected the whole

PEM stability. Whereas, the equilibrated system can be only established if complex coacervates existed. [175] These screening effect arguments were well supported for PEM/ATP complex for ATP concentration > 0.6 mg mL^{-1}, where no more stable PEM has been created and the whole PEM was dissociated. Thus, it was assumed that at ATP critical concentration, 0.5 mg mL^{-1}, equilibrium was held between all PEM counterparts (polyanion, polycation and the counterions). On the basis of these attributes, it was hypothesized that at ATP 0.5 mg mL^{-1} the most equilibrated system has been created and the most efficient PA/ATP and PC/ATP ratios (**Figure 4-21, 4-22**).

ATP release out of PEM ($PEI(HE\text{-}Na^{+}/PEI\text{-}Mal\text{-}C/ATP)_{20}$) has been performed on subjecting PEM to charge-free and charged solution under physiological pH value. ATR-FTIR results gave great evidence that PEMs with different ATP concentrations showed a profound stability toward the Millipore and HEPES buffer solutions and no ATP release has been initiated in those mediums (Appendix, **Figure 8-34 - 8-36**). This in turn means that PEM/ATP inner structure was kinetically stable and extrinsic/intrinsic potential sites were in equilibrium. PEM/ATP kinetic disturbance and ATP release has been performed only in the mixture HEPES+NaCl at pH 7.4. The higher ATP uptake and the lower release rate were at ATP critical concentration (0.5 mg mL^{-1}) (**Figure 4-21**, **4-22**). ATP release amount in case of ATP concentration 0.5 mg mL^{-1} was lower than that of ATP at concentrations 0.3 and 0.6 mg mL^{-1} with about 7% and 10%, respectively. According to latter, it is assumed that at kinetically stable uploaded PEM, lower drug release will be achieved.

ATP (0.5 mg mL^{-1}) release out of PEM/ATP was also traced with ellipsometry (**Figure 4-23**). PEM/ATP has swollen in different media of different ionic strength. PEM/ATP exerted high SD% of values 695%, 550% and 646% for Millipore water, HEPES(0.01M) and PBS(0.01M) buffer solutions, respectively. SD% in case of HEPES+NaCl was calculated to be 543%. Most likely, this behavior reflects a balance between hydrolysis and swelling immediately following immersion of the dry PEMs. It was addressed by Volodkin and Klitzing that in case of pronounced extrinsic charge compensation the PEM is denser with fewer voids in the dry state due to stronger screening of the PE charges. [167] This gives a higher flexibility of the polymer chains and an easier adjustment of the chains to the environment. In contrast, these PEMs swell more strongly in water than the ones built up in presence of small ions. Due to the lower density of

complexation sites the "mesh sizes" are larger and can take up more water. Following this brief swelling period, films reach saturation and hydrolysis begins to act as the dominant factor effecting film thickness. [167]

The discussion will focus on two different points: (**i**) on the one hand the difference between the ATP concentration in the prepared PEM and release rate versus time. (**ii**) On the other hand the drug release, for all different ATP concentrations, has not been achieved except in the presence of salt, neither in the presence of pure Millipore-water or in the pure buffer medium (Appendix, **Figure 8-34 – 8-36**). Firstly, for fewer ATP amounts (0.08- 0.2 mg mL^{-1}) in the PEM, ATP is bound more specifically at potential binding sites. Whereas, for larger ATP amounts (0.3, 0.5, 0.6 mg mL^{-1}) in the PEM, ATP might form aggregates or clusters within the PEM phase, which might be simply disturbed in the presence of salt medium. These kinetically disturbed PEMs with larger amount of ATP have been released rapidly within 1000 min in the presence of salt medium. Among such specific ATP/PEM interactions, electrostatic attraction of ATP in a counterion-like fashion at PEI-Mal-C or other interaction forces like, e.g. hydrogen bonding between ATP and both PEI-Mal-C maltose shell and HE-Na^+ may prevail. Also a change in the internal structure of PEM/ATP, e.g. concerning density, being more pronounced for higher ATP/PE ratios , e.g. 0.5 – 0.6 mg mL^{-1} (**Figure 4-21**), might contribute. Thus, ATP migration was less hindered. PEM equilibrium in case of 0.5 mg mL^{-1} was the highest for both uptake and controlled release. However, the equilibrium was reversed once the ATP concentration rose to 0.6 mg mL^{-1}.

In 2013, Torger and Müller, [220] have investigated about PEM PEI/PAA loaded with antibiotic streptomycin (STRP). They used polycationic HPEI (65% branching degree, M_w= 750,000 g mol^{-1}, 50% (w/v) solution). The release of STRP out of PEM using ATR-FTIR spectroscopy was studied. They prepared the loaded PEM by consecutively adsorption of STRP/HPEI and STRP/PAA solution onto a Ge-IRE using LbL technique in a flow in-situ ATR-FTIR cell. Different ratios of drug/PE (1:25, 1:10 and 1:5) were prepared. The STPR/PE ratio showed a significant influence on release kinetics, whereby the slowest released was for STPR/PE of ratio 1:25, while the fastest release was for STPR/PE of ratio 1:5. The cationic drug STRP's release, for different STPR/PE ratio, has been done in Millipore water within 240 minutes. [220] In case of this work, it was assumed that the release time for anionic ATP attached to PEM (PEI(HE-Na^+/PEI-Mal-

C/ATP)$_{20}$) was enhanced due to the strong interaction forces, which exist additionally to the maltose-decorated shell (PEI-Mal-C), in addition to those normal interactions stated previously. The hydrogen bonding initiated between maltose-shell of PEI-Mal-C and ATP has created a retarded controlled release for ATP out of PEM.

Secondly, the release has been done in the presence of salt solution Na^+ Cl^-. It is shown in **Scheme 2-13**, that the size of Na^+ ions and Cl^- ions are with atomic radii, 0.98 Å and 1.81 Å, respectively, is smaller than PO_2^- of atomic radius equal to 1.49 Å. [381] It is important to know that the atom size increases as one moves down the periodic table. Besides the type of PE, the type of counterions also plays an important role in ML formation. Usually, the ions are chosen according to the ‘‘Hofmeister series’’. [185] It has been previously discussed in **Section 2.6.2** that the smaller ions have a relatively low polarizability, low ionic strength and prefer to keep their water of hydration. However for larger ions, they are with a high polarizability, high ionic strength and their hydration water can be easily removed (**Scheme 2-13**). Thus, logically one may interpret that all the time it is important for the system to search for stability and equilibrium; therefore in case of weak/strong system both the PO_2^- and Cl^- ions exchange positions. Thus, PO_2^- prefers to ionically attach with Na^+ rather than PEI-Mal-C. In addition to the negative counterions, positive Na^+ ions take their role in compensating extrinsically the uncompensated sites on the polyanion HE-Na^+. Thus, it was assumed that this mission led to higher swelling effect for inner PEM structure and then followed by ATP molecules release. In contrary, in case of pure Millipore-water and buffer (Appendix, **Figure 8-34 – 8-36**), there was no kinetic disturbance for PEM and meanwhile no/nearly no drug release has been achieved.

4.8.2. Drug preloading for weak/weak system

4.8.2.1. Result: Drug preloading and release for weak/weak system

In these studies, the drug molecules ATP served as both functional drugs and film components. It is important to mention that in contrary to the weak/strong system, weak/weak system has a higher kinetic affinity. It was expected from the previous results that the drug loading affinity and the stability for the weak/weak system would be much better than that of weak/strong system. In this part, drug preloading for the weak/weak system will be investigated. ATP preloading for PEM (PEI(HA-Na^+/PEI-Mal-C/ATP)$_{20}$) has been created exactly like in weak/strong system. When ATP amount increased more

than >0.5 mg mL^{-1} the film was no longer stable and decomposed. It has been previously assumed, that anionic ATP was attached to PEM in a counterion-like fashion. PEM (PEI(HA-Na^+/PEI-Mal-C/ATP)$_{20}$) ATR-FTIR spectra for upload and release are shown in Appendix, **Figure 8-42 – 8-44**. ATP isolated band at 900 cm^{-1} was integrated and **Figure 4-24** was plotted**.** It is shown in **Figure 4-24** that ATP uptake affinities started to increase till reaching its maximum with value 0.3 mg mL^{-1}. ATR-FTIR spectrum for PEM/ATP complex with ATP (0.3 mg mL^{-1}) (Appendix, **Figure 8-43)**, demonstrated that ATP isolated band has achieved a small shift from 900 to 897 cm^{-1}. However, for higher ATP concentrations, 0.4 and 0.5 mg mL^{-1}, PEM (PEI(HA-Na^+/PEI-Mal-C/ATP)$_{20}$) has shown lower affinities than for ATP critical concentration (0.3 mg mL^{-1}) (**Figure 4-24**) and no band shift has been observed in ATR-FTIR spectra (Appendix, **Figure 8-42**, **8-44**).

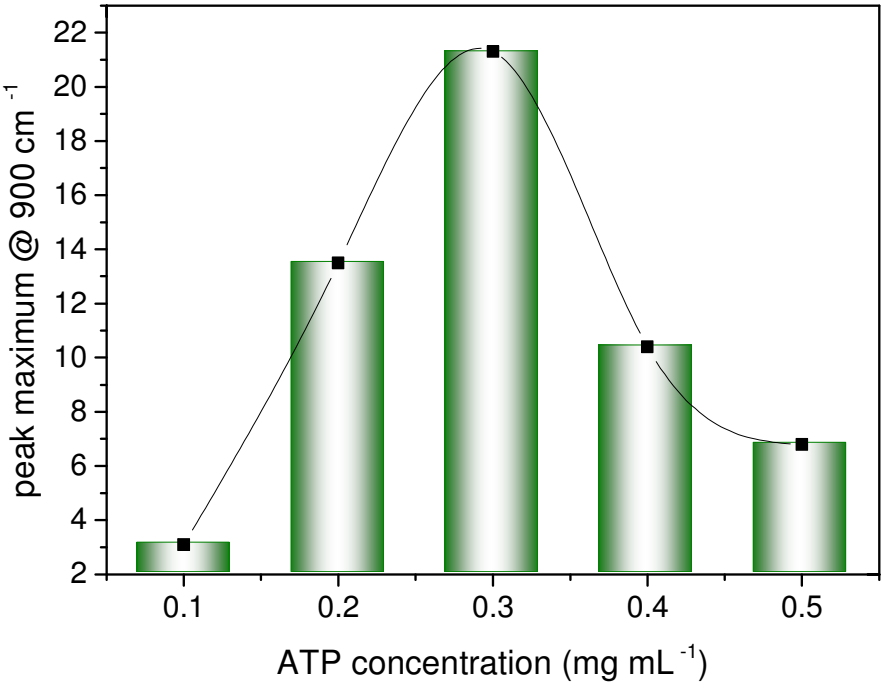

Figure 4-24. ATR-FTIR study for ATP of different concentration PEM (PEI(HA-Na^+/PEI-Mal-C/ATP)$_{20}$). The integration calculation was done at wavelength 900 cm^{-1}.

Similar to loading, release profile is also very important for a drug delivery system. For PEM (PEI(HA-Na^+/PEI-Mal-C/ATP)$_{20}$), ATP release has been investigated in different ionic strengths and pH values. The release of ATP of concentrations 0.2, 0.3, 0.5 mg mL^{-1} out of PEM (PEI(HA-Na^+/PEI-Mal-C/ATP)$_{20}$) was investigated in Millipore water and pure HEPES (shown in Appendix, **Figure 39 – 8-41,** respectively). Almost identical to

weak/strong system, no release has been established on immersing PEM/ATP complex for weak/weak system in charge-free solutions at physiological pH, e.g. Millipore and pure HEPES buffer (Appendix, **Figure 39 – 8-41**). PEM (PEI(HA-Na^+/PEI-Mal-C/ATP)$_{20}$) was subjected to HEPES buffer (0.05M) mixed to NaCl (0.1M) and the mixture pH has been adjusted using NaOH (0.1M), this 1:1 mixture will be notified in an abbreviated version so called HEPES (0.05M)+NaCl (0.1M). PEM/ATP complexes have shown ATP release in HEPES (0.05M) + NaCl (0.1M) at physiological (pH 7.4) and alkaline pH (pH 9) (Appendix, **Figure 8-42 – 8-44**). In contrary, the total PEM/ATP complex degradation has been established in HEPES (0.05M) + NaCl (0.1M) of acidic pH (pH 5.5). ATR-FTIR spectra of PEM/ATP complex are shown in Appendix **Figure 8-42** – **8-44**. Isolated ATP band at 900 cm^{-1} for ATP of concentrations 0.2 and 0.5 mg mL^{-1}, as well as the shifted band at 897 cm^{-1} for ATP 0.3 mg mL^{-1} have been integrated and **Figure 4-25** was plotted. For ATP release out of PEM/ATP complex in HEPES+NaCl mixture at pH 7.4 (**Figure 4-25 a**), after 1000 min about ~17, ~37 and ~60% for ATP loaded amounts of mass values of ~0.2, ~0.3, ~0.5 mg mL^{-1}, respectively have been released. However, in HEPES+NaCl mixture of pH 9 (**Figure 4-25 b**), after 1000 min about ~35, ~57 and ~90% for ATP loaded amounts of mass values of 0.2, 0.3, 0.5 mg mL^{-1}, respectively have been released. It was obvious that the ATP release for PEM/ATP complex was faster in case of pH 9 than that of pH 7.4 (**Figure 4-25**).

The release of ATP molecules of mass values 0.3 mg mL^{-1} and 0.5 mg mL^{-1} ($ATP_{0.3}$ and $ATP_{0.5}$) out of PEM/ATP complex have been retraced via ellipsometry (**Figure 4-26**). Ellipsometric investigations gave an agreement to data investigated via ATR-FTIR spectroscopy (**Figure 4-25**). The PEM (PEI(HA-Na^+/PEI-Mal-C/$ATP_{0.3}$)$_{20}$) initial dry thickness and the end dry thickness after being soaked in different media for 1 day has been investigated (Appendix**, Table 8-7**). Initial SD% for PEM (PEI(HA-Na^+/PEI-Mal-C/$ATP_{0.3}$)$_{20}$) was calculated to the approximated percentage value of ~67, ~42, ~86 and ~71% for Millipore water, HEPES (0.05M and pH7.4), PBS (0.01M and pH 7.4) and HEPES+NaCl (pH9), respectively (**Figure 4-26,** Appendix**, Table 8-7**). However when PEM (PEI(HA-Na^+/PEI-Mal-C/$ATP_{0.5}$)$_{20}$) was immersed in HEPES+NaCl (pH9), the initial SD% was of value 86%. The calculated SD% was considered to be lower than that of the weak/strong system, although PEM/ATP complex's thickness has approximately doubled its original thickness (Appendix**, Table 8-7**).

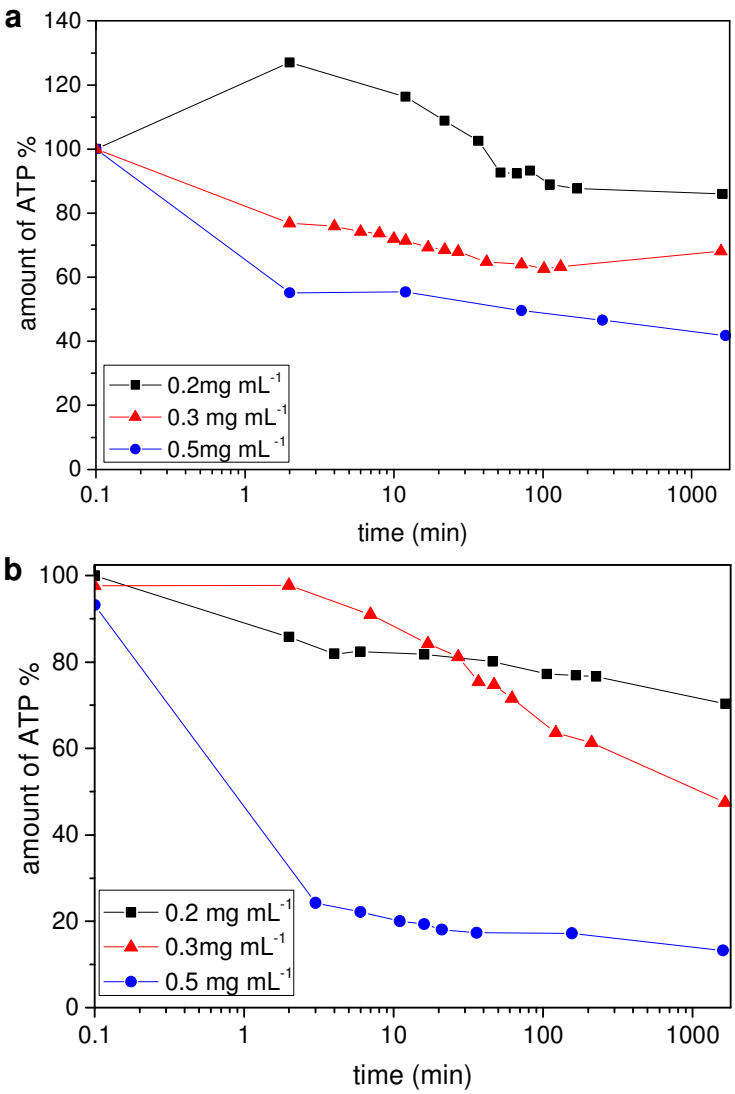

Figure 4-25. Release study using ATR-FTIR, PEM (PEI(HA^{-}Na^{+}/PEI-Mal-C)$_{20}$) prepared via Approach C for different concentration of ATP , the release study was done in HEPES buffer (0.05M) and NaCl (0.1M) mixed with ratio (1:1) (**a**) pH 7.4 (**b**) pH 9, pH was adjusted using NaOH 0.1M

In addition to SD%, initial dry thickness for PEM (PEI(HA-Na^{+}/PEI-Mal-C/ATP)$_{20}$) was measured by ellipsometry in value of ~300 nm (Appendix**, Table 8-7**). By calculating the differences between start dry and end dry thickness after being immersed in rinsing solutions (Δd nm) for ATP 0.3 mg mL^{-1}, Δd was calculated in values ~71, ~3, ~56 and ~130 nm for Millipore water, HEPES (0.05M pH 7.4), PBS (0.01M pH7.4) and HEPES+NaCl (pH9), respectively. However, Δd for PEM/ATP complex for ATP 0.5mg mL^{-1} was of value ~152 nm when immersed in HEPES+NaCl (pH9). When calculating the percentage release value for PEM/ATP complex with ATP 0.3 and 0.5 mg mL^{-1} after one

day in HEPES+NaCl (pH9), the resultant value was approximately equal ~43% and ~50%, respectively. PEM/ATP complex thickness readily decreased after being immersed in HEPES +NaCl pH 9.0, indicating ATP molecules release at a constant rate of ~ 0.8, ~1.2 nm/min for ATP 0.3 and 0.5 mg mL^{-1}, respectively (Appendix**, Table 8-7**).

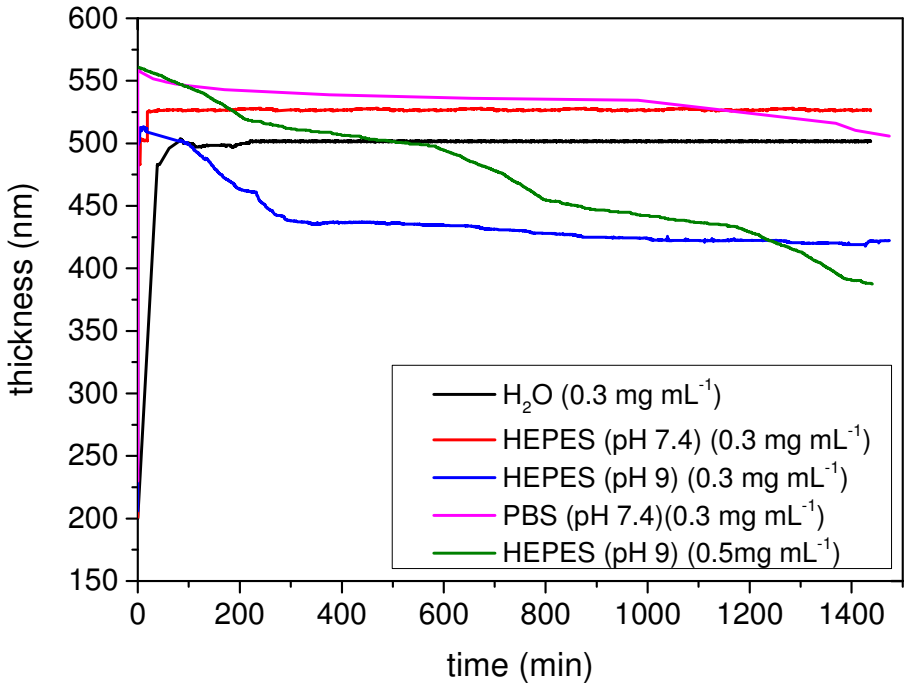

Figure 4-26. Drug preloading process traced by ellipsometric measurements – for ATP of 0.3mg mL^{-1} and 0.5mg mL^{-1}. ATP release was checked in Millipore water, HEPES (0.05M) (pH 7.4) and HEPES (0.05M) + NaCl (0.1M) (pH 9) mixed with ratio (1:1) adjusted with NaOH (0.1M) and PBS (PO_4^{3-} (0.01M) + NaCl (137 mM)+ KCl (2.7 mM)) at pH 7.4.

4.8.2.2. Discussion: Drug preloading and release for weak/weak system

Upon complexing ATP molecules with polyanion (HA-Na^+) and polycation (PEI-Mal-C), the probability for ATP molecules to interact with cationic charges was high. It is assumed that ATP molecules have interacted to both polyions through different electrostatic and non-electrostatic interactions. The most likely assumption is directed toward strong electrostatic interaction between anionic ATP and polycationic PEI-Mal-C. In addition to electrostatic forces, other forces are assumed to be contributed and to increase PEM/ATP interactions probabilities, e.g. hydrogen bonds toward PEI-Mal-C shell in addition to the hydrogen bond which may be established between ATP and HA-Na^+. In

case of weak/weak system, the polycationic charge of protonized amino groups in PEI-Mal-C chain was higher than the polyanionic charges of HA-Na^+ and cannot be totally compensated (**Table 4-3**). There were still free ionized uncompensated $–NH_3^+$ groups to bind ATP, thus making the interaction with the charged surface more favorable and accelerate the interacting process. Therefore, the electrostatic attractive forces between negative ATP and positive $–NH_3^+$ were promoted and the loading amount for ATP reached its maximum at ATP 0.3mg mL^{-1}. PEM/ATP complex with critical ATP mass concentration (0.3 mg mL^{-1}) is shown in Appendix, **Figure 8-43**, where there was a small shift in the ATP peak from 900 to 897 cm^{-1}. These results suggested that most of ATP within PEM (PEI(HA-Na^+/PEI-Mal-C/$ATP_{0.3}$)$_{20}$) formed molecular aggregates. [158, 382, 383] However, when ATP amounts increased to concentration ≥0.6 mg mL^{-1}, PEM was no longer stable and decomposed. The reason is that at ATP mass value of 0.6 mg mL^{-1}, the screening effect was increased and in turn the charge balance between PEI-Mal-C and HA-Na^+ has been destroyed. In addition to the latter reason, PEMs built-up in presence of larger ions were less stable. [145] It strongly decreases the number of complexation sites due to strong polyion–ion interactions and/or high ionic strength and the PEM formation might even become impossible. This in turn leads to the whole PEM destruction. [167] Gain of entropy forces also play an important role in these kind of interactions, where ATP interacted to PEM in a counterion-like fashion. The ATP molecules are larger in size than that of monomer unit of PE. It was reported by Volodkin and Klitzing that there is a competition between the formation of complexes of oppositely charged polyions on one hand and polyion–ion interactions on the other hand. Large ions of high polarizability and a small hydration shell can easier act with the oppositely charged PEs than small ions with a large hydration shell. [167]

On discussing the represented results for the ATP release out of PEM/ATP complex, it has been mentioned that ATP release was subjected and tuned via different ionic strength and pH values. Similarly to weak/strong system no release has been established in Millipore water or pure HEPES pH 7.4 media (Appendix, **Figure 8-39 - 8-41**). In contrary to weak/strong system, the release was slower in HEPES buffer (0.05M) + NaCl (0.1M) at the physiological pH 7.4, and was faster in alkaline pH 9 for the same buffer mixture. PEM/ATP complex stability faced difficulties in acidic medium pH 5.5 and instantly the whole PEM system was destroyed. It is assumed that this kind of degradation has been established due to the rapid release of the outermost HA-Na^+ layer, which was

followed by the instant release of ATP from adjacent and thus the underlying layers. At pH 5.5, HA-Na^+ was deprotonated that in turn leads to the breaking down of the intrinsic interaction sites between HA-Na^+ and PEI-Mal-C and the whole PEM degradation. This assumption is due to the previous investigation that PEM degrades from top to down. [384] These data suggest an interesting hypothesis with respect to PEM composition and drug release tuning properties under the effect of ionic strength and pH values. The change in net charges results in attraction or repulsion between charged drug molecules and PEM components thereby leading to the tuning of drug release. [236] In comparing the immersion solution of pH 7.4 and pH 9.0, faster release in case of pH 9.0 has been observed. For HEPES (0.05M)+NaCl (0.1M)at pH 9.0, the ionized amino group NH_3^+ will be deprotonated slowly and there will be less and less protonated PEI-Mal-C to bind with ATP molecules. In other word, when the pH value reached pH 9.0, there was no free PEI-Mal-C to combine with negatively charged ATP molecules, even electrostatic repulsive forces were emerged and might become dominant in the release process, so burst release has been observed in case of pH 9.0 (**Figure 4-25 b**) other than at pH 7.4 (**Figure 4-25 a**). In addition to pH, ionic strength in this part also plays an important role. It was shown that no release has been observed in case of immersion solution with approximately no ionic strength. Meanwhile, rate of ATP release became faster with the increasing of NaCl concentration, which suggested a significant effect of ionic strength on the release rate. Such phenomenon could be explained by weakening the electrostatic interactions between PEI-Mal-C and HA-Na^+ in the film due to the electrostatic screening of salt, which led to increase the swelling behavior of PEM/ATP complex. Additionally, the electrostatic interaction between ATP and binding sites in the films were also weakened. Similar effects of ionic strength on the release rates of drugs in LbL films have been reported previously in Reference.[385]

4.8.3. Conclusion for preloading and release for both weak/weak and strong/weak system

Tunable drug release nowadays is one of the most important issues under investigation. In turn, LbL thin films have been also investigated extensively for drug delivery applications in recent years based on the hypothesis that their highly tunable properties may lead to controllable drug release behavior. Drug release profile in PEM nanofilms depends mainly on the PEM stability, efficient drug molecules loading as well

as the stable interaction between charged drug molecules and nanofilm components. In this study, it was shown that pH-triggered drug release could also be used in addition to ionic strength to tune the release of electrostatically-bound drug molecules and the drug release was due to the change of net charges of weak PEs within the nanofilms. [386] PEM/ATP complex for both weak/strong and weak/weak systems uploaded with different ATP concentrations (0.2, 0.3, 0.5, 0.6 mg mL^{-1}) were immersed in different pH and ionic strength mediums, e.g. pure HEPES buffer , Millipore water, PBS, HEPES+NaCl (pH 7.4 and 9). In this part, a set of guiding principles have been covered that should significantly aid future attempt to build up a high affinity loading and controlled sustained release PEM. These principles may be stated as follows:

1- In case of both weak/strong and weak/weak systems, it is assumed that ATP molecules can be bound to PEM through electrostatic force and non-electrostatic interactions. The electrostatic interaction lead to an attraction forces between cationic PEI-Mal-C and anionic ATP. In addition, hydrogen bonds may be formed between ATP and both PEI-Mal-C (maltose shell) and counterparts polyanions ($HE\text{-}NA^+$ and $HA\text{-}Na^+$).
2- It has been also observed from ATR-FTIR spectra that small shift for ATP band at 900 to 897 cm^{-1} was demonstrated in case of weak/weak system (Appendix, **Figure 8-43**) which give a proof those ATP molecules uploaded in the form of aggregates in the PEM films due to gain of entropy influences. However, ATP uploading process may lead to different PEM internal structure in order to create potential sites of interactions and avoid competition with the polyanion.
3- The release rate of ATP out of PEM/ATP complex depends significantly on pH and ionic strength of the release medium. Approximately no release has been observed in case of charged-free media, Millipore-water and pure buffer solutions. The release was only taken place in case of salt solutions. In addition to ionic strength, the weak/weak system has shown pH tunable release properties. The release rate was faster in basic solution and in media with higher ionic strength.
4- In case of critical molar ratio for ATP, PEM exhibited the most stable PEM/ATP complex, the highest ATP uploading efficiency and the slowest release profile for both created systems.

5. CONCLUSION AND OUTLOOK

This study has been devoted to building up polyelectrolyte multilayers and to investigate for host-guest interaction of biocompatible HB core-shell polymers with anionic ATP molecules. Among the total non-viral gene vectors, PEI with high transfection efficiency has shown bright prospects in these directions. [45, 46] However, PEI is not fit for keeping on gene expression, [46, 47] due to its serious cytotoxicity. [48-50] Actually, the transfection efficiency and cytotoxicity are almost antagonistic. PEI with a low molecular weight, including 800-Da, 25-kDa or less, displays a low cytotoxicity and transfection efficiency. In contrary, PEI with higher molecular weight (up to 750 kDa) shows higher transfection efficiency and cytotoxicity. Investigators attempted to make some modification against PEI properties. [45, 46] PEI-25k was modified by Appelhans *et al.,* [56] who have presented a rapid method for the development of HPEI decorated with different oligosaccharide architectures as carrier systems (CS) for drug and bioactive molecules for in-vitro and in-vivo experiments. Reductive amination resulted in HPEI with readily available oligosaccharide shells of different densities. The core-shell polymers PEI with different degrees of substitution (DS%) with maltose (PEI-Mal) were applied in the present study. PEI-Mal was prepared according to the scheme described by Appelhans *et al*. [56] Structures with different DS% , ~ 50% and ~ 20% for PEI-Mal-B and PEI-Mal-C, respectively were achieved. Therefore, different densities of maltose shell were obtained (**Scheme 2-4**) by reductive amination. Both PEI-Mal-B and PEI-Mal-C are characterized by their open shell. With the increase of DS%, both the isoelectric point and the surface charge of the PEI-Mal macromolecules will be decreased. At pH 7.5 PEI-Mal-B has less positive charge than PEI-Mal-C (**Table 4-3**).

The formation of a new kind of biocompatible PEMs based on the novel polycationic PEI-Mal was due to an alternative adsorption of PEI-Mal (PEI-Mal-B and PEI-Mal-C) (**Scheme 5-1**), combined with strongly charged polyanion HE-Na^+ (**Scheme 5-1**) forming weak/strong system or weakly charged polyanion HA-Na^+ (**Scheme 5-1**) forming weak/weak system. In order to summarize observations in this study, two divisions will be addressed: (**i**) The first part was the building up studies for both PEM systems (**ii**) the second was the drug loading and release study, whether via preloading or postloading strategies. ATP was the drug model in this study, which has been

loaded and released for both created systems, weak/strong and weak/weak systems. Accordingly, one can expect that the coating composed of PEI-Mal, HE-Na^+ and HA-Na^+, serving as PE with opposite charges to fabricate thin PEM, in addition to ATP as a drug model, should promote a favorable responses to tissue regeneration and controlling cell behaviors.

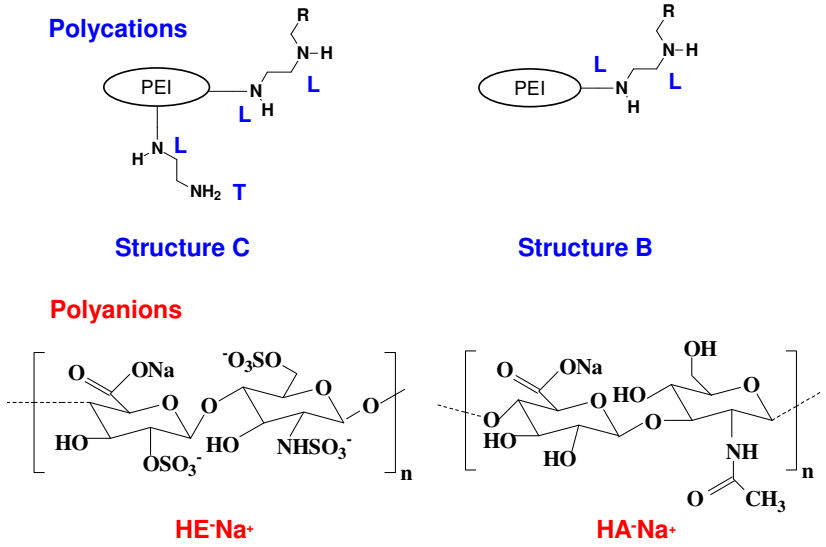

Scheme 5-1. Polycations and polyanions structures

Although some previous studies have focused on studying the dissociation behavior in ML films of weak PEs, built with 2 or more counterparts of equal kinetic affinities, [387-389] this is the first study that uses maltose modified poly(ethyleneimine) as PEM weakly charged polycationic counterpart and it is also one of the few studies which gives a clear link to:

(i) The possibly to build up stable PEM structure although the kinetic affinities between PEM counterparts are not equal and of different stoichiometric ratio. PE‘s charge densities may be adjusted by adjusting their concentrations toward each other. The charge densities adjustments have been investigated through PCD, DLS and zeta potential measurements. The main role in this scenario was given to PEI-Mals, e.g. PEI-Mal-B and PEI-Mal-C, of weak charge densities.

(ii) Although electrostatic interactions between polyions forming PEM are one of the most important interactions in the PEM formation, in comparing the electrostatic to non-electrostatic interactions, the priorities are to the non-electrostatic interactions, e.g.

short rang interaction, Van der Waal forces, double layer force, hydrogen bonds, DLVO and non DLVO forces, etc.

(iii) Both electrostatic and non-electrostatic driving forces profoundly affect PEM growing regime, which in turn has a dramatic influence on PEM stability and its performed interactions toward the surrounding.

(iv) The growth regime is highly affected by the polyions kinetic affinities to each other. In case of weakly charged polyions, the PEM growth is profoundly responsive to the assembly pH, where it is possible for the growth regime to be converted from kinetically blocked to labile kinetically growing system

(v) In addition to previous points, a further study on how the conformational secondary changes are manifested in the physicochemical properties of fabricated PEM has been done. Hence, controlling the dissociation behavior of weak PE is a valuable tool for tailoring PEMs with desired properties. This phenomenon is a particularly important consideration for many potential biomaterials applications for PEMs, which have specific requirements for the fundamental physical properties such as wettability, surface friction, and degree of swelling (SD %). These properties dictate how the material will interact with biological structures such as proteins and cells and, therefore, determine the suitability of the material to a particular application. Drastic changes in the character of the films can be created, readily and reversibly making these films promising for a diversity of applications.

5.1. Polyions stoichiometric ratio calculation

This step was one of the important steps in this study, where calculation of the optimal stoichiometric ratio for both weak/strong and weak/weak system has been performed. In this step, different modalities have been used to emphasis becoming results, e.g. zeta potential, DLS, PCD and ATR-FTIR. It has been proved that PEM optimal ratio for PEI-Mal-B against HE-Na^+ and HA-Na^+ was 20:1 (Appendix, **Figure 8-2, 4-3**) and 2:1(Appendix, **Figure 8-4** and **Figure 4-4**), respectively. However, for PEI-Mal-C the ratio was 7:1 (Appendix, **Figure 8-3** and **Figure 4-3**) and 1:1 (Appendix, **Figure 8-5** and **Figure 4-4**), for HE-Na^+ and HA-Na^+, respectively. This different stoichiometric ratio was

to adjust the kinetic affinities by varying polyions concentrations and ratios toward each other. On the basis of these attributes, it is hypothesized that it is possible to build-up PEM with non-equal stoichiometric ratio. This will open a new future in creating stable PEM with polyions of different kinetic affinities and charge strength.

5.2. Precoating formation

PEI-25k was selected as polycation to form pre-coatings on the surface of negatively charged substrate acting as uniform anchoring network for consecutive layers formation featured with a homogeneous and smooth PEM surface at higher number of bilayer formation. Two different precoating have been created on the surface of planar substrates. According to the precoating formation method, different approaches have been used. Precoating of PEI-25k has been created at pH 11 (PEI-11) and at pH 9.5 (PEI-9.5), for Approach A and B, respectively. Thickness of precoating has been traced as a function of time for different pHs values 11, 9.5, 5.5 for 2 day (**Figure 4-5**). It is important to mention that PEI-25k is practically neutral at pH ≥ 10.5, whereas it possesses considerable charge density in the acidic pH range. [320] At pH 11, thick precoating (~ 60 nm) (Appendix, **Figure 8-7**and **Figure 4-6, 4-5**), measured by means of ellipsometry as well as AFM, has been created on deposition of PEI-25k onto freshly activated planar surface for 2 days. This thickness (*d*) was significantly affected at pH 9.5 and 5.5, where *d* was ~ 30 nm (Appendix**, Figure 8-8, 4-5**) in case of pH-9.5 and ~ 4nm in case of pH 5.5 (**Figure 4-5**). This variation in PE adsorbed amount and the layer thickness may be due to the pronounced role of the electrostatic segment/segment repulsion. I.e., by increasing degree of the protonation of PEI, the deviation from the initial adsorption rate becomes steeper and the adsorption decreases monotonically with the increase of pH value at a fixed ionic strength. [319] Only the thick layers PEI-11 (~ 60 nm) and PEI-9.5 (~ 30 nm) were chosen for further experiments. It was also important to check the topology and morphology via AFM for both chosen precoatings for later PEM building up. In case of PEI-11 (thicker layer) the surface topography appeared smooth with rms of 10 nm with no bloblike shapes or island appeared on its surface (**Figure 4-6, Table 4-4**). However, in case of PEI-9.5, a seemly rougher surface of rms ~ 30nm has been observed (**Figure 4-7** and **Table 4-4).**

5.3. PEM formation and building up regime

The driving force of the buildup process appears, as for ''conventional'' PEM systems, to be the alternate overcompensation of the surface charge after PEI-Mal and the polyanion deposition. It has been shown in this study that the PEM construction seems to take place by the formation of isolated islands, islets and then bloblike structure dispersed on the surface, which in turn grow by addition of new PEs on their top and by mutual coalescence. [321] AFM has shown in the first stages of building up that both higher rms and pores are presented (Appendix, **Figure 8-10 – 8-19**). AFM has also shown that after reaching higher number of bilayers depositions, a continuous PEM film is formed without any holes or pores .(Appendix, **Figure 8-10 – 8-19**).

PEM building up has been established with three different approaches, Approach A, B and C. The main distinguish character between Approach A and B was the precoating, where PEI-11 and PEI-9.5 was used for Approach A and B, respectively. While for Approach C, the polycationic PEI-Mal was protonated with HCl (0.5M) and its pH was adjusted to value 5.5. For weak/strong system, it has been shown via ellipsometric investigations that PEM growing regime and its overall mass seem to increase in a pseudo-linear or exponential way in case of Approach A and Approach B for PEI-Mal-B and PEI-Mal-C, respectively. For PEM ($PEI(HE\text{-}Na^{+}/PEI\text{-}Mal\text{-}B)_{50}$), no growth differences have been observed between Approach A and C, while B was of linear growing regime, however, more investigations are recommended. For PEM ($PEI(HE\text{-}Na^{+}/PEI\text{-}Mal\text{-}C)_{50}$), it was clearly observed that the exponential growing regime has switched to completely linear growing up after changing Approach A and B to C (**Figure 4-8 b**). In Approach C, it was assumed that after PEI-Mal was protonated and adjusted to pH 5.5, it lost part of its flexibility and a kind of labile/kinetically blocked growth transition has been achieved (**Scheme 4-4**). PEM thickness was measured by ellipsometry. In case of PEM ($PEI(HE\text{-}Na^{+}/PEI\text{-}Mal\text{-}B)_{50}$), thickness of 50 bilayers was measured in range of ~165 nm and ~139 nm for Approach A and B, respectively. The highest thickness was measured for PEM fabricated with Approach C and it was ~175 nm. For PEM ($PEI(HE\text{-}Na^{+}/PEI\text{-}Mal\text{-}C)_{50}$), thickness for 50 bilayers has been measured in values: 1.29 µm, 1.13 µm and 185 nm for Approach A, B and C respectively.

In case of weak/weak system, PEM (PEI(HA-Na^+/PEI-Mal-C)$_{25}$) has been successfully built-up. Both charge densities for PEI-Mal-B and PEI-Mal-C have been investigated. Only PEI-Mal-C for building up weak/weak PEM with stoichiometric ratio of 1:1 has been chosen. PEM (PEI(HA-Na^+/PEI-Mal-C)$_{25}$) thickness has been measured via ellipsometry with values 1.44 µm. 1.43 µm and 479 nm for Approach A, B and C, respectively. It has been emphasized according to ellipsometric measurements, that there were two different growing regimes with switching point involved in the same PEM system (**Figure 4-9**). This PEM switching point was clearly obvious after the 10^{th} bilayer (Appendix, **Figure 8-20**). The only logical postulations for this phenomenon are that both polyions PEI-Mal-C and HA-Na^+ are diffusing in-and-out of PEM structure. This would throw more light upon the kinetic behavior of the prepared PEM. It was shown in **Table 4-3** that the calculated charge density of HA-Na^+ is lower than that of the protonated PEI-Mal-C. This means that it was not possible to compensate all the cationic sites on PEI-Mal-C in one deposition step. Otherwise, PEI-Mal-C compensation has been established in a successive way and when the film is further brought in contact with HA-Na^+ solution during the layering up process.

5.3.1. PEM swelling and stability

The main task in this study and the most challenging point was to have a stable PEM against different environmental circumstances. Intensive effort has been carried out to adjust the whole polyions affinities to one another in the building up. Thus, it was logic to measure both swelling and stability behaviors for both weak/strong and weak/weak systems. The high stability of PEMs, which was generally observed, was attributed to the large number of electrostatic and non-electrostatic interactions formed between polyions in subsequent layers. These results were discussed in two different directions, which were swelling and stability. Actually both behaviors cannot be separated; the resultant PEM must have the ability to swell in order to interact with surrounding and this swelling must be accomplished with stable PEM.

In case of weak/strong system, Approach A, B and C have been examined for four days in three different submersion media; Millipore water, PBS and NaCl (0.1M). Firstly, in the direction of swelling and for PEM (PEI(HE-Na^+/PEI-Mal-B)$_{50}$) : for the three approaches, SD% in PBS buffer was ~107%, ~105% and ~130%, for Approach A, B and C

, respectively (**Figure 4-12 a, Table 4-6**). However, for PEM (PEI(HE-Na^+/PEI-Mal-C)$_{50}$), SD% in PBS buffer was ~171%, ~248% and ~67%, for Approach A, B and C, respectively (**Figure 4-12 b, Table 4-6**). Secondly, in the direction of stability: all of the approaches for both PEI-Mal-B and PEI-Mal-C were stable in Millipore water. The most stable PEM was that fabricated by Approach C. Approach C for both PEI-Mal-B and PEI-Mal-C was kinetically stable in the three stated media for the whole subjected period. This may be relied on the linear growing regime and PEM formation features. The lower the pH of weak polycation, the higher the degree of its charge ionization will be achieved. Therefore, its ionic interactions with strongly charged polyanion in PEM will be enhanced. This increase in ionic interactions may lead to impaired mobility of the polycation. Only about ~5 nm for both PEMs by PEI-Mal-B and PEI-Mal-C were reduced from the total dry initial thickness after being subjected to PBS buffer solution for four days (**Table 4-5**).

In case of weak/weak system, PEM (PEI(HA-Na^+/PEI-Mal-C)$_{25}$) was subjected to the same submersion media for four days. Firstly, in the direction of swelling, all the approaches have swollen with the same SD%, which was ~50% (**Table 4-9**). Secondly, for stability and equilibrium, the most stable approach was Approach C; there was no variation between the initial thickness and the final after subjecting the PEM to PBS buffer solution for 4 days (**Table 4-9** and **4-10**). Approach A and B lost about ~6% of their total thickness after being subjected to PBS buffer solution for 4 days.

In case of Approaches A and B for both systems, weak/strong and weak/weak systems, they were not totally stable in the presence of counterions, e.g. PBS and NaCl, in contrary to Millipore water. The situation for weak/strong system was worse than that of weak/weak system. This may be due to the different growth regimes which are followed by both systems. This degradation may be explained that there was a kind of reduction in the complexation sites and densities related to the transition from intrinsic to more extrinsic charge compensation. These different interactions have led to a high SD%, which in turn simply led to a successive degradation of the system over time, e.g. weak/weak system in NaCl (0.1M) (**Figure 4-14**), or in other cases the instant destruction of the whole system once subjected to the charged medium, e.g. weak/strong system in NaCl (0.1M) (**Figure 4-11**). This may emphasize the idea that counterions have kinetically disturbed PEM built-up fabricated by Approach A and B, however, the disturbance was lower in case

of Approach C which was more kinetically blocked. The SD% for PEM via Approach C was lower than the others (**Table 4-6**, **4-9**), this was probably due to counterions penetration difficulties and extrinsic/intrinsic transition creation. From here it was concluded that the higher the chain mobility, the stronger the ability for the system to swell and the lower stability.

5.4. Drug loading and release methods

ATP anionic molecules were considered as the drug model in this study. This part was divided in to main sections: (**i**) drug cyclic loading and release or the drug postloading, (**ii**) and secondly, ATP molecules were considered to be one of main PEM counterparts or drug preloading. In the latter case ATP was mixed with both polyions and the chosen ATP concentrations was depending on the molecular weight of the respective monomer units of the used polyanion (Experimental, **Section 6.2.2**). For the drug loading and release step, the most stable PEM (fabricated by Approach C and polycationic PEI-Mal-C) has been used.

5.4.1. Drug postloading and release

In this part ATP has been treated exactly similar to counterion-like fashion. For both systems excess concentration of ATP (0.5 mg mL^{-1}) has been used. The most important difficulty in this part of study is that PEM has to be stable even after the uploading of anionic ATP molecules. For both systems cyclic upload and release has been achieved. The ATP absorbance fluctuated regularly with the successive loading and release of ATP molecules in both weak/strong and weak/weak systems and the adsorption efficiency of PEM to ATP were almost unchanged after ≥ 20 times of loading and release (**Table 4-10, 4-11**). Intriguingly, two different features have been observed: the first observation was in case of weak/strong, where after PEM being subjected to ATP (0.5mg mL^{-1}) PEM swelling has been demonstrated (**Figure 4-19**). However, in case of weak/weak system the contrary and PEM shrinkage has been observed (**Figure 4-20**). For linearly kinetically blocked weak/strong system, a group of adjacent intrinsic ion pairs has sequentially dissociated, moved and reassociated in the presence of ATP (**Scheme 5-2**). Side-to-side to the intrinsic sites new interaction sites so called extrinsic sites of interaction has been created. This dissociation and new interaction has led to the swelling behavior.

The conformational structure of PEM counterparts plays an important role in suggesting the growing regime, which in turn affects drug loading affinity and release.

Surprisingly, the previous observations have been reversed in case of weak/weak system (**Figure 4-20**). For explaining this behavior, two different reasons have to be presented: (**i**) presence of uncompensated sites of positive PEI-Mal-C, especially on the top of PEM (anomalous inter-diffusion portion), this with no doubt increases the probability for the anionic ATP molecules to interact via extrinsic sites with PEI-Mal-C, which led to the formation of interlayer bridge between layers (**Scheme 5-2**). These interlayer bridges compressed fabricated PEM and reduced its thickness (**ii**) The second reason for the PEM collapsing feature represented for PEM (PEI(HA-Na^+/PEI-Mal-C)$_{20}$) might be due to the presence of the polyanion HA-Na^+. Previously polyelectrolyte gel behavior and the conformational changes for HA-Na^+ have been discussed (**Scheme 4-7**). [370] The PE-gel in this case was that in higher ionic strength, it preferred to shrink exactly like natural gel. It was assumed from the previous data that ATP molecules were stable and interacted with PEM mainly through strong electrostatic interactions in the presence of additional non-electrostatic interactions, e.g. hydrogen bond, gain of entropy... etc., for PEI-Mal-C and HA-Na^+. Therefore, it was difficult for ATP to be released in the presence of Millipore-water and pure buffer as submersion solutions and without PEM kinetic disturbance action. The complete ATP release was achieved only in NaCl (0.1M) pH 6.5 in case of weak/strong system (**Table 4-10**) and through HEPES (0.05M) + NaCl (0.1M) pH 9 (**Table 4-11**).

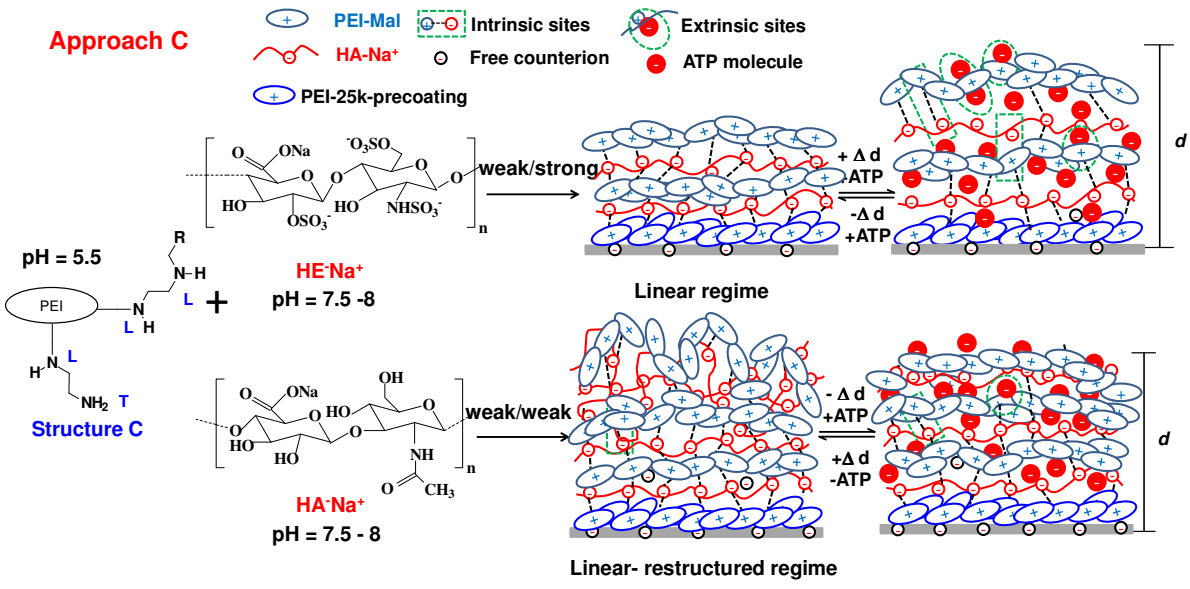

Scheme 5-2. ATP loaded PEM via Approach C for weak/strong and weak/weak systems

5.4.2. Drug preloading and release

In case of drug preloading, addition of salt (ATP molecules) to the PE solution during ML preparation introduced counterions which also contributed to complex formation. [145, 390, 391] It was expected that the loading process has been performed due to PC/ATP complexation, with molar ratio arranged in descending order : 1: 35, 1:29, 1:23 1:18, 1:12 and 1:5, for ATP mass values with descending arrangement 0.6, 0.5, 0.4, 0.3, 0.2 and 0.08 mg mL^{-1}. ATP molecules have been also mixed to polyanions (HE-Na^+ and HA-Na^+) with different molar ratios. The mixing ratio of both PA and PC was 1:5. This ATP/polyanion mixing has raised non-electrostatic interactions between ATP and the presented polyanions. From the previous data investigated from ATR-FTIR and a small shifting in the ATP isolated band in weak/weak system from 900 to 897 cm^{-1}, one can conclude that ATP molecules formed aggregates in the PEM films. For the assumption that ATP contributed to PEM in counterions-like fashion, therefore as if ATP molecules concentration increase, the counterions screening effect will be also further increased till reaching the threshold. After this critical ATP concentration, PEM existence probability will be decreased till destroying the whole PEM equilibrium and no PEM structure will be found onto the interface's surface. In the threshold, maximum loading affinity and system equilibrium will be achieved (**Figure 4-21, 4-24**). Those strong electrostatic and non-electrostatic loading interactions affect profoundly the release profiles. The release rates of ATP molecules from PEM structure significantly depend on pH and ionic strength of the medium in which ATP was released. No release has been achieved in either Millipore water or pure buffer solution. The release has been only achieved for both weak/strong and weak/weak systems, when they subjected to a kinetic disturbance conditions. For weak/strong system, harsh immersion solution of HEPES buffer solution (0.01M) in addition to NaCl (0.1M) pH 7.4 was used (**Figure 4-22**). However for weak/weak system, PEM has been subjected to HEPES buffer solution (0.05M) in addition to NaCl (0.1M) pH 7.4 , whereas the release was faster in pH 9 (**Figure 4-25**). At pH 9.0, PEI-Mal-C will be deprotonated and the positive charge will be less to combine with anionic ATP molecules and thus the electrostatic repulsive forces will be emerged and become dominant in the release process. Therefore, burst release has been observed in case of pH 9.0 (**Figure 4-25 b**) than that of pH 7.4 (**Figure 4-25 a**).These data suggest an interesting hypothesis with respect to PEM composition and drug release tuning properties under the effect of ionic strength and pH values. The change in net charges results in attraction or repulsion

between charged drug molecules and PEM film components thereby leading to the tuning of drug release. [236]

Finally, it is important to conclude that a stable glycopolymers PEM based on a novel polycationic maltose modified hyperbranched poly(ethylenimine) has been successfully created. Optimum conditions for PEM building up were observed whether in case of equal (1:1) (weak/weak system) or variable stoichiometric ratio (weak/strong system). A stable swelling PEM without degradation has been achieved. The finally created PEMs for both weak/strong and weak/weak systems have been efficiently loaded with a drug model (ATP). ATP release out of PEM has been achieved without PEM degradation for both preloading and postloading strategies. These biocompatible PEMs built-up with polycationic PEI-Mal and polyanionic HE-Na^+ and HA-Na^+ being a natural extracellular matrix polysaccharide are profoundly considered as a model substrates for the design of bioactive films and drug delivery coatings. In particular, this kind of film should enhance specific cell proliferation or adhesion. The incorporation of biologically active compounds in the films or their coupling to PEI-Mal molecules is also foreseen. Indeed, investigation of living cells interaction with these fabricated PEMs should be investigated in a future work.

6. EXPRIMENTAL PART

6.1. Chemical reagents and preparation methods

6.1.1. Polyelectrolytes

6.1.1.1. Polycations

Cationic maltose-modified hyperbranched poly(ethyleneimine) (PEI-Mal) was received by reductive amination of hyperbranched PEI in the presence of minor maltose as previously described by Appelhans *et al.* [56] Two different architectures of PEI-Mal were used in this study: PEI-Mal-B and PEI-Mal-C. Poly(ethyleneimine) (Lupasol WF) (PEI-25k) (M_w = 25,000 g mol^{-1}, M_n = 9,600 g mol^{-1}, PDI = 2.6, DB = 70.6 %) was used as the core of PEI-Mal and PEM precoating. It was purchased from BASF SE (Ludwigshafen/Germany)

Synthesis of PE-Mal-B and PEI-Mal-C

The following general experimental procedure was applied to obtain various maltose modified PEI (**Scheme 6-1**); it corresponds to the original procedure described by Appelhans *et al.* [56]

(i) Synthesis of PEI-Mal structure B (1:0.5): 5 g of PEI-25k was dissolved in 100 mL of 0.1 M sodium borate solution followed by the addition of 21g D(+)-maltose monohydrate and 7.3 mL of borane pyridine complex (BH_3·Py) purchased from sigma (Germany) in round bottom flask of 250 mL, i.e. BH_3·Py complex was injected under being stored in nitrogen gas. The reaction solution was vigorously stirred at 50°C for 7 days and stored in oil bath to avoid change in temperature (**Scheme 6-1**). Then, the crude product was purified by dialysis toward Millipore-water for 3-4 days, taking in account that dialytic Millipore water must be changed 3-4 times/day.

(ii) Synthesis of PEI-Mal structure C (1:0.2): 5 g of PEI-25k was dissolved in 60 mL of 0.1 M sodium borate solution followed by the addition of 8.395 g D(+)-maltose monohydrate and 2.9 mL of BH_3·Py complex in round bottom flask of 250 mL in oil bath (**Scheme 6-1**), i.e. BH_3·Py complex was injected under being stored in nitrogen gas. The reaction solution was vigorously stirred at 50°C for 7 days. Then, the crude product was purified by dialysis toward Millipore-water for 3-4 days.

For dialysis, membrane of approximately 2000 MWCO was used. The different maltose-modified PEIs were obtained via freeze-drying. The yields were between 60 and 90 %. The molar ratio NH-groups/maltose and masses of D(+)-maltose monohydrate required for the reaction with 1 g of PEI. The molar amount of D(+)-maltose monohydrate and the reduction agent was taken in an equimolar ratio. Structural characterization of various PEI-Mal architectures was shown in **Scheme 4-1**.

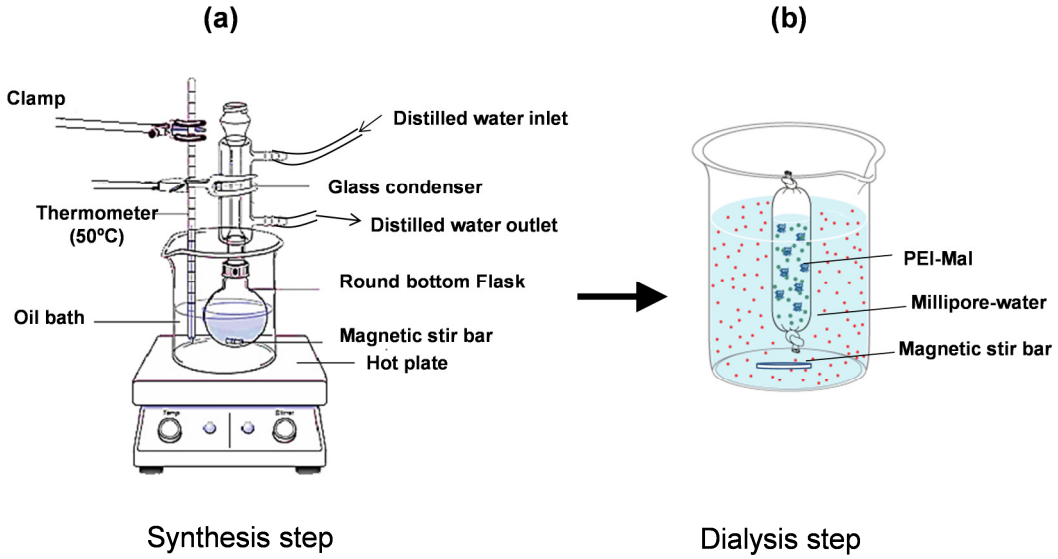

Scheme 6-1. Simplified schematic diagram showing PEI-Mal (**a**) synthesis step followed by (**b**) dialysis step

For the synthesis of PEI-Mal, poly(ethyleneimine) (PEI 25k) (Lupasol WF with molecular weight (M_w) 25000 g mol^{-1} , Mass number (M_n) 9600 g mol^{-1}, [56] and degree of branching of about 71%, using ^{13}C NMR method, [56] was used. Lupasol WF was received by BASF SE (Ludwigshafen/Germany). Molecular properties (Molecular weight and degree of maltose substitution of amino groups in PEI-Mal) of PEI-Mal are summarized in **Table 4-1**. Maltose was purchased from Sigma–Aldrich.

6.1.1.2. Polyanions

Two different systems have been established with two different polyanions: (**i**) weak/strong system (**ii**) weak/weak system.

(**i**) For weak/strong system - anionic heparin sodium salt (HE–Na^+) was purchased from Roth (Germany), (M_w = 2×10^4 g mol^{-1}). (**ii**) For weak/weak system - anionic hyaluronic acid sodium salt from streptococcus (HA-Na^+) (M_w = 1500-1800 kDa) was

purchased from Sigma–Aldrich (Germany). HA-Na^+ solution was always prepared the day before the dipping deposition experiment and stored overnight at room temperature to allow for a complete dissolution of the initially formed gel. Adenosine 5′-triphosphate disodium salt hydrate (ATP) (≥99%) was purchased from Sigma–Aldrich (Germany). Polyanions were used directly without being further purified or chemically treated.

6.1.2. Substrate activation

In this study, two different types of planar solid substrates have been used (**i**) for ATR-FTIR measurement: rough attenuated total reflection-Fourier-transform infrared (ATR-FTIR) internal reflection prism/element (IRE) from silicon (Si-IRE) and germanium (Ge-IRE) single crystal have been used. A specific trapezoidal polished silicon single crystal was used and purchased from Komlas GmbH (Berlin, Germany). (**ii**) Thermally grown oxide layer treated smooth Si wafers were also used as a solid substrate. Si wafers with thermal silicon oxide SiO_2 layer thickness measured (25–30 nm) by multi-wavelength ellipsometry were purchased from Institute of Semiconductor and Microsystem Technique, Technische Universität Dresden (Germany). Si-IRE was cleaned by piranha solution (H_2SO_4:H_2O_2) (1:1) for 30 min then Si-IRE was re-cleaned using remote chemical analysis (RCA) protocol or called standard cleaning. The slides were immersed in a mixture (H_2O_2 (pa, 30% aqueous solution, Fluka): NH_4OH (pa, 28% aqueous solution, sigma aldrich): Millipore-water) (1:1:5) for another 30 min at 70ºC, then rinsed thoroughly with Millipore water and ethanol.

Ge-IRE is so fragile and on subjected to these harsh condition will be instantly damaged. Ge-IREs were practically cleaned by mechanically rubbing by humid tissue pads. Latter was followed by UV plasma treatment under low pressure (Sterilizer PDC-32 G, Harrick, Ossining, NY, U.S.A., medium RF power level of 10.5 W) for 10 min. to remove organic impurities and create reproducible surface properties. The latter step was followed by being immersed in absolute ethanol for 1 minute and then dried thoroughly under a stream of dry nitrogen.

Si wafers were activated via sonication for 30 min in Millipore water, then they were once more sonicated for 30 min in absolute ethanol and finally another 30 min in

remote RCA protocol (1:1:5) (NH_4OH: H_2O_2: Millipore) at 70ºC, rinsed thoroughly with Millipore water and ethanol, and then blow-dried carefully with N_2 stream.

6.1.3. Solvents, buffer solutions and submersion solutions

(**i**) Phosphate buffered saline (PBS) tablets were purchased from Sigma–Aldrich (Germany). PBS buffer solution was of concentration 137 mM NaCl, 2.7 mM KCl, 0.01M PO_4^{3-} and pH7.4. (**ii**) NaCl solution (0.1M) was purchased from Sigma–Aldrich (Germany). (**iii**) 4-(2-Hydroxyethyl) piperazine-1-ethanesulfonic acid (HEPES buffer) (0.01M and 0.05M) of pH 7.4 adjusted by using NaOH 0.1M. Both HEPES buffer and NaOH were purchased from Sigma–Aldrich (Germany). (**iv**) HEPES (0.01M) +NaCl (0.1M) mixed with ratio 1:1 at pH 7.4, solution pH was adjusted by using NaOH (0.1M) (**v**) HEPES (0.05M) + NaCl (0.1M) mixed with ratio 1:1 at pH 9, solution pH was adjusted by using NaOH (0.1M). (**vi**) Deionized water (Millipore, Germany) was used having a resistance of 18.2 MΩ cm (25ºC). Hydrochloric acid concentrate (HCl) (0.5M) and sodium hydroxide (NaOH) (0.1M) were purchased from Fluka (Germany). This was sufficient to stabilize the pH of all polyelectrolytes within 0.05 pH unit. All chemicals were used without further purification.

6.1.4. Precoating preparation

The precoating is always PEI-25k (Lupasol WF) that was received from BASF SE (Ludwigshafen, Germany).The freshly activated substrates were being directly stored in the stirring direction of a slow-wise stirring PEI-25k solution (2mg mL^{-1}) for 20 hours. PEI-25k with pH 11 (PEI-11) fabricate thick precoating 60 nm, measured by ellipsometry (Approach A). However, when PEI-25k pH was adjusted by using HCl (0.5M) to pH 9.5, PEI-9.5 was fabricated. Solvent used in precoating was Millipore-water.

6.1.5. Preparation protocol (polyelectrolyte multilayer self-assembly formation)

The multilayers were prepared according to the LbL technique suggested by Decher. [131] The LbL technique was performed using automatic dip-coating device, dip-coater with variable dipping speed (DIP COATING ROBOT DR-3, Riegler & Kierstein

GmbH, Berlin , Germany). PEMs are built up with a rather simple experimental setup sketched in **Scheme 2-6**. If the cycle process starts for example from a negatively charged substrate to grow the film, the first layer is deposited through polymer adsorption by dipping the surface into a polycationic solution (positively charged). The next step is to rinse the surface in Millipore-water in order to remove the polymers that are not tightly bound to the substrate. This ensures that no free polycations interact in solution with the other components would be still in contact to the film. The next layer is deposited by immersion of the substrate containing the first layer into a solution of the oppositely charged polymer. The new layer is then washed. This cyclic process is carried out until the desired number of layers is achieved. The solution dip method has been automated using a variety of commercially available instruments (M. Müller, IPF Dresden e.V., Germany).

6.1.5.1. Systems under investigation

Two different systems have been created and investigated. (**i**) weak/strong system: (**a**) polycations used for PEM formation were PEI-Mal-B and PEI-Mal-C (**b**) polyanion used in this system is strong negatively charged heparin sodium salt (HE-Na^+). (**ii**) weak/weak system: (**a**) polycation used for PEM formation was PEI-Mal-C, however (**b**) polyanion was weak negatively charged hyaluronic acid sodium salt (HA-Na^+). All PEM systems have been created using three different approaches, Approaches A, B and C. PEM system were build-up on planar substrates.

6.1.5.2. PEM Approach A, B and C

PEM were prepared using Approach A, B and C, presented in **Scheme 4-2**, and described as follows where the outermost layer is always polyanion: All substrates were first primed with a layer of PEI-25k for 20 hours (pre-coating's pH depends on which approach has been used).

Approach A - activated substrate was dipped into a precoating solution of PEI-11, composed of PEI-25k 2mg mL^{-1} in 18.2 MΩ Millipore water with pH 11 for 20 hours, then this is followed by alterative deposition of PEI-Mal at pH 7.5-8 for 20 min followed up by 1 min rinsing step in Millipore water and polyanions (HE-Na^+ or HA-Na^+) pH 7.5-8 for 20 min followed up by 1 min rinsing step in Millipore water. This process will be repeated

several times until the desired number on bilayer formation is achieved for fabricating defined PEM. For weak/strong system: 20 wt% aqueous solution of PEI-Mal-B adjusted to pH 7.5-8, 7 wt% aqueous solution of PEI-Mal-C adjusted to pH 7.5-8 against 1wt% aqueous solution of HE-Na^+ , kept at its physiological pH 7.5-8, were used for establishing different PEM . However, for weak/weak system PEM was fabricated with PEI-Mal-C: HA-Na^+ with concentration ratio 1:1 (0.5mg mL^{-1}). The pH of both polyanions and polycations solutions were depended on Millipore solution used to dissolve them within the experimental and with uncertainty of 0.5 pH units.

Approach B - Approach B was exactly similar to Approach A except in the precoating. PEI-9.5 was used as a positively charged precoating for PEM formation. PEI-25k (2mg mL) dissolved in 100mL 18.2 MΩ Millipore water adjusted by using HCl (0.5M) to pH 9.5. The precoating is followed by PEM deposition to the desired number of cycles per depositions (**Scheme 4-2**).

Approach C - activated substrate was soaked into a pre-coating solution of PEI-25k 2mg mL^{-1} dissolved in 18.2 MΩ Millipore water with pH 11 (PEI-11) , for 20 hours, then this was followed by alterative deposition of polyanions (HE-Na^+ or HA-Na^+) pH 7.5-8 for 20 min followed up by 1 min rinsing step with Millipore water and PEI-Mal at pH 5.5 , adjusted by HCl (0.5M) for 20 min followed up by 1 min rinsing step with Millipore water. This process is steadily repeated until the desired number on bilayer formation was achieved. The same mass ratios of PEI-Mal-B and PEI-Mal-C against HE-Na^+ and HA-Na^+ as mentioned in Approach A have been used.

6.1.6. Preparation in-situ PEM

The precoated internal reflection elements (ATR crystals) were placed in an in situ ATR cell (M. Müller, IPF Dresden e.V., Germany) forming an upper sample (S) and a lower reference (R) compartment on the front side of the Ge-IRE, respectively, sealed by O-rings. PEM deposition was achieved by contacting alternately the S compartment of the IRE with polycation solution (**i**), Millipore water (**ii**), polyanion solution (**iii**), Millipore water (**iv**) and again with (**i**) using a peristaltic pump (ISM 931, Ismatec®, Germany) at a flow rate of 5 mL min^{-1} for a defined number of adsorption steps. Every adsorption step polycation takes 20 min and every rinsing step (Millipore water) 1min. The R compartment

was filled with Millipore water. The layering up was achieved by flowing 50 mL of desired solution in a closed-loop mode at the same mentioned flow rate (**Scheme 6-2**).

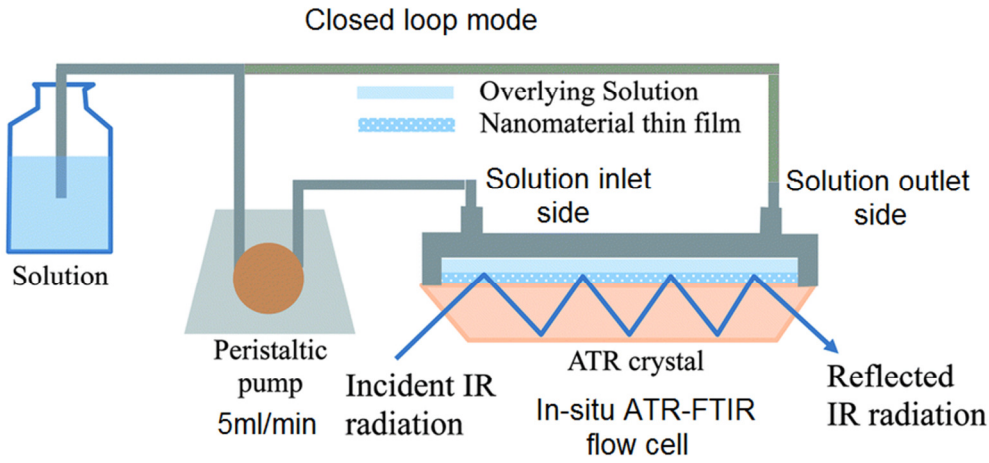

Scheme 6-2. Simplified schematic diagram represents the protocol for preparation of in-situ PEM via in-situ ATR-FTIR flow cell. PEM deposition is performed on the surface of Si-IRE. The same procedure was used in case of the postloading drug release, taking in account that the solution is changed from the polyions to the immersion solutions with different ionic strengths and pH values.

6.2. Uptake and release process

6.2.1. Drug cyclic upload and release (drug postloading)

PEM of only 20 bilayers for both weak/strong system and weak/weak system has been created, in order to facilitate measurements via ATR-FTIR as it was difficult for ATR-FTIR to detect more than 1 μm. In case of ellipsometric measurements: PEM was built-up on silicon wafers, while for ATR-FTIR spectroscopy measurements: PEM was built on ATR-IRE. The drug model in all cases is adenosine tri-5' phosphate disodium salt (ATP) 0.5mg mL^{-1}. The prepared PEM was built in the in-situ cell: (**i**) ellipsometry cuvette and/or (**ii**) ATR-flow cell (**Scheme 4-8 and 6-2**). (**i**) The PEM is subjected to Millipore water or PBS buffer (**Scheme 6-3**) in order to swell and increase the probabilities for ATP loading to the PEM bulk structure. The latter step is followed by ATP addition, taking in account that PEM structure must be kept in the wet state. ATP absorption lasted about 40 minutes. The previous step was followed by several number of rinsing steps. It is worth to mention that the PEM surface must be wet during the whole in-situ experiment. The in-situ cuvette occupied for 5mL of total liquid content. The submersion solution in contact to the

surface was squeezed away, keeping one centimeter square from this solution. The concentration of ATP solution (0.5 mg mL^{-1}) was calculated using dilution equation, **Eq. 6-1** is represented in Reference [392]:

$$C_{initial}V_{initial} = C_{final}V_{final} \qquad \textbf{Eq. 6-1}$$

Where, $C_{initial}$ and $V_{initial}$ are the initial concentration and the initial volume of the submersion solution, respectively. C_{final} and V_{final} are the final concentration and the final volume of ATP solution in cuvette, respectively.

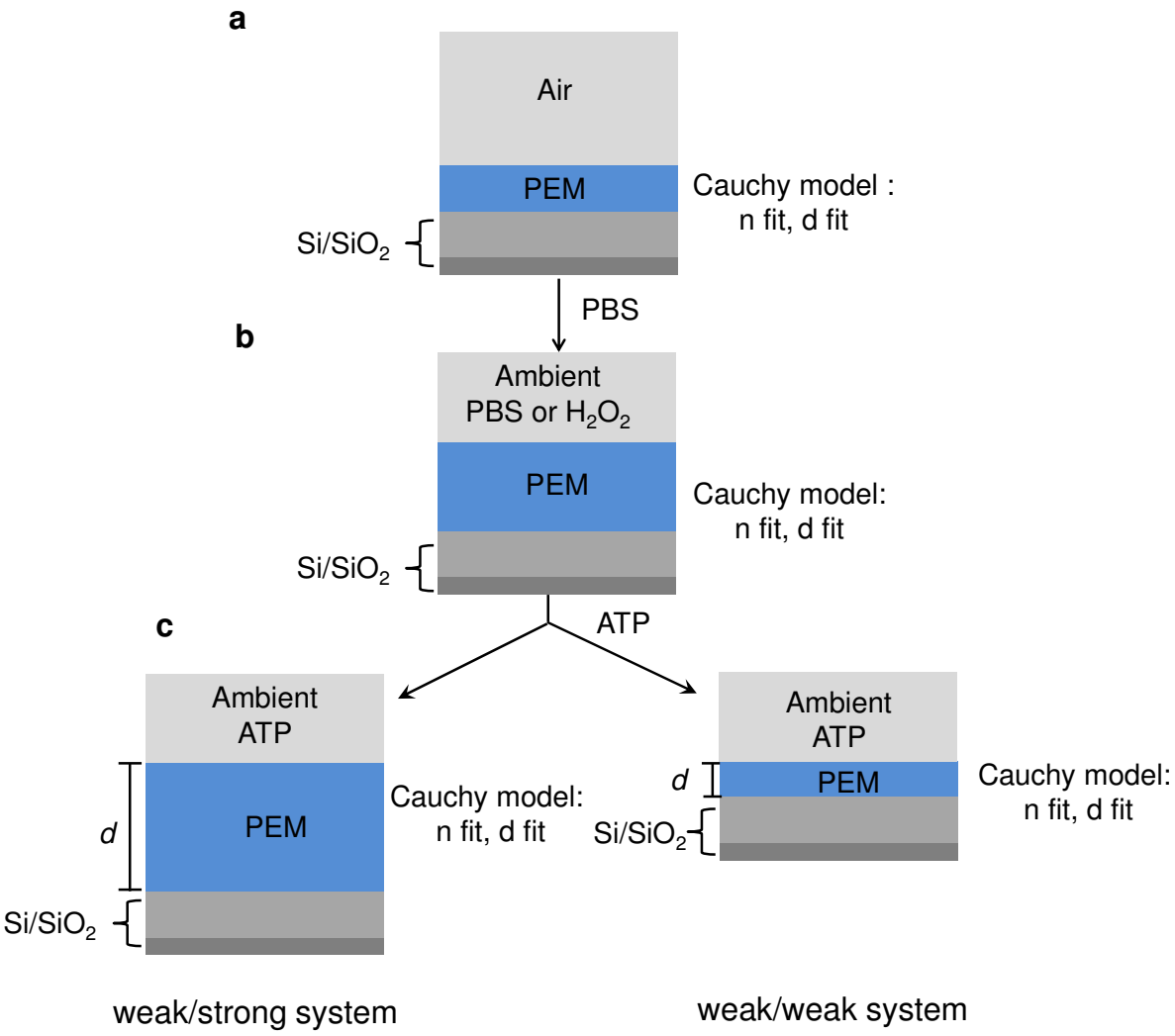

Scheme 6-3. Ellipsometric models for weak/strong and weak/weak systems for ATP absorption with the top Cauchy PEM where d and n were simultaneously fitted. (**a**) Dried PEM, (**b**) swollen PEM and (**c**) PEM state after ATP addition

(**ii**) In case of in-situ ATR-FTIR, cycling loading and release have been done in closed system by using a peristaltic pump at a flow rate of 5mL min^{-1} for both swelling and immersion solutions (**Scheme 6-2**). Then, PEM was subjected to Millipore water, as a swallowing medium, till reaching the maximum equilibrium. The latter step was followed by the ATP (0.5 mg mL^{-1}) addition with keeping in mind that the PEM system must be all the time in a wet state. The ATP addition lasted around 40 minutes and then was followed by 5 cycles of fresh Millipore water rinsing steps. Then the complete rinsing steps have been done.

In case of weak/strong system the complete ATP release has been performed via submersion solution NaCl 0.1M pH 6.4. Moreover, in case of weak/weak system the instant and complete release has been performed after the addition of the immersion solution HEPES (0.05M) +NaCl (0.1M) (1:1) solution pH 9.

6.2.2. Drug preloading and release

In this part ATP molecules are considered to be one of the PEM's counterparts (**Scheme 4-9**)**.** The built up PEM/dug complexation: polycation/polyanion/ATP is shown in **Scheme 6-4**.

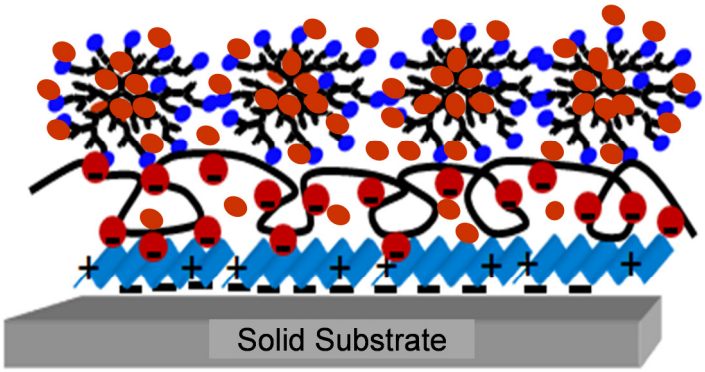

Scheme 6-4. Simplified sketch presenting PEM/ATP complexation interaction

In case of weak/strong system: In this method, PEM deposition was adjusted by preparing an equal concentration of the anionic drug (ATP) and used polyanion. Only polycationic PEI-Mal-C was used for drug loading and release experiments. The chosen molar concentration was depending on the molecular weight of the respective monomer units (M_wm) of the used polyanion (PA). For HE-NA^+, HA-Na^+, PEI-Mal-C and ATP,

[393] the M_wm were 332.5 , 365.31 , 29,610 and 507.18 g mol^{-1}, respectively. The calculated PC: ATP values in descending arrangement were 1: 35, 1:29, 1:23 1:18, 1:12 and 1:5, for ATP mass values with descending arrangement 0.6, 0.5, 0.4, 0.3, 0.2 and 0.08 mg mL^{-1}.

For weak/strong system: In order to seek for the most equilibrated system the highest uptake efficiency, different molar ratios of PA: ATP, 3:1, 1:1, 1:1.3, 1:2, 1:3 were prepared. A fixed mixing ratio of 5:1 was used for both polyelectrolyte (PE) solutions. The calculated net w/v concentrations of ATP after being mixed with HE-Na^+ (0.143mg. mL^{-1}) and complexed with PEI-Mal-C (1mg mL^{-1}) were 0.08, 0.2, 0.3, 0.5 and 0.6 mg mL^{-1}. In case of weak/weak system the same procedure has been postulated for ATP molecules concentration calculation. In order to seek for the most equilibrated system the highest uptake efficiency, different molar ratios of PA: ATP, 7:1, 3:1, 2:1, 1:1, were prepared. The calculated net w/v concentrations of ATP after being mixed with HA-Na^+ (0.5 mg mL^{-1}) and complexed with polycation (0.5 mg mL^{-1}) were 0.1, 0.2, 0.3, and 0.5 mg mL^{-1}. For 0.6 mg mL^{-1} no PEM buildup was achieved.

The release step was established in different immersion solution. For both systems, loaded with ATP (PEM/ATP), they were subjected to Millipore water and pure buffer HEPES. The complete release was performed in NaCl (0.1M) and HEPES (0.05M) and NaCl (0.1M) mixed with ratio (1:1) pH 9, for weak/strong and weak/weak systems, respectively.

6.3. Instruments and characterization methods

6.3.1. Polyelectrolyte titration

6.3.1.1. Colloid titration (particle charge detector PCD)

The cationic or anionic charge of the polyelectrolyte complex (PEC) particles was determined by the particle charge detector (PCD, BTG Mütek GmbH, Herrsching, Germany) based on titration with low molecular-weight polyanionic poly(ethylenesulfate) (PES) (0.001M) and polycationic poly(diallyldimethyl-ammonium chloride) (PDADMAC) (0.001M), respectively, under control of the zetapotential. In a hollow cylinder of chemically inert PTFE material a diluted PEC dispersion is exposed to a shear field of a

cyclic moving pestle of the same material. Moving of the pestle leads to distortion of the counterion cloud of adsorbed particles and potential results. This streaming potential, which is measured between two gold contact electrodes, is linearly correlated to the zetapotential. It becomes zero in case of charge neutrality. Based on exact charge compensation of the PEC particles by the dropwise added PES or PDADMAC solution (high ionic activity and pH independence), the titration of the PEC dispersion reveals a quantitative and reproducible estimate of the particle charges. Two different experiments have been performed to calculate the isoelectric points for polyelectrolyte complex (PEC). (**i**) The first titration was for polyions titration against the PCD standards: PES and PDADMAC. (**ii**) Secondary, to titrate polycations: PEI-Mal-B and PEI-Mal-C against polyanions: HE-Na^+ and HA-Na^+. In all cases 1mg mL^{-1} as the polyions concentration was used. 1mL of the PEI-Mal (1mg mL^{-1}) in addition to 9mL Millipore water was added to PCD pulp and whether has been titrated using standard polyanion PES or polyanions HE-Na^+ and HA-Na^+.

6.3.1.2. Charge density calculation

Charge densities q (C g^{-1}) of PEI-Mal were determined by PE titration via particle charge detector (PCD-03, Mütek, Germany), combined with a 702 SM Titrino (Metrohm, Switzerland). 0.001 M Solutions of low molecular weight sodium poly (ethylene sulfonate) (PES-Na) or poly (diallyldimethylammonium chloride) (PDADMAC) were used as titrants for cationic and anionic systems, respectively. q (C g^{-1}) was calculated according to the following equation, represented in Reference [394]:

$$q = \frac{C_{titrant} \cdot V_{titrant}}{V.m} \qquad \textbf{Eq. 6-2}$$

where $C_{titrant}$ is the concentration of titrant (meq L^{-1}), $V_{titrant}$ is the equivalent titrant volume, V is the volume of titrated solution (L) and m is the mass of polyelectrolyte in the titrated solution (g L^{-1}). Measurements were performed by Dr. Simona Schwarz.

6.3.1.3. Charge density per macromolecule

Charge density per macromolecule q (e/macromolecule) was calculated according to the following equation, represented in Reference [395] :

$$q = \frac{q \,.M.N_A}{e} \qquad \textbf{Eq. 6-3}$$

where q is the charge density of macromolecule (C g^{-1}), M is the molar mass of macromolecule, N_A is the Avogadro's constant (6.022×10^{23}) (mol^{-1}), and e is the elementary charge (electric charge carried on a single proton) (1.602×10^{-19}) (Coulombs).

6.3.2. DLS and zeta potential measurements

Zetasizer Nano (Malvern Instruments/UK) was used for the determination of the hydrodynamic diameter of investigated PEI-Mal/polyanion complex. Zetasizer was equipped with a 633 nm He/Ne laser and a non-invasive back scatter (NIBS®) technology. DLS measurements conditions were 3 × 25 runs per 5 seconds with normal resolution and backscatter mode. It was also used for electrophoretic experiments to determine the electrophoretic velocity of the complexes. The complex velocity in an electric field, using 120 V cm^{-1}, was measured by laser Doppler anemometry employing the He/Ne laser. The apparent electrokinetic potential (zeta potential,ζ) values were calculated from the complex velocity according to the Henry equation (**Eq. 6-4)**, represented in Reference [396]:

$$\mu = \frac{2\varepsilon\zeta f(\kappa a)}{3\eta} \qquad \textbf{Eq. 6-4}$$

where ε is the dielectric constant, $f(\kappa a)$ is the Henry's function, and η is dynamic viscosity of the dispersion medium (Pa·s). Since, the presented measurements had been done in aqueous media and moderate electrolyte concentration, $f(\kappa a)$ is 1.5, ε is 78.9 (at 24°C), and η is 0.9086 mPa·s (at 24°C). Zetapotential monomodel measurements conditions were 3 × 50 runs per 5 seconds at 40V. Prior to measurement, samples were filtered with 0.2µm Millipore water syringe filter to remove dust particles.

Series of concentration ratios for PEI-Mal and polyanions (HE-Na^+ and HA-Na^+) have been prepared in order to investigate the complex aggregation particle size and their isoelectric point. PEI-Mal concentration was 1 mg mL^{-1}. The concentration series was mixed with ratio 1:1. For weak/strong system, PEC (PEI-Mal/HE-Na^+) was of ratios: 1:0, 1:1, 2:1, 5:1, 10:1, 20:1 and 0:1. However for weak/weak system, PEC (PEI-Mal/ HA-Na^+)

was of ratios: 1:0, 1:1, 2:1, 5:1, 10:1, 20:1 and 0:1. DLS and zeta potential measurements were carried out by Mrs. Anja Caspari.

6.4. Ellipsometry

6.4.1. PEM dry, swollen and stability measurements

The determination of PEM thickness (d) and the refractive index (n) of dry and swollen states , as well as ATP adsorption was performed by using a multiwavelength ellipsometer in the spectral range of 380-900 nm and an incidence angle of 70º [Rotating compensator ellipsometer alpha-SE® (J. A. Woollam Co., Inc)]. n (λ) of the PEM as an effective polymer top layer as well as its thickness d were calculated from spectroscopic ellipsometry data, amplitute ratio (ψ) and phase difference (Δ) obtained by fitting to a multilayer box model (**Scheme 6-5**). For the Si wafers with thermal SiO_2 and PEM on top a three layer model was used: (Si substrate with Si-SiO_2 interface/ thermal SiO_2/ polymeric PEM film (**Scheme 6-5**). The refractive index n (λ) of the polymer film was fitted to a two-parameter Cauchy equation (**Eq. 6-5**) represented in Reference, [397] :

$$n\,(\lambda) = A_n + \frac{B_n}{\lambda^2} \qquad \textbf{Eq. 6-5}$$

where A_n and B_n are the Cauchy parameters at an extinction coefficient k=0, for nonabsorbing films in applied spectral range. All the refractive index (n) values mentioned in this work are presented for λ = 632.8 nm for a better comparison with literature data. The dried PEM can be measured directly; however for in-situ swelling special quartz cuvettes were used. These cuvettes have an incidence angle of 70° which is analogue to the angle of incidence of the light from the ellipsometer. Additionally, the Si wafers were fixed with special teflon cuvette holders. PEM thickness was measured in dry and then swelling measurements were subsequently made by addition of solutions: Millipore water, PBS (0.01M) of pH 7.4 and NaCl (0. 1M). Ambient refractive index of 1.332 for water was taken from literature. [398] The ambient refractive indices for all immersion solutions were measured by using Digital multiple wavelength refractometer DSR (SCHMIDT + HAENSCH GmbH & Co.), the measurements were established in Dr. Klaus-Jochen Eichhorn laboratory. Firstly, the dried PEM was measured without and with cuvette. Afterwards, 3 mL of one of the three different solutions were added to the PEM fixed in

the cuvette and the according swelling was determined for 4 days. For the determination of the percent swelling of the PEM with defined number on (PEI(PEI-Mal/HE-Na^+)$_n$) bilayers, in-situ experiments were performed on the multilayers samples. The percentage degree of swelling is defined as (**Eq. 6-6**), represented in Reference [338]:

$$Degree\ of\ swelling\ \% = 100 \times \frac{d_{\ Swollen\ state} - d_{\ Dry\ state}}{d_{Dry\ state}} \qquad \textbf{Eq. 6-6}$$

where d_{Swollen} state and $d_{\text{Dry state}}$ are the PEM thickness (nm) in dry and in swollen states, respectively.

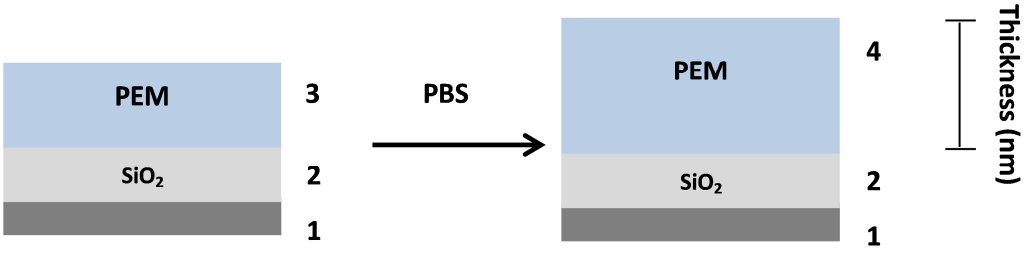

Scheme 6-5. Optical models used for fitting of the ellipsometric data ψ and Δ to obtain the thickness and refractive index of the polymer film thickness. 1- Si substrate, 2-SiO_2, 3-Cauchy layer for polymer's PEM film in dry (d and n fit), 4- Cauchy layer for polymer´s PEM film in swollen state (*d* and *n* fit).

Within all measurements amplitude ratio (ψ) and phase difference (Δ) values were recorded and later on the thickness d and the refractive index *n* (as an effective value) of all PEM films can be fitted with the described optical model. The resulting mean square errors (MSE) and the parameter correlation matrix of the fits were checked and evaluated. As expected relatively high MSE (>10) were obtained for some rough PEM surfaces and for very thick (*d* > ~1000nm) or less homogeneous layers. Unfortunately, modifications of the optical model and introduction of parameters like surface roughness and thickness non-uniformity or index gradient as well as effective medium approaches (EMA) were not successful because of parameter correlation.

For the recording of the measurements and the fitting of *d* and *n* the program CompleteEASE version 4.32 was used. Optical model for the evaluation of thickness and

refractive index (n) of PEM were used depending on the type of Si-wafer. For samples, Si-substrates with thermal SiO_2 and PEM layer on top following optical box model (**Scheme 6-5**) were used: (Si substrate with Si-SiO_2 interface /thermal SiO_2/polymer PEM film). The model for the Si-SiO_2 wafers is available as standard model in the CompleteEASE software and was used without any modification. [399]

6.5. Atomic force microscopy (AFM)

The AFM measurements of dry samples were done in peak force tapping mode by a Dimension Icon® 3100 NanoScope V (Bruker-Nano, USA) with a scan rate of 1 Hz and a peak force setpoint of 1 nN. Silicon-SPM-sensors BS-Tap300 (BudgetSensors, Bulgaria) with spring constant of ca. 40 N m^{-1} was used; the tip radius was lower than 10 nm. The left part of the images shows the topography and the right one the error signal, where structure details can be better seen. All samples were prepared on silicon wafers as a planar solid substrate. AFM measurements were carried out by Mr. Andreas Janke.

6.6. In-situ attenuated total reflection-Fourier-transform infrared (ATR-FTIR) spectroscopy

In-situ ATR-FTIR spectroscopy was applied to characterize PEM with defined numbers on PEI-Mal bilayers in the dry state and in contact to overlaying solutions of different ionic strength and pH values, e.g. Millipore water , PBS buffer etc. to determine the swelling and stability of PEM. A commercial ATR-FTIR attachment operated by the single-beam-sample-reference (SBSR) concept (OPTISPEC, Zürich, Switzerland) was used, which in turn record the ATR-FTIR spectra. [400-402] The ATR-FTIR attachment was installed on the IFS 55 Equinox FTIR spectrometer (BRUKER-Optics GmbH, Ettlingen Germany) equipped with globar source and highly sensitive mercury cadmium telluride (MCT) detector. A transparent in-situ cell (M. Müller, IPF Dresden, Germany) was used, which sealed the upper sample (S) half and the lower reference (R) half of the Si-IRE by oval O-rings forming S- and R-compartments, respectively, both sections can be filled with various aqueous solutions. In this work the PEM were located solely on the S half of the Si-IRE and the R half was uncoated. Applying the SBSR concept single channel spectra $I_{S,R}(\nu)$ can be recorded of separately the S and R half of the Si-IRE, respectively,

by guiding one IR beam alternately through these halves. Normalizing the single-channel spectra according to the Lambert- Beer law, represented in Reference [403] :

$$A\ (\nu) = \ -log_{10}\left(\frac{I_S(\nu)}{I_R(\nu)}\right) \qquad \textbf{Eq. 6-7}$$

resulted in absorbance spectra (A(ν)) with proper compensation of the background absorptions due to the SiO_2 layer, solvent, water vapor (spectrometer) and ice on MCT detector window.

7. REFERENCES

1. C. Picart, R. Elkaim, L. Richert, F. Audoin, Y. Arntz, M. Da Silva Cardoso, P. Schaaf, J.C. Voegel, and B. Frisch, *Primary Cell Adhesion on Rgd-Functionalized and Covalently Crosslinked Thin Polyelectrolyte Multilayer Films.* Advanced Functional Materials, 2005. **15**(1): p. 83-94.
2. F. Likibi, B. Jiang, and B. Li, *Biomimetic Nanocoating Promotes Osteoblast Cell Adhesion on Biomedical Implants.* Journal of Materials Research, 2008. **23**(12): p. 3222-3228.
3. L. Richert, P. Lavalle, E. Payan, X.Z. Shu, G.D. Prestwich, J.-F. Stoltz, P. Schaaf, J.-C. Voegel, and C. Picart, *Layer by Layer Buildup of Polysaccharide Films: Physical Chemistry and Cellular Adhesion Aspects.* Langmuir, 2004. **20**(2): p. 448-458.
4. L. Richert, A. Schneider, D. Vautier, C. Vodouhe, N. Jessel, E. Payan, P. Schaaf, J.-C. Voegel, and C. Picart, *Imaging Cell Interactions with Native and Crosslinked Polyelectrolyte Multilayers.* Cell Biochemistry and Biophysics, 2006. **44**(2): p. 273-285.
5. C.m. Pozos Vázquez, T. Boudou, V. Dulong, C. Nicolas, C. Picart, and K. Glinel, *Variation of Polyelectrolyte Film Stiffness by Photo-Cross-Linking: A New Way to Control Cell Adhesion.* Langmuir, 2009. **25**(6): p. 3556-3563.
6. A. Schneider, L. Richert, G. Francius, J.-C. Voegel, and C. Picart, *Elasticity, Biodegradability and Cell Adhesive Properties of Chitosan/Hyaluronan Multilayer Films.* Biomedical Materials, 2007. **2**(1): p. S45.
7. L. Richert, F. Boulmedais, P. Lavalle, J. Mutterer, E. Ferreux, G. Decher, P. Schaaf, J.-C. Voegel, and C. Picart, *Improvement of Stability and Cell Adhesion Properties of Polyelectrolyte Multilayer Films by Chemical Cross-Linking.* Biomacromolecules, 2004. **5**(2): p. 284-294.
8. G. Decher, *Fuzzy Nanoassemblies: Toward Layered Polymeric Multicomposites.* science, 1997. **277**(5330): p. 1232-1237.
9. S.T. Dubas and J.B. Schlenoff, *Factors Controlling the Growth of Polyelectrolyte Multilayers.* Macromolecules, 1999. **32**(24): p. 8153-8160.
10. M. Lösche, J. Schmitt, G. Decher, W.G. Bouwman, and K. Kjaer, *Detailed Structure of Molecularly Thin Polyelectrolyte Multilayer Films on Solid Substrates as Revealed by Neutron Reflectometry.* Macromolecules, 1998. **31**(25): p. 8893-8906.
11. A. Fery, B. Schöler, T. Cassagneau, and F. Caruso, *Nanoporous Thin Films Formed by Salt-Induced Structural Changes in Multilayers of Poly (Acrylic Acid) and Poly (Allylamine).* Langmuir, 2001. **17**(13): p. 3779-3783.
12. D. Yoo, S.S. Shiratori, and M.F. Rubner, *Controlling Bilayer Composition and Surface Wettability of Sequentially Adsorbed Multilayers of Weak Polyelectrolytes.* Macromolecules, 1998. **31**(13): p. 4309-4318.
13. S.T. Dubas, T.R. Farhat, and J.B. Schlenoff, *Multiple Membranes from "True" Polyelectrolyte Multilayers.* Journal of the American Chemical Society, 2001. **123**(22): p. 5368-5369.
14. M. Marks, S. Munjal, S. Namhata, D. Scott, F. Bosscher, J. De Letter, and B. Klumperman, *Randomly Branched Bisphenol a Polycarbonates. I. Molecular Weight Distribution Modeling, Interfacial Synthesis, and Characterization.* Journal of Polymer Science Part A: Polymer Chemistry, 2000. **38**(3): p. 560-570.
15. F. Vögtle, S. Gestermann, R. Hesse, H. Schwierz, and B. Windisch, *Functional Dendrimers.* Progress in Polymer Science, 2000. **25**(7): p. 987-1041.
16. D.A. Tomalia, H. Baker, J. Dewald, M. Hall, G. Kallos, S. Martin, J. Roeck, J. Ryder, and P. Smith, *A New Class of Polymers: Starburst-Dendritic Macromolecules.* Polymer Journal, 1985. **17**(1): p. 117-132.

17. D.A. Tomalia, A.M. Naylor, and W.A. Goddard, *Starburst Dendrimers: Molecular-Level Control of Size, Shape, Surface Chemistry, Topology, and Flexibility from Atoms to Macroscopic Matter.* Angewandte Chemie International Edition in English, 1990. **29**(2): p. 138-175.
18. C. Hawker, R. Lee, and J. Fréchet, *One-Step Synthesis of Hyperbranched Dendritic Polyesters.* Journal of the American Chemical Society, 1991. **113**(12): p. 4583-4588.
19. B.I. Voit, *Hyperbranched Polymers: A Chance and a Challenge.* Comptes Rendus Chimie, 2003. **6**(8–10): p. 821-832.
20. M. Seiler, *Hyperbranched Polymers: Phase Behavior and New Applications in the Field of Chemical Engineering.* Fluid Phase Equilibria, 2006. **241**(1): p. 155-174.
21. J.M. Fréchet, C.J. Hawker, I. Gitsov, and J.W. Leon, *Dendrimers and Hyperbranched Polymers: Two Families of Three-Dimensional Macromolecules with Similar but Clearly Distinct Properties.* Journal of Macromolecular Science, Part A: Pure and Applied Chemistry, 1996. **33**(10): p. 1399-1425.
22. B. Pettersson, *Hyperbranched Polymers: Unique Design Tools for Multi-Property Control in Resins and Coatings.* Pigment & resin technology, 1996. **25**(4): p. 4-14.
23. D. Hölter, A. Burgath, and H. Frey, *Degree of Branching in Hyperbranched Polymers.* Acta Polymerica, 1997. **48**(1-2): p. 30-35.
24. L.J. Markoski, J.L. Thompson, and J.S. Moore, *Indirect Method for Determining Degree of Branching in Hyperbranched Polymers.* Macromolecules, 2002. **35**(5): p. 1599-1603.
25. H. Liu, Y. Chen, D. Zhu, Z. Shen, and S.-E. Stiriba, *Hyperbranched Polyethylenimines as Versatile Precursors for the Preparation of Different Type of Unimolecular Micelles.* Reactive and Functional Polymers, 2007. **67**(5): p. 383-395.
26. Y.H. Kim, *Hyperbranched Polymers 10 Years After.* Journal of Polymer Science Part A: Polymer Chemistry, 1998. **36**(11): p. 1685-1698.
27. S.-E. Stiriba, H. Kautz, and H. Frey, *Hyperbranched Molecular Nanocapsules: Comparison of the Hyperbranched Architecture with the Perfect Linear Analogue.* Journal of the American Chemical Society, 2002. **124**(33): p. 9698-9699.
28. J.L. Hedrick, C.J. Hawker, R.D. Miller, R. Twieg, S. Srinivasan, and M. Trollsås, *Structure Control in Organic-Inorganic Hybrids Using Hyperbranched High-Temperature Polymers.* Macromolecules, 1997. **30**(24): p. 7607-7610.
29. Q. Sun, J.W. Lam, K. Xu, H. Xu, J.A. Cha, P.C. Wong, G. Wen, X. Zhang, X. Jing, and F. Wang, *Nanocluster-Containing Mesoporous Magnetoceramics from Hyperbranched Organometallic Polymer Precursors.* Chemistry of Materials, 2000. **12**(9): p. 2617-2624.
30. C. Gao and D. Yan, *Hyperbranched Polymers: From Synthesis to Applications.* Progress in Polymer Science, 2004. **29**(3): p. 183-275.
31. G. Maier and T. Griebel. *" Core Shell" Hyperbranched Polymers for Molecular Imprinting*. in *Abstracts of Papers of the American Chemical Society*. 2000. Journal of the American Chemical Society 1155 16TH ST, NW, WASHINGTON, DC 20036 USA.
32. R.M. Crooks, *Patterning of Hyperbranched Polymer Films.* ChemPhysChem, 2001. **2**(11): p. 644-654.
33. W.M. Lackowski, P. Ghosh, and R.M. Crooks, *Micron-Scale Patterning of Hyperbranched Polymer Films by Micro-Contact Printing.* Journal of the American Chemical Society, 1999. **121**(6): p. 1419-1420.
34. A. Aoki, P. Ghosh, and R.M. Crooks, *Micrometer-Scale Patterning of Multiple Dyes on Hyperbranched Polymer Thin Films Using Photoacid-Based Lithography.* Langmuir, 1999. **15**(22): p. 7418-7421.
35. M. Johansson, E. Malmström, A. Jansson, and A. Hult, *Novel Concept for Low Temperature Curing Powder Coatings Based on Hyperbranched Polyesters.* Journal of Coatings Technology, 2000. **72**(906): p. 49-54.

36. S.W. Zhu and W.F. Shi, *Synthesis and Photopolymerization of Hyperbranched Polyurethane Acrylates Applied to Uv Curable Flame Retardant Coatings.* Polymer international, 2002. **51**(3): p. 223-227.
37. J. Lange and Y. Wyser, *Recent Innovations in Barrier Technologies for Plastic Packaging—a Review.* Packaging Technology and Science, 2003. **16**(4): p. 149-158.
38. B. Maichel, B. Potocek, E. Kenndler, B. Gas, and M. Chiari, *Separation of Neutral Compounds by Capillary Electrokinetic Chromatography Using Polyethyleneimine as Replaceable Cationic Pseudostationary Phase.* Electrophoresis, 1998. **19**(12): p. 2124-2128.
39. W. Godbey, M.A. Barry, P. Saggau, K.K. Wu, and A.G. Mikos, *Poly (Ethylenimine)-Mediated Transfection: A New Paradigm for Gene Delivery.* Journal of Biomedical Materials Research, 2000. **51**(3): p. 321-328.
40. J. Huang, K. Sooklal, C.J. Murphy, and H.J. Ploehn, *Polyamine-Quantum Dot Nanocomposites: Linear Versus Starburst Stabilizer Architectures.* Chemistry of Materials, 1999. **11**(12): p. 3595-3601.
41. A. Cifuentes, H. Poppe, J.C. Kraak, and F. Bedia Erim, *Selectivity Change in the Separation of Proteins and Peptides by Capillary Electrophoresis Using High-Molecular-Mass Polyethyleneimine.* Journal of Chromatography B: Biomedical Sciences and Applications, 1996. **681**(1): p. 21-27.
42. D.R. Coleman and G.P. Royer, *New Hydrogenation Catalyst: Palladium-Poly (Ethylenimine)" Ghosts". Applications in Peptide Synthesis.* The Journal of Organic Chemistry, 1980. **45**(11): p. 2268-2269.
43. A. Haimov, H. Cohen, and R. Neumann, *Alkylated Polyethyleneimine/Polyoxometalate Synzymes as Catalysts for the Oxidation of Hydrophobic Substrates in Water with Hydrogen Peroxide.* Journal of the American Chemical Society, 2004. **126**(38): p. 11762-11763.
44. Z. Shen, Y. Chen, H. Frey, and S.-E. Stiriba, *Complex of Hyperbranched Polyethylenimine with Cuprous Halide as Recoverable Homogeneous Catalyst for the Atom Transfer Radical Polymerization of Methyl Methacrylate.* Macromolecules, 2006. **39**(6): p. 2092-2099.
45. K. Aoki, S. Furuhata, K. Hatanaka, M. Maeda, J. Remy, J. Behr, M. Terada, and T. Yoshida, *Polyethylenimine-Mediated Gene Transfer into Pancreatic Tumor Dissemination in the Murine Peritoneal Cavity.* Gene Therapy, 2001. **8**(7): p. 508-514.
46. O. Boussif, F. Lezoualc'h, M.A. Zanta, M.D. Mergny, D. Scherman, B. Demeneix, and J.-P. Behr, *A Versatile Vector for Gene and Oligonucleotide Transfer into Cells in Culture and in Vivo: Polyethylenimine.* Proceedings of the National Academy of Sciences, 1995. **92**(16): p. 7297-7301.
47. W. Godbey, K.K. Wu, and A.G. Mikos, *Poly (Ethylenimine)-Mediated Gene Delivery Affects Endothelial Cell Function and Viability.* Biomaterials, 2001. **22**(5): p. 471-480.
48. E. Heurich, S. Zankovych, M. Beyer, M. Schnabelrauch, A. Berg, and K.D. Jandt, *A Comparison of the Cell Compatibility of Poly (Ethyleneimine) with That of Other Cationic Biopolymers Used in Applications at Biointerfaces.* Advanced Engineering Materials, 2011. **13**(9): p. B285-B295.
49. Z. Xu, G. Shen, X. Xia, X. Zhao, P. Zhang, H. Wu, Q. Guo, Z. Qian, Y. Wei, and S. Liang, *Comparisons of Three Polyethyleneimine-Derived Nanoparticles as a Gene Therapy Delivery System for Renal Cell Carcinoma.* J Transl Med, 2011. **9**(1): p. 46.
50. W. Godbey, K.K. Wu, and A.G. Mikos, *Poly (Ethylenimine) and Its Role in Gene Delivery.* Journal of Controlled Release, 1999. **60**(2): p. 149-160.
51. A. Akinc, M. Thomas, A.M. Klibanov, and R. Langer, *Exploring Polyethylenimine-Mediated DNA Transfection and the Proton Sponge Hypothesis.* The journal of Gene Medicine, 2005. **7**(5): p. 657-663.
52. S.H. Pun, N.C. Bellocq, A. Liu, G. Jensen, T. Machemer, E. Quijano, T. Schluep, S. Wen, H. Engler, and J. Heidel, *Cyclodextrin-Modified Polyethylenimine Polymers for Gene Delivery.* Bioconjugate Chemistry, 2004. **15**(4): p. 831-840.

53. M. Ogris, G. Walker, T. Blessing, R. Kircheis, M. Wolschek, and E. Wagner, *Tumor-Targeted Gene Therapy: Strategies for the Preparation of Ligand–Polyethylene Glycol–Polyethylenimine/DNA Complexes.* Journal of Controlled Release, 2003. **91**(1): p. 173-181.
54. S. Hwa Kim, J. Hoon Jeong, K. Chul Cho, S. Wan Kim, and T. Gwan Park, *Target-Specific Gene Silencing by Sirna Plasmid DNA Complexed with Folate-Modified Poly (Ethylenimine).* Journal of Controlled Release, 2005. **104**(1): p. 223-232.
55. O. Larm, R. Larsson, and P. Olsson, *A New Non-Thrombogenic Surface Prepared by Selective Covalent Binding of Heparin Via a Modified Reducing Terminal Residue.* Artificial Cells, Blood Substitutes and Biotechnology, 1983. **11**(2-3): p. 161-173.
56. D. Appelhans, H. Komber, M.A. Quadir, S. Richter, S. Schwarz, J. van der Vlist, A. Aigner, M. Müller, K. Loos, and J.r. Seidel, *Hyperbranched PEI with Various Oligosaccharide Architectures: Synthesis, Characterization, ATP Complexation, and Cellular Uptake Properties.* Biomacromolecules, 2009. **10**(5): p. 1114-1124.
57. M.S. Huh, S.-Y. Lee, S. Park, S. Lee, H. Chung, S. Lee, Y. Choi, Y.-K. Oh, J.H. Park, and S.Y. Jeong, *Tumor-Homing Glycol Chitosan/Polyethylenimine Nanoparticles for the Systemic Delivery of Sirna in Tumor-Bearing Mice.* Journal of Controlled Release, 2010. **144**(2): p. 134-143.
58. J.-Q. Gao, Q.-Q. Zhao, T.-F. Lv, W.-P. Shuai, J. Zhou, G.-P. Tang, W.-Q. Liang, Y. Tabata, and Y.-L. Hu, *Gene-Carried Chitosan-Linked-Pei Induced High Gene Transfection Efficiency with Low Toxicity and Significant Tumor-Suppressive Activity.* International journal of Pharmaceutics, 2010. **387**(1): p. 286-294.
59. H.-L. Jiang, T.-H. Kim, Y.-K. Kim, I.-Y. Park, M.-H. Cho, and C.-S. Cho, *Efficient Gene Delivery Using Chitosan–Polyethylenimine Hybrid Systems.* Biomedical Materials, 2008. **3**(2): p. 025013.
60. K. Kunath, A. von Harpe, D. Fischer, and T. Kissel, *Galactose-Pei–DNA Complexes for Targeted Gene Delivery: Degree of Substitution Affects Complex Size and Transfection Efficiency.* Journal of Controlled Release, 2003. **88**(1): p. 159-172.
61. K. Sagara and S.W. Kim, *A New Synthesis of Galactose-Poly (Ethylene Glycol)-Polyethylenimine for Gene Delivery to Hepatocytes.* Journal of Controlled Release, 2002. **79**(1): p. 271-281.
62. S.E. Cook, I.K. Park, E.M. Kim, H.J. Jeong, T.G. Park, Y.J. Choi, T. Akaike, and C.S. Cho, *Galactosylated Polyethylenimine-Graft-Poly (Vinyl Pyrrolidone) as a Hepatocyte-Targeting Gene Carrier.* Journal of Controlled Release, 2005. **105**(1): p. 151-163.
63. S.S. Diebold, M. Kursa, E. Wagner, M. Cotten, and M. Zenke, *Mannose Polyethylenimine Conjugates for Targeted DNA Delivery into Dendritic Cells.* Journal of Biological Chemistry, 1999. **274**(27): p. 19087-19094.
64. F. Leclercq, C. Dubertret, B. Pitard, D. Scherman, and J. Herscovici, *Synthesis of Glycosylated Polyethylenimine with Reduced Toxicity and High Transfecting Efficiency.* Bioorganic and Medicinal Chemistry Letters, 2000. **10**(11): p. 1233-1235.
65. S. Grosse, G. Thévenot, Y. Aron, E. Duverger, M. Abdelkarim, A.-C. Roche, M. Monsigny, and I. Fajac, *In Vivo Gene Delivery in the Mouse Lung with Lactosylated Polyethylenimine, Questioning the Relevance of In Vitro Experiments.* Journal of Controlled Release, 2008. **132**(2): p. 105-112.
66. S. Höbel, A. Loos, D. Appelhans, S. Schwarz, J. Seidel, B. Voit, and A. Aigner, *Maltose-and Maltotriose-Modified, Hyperbranched Poly (Ethylene Imine) S (Om-Peis): Physicochemical and Biological Properties of DNA and Sirna Complexes.* Journal of Controlled Release, 2011. **149**(2): p. 146-158.
67. M.J. Cloninger, *Biological Applications of Dendrimers.* Current Opinion in Chemical Biology, 2002. **6**(6): p. 742-748.
68. A.R. Menjoge, R.M. Kannan, and D.A. Tomalia, *Dendrimer-Based Drug and Imaging Conjugates: Design Considerations for Nanomedical Applications.* Drug Discovery Today, 2010. **15**(5): p. 171-185.

69. M. El-Sayed, M. Ginski, C. Rhodes, and H. Ghandehari, *Transepithelial Transport of Poly (Amidoamine) Dendrimers across Caco-2 Cell Monolayers.* Journal of Controlled Release, 2002. **81**(3): p. 355-365.
70. K. Jain, P. Kesharwani, U. Gupta, and N. Jain, *Dendrimer Toxicity: Let's Meet the Challenge.* International Journal of Pharmaceutics, 2010. **394**(1): p. 122-142.
71. K.J. Doores, D. Gamblin, and B.G. Davis, *Exploring and Exploiting the Therapeutic Potential of Glycoconjugates.* Chemistry-A European Journal, 2006. **12**(3): p. 656-665.
72. T. Dutta and N.K. Jain, *Targeting Potential and Anti-Hiv Activity of Lamivudine Loaded Mannosylated Poly (Propyleneimine) Dendrimer.* Biochimica et Biophysica Acta (BBA)-General Subjects, 2007. **1770**(4): p. 681-686.
73. P.V. Kumar, A. Asthana, T. Dutta, and N.K. Jain, *Intracellular Macrophage Uptake of Rifampicin Loaded Mannosylated Dendrimers.* Journal of Drug Targeting, 2006. **14**(8): p. 546-556.
74. H. Arima, Y. Chihara, M. Arizono, S. Yamashita, K. Wada, F. Hirayama, and K. Uekama, *Enhancement of Gene Transfer Activity Mediated by Mannosylated Dendrimer/A-Cyclodextrin Conjugate (Generation 3, G3).* Journal of Controlled Release, 2006. **116**(1): p. 64-74.
75. B. Voit and D. Appelhans, *Glycopolymers of Various Architectures—More Than Mimicking Nature.* Macromolecular Chemistry and Physics, 2010. **211**(7): p. 727-735.
76. G. Mitsuaki, Y. Hirohumi, C. Chia-Wun, K. Akira, S. Tatsuki, M. Atsushi, K. Seiki, K. Kazukiyo, and A. Toshihiro, *Lactose-Carrying Polystyrene as a Drug Carrier: Investigation of Body Distributions to Parenchymal Liver Cells Using ^{125}I-Labelled Lactose-Carrying Polystyrene.* Journal of Controlled Release, 1994. **28**(1): p. 223-233.
77. W.B. Turnbull and J.F. Stoddart, *Design and Synthesis of Glycodendrimers.* Reviews in Molecular Biotechnology, 2002. **90**(3): p. 231-255.
78. M. Ogata, K.I. Hidari, W. Kozaki, T. Murata, J. Hiratake, E.Y. Park, T. Suzuki, and T. Usui, *Molecular Design of Spacer-N-Linked Sialoglycopolypeptide as Polymeric Inhibitors against Influenza Virus Infection.* Biomacromolecules, 2009. **10**(7): p. 1894-1903.
79. A.F. Thünemann, R. Bienert, D. Appelhans, and B. Voit, *Core-Shell Structures of Oligosaccharide-Functionalized Hyperbranched Poly(Ethylene Imines).* Macromolecular Chemistry and Physics, 2012. **213**(22): p. 2362-2369.
80. M. Mkandawire, A. Pohl, T. Gubarevich, V. Lapina, D. Appelhans, G. Rödel, W. Pompe, J. Schreiber, and J. Opitz, *Selective Targeting of Green Fluorescent Nanodiamond Conjugates to Mitochondria in Hela Cells.* Journal of Biophotonics, 2009. **2**(10): p. 596-606.
81. M. Kubeil, H. Stephan, H.J. Pietzsch, G. Geipel, D. Appelhans, B. Voit, J. Hoffmann, B. Brutschy, Y.V. Mironov, and K.A. Brylev, *Sugar-Decorated Dendritic Nanocarriers: Encapsulation and Release of the Octahedral Rhenium Cluster Complex [Re6s8 (Oh) 6] 4–.* Chemistry–An Asian Journal, 2010. **5**(12): p. 2507-2514.
82. A. Köth, D. Appelhans, D. Robertson, B. Tiersch, and J. Koetz, *Use of Weakly Cationic Dendritic Glycopolymer for Morphological Transformation of Phospholipid Vesicles into Tube-Like Networks.* Soft Matter, 2011. **7**(22): p. 10581-10584.
83. M. Fischer, D. Appelhans, S. Schwarz, B. Klajnert, M. Bryszewska, B. Voit, and M. Rogers, *Influence of Surface Functionality of Poly (Propylene Imine) Dendrimers on Protease Resistance and Propagation of the Scrapie Prion Protein.* Biomacromolecules, 2010. **11**(5): p. 1314-1325.
84. A. Richter, A. Janke, S. Zschoche, R. Zimmermann, F. Simon, K.-J. Eichhorn, B. Voit, and D. Appelhans, *pH-Stable Hyperbranched Poly (Ethyleneimine)-Maltose Films for the Interaction with Phosphate Containing Drugs.* New Journal of Chemistry, 2010. **34**(10): p. 2105-2108.
85. A. Szulc, D. Appelhans, B. Voit, M. Bryszewska, and B. Klajnert, *Characteristics of Complexes between Poly (Propylene Imine) Dendrimers and Nucleotides.* New Journal of Chemistry, 2012. **36**(8): p. 1610-1615.

86. N. Polikarpov, D. Appelhans, P. Welzel, A. Kaufmann, P. Dhanapal, C. Bellmann, and B. Voit, *Tailoring Uptake and Release of Atp by Dendritic Glycopolymer/Pnipaam Hydrogel Hybrids: First Approaches Towards Multicompartment Release Systems.* New Journal of Chemistry, 2012. **36**(2): p. 438-451.
87. S. Tripp, D. Appelhans, C. Striegler, and B. Voit, *Oligosaccharide Shells as a Decisive Factor for Moderate and Strong Ionic Interactions of Dendritic Poly (Ethylene Imine) Scaffolds under Shear Forces.* Chemistry-A European Journal, 2014.
88. S. Förster and M. Schmidt, *Polyelectrolytes in Solution*, in *Physical Properties of Polymers*. 1995, Springer. p. 51-133.
89. A.V. Dobrynin and M. Rubinstein, *Theory of Polyelectrolytes in Solutions and at Surfaces.* Progress in Polymer Science, 2005. **30**(11): p. 1049-1118.
90. J.L. Stair, J.J. Harris, and M.L. Bruening, *Enhancement of the Ion-Transport Selectivity of Layered Polyelectrolyte Membranes through Cross-Linking and Hybridization.* Chemistry of Materials, 2001. **13**(8): p. 2641-2648.
91. K. Vaynberg, A. Berta, and P. Dunckley, *Predicting Shear Adhesion of Water-Based Pressure-Sensitive Adhesives Via Transient Rheological Measurements.* The journal of Adhesion, 2001. **77**(4): p. 275-284.
92. E.J. Vandenberg, W.R. Diveley, L.J. Filar, S.R. Patel, and H.G. Barth, *The Synthesis and Solution Properties of Some Rigid-Chain, Water-Soluble Polymers: Poly[N,N'-(Sulfo-Phenylene)Phthalamide]S and Poly[N,N'-(Sulfo-P-Phenylene)Pyromellitimide].* Journal of Polymer Science Part A: Polymer Chemistry, 1989. **27**(11): p. 3745-3757.
93. B. Bolto and J. Gregory, *Organic Polyelectrolytes in Water Treatment.* Water Research, 2007. **41**(11): p. 2301-2324.
94. M.T. Radoiu, D.I. Martin, I. Calinescu, and H. Iovu, *Preparation of Polyelectrolytes for Wastewater Treatment.* Journal of Hazardous Materials, 2004. **106**(1): p. 19-24.
95. Y. Watanabe, K. Kubo, and S. Sato, *Application of Amphoteric Polyelectrolytes for Sludge Dewatering.* Langmuir, 1999. **15**(12): p. 4157-4164.
96. A.M. Howe, A. Clarke, and T.H. Whitesides, *Viscosity of Emulsions of Polydisperse Droplets with a Thick Adsorbed Layer.* Langmuir, 1997. **13**(10): p. 2617-2626.
97. I. Szilagyi, G. Trefalt, A. Tiraferri, P. Maroni, and M. Borkovec, *Polyelectrolyte Adsorption, Interparticle Forces, and Colloidal Aggregation.* Soft Matter, 2014. **10**(15): p. 2479-2502.
98. P.M. Claesson, A. Dedinaite, and O.J. Rojas, *Polyelectrolytes as Adhesion Modifiers.* Advances in Colloid and Interface Science, 2003. **104**: p. 53-74.
99. E. Akyol, S. Kirboga, and M. Öner, *Polyelectrolytes: Science and Application*, in *Polyelectrolytes*, V. P. M, O. Bayraktar, and G.A. Picó, Editors. 2014, Springer International Publishing. p. 87-112.
100. R.M. Fuoss and H. Sadek, *Mutual Interaction of Polyelectrolytes.* Science, 1949. **110**(2865): p. 552-554.
101. A.S. Michaels and R.G. Miekka, *Polycation-Polyanion Complexes: Preparation and Properties of Poly-(Vinylbenzyltrimethylammonium) Poly-(Styrenesulfonate).* The Journal of Physical Chemistry, 1961. **65**(10): p. 1765-1773.
102. A. Thünemann, M. Müller, H. Dautzenberg, J.-F. Joanny, and H. Löwen, *Polyelectrolyte Complexes*, in *Polyelectrolytes with Defined Molecular Architecture Ii*, M. Schmidt, Editor. 2004, Springer Berlin Heidelberg. p. 113-171.
103. H.G. Bungenberg de Jong, H.R. Kruyt, and J. Lens, *Zur Kenntnis Der Lyophilen Kolloide.* Kolloid-Beihefte, 1932. **36**(11-12): p. 429-462.
104. K.N. Bakeev, Y.M. Shu, A.B. Zezin, V.A. Kabanov, A.V. Lezov, A.B. Mel'nikov, I.P. Kolomiets, E.I. Rjumtsev, and W.J. MacKnight, *Structure and Properties of Polyelectrolyte–Surfactant Nonstoichiometric Complexes in Low-Polarity Solvents.* Macromolecules, 1996. **29**(4): p. 1320-1325.

105. A.Y. Grosberg, T.T. Nguyen, and B.I. Shklovskii, *Colloquium: The Physics of Charge Inversion in Chemical and Biological Systems.* Reviews of Modern Physics, 2002. **74**(2): p. 329-345.
106. M. Kawaguchi and A. Takahashi, *Polymer Adsorption at Solid-Liquid Interfaces.* Advances in Colloid and Interface Science, 1992. **37**(3–4): p. 219-317.
107. A.K. Bajpai, *Interface Behaviour of Ionic Polymers.* Progress in Polymer Science, 1997. **22**(3): p. 523-564.
108. F. Wiegel, *Adsorption of a Macromolecule to a Charged Surface.* Journal of Physics A: Mathematical and General, 1977. **10**(2): p. 299.
109. T. Odijk, *Binding of Long Flexible Chains to a Rodlike Macromolecule.* Macromolecules, 1980. **13**(6): p. 1542-1546.
110. M. Muthukumar, *Adsorption of a Polyelectrolyte Chain to a Charged Surface.* The Journal of Chemical Physics, 1987. **86**(12): p. 7230-7235.
111. M. Muthukumar, *Pattern Recognition by Polyelectrolytes.* The Journal of Chemical Physics, 1995. **103**(11): p. 4723-4731.
112. C. Kong and M. Muthukumar, *Monte Carlo Study of Adsorption of a Polyelectrolyte onto Charged Surfaces.* The Journal of Chemical Physics, 1998. **109**(4): p. 1522-1527.
113. M. Ellis, C. Kong, and M. Muthukumar, *Polyelectrolyte Adsorption on Heterogeneously Charged Surfaces.* The Journal of Chemical Physics, 2000. **112**(19): p. 8723-8729.
114. O. Borisov, E. Zhulina, and T. Birshtein, *Polyelectrolyte Molecule Conformation near a Charged Surface.* Journal of Physics II, 1994. **4**(6): p. 913-929.
115. V. Yamakov, A. Milchev, O. Borisov, and B. Dünweg, *Adsorption of a Polyelectrolyte Chain on a Charged Surface: A Monte Carlo Simulation of Scaling Behaviour.* Journal of Physics: Condensed Matter, 1999. **11**(49): p. 9907.
116. S. Beltran, H.H. Hooper, H.W. Blanch, and J.M. Prausnitz, *Monte Carlo Study of Polyelectrolyte Adsorption: Isolated Chains on a Planar Charged Surface.* Macromolecules, 1991. **24**(11): p. 3178-3184.
117. C. Hoeve. *Theory of Polymer Adsorption at Interfaces*. Journal of Polymer Science Part C: Polymer Symposia. 1971. Wiley Online Library.
118. C. Hoeve. *On the General Theory of Polymer Absorption at a Surface*. Journal of Polymer Science Part C: Polymer Symposia. 1970. Wiley Online Library.
119. F.T. Hesselink, *On the Theory of Polyelectrolyte Adsorption: The Effect on Adsorption Behavior of the Electrostatic Contribution to the Adsorption Free Energy.* Journal of Colloid and Interface Science, 1977. **60**(3): p. 448-466.
120. J. Scheutjens and G. Fleer, *Statistical Theory of the Adsorption of Interacting Chain Molecules. 1. Partition Function, Segment Density Distribution, and Adsorption Isotherms.* Journal of Physical Chemistry, 1979. **83**(12): p. 1619-1635.
121. J. Scheutjens and G. Fleer, *Statistical Theory of the Adsorption of Interacting Chain Molecules. 2. Train, Loop, and Tail Size Distribution.* The Journal of Physical Chemistry, 1980. **84**(2): p. 178-190.
122. H. Van der Schee and J. Lyklema, *A Lattice Theory of Polyelectrolyte Adsorption.* The Journal of Physical Chemistry, 1984. **88**(26): p. 6661-6667.
123. O.A. Evers, G.J. Fleer, J.M.H.M. Scheutjens, and J. Lyklema, *Adsorption of Weak Polyelectrolytes from Aqueous Solution.* Journal of Colloid and Interface Science, 1986. **111**(2): p. 446-454.
124. M.R. Bohmer, O.A. Evers, and J.M.H.M. Scheutjens, *Weak Polyelectrolytes between Two Surfaces: Adsorption and Stabilization.* Macromolecules, 1990. **23**(8): p. 2288-2301.
125. A.W. Vermeer, F.A. Leermakers, and L.K. Koopal, *Adsorption of Weak Polyelectrolytes on Surfaces with a Variable Charge. Self-Consistent-Field Calculations.* Langmuir, 1997. **13**(16): p. 4413-4421.
126. M.A. Dahlgren and F.A. Leermakers, *Depletion Zones in Polyelectrolyte Systems: Polydispersity Effects and Colloidal Stability.* Langmuir, 1995. **11**(8): p. 2996-3006.

127. J. Lyklema, *Fundamentals of Interface and Colloid Science: Soft Colloids*. Vol. 5. 2005: Academic press.
128. R.K. Iler, *Multilayers of Colloidal Particles.* Journal of Colloid and Interface Science, 1966. **21**(6): p. 569-594.
129. G. Decher, J.D. Hong, and J. Schmitt, *Buildup of Ultrathin Multilayer Films by a Self-Assembly Process: Iii. Consecutively Alternating Adsorption of Anionic and Cationic Polyelectrolytes on Charged Surfaces.* Thin Solid Films, 1992. **210–211, Part 2**(0): p. 831-835.
130. P. Schaaf and J.C. Voegel, *Polyelectrolyte Multilayers*, in *Nanoscience*, P. Boisseau, P. Houdy, and M. Lahmani, Editors. 2009, Springer Berlin Heidelberg. p. 1017-1042.
131. G. Decher and J.-D. Hong, *Buildup of Ultrathin Multilayer Films by a Self-Assembly Process, 1 Consecutive Adsorption of Anionic and Cationic Bipolar Amphiphiles on Charged Surfaces.* Makromolekulare Chemie. Macromolecular Symposia, 1991. **46**(1): p. 321-327.
132. J. Kang. The Application of Layer-by-Layer Technology in Nucleic Acid Sensing Systems. Freie Universität Berlin2011.
133. J. Dejeu, S. Diziain, C. Dange, F. Membrey, D. Charraut, and A. Foissy, *Stability of Self-Assembled Polymer Films Investigated by Optical Laser Reflectometry.* Langmuir, 2008. **24**(7): p. 3090-3098.
134. M.T. Kumara, B.C. Tripp, and S. Muralidharan, *Layer-by-Layer Assembly of Bioengineered Flagella Protein Nanotubes.* Biomacromolecules, 2007. **8**(12): p. 3718-3722.
135. S. Förster and M. Schmidt, *Polyelectrolytes in Solution*, in *Physical Properties of Polymers*. 1995, Springer Berlin Heidelberg. p. 51-133.
136. A. Katchalsky, O. Künzle, and W. Kuhn, *Behavior of Polyvalent Polymeric Ions in Solution.* Journal of Polymer Science, 1950. **5**(3): p. 283-300.
137. J.A. Jaber and J.B. Schlenoff, *Mechanical Properties of Reversibly Cross-Linked Ultrathin Polyelectrolyte Complexes.* Journal of the American Chemical Society, 2006. **128**(9): p. 2940-2947.
138. Y. Lvov, K. Ariga, I. Ichinose, and T. Kunitake, *Assembly of Multicomponent Protein Films by Means of Electrostatic Layer-by-Layer Adsorption.* Journal of the American Chemical Society, 1995. **117**(22): p. 6117-6123.
139. G. Sukhorukov, H. Möhwald, G. Decher, and Y.M. Lvov, *Assembly of Polyelectrolyte Multilayer Films by Consecutively Alternating Adsorption of Polynucleotides and Polycations.* Thin Solid Films, 1996. **284**: p. 220-223.
140. R. Georgieva, S. Moya, S. Leporatti, B. Neu, H. Bäumler, C. Reichle, E. Donath, and H. Möhwald, *Conductance and Capacitance of Polyelectrolyte and Lipid-Polyelectrolyte Composite Capsules as Measured by Electrorotation.* Langmuir, 2000. **16**(17): p. 7075-7081.
141. Y. Lvov, H. Haas, G. Decher, H. Moehwald, A. Mikhailov, B. Mtchedlishvily, E. Morgunova, and B. Vainshtein, *Successive Deposition of Alternate Layers of Polyelectrolytes and a Charged Virus.* Langmuir, 1994. **10**(11): p. 4232-4236.
142. A.A. Mamedov, N.A. Kotov, M. Prato, D.M. Guldi, J.P. Wicksted, and A. Hirsch, *Molecular Design of Strong Single-Wall Carbon Nanotube/Polyelectrolyte Multilayer Composites.* Nature materials, 2002. **1**(3): p. 190-194.
143. K. Ariga, Y. Lvov, and T. Kunitake, *Assembling Alternate Dye-Polyion Molecular Films by Electrostatic Layer-by-Layer Adsorption.* Journal of the American Chemical Society, 1997. **119**(9): p. 2224-2231.
144. O. Guillaume-Gentil, R. Zahn, S. Lindhoud, N. Graf, J. Voros, and T. Zambelli, *From Nanodroplets to Continuous Films: How the Morphology of Polyelectrolyte Multilayers Depends on the Dielectric Permittivity and the Surface Charge of the Supporting Substrate.* Soft Matter, 2011. **7**(8): p. 3861-3871.
145. R.v. Klitzing, *Internal Structure of Polyelectrolyte Multilayer Assemblies.* Physical Chemistry Chemical Physics, 2006. **8**(43): p. 5012-5033.

146. L.D. Landau, J. Bell, M. Kearsley, L. Pitaevskii, E. Lifshitz, and J. Sykes, *Electrodynamics of Continuous Media*. Vol. 8. 1984: Elsevier.
147. R. Messina, *Effect of Image Forces on Polyelectrolyte Adsorption at a Charged Surface.* Physical Review E, 2004. **70**(5): p. 051802.
148. J.J. Cerdà, B. Qiao, and C. Holm, *Understanding Polyelectrolyte Multilayers: An Open Challenge for Simulations.* Soft Matter, 2009. **5**(22): p. 4412-4425.
149. P.A. Patel, J. Jeon, P.T. Mather, and A.V. Dobrynin, *Molecular Dynamics Simulations of Multilayer Polyelectrolyte Films: Effect of Electrostatic and Short-Range Interactions.* Langmuir, 2006. **22**(24): p. 9994-10002.
150. J. Jeon, V. Panchagnula, J. Pan, and A.V. Dobrynin, *Molecular Dynamics Simulations of Mutilayer Films of Polyelectrolytes and Nanoparticles.* Langmuir, 2006. **22**(10): p. 4629-4637.
151. R. Messina, *Polyelectrolyte Multilayering on a Charged Planar Surface.* Macromolecules, 2003. **37**(2): p. 621-629.
152. A.V. Dobrynin, *Theory and Simulations of Charged Polymers: From Solution Properties to Polymeric Nanomaterials.* Current Opinion in Colloid and Interface Science, 2008. **13**(6): p. 376-388.
153. C. Picart, P. Lavalle, P. Hubert, F. Cuisinier, G. Decher, P. Schaaf, and J.-C. Voegel, *Buildup Mechanism for Poly (L-Lysine)/Hyaluronic Acid Films onto a Solid Surface.* Langmuir, 2001. **17**(23): p. 7414-7424.
154. C. Buron, C. Filiâtre, F. Membrey, C. Bainier, D. Charraut, and A. Foissy, *Effect of Substrate on the Adsorption of Polyelectrolyte Multilayers: Study by Optical Fixed-Angle Reflectometry and Afm.* Colloids and Surfaces A: Physicochemical and Engineering Aspects, 2007. **305**(1): p. 105-111.
155. J. Zhang, B. Senger, D. Vautier, C. Picart, P. Schaaf, J.-C. Voegel, and P. Lavalle, *Natural Polyelectrolyte Films Based on Layer-by Layer Deposition of Collagen and Hyaluronic Acid.* Biomaterials, 2005. **26**(16): p. 3353-3361.
156. H. Krass, G. Papastavrou, and D.G. Kurth, *Layer-by-Layer Self-Assembly of a Polyelectrolyte Bearing Metal Ion Coordination and Electrostatic Functionality.* Chemistry of materials, 2003. **15**(1): p. 196-203.
157. A.J. Nolte, M.F. Rubner, and R.E. Cohen, *Determining the Young's Modulus of Polyelectrolyte Multilayer Films Via Stress-Induced Mechanical Buckling Instabilities.* Macromolecules, 2005. **38**(13): p. 5367-5370.
158. F. Caruso, H. Lichtenfeld, E. Donath, and H. Möhwald, *Investigation of Electrostatic Interactions in Polyelectrolyte Multilayer Films: Binding of Anionic Fluorescent Probes to Layers Assembled onto Colloids.* Macromolecules, 1999. **32**(7): p. 2317-2328.
159. X. Jiang, Z. Chen, D. Lv, Q. Wu, and X. Lin, *Basic Law Controlling the Growth Regime of Layer-by-Layer Assembled Polyelectrolyte Multilayers.* Macromolecular Chemistry and Physics, 2008. **209**(2): p. 175-183.
160. P. Lavalle, C. Gergely, F. Cuisinier, G. Decher, P. Schaaf, J. Voegel, and C. Picart, *Comparison of the Structure of Polyelectrolyte Multilayer Films Exhibiting a Linear and an Exponential Growth Regime: An in Situ Atomic Force Microscopy Study.* Macromolecules, 2002. **35**(11): p. 4458-4465.
161. F. Boulmedais, V. Ball, P. Schwinte, B. Frisch, P. Schaaf, and J.-C. Voegel, *Buildup of Exponentially Growing Multilayer Polypeptide Films with Internal Secondary Structure.* Langmuir, 2003. **19**(2): p. 440-445.
162. G. Ladam, P. Schaad, J. Voegel, P. Schaaf, G. Decher, and F. Cuisinier, *In Situ Determination of the Structural Properties of Initially Deposited Polyelectrolyte Multilayers.* Langmuir, 2000. **16**(3): p. 1249-1255.
163. J.B. Schlenoff and S.T. Dubas, *Mechanism of Polyelectrolyte Multilayer Growth: Charge Overcompensation and Distribution.* Macromolecules, 2001. **34**(3): p. 592-598.

164. B. Schoeler, E. Poptoshev, and F. Caruso, *Growth of Multilayer Films of Fixed and Variable Charge Density Polyelectrolytes: Effect of Mutual Charge and Secondary Interactions.* Macromolecules, 2003. **36**(14): p. 5258-5264.
165. R.A. McAloney, M. Sinyor, V. Dudnik, and M.C. Goh, *Atomic Force Microscopy Studies of Salt Effects on Polyelectrolyte Multilayer Film Morphology.* Langmuir, 2001. **17**(21): p. 6655-6663.
166. N. Madaboosi, K. Uhlig, M.S. Jäger, H. Möhwald, C. Duschl, and D.V. Volodkin, *Microfluidics as a Tool to Understand the Build-up Mechanism of Exponential-Like Growing Films.* Macromolecular rapid communications, 2012. **33**(20): p. 1775-1779.
167. D. Volodkin and R. von Klitzing, *Competing Mechanisms in Polyelectrolyte Multilayer Formation and Swelling: Polycation–Polyanion Pairing Vs. Polyelectrolyte–Ion Pairing.* Current Opinion in Colloid and Interface Science, 2014. **19**(1): p. 25-31.
168. L. Richert, Y. Arntz, P. Schaaf, J.-C. Voegel, and C. Picart, *Ph Dependent Growth of Poly(L-Lysine)/Poly(L-Glutamic) Acid Multilayer Films and Their Cell Adhesion Properties.* Surface Science, 2004. **570**(1–2): p. 13-29.
169. C. Porcel, P. Lavalle, V. Ball, G. Decher, B. Senger, J.-C. Voegel, and P. Schaaf, *From Exponential to Linear Growth in Polyelectrolyte Multilayers.* Langmuir, 2006. **22**(9): p. 4376-4383.
170. C. Porcel, P. Lavalle, G. Decher, B. Senger, J.C. Voegel, and P. Schaaf, *Influence of the Polyelectrolyte Molecular Weight on Exponentially Growing Multilayer Films in the Linear Regime.* Langmuir, 2007. **23**(4): p. 1898-1904.
171. D.T. Haynie, E. Cho, and P. Waduge, *"In and out Diffusion" Hypothesis of Exponential Multilayer Film Buildup Revisited.* Langmuir, 2011. **27**(9): p. 5700-5704.
172. R.A. Ghostine, M.Z. Markarian, and J.B. Schlenoff, *Asymmetric Growth in Polyelectrolyte Multilayers.* Journal of the American Chemical Society, 2013. **135**(20): p. 7636-7646.
173. A.S. Michaels, L. Mir, and N.S. Schneider, *A Conductometric Study of Polycation—Polyanion Reactions in Dilute Aqueous Solution.* The Journal of Physical Chemistry, 1965. **69**(5): p. 1447-1455.
174. R.B. Cundall, J.B. Lawton, D. Murray, and G.O. Phillips, *Polyelectrolyte Complexes, 1. The Effect of Ph and Ionic Strength on the Stoichiometry of Model Polycation—Polyanion Complexes.* Die Makromolekulare Chemie, 1979. **180**(12): p. 2913-2922.
175. H. Mjahed, J.-C. Voegel, A. Chassepot, B. Senger, P. Schaaf, F. Boulmedais, and V. Ball, *Turbidity Diagrams of Polyanion/Polycation Complexes in Solution as a Potential Tool to Predict the Occurrence of Polyelectrolyte Multilayer Deposition.* Journal of Colloid and Interface Science, 2010. **346**(1): p. 163-171.
176. A. Plech, T. Salditt, C. Münster, and J. Peisl, *Investigation of Structure and Growth of Self-Assembled Polyelectrolyte Layers by X-Ray and Neutron Scattering under Grazing Angles.* Journal of Colloid and Interface Science, 2000. **223**(1): p. 74-82.
177. X. Arys, A. Laschewsky, and A.M. Jonas, *Ordered Polyelectrolyte "Multilayers". 1. Mechanisms of Growth and Structure Formation: A Comparison with Classical Fuzzy "Multilayers".* Macromolecules, 2001. **34**(10): p. 3318-3330.
178. P. Bertrand, A. Jonas, A. Laschewsky, and R. Legras, *Ultrathin Polymer Coatings by Complexation of Polyelectrolytes at Interfaces: Suitable Materials, Structure and Properties.* Macromolecular Rapid Communications, 2000. **21**(7): p. 319-348.
179. G.B. Sukhorukov, E. Donath, H. Lichtenfeld, E. Knippel, M. Knippel, A. Budde, and H. Möhwald, *Layer-by-Layer Self Assembly of Polyelectrolytes on Colloidal Particles.* Colloids and Surfaces A: Physicochemical and Engineering Aspects, 1998. **137**(1–3): p. 253-266.
180. J. Joanny, *Polyelectrolyte Adsorption and Charge Inversion.* The European Physical Journal B-Condensed Matter and Complex Systems, 1999. **9**(1): p. 117-122.

181. B. Schoeler, G. Kumaraswamy, and F. Caruso, *Investigation of the Influence of Polyelectrolyte Charge Density on the Growth of Multilayer Thin Films Prepared by the Layer-by-Layer Technique.* Macromolecules, 2002. **35**(3): p. 889-897.
182. P.A. Neff, A. Naji, C. Ecker, B. Nickel, R. v. Klitzing, and A.R. Bausch, *Electrical Detection of Self-Assembled Polyelectrolyte Multilayers by a Thin Film Resistor.* Macromolecules, 2006. **39**(2): p. 463-466.
183. R. Messina, C. Holm, and K. Kremer, *Polyelectrolyte Multilayering on a Charged Sphere.* Langmuir, 2003. **19**(10): p. 4473-4482.
184. C. Picart, J. Mutterer, L. Richert, Y. Luo, G. Prestwich, P. Schaaf, J.-C. Voegel, and P. Lavalle, *Molecular Basis for the Explanation of the Exponential Growth of Polyelectrolyte Multilayers.* Proceedings of the National Academy of Sciences, 2002. **99**(20): p. 12531-12535.
185. E. Leontidis, *Hofmeister Anion Effects on Surfactant Self-Assembly and the Formation of Mesoporous Solids.* Current Opinion in Colloid & Interface Science, 2002. **7**(1–2): p. 81-91.
186. T. López-León, A.B. Jódar-Reyes, D. Bastos-González, and J.L. Ortega-Vinuesa, *Hofmeister Effects in the Stability and Electrophoretic Mobility of Polystyrene Latex Particles.* The Journal of Physical Chemistry B, 2003. **107**(24): p. 5696-5708.
187. T. Boudou, T. Crouzier, K. Ren, G. Blin, and C. Picart, *Multiple Functionalities of Polyelectrolyte Multilayer Films: New Biomedical Applications.* Advanced Materials, 2010. **22**(4): p. 441-467.
188. J.N. Israelachvili, *Intermolecular and Surface Forces: Revised Third Edition*. 2011: Academic press.
189. M. Salomäki, I.A. Vinokurov, and J. Kankare, *Effect of Temperature on the Buildup of Polyelectrolyte Multilayers.* Langmuir, 2005. **21**(24): p. 11232-11240.
190. L. Ghimici and S. Dragan, *Behaviour of Cationic Polyelectrolytes Upon Binding of Electrolytes: Effects of Polycation Structure, Counterions and Nature of the Solvent.* Colloid and Polymer Science, 2002. **280**(2): p. 130-134.
191. E. Görnitz, M. Hahn, W. Jaeger, and H. Dautzenberg, *Sedimentation Equilibrium Studies of Synthetic Polyelectrolytes by Means of Interference Optical Methods*, in *Analytical Ultracentrifugation Iv*. 1997, Springer. p. 127-135.
192. R.A. Jones, *Soft Condensed Matter*. 2002, IOP Publishing.
193. R.R. Netz and D. Andelman, *Neutral and Charged Polymers at Interfaces.* Physics Reports, 2003. **380**(1): p. 1-95.
194. M. Kotelyanskii and D.N. Theodorou, *Simulation Methods for Polymers*. 2004: CRC Press.
195. R.R. Netz and J.-F. Joanny, *Adsorption of Semiflexible Polyelectrolytes on Charged Planar Surfaces: Charge Compensation, Charge Reversal, and Multilayer Formation.* Macromolecules, 1999. **32**(26): p. 9013-9025.
196. E. Leontidis, *Hofmeister Anion Effects on Surfactant Self-Assembly and the Formation of Mesoporous Solids.* Current Opinion in Colloid and Interface Science, 2002. **7**(1): p. 81-91.
197. D. Kovacevic, S. van der Burgh, A. de Keizer, and M.A. Cohen Stuart, *Kinetics of Formation and Dissolution of Weak Polyelectrolyte Multilayers: Role of Salt and Free Polyions.* Langmuir, 2002. **18**(14): p. 5607-5612.
198. D. Kovacevic, S. Van der Burgh, A. De Keizer, and M. Cohen Stuart, *Kinetics of Formation and Dissolution of Weak Polyelectrolyte Multilayers: Role of Salt and Free Polyions.* Langmuir, 2002. **18**(14): p. 5607-5612.
199. J.D. Mendelsohn, C.J. Barrett, V.V. Chan, A.J. Pal, A.M. Mayes, and M.F. Rubner, *Fabrication of Microporous Thin Films from Polyelectrolyte Multilayers.* Langmuir, 2000. **16**(11): p. 5017-5023.
200. S.E. Burke and C.J. Barrett, *Ph-Dependent Loading and Release Behavior of Small Hydrophilic Molecules in Weak Polyelectrolyte Multilayer Films.* Macromolecules, 2004. **37**(14): p. 5375-5384.
201. A. Chung and M. Rubner, *Methods of Loading and Releasing Low Molecular Weight Cationic Molecules in Weak Polyelectrolyte Multilayer Films.* Langmuir, 2002. **18**(4): p. 1176-1183.

202. S.Y. Park, C.J. Barrett, M.F. Rubner, and A.M. Mayes, *Anomalous Adsorption of Polyelectrolyte Layers.* Macromolecules, 2001. **34**(10): p. 3384-3388.
203. J. Hodak, R. Etchenique, E.J. Calvo, K. Singhal, and P.N. Bartlett, *Layer-by-Layer Self-Assembly of Glucose Oxidase with a Poly (Allylamine) Ferrocene Redox Mediator.* Langmuir, 1997. **13**(10): p. 2708-2716.
204. P.-G.d. De Gennes, P. Pincus, R. Velasco, and F. Brochard, *Remarks on Polyelectrolyte Conformation.* Journal de physique, 1976. **37**(12): p. 1461-1473.
205. O. Mermut and C.J. Barrett, *Effects of Charge Density and Counterions on the Assembly of Polyelectrolyte Multilayers.* The Journal of Physical Chemistry B, 2003. **107**(11): p. 2525-2530.
206. S. Salem, M. Müller, B. Torger, A. Janke, K.-J. Eichhorn, B. Voit, and D. Appelhans, *Glycopolymer Polyelectrolyte Multilayers Composed of Heparin and Maltose-Modified Poly(Ethylene Imine) as a Strong/Weak Polyelectrolyte System for Future Drug Delivery Coatings: Influence of Ph and Sugar Architecture on Growth of Multilayers and Multilayer Swelling and Stability.* Macromolecular Chemistry and Physics, 2015. **216**(2): p. 182-195.
207. S.S. Shiratori and M.F. Rubner, *Ph-Dependent Thickness Behavior of Sequentially Adsorbed Layers of Weak Polyelectrolytes.* Macromolecules, 2000. **33**(11): p. 4213-4219.
208. A. Katchalsky and P. Spitnik, *Potentiometric Titrations of Polymethacrylic Acid.* Journal of Polymer Science, 1947. **2**(4): p. 432-446.
209. R. Speiser, C. Eddy, and C. Hills, *Kinetics of Deesterification of Pectin.* The Journal of Physical Chemistry, 1945. **49**(6): p. 563-579.
210. H.H. Rmaile and J.B. Schlenoff, *"Internal P K A's" in Polyelectrolyte Multilayers: Coupling Protons and Salt.* Langmuir, 2002. **18**(22): p. 8263-8265.
211. S. Dodoo, R. Steitz, A. Laschewsky, and R. von Klitzing, *Effect of Ionic Strength and Type of Ions on the Structure of Water Swollen Polyelectrolyte Multilayers.* Physical Chemistry Chemical Physics, 2011. **13**(21): p. 10318-10325.
212. O.M. Tanchak and C.J. Barrett, *Swelling Dynamics of Multilayer Films of Weak Polyelectrolytes.* Chemistry of Materials, 2004. **16**(14): p. 2734-2739.
213. T.d.V. Naylor, *Permeation Properties.* Comprehensive Polymer Science, 1989. **2**: p. 643-668.
214. J.B. Schlenoff, A.H. Rmaile, and C.B. Bucur, *Hydration Contributions to Association in Polyelectrolyte Multilayers and Complexes: Visualizing Hydrophobicity.* Journal of the American Chemical Society, 2008. **130**(41): p. 13589-13597.
215. D.S. Salloum and J.B. Schlenoff, *Rectified Ion Currents through Ultrathin Polyelectrolyte Complex: Toward Chemical Transistors.* Electrochemical and Solid-State Letters, 2004. **7**(11): p. E45-E47.
216. L. Shen, P. Chaudouet, J. Ji, and C. Picart, *pH-Amplified Multilayer Films Based on Hyaluronan: Influence of Ha Molecular Weight and Concentration on Film Growth and Stability.* Biomacromolecules, 2011. **12**(4): p. 1322-1331.
217. B.M. Wohl and J.F. Engbersen, *Responsive Layer-by-Layer Materials for Drug Delivery.* Journal of Controlled Release, 2012. **158**(1): p. 2-14.
218. P. D Marcato, L. F Adami, R. de Melo Barbosa, P. S Melo, I. R Ferreira, L. de Paula, N. Duran, and A. B Seabra, *Development of a Sustained-Release System for Nitric Oxide Delivery Using Alginate/Chitosan Nanoparticles.* Current Nanoscience, 2013. **9**(1): p. 1-7.
219. J. Hong, B.-S. Kim, K. Char, and P.T. Hammond, *Inherent Charge-Shifting Polyelectrolyte Multilayer Blends: A Facile Route for Tunable Protein Release from Surfaces.* Biomacromolecules, 2011. **12**(8): p. 2975-2981.
220. B. Torger and M. Müller, *In Situ-Atr–Ftir Analysis on the Uptake and Release of Streptomycin from Polyelectrolyte Complex Layers.* Spectrochimica Acta Part A: Molecular and Biomolecular Spectroscopy, 2013. **104**: p. 546-553.

221. S. Ye, C. Wang, X. Liu, Z. Tong, B. Ren, and F. Zeng, *New Loading Process and Release Properties of Insulin from Polysaccharide Microcapsules Fabricated through Layer-by-Layer Assembly.* Journal of Controlled Release, 2006. **112**(1): p. 79-87.
222. C.S. Peyratout and L. Dähne, *Tailor-Made Polyelectrolyte Microcapsules: From Multilayers to Smart Containers.* Angewandte Chemie International Edition, 2004. **43**(29): p. 3762-3783.
223. A.A. Antipov, G.B. Sukhorukov, and H. Möhwald, *Influence of the Ionic Strength on the Polyelectrolyte Multilayers' Permeability.* Langmuir, 2003. **19**(6): p. 2444-2448.
224. M.C. Berg, L. Zhai, R.E. Cohen, and M.F. Rubner, *Controlled Drug Release from Porous Polyelectrolyte Multilayers.* Biomacromolecules, 2006. **7**(1): p. 357-364.
225. X. Tao, H. Chen, X.-J. Sun, J.-F. Chen, and W.H. Roa, *Formulation and Cytotoxicity of Doxorubicin Loaded in Self-Assembled Bio-Polyelectrolyte Microshells.* International Journal of Pharmaceutics, 2007. **336**(2): p. 376-381.
226. O. Etienne, A. Schneider, C. Taddei, L. Richert, P. Schaaf, J.-C. Voegel, C. Egles, and C. Picart, *Degradability of Polysaccharides Multilayer Films in the Oral Environment: An in Vitro and in Vivo Study.* Biomacromolecules, 2005. **6**(2): p. 726-733.
227. E. Vázquez, D.M. Dewitt, P.T. Hammond, and D.M. Lynn, *Construction of Hydrolytically-Degradable Thin Films Via Layer-by-Layer Deposition of Degradable Polyelectrolytes.* Journal of the American Chemical Society, 2002. **124**(47): p. 13992-13993.
228. K.C. Wood, H.F. Chuang, R.D. Batten, D.M. Lynn, and P.T. Hammond, *Controlling Interlayer Diffusion to Achieve Sustained, Multiagent Delivery from Layer-by-Layer Thin Films.* Proceedings of the National Academy of Sciences, 2006. **103**(27): p. 10207-10212.
229. M. Macdonald, N.M. Rodriguez, R. Smith, and P.T. Hammond, *Release of a Model Protein from Biodegradable Self Assembled Films for Surface Delivery Applications.* Journal of Controlled Release, 2008. **131**(3): p. 228-234.
230. L. Loretta, P. Rivera-Gil, A.Z. Abbasi, M. Ochs, C. Ganas, I. Zins, C. Sönnichsen, and W.J. Parak, *Lbl Multilayer Capsules: Recent Progress and Future Outlook for Their Use in Life Sciences.* Nanoscale, 2010. **2**(4): p. 458-467.
231. S. Yan, J. Zhu, Z. Wang, J. Yin, Y. Zheng, and X. Chen, *Layer-by-Layer Assembly of Poly (L-Glutamic Acid)/Chitosan Microcapsules for High Loading and Sustained Release of 5-Fluorouracil.* European Journal of Pharmaceutics and Biopharmaceutics, 2011. **78**(3): p. 336-345.
232. H.W. Jomaa and J.B. Schlenoff, *Salt-Induced Polyelectrolyte Interdiffusion in Multilayered Films: A Neutron Reflectivity Study.* Macromolecules, 2005. **38**(20): p. 8473-8480.
233. J.E. Wong, A.K. Gaharwar, D. Müller-Schulte, D. Bahadur, and W. Richtering, *Dual-Stimuli Responsive Pnipam Microgel Achieved Via Layer-by-Layer Assembly: Magnetic and Thermoresponsive.* Journal of Colloid and Interface Science, 2008. **324**(1–2): p. 47-54.
234. K.C. Wood, N.S. Zacharia, D.J. Schmidt, S.N. Wrightman, B.J. Andaya, and P.T. Hammond, *Electroactive Controlled Release Thin Films.* Proceedings of the National Academy of Sciences, 2008. **105**(7): p. 2280-2285.
235. B.-S. Kim, S.W. Park, and P.T. Hammond, *Hydrogen-Bonding Layer-by-Layer-Assembled Biodegradable Polymeric Micelles as Drug Delivery Vehicles from Surfaces.* Acs Nano, 2008. **2**(2): p. 386-392.
236. W. Jian, S. Xu, J. Wang, and S. Feng, *Layer-by-Layer Assembly of Poly (Allylamine Hydrochloride)/Polyurethane and Its Loading and Release Behavior for Methylene Orange.* Journal of Applied Polymer Science, 2013. **129**(4): p. 2070-2075.
237. K. Ariga, J.P. Hill, and Q. Ji, *Layer-by-Layer Assembly as a Versatile Bottom-up Nanofabrication Technique for Exploratory Research and Realistic Application.* Physical Chemistry Chemical Physics, 2007. **9**(19): p. 2319-2340.

238. C.W. Tse, K.Y.K. Man, K.W. Cheng, C.S. Mak, W.K. Chan, C.T. Yip, Z.T. Liu, and A.B. Djurišić, *Layer-by-Layer Deposition of Rhenium-Containing Hyperbranched Polymers and Fabrication of Photovoltaic Cells.* Chemistry-a European Journal, 2007. **13**(1): p. 328-335.
239. S.-H. Lee, J. Kumar, and S. Tripathy, *Thin Film Optical Sensors Employing Polyelectrolyte Assembly.* Langmuir, 2000. **16**(26): p. 10482-10489.
240. T. Ogawa, B. Ding, Y. Sone, and S. Shiratori, *Super-Hydrophobic Surfaces of Layer-by-Layer Structured Film-Coated Electrospun Nanofibrous Membranes.* Nanotechnology, 2007. **18**(16): p. 165607.
241. F.Ç. Cebeci, Z. Wu, L. Zhai, R.E. Cohen, and M.F. Rubner, *Nanoporosity-Driven Superhydrophilicity: A Means to Create Multifunctional Antifogging Coatings.* Langmuir, 2006. **22**(6): p. 2856-2862.
242. L. Krasemann and B. Tieke, *Selective Ion Transport across Self-Assembled Alternating Multilayers of Cationic and Anionic Polyelectrolytes.* Langmuir, 1999. **16**(2): p. 287-290.
243. M. Adusumilli and M.L. Bruening, *Variation of Ion-Exchange Capacity, Z Potential, and Ion-Transport Selectivities with the Number of Layers in a Multilayer Polyelectrolyte Film.* Langmuir, 2009. **25**(13): p. 7478-7485.
244. T. Crouzier, K. Ren, C. Nicolas, C. Roy, and C. Picart, *Layer-by-Layer Films as a Biomimetic Reservoir for Rhbmp-2 Delivery: Controlled Differentiation of Myoblasts to Osteoblasts.* Small, 2009. **5**(5): p. 598-608.
245. A.A. Antipov, G.B. Sukhorukov, E. Donath, and H. Möhwald, *Sustained Release Properties of Polyelectrolyte Multilayer Capsules.* The Journal of Physical Chemistry B, 2001. **105**(12): p. 2281-2284.
246. N.G. Balabushevich, G.B. Sukhorukov, and N.I. Larionova, *Polyelectrolyte Multilayer Microspheres as Carriers for Bienzyme System: Preparation and Characterization.* Macromolecular rapid communications, 2005. **26**(14): p. 1168-1172.
247. V. Smuleac, D. Butterfield, and D. Bhattacharyya, *Layer-by-Layer-Assembled Microfiltration Membranes for Biomolecule Immobilization and Enzymatic Catalysis.* Langmuir, 2006. **22**(24): p. 10118-10124.
248. O. Guillaume-Gentil, Y. Akiyama, M. Schuler, C. Tang, M. Textor, M. Yamato, T. Okano, and J. Voeroes, *Polyelectrolyte Coatings with a Potential for Electronic Control and Cell Sheet Engineering.* Advanced Materials, 2008. **20**(3): p. 560-565.
249. C. Picart, *Polyelectrolyte Multilayer Films: From Physico-Chemical Properties to the Control of Cellular Processes.* Current Medicinal Chemistry, 2008. **15**(7): p. 685-697.
250. Z. Li, D. Lee, X. Sheng, R.E. Cohen, and M.F. Rubner, *Two-Level Antibacterial Coating with Both Release-Killing and Contact-Killing Capabilities.* Langmuir, 2006. **22**(24): p. 9820-9823.
251. R. Kügler and W. Knoll, *Polyelectrolyte-Supported Lipid Membranes.* Bioelectrochemistry, 2002. **56**(1): p. 175-178.
252. L. Wang, M. Schönhoff, and H. Möhwald, *Lipids Coupled to Polyelectrolyte Multilayers: Ultraslow Diffusion and the Dynamics of Electrostatic Interactions.* The Journal of Physical Chemistry B, 2002. **106**(35): p. 9135-9142.
253. W.D. Comper, *Heparin (and Related Polysaccharides): Structural and Functional Properties*. 1981: Gordon and Breach Science Publishers.
254. N. Flint, F. Cove, and G.S. Evans, *Heparin Stimulates the Proliferation of Intestinal Epithelial Cells in Primary Culture.* Journal of Cell Science, 1994. **107**(2): p. 401-411.
255. S. Cavari, M. Ruggiero, and S. Vannucchi, *Antiproliferative Effects of Heparin on Normal and Transformed Nih/3t3 Fibroblasts.* Cell Biology International, 1993. **17**(8): p. 781-786.
256. B. Casu, *Structure and Biological Activity of Heparin.* Advances in Carbohydrate Chemistry and Biochemistry, 1985. **43**: p. 51-134.

257. R. Linhardt, J.E. Turnbull, H. Wang, D. Loganathan, and J.T. Gallagher, *Examination of the Substrate Specificity of Heparin and Heparan Sulfate Lyases.* Biochemistry, 1990. **29**(10): p. 2611-2617.
258. B. Mulloy and M.J. Forster, *Conformation and Dynamics of Heparin and Heparan Sulfate.* Glycobiology, 2000. **10**(11): p. 1147-1156.
259. D.R. Ferro, A. Provasoli, M. Ragazzi, G. Torri, B. Casu, G. Gatti, J.C. Jacquinet, P. Sinay, M. Petitou, and J. Choay, *Evidence for Conformational Equilibrium of the Sulfated L-Iduronate Residue in Heparin and in Synthetic Heparin Mono- and Oligo-Saccharides: NMR and Force-Field Studies.* Journal of the American Chemical Society, 1986. **108**(21): p. 6773-6778.
260. G.A. Jeffrey and J.H. Yates, *Stereographic Representation of the Cremer-Pople Ring-Puckering Parameters for Pyranoid Rings.* Carbohydrate Research, 1979. **74**(1): p. 319-322.
261. B. Mulloy, M.J. Forster, C. Jones, A.F. Drake, E.A. Johnson, and D.B. Davies, *The Effect of Variation of Substitution on the Solution Conformation of Heparin: A Spectroscopic and Molecular Modelling Study.* Carbohydrate Research, 1994. **255**(0): p. 1-26.
262. M.S. Niepel, D. Peschel, X. Sisquella, J.A. Planell, and T. Groth, *Ph-Dependent Modulation of Fibroblast Adhesion on Multilayers Composed of Poly (Ethylene Imine) and Heparin.* Biomaterials, 2009. **30**(28): p. 4939-4947.
263. J.R.E. Fraser, T.C. Laurent, and U.B.G. Laurent, *Hyaluronan: Its Nature, Distribution, Functions and Turnover.* Journal of Internal Medicine, 1997. **242**(1): p. 27-33.
264. D. Scott, P.J. Coleman, R.M. Mason, and J.R. Levick, *Concentration Dependence of Interstitial Flow Buffering by Hyaluronan in Synovial Joints.* Microvascular Research, 2000. **59**(3): p. 345-353.
265. L. Lapčík, L. Lapčík, S. De Smedt, J. Demeester, and P. Chabreček, *Hyaluronan: Preparation, Structure, Properties, and Applications.* Chemical Reviews, 1998. **98**(8): p. 2663-2684.
266. W. Winter and S. Arnott, *Hyaluronic Acid: The Role of Divalent Cations in Conformation and Packing.* Journal of Molecular Biology, 1977. **117**(3): p. 761-784.
267. R. Cortivo, P. Brun, A. Rastrelli, and G. Abatangelo, *In Vitro Studies on Biocompatibility of Hyaluronic Acid Esters.* Biomaterials, 1991. **12**(8): p. 727-730.
268. L. Lapčík, L. Lapcik, S. De Smedt, J. Demeester, and P. Chabrecek, *Hyaluronan: Preparation, Structure, Properties, and Applications.* Chemical Reviews, 1998. **98**(8): p. 2663-2684.
269. J. Fraser, T. Laurent, and U. Laurent, *Hyaluronan: Its Nature, Distribution, Functions and Turnover.* Journal of Internal Medicine, 1997. **242**(1): p. 27-33.
270. E.A. Balazs and T.C. Laurent, *Viscosity Function of Hyaluronic Acid as a Polyelectrolyte.* Journal of Polymer Science, 1951. **6**(5): p. 665-667.
271. S.E. Burke and C.J. Barrett, *Ph-Responsive Properties of Multilayered Poly (L-Lysine)/Hyaluronic Acid Surfaces.* Biomacromolecules, 2003. **4**(6): p. 1773-1783.
272. R.L. Cleland, J.L. Wang, and D.M. Detweiler, *Polyelectrolyte Properties of Sodium Hyaluronate. 2. Potentiometric Titration of Hyaluronic Acid.* Macromolecules, 1982. **15**(2): p. 386-395.
273. M.B. Mathews and L. Decker, *Conformation of Hyaluronate in Neutral and Alkaline Solutions.* Biochimica et Biophysica Acta (BBA)-General Subjects, 1977. **498**(1): p. 259-263.
274. A. Darke, E. Finer, R. Moorhouse, and D. Rees, *Studies of Hyaluronate Solutions by Nuclear Magnetic Relaxation Measurements. Detection of Covalently-Defmed, Stiff Segments within the Flexible Chains.* Journal of Molecular Biology, 1975. **99**(3): p. 477-486.
275. E. Fouissac, M. Milas, M. Rinaudo, and R. Borsali, *Influence of the Ionic Strength on the Dimensions of Sodium Hyaluronate.* Macromolecules, 1992. **25**(21): p. 5613-5617.
276. K. Hayashi, K. Tsutsumi, F. Nakajima, T. Norisuye, and A. Teramoto, *Chain-Stiffness and Excluded-Volume Effects in Solutions of Sodium Hyaluronate at High Ionic Strength.* Macromolecules, 1995. **28**(11): p. 3824-3830.
277. T. Odijk, *Polyelectrolytes near the Rod Limit.* Journal of Polymer Science: Polymer Physics Edition, 1977. **15**(3): p. 477-483.

278. S. Ghosh, I. Kobal, D. Zanette, and W.F. Reed, *Conformational Contraction and Hydrolysis of Hyaluronate in Sodium Hydroxide Solutions.* Macromolecules, 1993. **26**(17): p. 4685-4693.
279. M.K. Cowman, D.M. Hittner, and J. Feder-Davis, *13c-Nmr Studies of Hyaluronan: Conformational Sensitivity to Varied Environments.* Macromolecules, 1996. **29**(8): p. 2894-2902.
280. J. Lee, S.H. Yang, S.-P. Hong, D. Hong, H. Lee, H.-Y. Lee, Y.-G. Kim, and I.S. Choi, *Chemical Control of Yeast Cell Division by Cross-Linked Shells of Catechol-Grafted Polyelectrolyte Multilayers.* Macromolecular Rapid Communications, 2013. **34**(17): p. 1351-1356.
281. R.F. Fakhrullin and R.T. Minullina, *Hybrid Cellular− Inorganic Core− Shell Microparticles: Encapsulation of Individual Living Cells in Calcium Carbonate Microshells.* Langmuir, 2009. **25**(12): p. 6617-6621.
282. B. Dutka, N. Nyholm, and J. Petersen, *Comparison of Several Microbiological Toxicity Screening Tests.* Water Research, 1983. **17**(10): p. 1363-1368.
283. V. Kozlovskaya, S. Harbaugh, I. Drachuk, O. Shchepelina, N. Kelley-Loughnane, M. Stone, and V.V. Tsukruk, *Hydrogen-Bonded LbL Shells for Living Cell Surface Engineering.* Soft Matter, 2011. **7**(6): p. 2364-2372.
284. J.T. Wilson, W. Cui, V. Kozlovskaya, E. Kharlampieva, D. Pan, Z. Qu, V.R. Krishnamurthy, J. Mets, V. Kumar, and J. Wen, *Cell Surface Engineering with Polyelectrolyte Multilayer Thin Films.* Journal of the American Chemical Society, 2011. **133**(18): p. 7054-7064.
285. C. Brunot, L. Ponsonnet, C. Lagneau, P. Farge, C. Picart, and B. Grosgogeat, *Cytotoxicity of Polyethyleneimine (PEI), Precursor Base Layer of Polyelectrolyte Multilayer Films.* Biomaterials, 2007. **28**(4): p. 632-640.
286. L. Schultz and S. Zimmerman, *Dendrimers: Potential Drugs and Drug Delivery Agents.* Pharmaceutical News, 1999. **6**(3): p. 25-29.
287. S.A. Sukhishvili, E. Kharlampieva, and V. Izumrudov, *Where Polyelectrolyte Multilayers and Polyelectrolyte Complexes Meet.* Macromolecules, 2006. **39**(26): p. 8873-8881.
288. N.G. Hoogeveen, M.A. Cohen Stuart, G.J. Fleer, and M.R. Böhmer, *Formation and Stability of Multilayers of Polyelectrolytes.* Langmuir, 1996. **12**(15): p. 3675-3681.
289. D. Laurent and J.B. Schlenoff, *Multilayer Assemblies of Redox Polyelectrolytes.* Langmuir, 1997. **13**(6): p. 1552-1557.
290. F. Caruso and H. Möhwald, *Protein Multilayer Formation on Colloids through a Stepwise Self-Assembly Technique.* Journal of the American Chemical Society, 1999. **121**(25): p. 6039-6046.
291. P. Bieker and M. Schönhoff, *Linear and Exponential Growth Regimes of Multilayers of Weak Polyelectrolytes in Dependence on pH.* Macromolecules, 2010. **43**(11): p. 5052-5059.
292. J.A. Jaber and J.B. Schlenoff, *Counterions and Water in Polyelectrolyte Multilayers: A Tale of Two Polycations.* Langmuir, 2007. **23**(2): p. 896-901.
293. J.A. Hiller and M.F. Rubner, *Reversible Molecular Memory and Ph-Switchable Swelling Transitions in Polyelectrolyte Multilayers.* Macromolecules, 2003. **36**(11): p. 4078-4083.
294. J. Früh, R. Köhler, H. Möhwald, and R. Krastev, *Changes of the Molecular Structure in Polyelectrolyte Multilayers under Stress.* Langmuir, 2010. **26**(19): p. 15516-15522.
295. J.E. Wong, F. Rehfeldt, P. Hänni, M. Tanaka, and R.v. Klitzing, *Swelling Behavior of Polyelectrolyte Multilayers in Saturated Water Vapor.* Macromolecules, 2004. **37**(19): p. 7285-7289.
296. S.E. Burke and C.J. Barrett, *Swelling Behavior of Hyaluronic Acid/Polyallylamine Hydrochloride Multilayer Films.* Biomacromolecules, 2005. **6**(3): p. 1419-1428.
297. H. Mjahed, J.-C. Voegel, B. Senger, A. Chassepot, A. Rameau, V. Ball, P. Schaaf, and F. Boulmedais, *Hole Formation Induced by Ionic Strength Increase in Exponentially Growing Multilayer Films.* Soft Matter, 2009. **5**(11): p. 2269-2276.
298. H. Mjahed, G. Cado, F. Boulmedais, B. Senger, P. Schaaf, V. Ball, and J.-C. Voegel, *Restructuring of Exponentially Growing Polyelectrolyte Multilayer Films Induced by Salt Concentration Variations after Film Deposition.* Journal of Materials Chemistry, 2011. **21**(23): p. 8416-8421.

299. M. Salomäki and J. Kankare, *Specific Anion Effect in Swelling of Polyelectrolyte Multilayers.* Macromolecules, 2008. **41**(12): p. 4423-4428.
300. L. Krasemann and B. Tieke, *Selective Ion Transport across Self-Assembled Alternating Multilayers of Cationic and Anionic Polyelectrolytes.* Langmuir, 2000. **16**(2): p. 287-290.
301. B. Tieke, F. Van Ackern, L. Krasemann, and A. Toutianoush, *Ultrathin Self-Assembled Polyelectrolyte Multilayer Membranes.* The European Physical Journal E, 2001. **5**(1): p. 29-39.
302. J.J. Harris, J.L. Stair, and M.L. Bruening, *Layered Polyelectrolyte Films as Selective, Ultrathin Barriers for Anion Transport.* Chemistry of Materials, 2000. **12**(7): p. 1941-1946.
303. R.A. Ghostine and J.B. Schlenoff, *Ion Diffusion Coefficients through Polyelectrolyte Multilayers: Temperature and Charge Dependence.* Langmuir, 2011. **27**(13): p. 8241-8247.
304. T.R. Farhat and J.B. Schlenoff, *Ion Transport and Equilibria in Polyelectrolyte Multilayers.* Langmuir, 2001. **17**(4): p. 1184-1192.
305. A.G. Skirtach, A.A. Antipov, D.G. Shchukin, and G.B. Sukhorukov, *Remote Activation of Capsules Containing Ag Nanoparticles and Ir Dye by Laser Light.* Langmuir, 2004. **20**(17): p. 6988-6992.
306. Z. Lu, M.D. Prouty, Z. Guo, V.O. Golub, C.S. Kumar, and Y.M. Lvov, *Magnetic Switch of Permeability for Polyelectrolyte Microcapsules Embedded with Co@Au Nanoparticles.* Langmuir, 2005. **21**(5): p. 2042-2050.
307. G.B. Sukhorukov, A.A. Antipov, A. Voigt, E. Donath, and H. Möhwald, *Ph-Controlled Macromolecule Encapsulation in and Release from Polyelectrolyte Multilayer Nanocapsules.* Macromolecular Rapid Communications, 2001. **22**(1): p. 44-46.
308. C. Déjugnat, D. Haložan, and G.B. Sukhorukov, *Defined Picogram Dose Inclusion and Release of Macromolecules Using Polyelectrolyte Microcapsules.* Macromolecular Rapid Communications, 2005. **26**(12): p. 961-967.
309. A.A. Antipov, G.B. Sukhorukov, S. Leporatti, I.L. Radtchenko, E. Donath, and H. Möhwald, *Polyelectrolyte Multilayer Capsule Permeability Control.* Colloids and Surfaces A: Physicochemical and Engineering Aspects, 2002. **198**: p. 535-541.
310. C. Schüler and F. Caruso, *Decomposable Hollow Biopolymer-Based Capsules.* Biomacromolecules, 2001. **2**(3): p. 921-926.
311. B.G. De Geest, A.M. Jonas, J. Demeester, and S.C. De Smedt, *Glucose-Responsive Polyelectrolyte Capsules.* Langmuir, 2006. **22**(11): p. 5070-5074.
312. I. Yannas, D. Orgill, E. Skrabut, and J. Burke, *Skin Regeneration with a Bioreplaceable Polymeric Template*. 1984: American Chemical Society, Washington, DC.
313. N. Polikarpov, *Complexation Properties of Maltosylated Hyperbranched Poly (Ethylene Imine) S in Solution and in Functional Hydrogels.* 2012.
314. O. Klementieva, E. Aso, D. Filippini, N. Benseny-Cases, M. Carmona, S. Juvés, D. Appelhans, J. Cladera, and I. Ferrer, *Effect of Poly (Propylene Imine) Glycodendrimers on B-Amyloid Aggregation in Vitro and in App/Ps1 Transgenic Mice, as a Model of Brain Amyloid Deposition and Alzheimer's Disease.* Biomacromolecules, 2013. **14**(10): p. 3570-3580.
315. O. Klementieva, N.r. Benseny-Cases, A. Gella, D. Appelhans, B. Voit, and J. Cladera, *Dense Shell Glycodendrimers as Potential Nontoxic Anti-Amyloidogenic Agents in Alzheimer's Disease. Amyloid–Dendrimer Aggregates Morphology and Cell Toxicity.* Biomacromolecules, 2011. **12**(11): p. 3903-3909.
316. R. Steitz, W. Jaeger, and R.v. Klitzing, *Influence of Charge Density and Ionic Strength on the Multilayer Formation of Strong Polyelectrolytes.* Langmuir, 2001. **17**(15): p. 4471-4474.
317. M.C. van Eijk and M.A. Cohen Stuart, *Polymer Adsorption Kinetics: Effects of Supply Rate.* Langmuir, 1997. **13**(20): p. 5447-5450.
318. H.M. Schneider, P. Frantz, and S. Granick, *The Bimodal Energy Landscape When Polymers Adsorb.* Langmuir, 1996. **12**(4): p. 994-996.

319. R. Mészáros, L. Thompson, M. Bos, and P. De Groot, *Adsorption and Electrokinetic Properties of Polyethylenimine on Silica Surfaces.* Langmuir, 2002. **18**(16): p. 6164-6169.
320. G.M. Lindquist and R.A. Stratton, *The Role of Polyelectrolyte Charge Density and Molecular Weight on the Adsorption and Flocculation of Colloidal Silica with Polyethylenimine.* Journal of Colloid and Interface Science, 1976. **55**(1): p. 45-59.
321. J. Dejeu, L. Buisson, M. Guth, C. Roidor, F. Membrey, D. Charraut, and A. Foissy, *Early Steps of the Film Growth Mechanism in Self-Assembled Multilayers of Pah and Pss on Silica: Polymer Uptake, Charge Balance and Afm Analysis.* Colloids and Surfaces A: Physicochemical and Engineering Aspects, 2006. **288**(1): p. 26-35.
322. H. Wang, D. Loganathan, and R.J. Linhardt, *Determination of the Pka of Glucuronic Acid and the Carboxy Groups of Heparin by 13c-Nuclear-Magnetic-Resonance Spectroscopy.* Biochemical Journal, 1991. **278**: p. 689-695.
323. S.S. Dukhin, R. Zimmermann, and C. Werner, *Charge Density Distribution at Interfaces between Polyelectrolyte Layers and Aqueous Solutions—Experimental Access and Limitations of Traditional Electrokinetics.* Journal of Colloid and Interface Science, 2008. **328**(2): p. 217-226.
324. V. Bosio, F. Dubreuil, G. Bogdanovic, and A. Fery, *Interactions between Silica Surfaces Coated by Polyelectrolyte Multilayers in Aqueous Environment: Comparison between Precursor and Multilayer Regime.* Colloids and Surfaces A: Physicochemical and Engineering Aspects, 2004. **243**(1): p. 147-155.
325. A. Mero and M. Campisi, *Hyaluronic Acid Bioconjugates for the Delivery of Bioactive Molecules.* Polymers, 2014. **6**(2): p. 346-369.
326. G. Francius, J. Hemmerlé, J.-C. Voegel, P. Schaaf, B. Senger, and V. Ball, *Anomalous Thickness Evolution of Multilayer Films Made from Poly-L-Lysine and Mixtures of Hyaluronic Acid and Polystyrene Sulfonate.* Langmuir, 2007. **23**(5): p. 2602-2607.
327. C. Üzüm, J. Hellwig, N. Madaboosi, D. Volodkin, and R. von Klitzing, *Growth Behaviour and Mechanical Properties of Pll/Ha Multilayer Films Studied by AFM.* Beilstein Journal of Nanotechnology, 2012. **3**(1): p. 778-788.
328. C. Porcel, P. Lavalle, G. Decher, B. Senger, J.-C. Voegel, and P. Schaaf, *Influence of the Polyelectrolyte Molecular Weight on Exponentially Growing Multilayer Films in the Linear Regime.* Langmuir, 2007. **23**(4): p. 1898-1904.
329. P.J. Yoo, N.S. Zacharia, J. Doh, K.T. Nam, A.M. Belcher, and P.T. Hammond, *Controlling Surface Mobility in Interdiffusing Polyelectrolyte Multilayers.* Acs Nano, 2008. **2**(3): p. 561-571.
330. D.M. DeLongchamp and P.T. Hammond, *Fast Ion Conduction in Layer-by-Layer Polymer Films.* Chemistry of Materials, 2003. **15**(5): p. 1165-1173.
331. N.S. Zacharia, M. Modestino, and P.T. Hammond, *Factors Influencing the Interdiffusion of Weak Polycations in Multilayers.* Macromolecules, 2007. **40**(26): p. 9523-9528.
332. D. Mertz, J. Hemmerlé, F. Boulmedais, J.-C. Voegel, P. Lavalle, and P. Schaaf, *Polyelectrolyte Multilayer Films under Mechanical Stretch.* Soft Matter, 2007. **3**(11): p. 1413-1420.
333. E. Zinoviev, R. Rakhmatullin, and I. Almazov, *New Bioplastic Material Based on Hyaluronic Acid Hydrocolloid.* Journal of Clinical and Experimental Dermatology Research, 2014. **5**: p. 215.
334. H. Xu, L. Ma, H. Shi, C. Gao, and C. Han, *Chitosan–Hyaluronic Acid Hybrid Film as a Novel Wound Dressing: In Vitro and in Vivo Studies.* Polymers for Advanced Technologies, 2007. **18**(11): p. 869-875.
335. Y. Lvov, G. Decher, and H. Moehwald, *Assembly, Structural Characterization, and Thermal Behavior of Layer-by-Layer Deposited Ultrathin Films of Poly (Vinyl Sulfate) and Poly (Allylamine).* Langmuir, 1993. **9**(2): p. 481-486.
336. S.T. Dubas and J.B. Schlenoff, *Swelling and Smoothing of Polyelectrolyte Multilayers by Salt.* Langmuir, 2001. **17**(25): p. 7725-7727.

337. N. Yui, R.J. Mrsny, and K. Park, *Reflexive Polymers and Hydrogels: Understanding and Designing Fast Responsive Polymeric Systems*. 2004: CRC Press.
338. I. Willerich, Y. Li, and F. Gröhn, *Influencing Particle Size and Stability of Ionic Dendrimer− Dye Assemblies.* The Journal of Physical Chemistry B, 2010. **114**(47): p. 15466-15476.
339. M. Schönhoff, *Layered Polyelectrolyte Complexes: Physics of Formation and Molecular Properties.* Journal of Physics: Condensed Matter, 2003. **15**(49): p. R1781.
340. N. Nuraje, R. Asmatulu, R.E. Cohen, and M.F. Rubner, *Durable Antifog Films from Layer-by-Layer Molecularly Blended Hydrophilic Polysaccharides.* Langmuir, 2010. **27**(2): p. 782-791.
341. A. Marti, G. Haehner, and N.D. Spencer, *Sensitivity of Frictional Forces to Ph on a Nanometer Scale: A Lateral Force Microscopy Study.* Langmuir, 1995. **11**(12): p. 4632-4635.
342. S. Asayama, M. Nogawa, Y. Takei, T. Akaike, and A. Maruyama, *Synthesis of Novel Polyampholyte Comb-Type Copolymers Consisting of a Poly (L-Lysine) Backbone and Hyaluronic Acid Side Chains for a DNA Carrier.* Bioconjugate Chemistry, 1998. **9**(4): p. 476-481.
343. A. Fery, B. Schöler, T. Cassagneau, and F. Caruso, *Nanoporous Thin Films Formed by Salt-Induced Structural Changes in Multilayers of Poly(Acrylic Acid) and Poly(Allylamine).* Langmuir, 2001. **17**(13): p. 3779-3783.
344. H.G. Garg and C.A. Hales, *Chemistry and Biology of Hyaluronan*. 2004: Elsevier.
345. P.C. Hoopes, *Sodium Hyaluronate (Healon®) in Anterior Segment Surgery: A Review and a New Use in Extracapsular Surgery.* American Intra-Ocular Implant Society Journal, 1982. **8**(2): p. 148-154.
346. R. Harland and R. Prudhomme. *Polyelectrolyte Gels: Properties, Preparation, and Application*. in *ACS Symposium Series*. 1992.
347. L. Brannon-Peppas and N. Peppas, *The Equilibrium Swelling Behavior of Porous and Non-Porous Hydrogels.* Absorbent Polymer Technology, 1990. **8**.
348. R. Skouri, F. Schosseler, J. Munch, and S. Candau, *Swelling and Elastic Properties of Polyelectrolyte Gels.* Macromolecules, 1995. **28**(1): p. 197-210.
349. M. Schönhoff, *Self-Assembled Polyelectrolyte Multilayers.* Current Opinion in Colloid and Interface Science, 2003. **8**(1): p. 86-95.
350. H.H. Rmaile and J.B. Schlenoff, *"Internal Pka's" in Polyelectrolyte Multilayers: Coupling Protons and Salt.* Langmuir, 2002. **18**(22): p. 8263-8265.
351. R. Gilli, M. Kacuráková, M. Mathlouthi, L. Navarini, and S. Paoletti, *Ftir Studies of Sodium Hyaluronate and Its Oligomers in the Amorphous Solid Phase and in Aqueous Solution.* Carbohydrate Research, 1994. **263**(2): p. 315-326.
352. M. Kačuráková and M. Mathlouthi, *Ftir and Laser-Raman Spectra of Oligosaccharides in Water: Characterization of the Glycosidic Bond.* Carbohydrate research, 1996. **284**(2): p. 145-157.
353. F.R. Quinn and F.A. Bettelheim, *Infrared Dichroism of Sodium Hyaluronate.* Biochimica et Biophysica acta, 1963. **69**: p. 544-551.
354. D. NAUMANN, G. BARNICKEL, H. BRADACZEK, H. LABISCHINSKI, and P. GIESBRECHT, *Infrared Spectroscopy, a Tool for Probing Bacterial Peptidoglycan.* European Journal of Biochemistry, 1982. **125**(3): p. 505-515.
355. H.J. Agteresch, P.C. Dagnelie, J.W.O. van den Berg, and J.P. Wilson, *Adenosine Triphosphate.* Drugs, 1999. **58**(2): p. 211-232.
356. R. Blankstein, L.D. Shturman, I.S. Rogers, J.A. Rocha-Filho, D.R. Okada, A. Sarwar, A.V. Soni, H. Bezerra, B.B. Ghoshhajra, and M. Petranovic, *Adenosine-Induced Stress Myocardial Perfusion Imaging Using Dual-Source Cardiac Computed Tomography.* Journal of the American College of Cardiology, 2009. **54**(12): p. 1072-1084.
357. A.S. Iskandrian, M.S. Verani, and J. Heo, *Pharmacologic Stress Testing: Mechanism of Action, Hemodynamic Responses, and Results in Detection of Coronary Artery Disease.* Journal of Nuclear Cardiology, 1994. **1**(1): p. 94-111.

358. Z. Song, K.J. Parker, I. Enoh, H. Zhao, and O. Olubajo, *Elucidation of Spermidine Interaction with Nucleotide Atp by Multiple Nmr Techniques.* Magnetic Resonance in Chemistry, 2010. **48**(2): p. 123-128.
359. L. El-Mahdaoui, J. Neault, and H. Tajmir-Riahi, *Carbohydrate-Nucleotide Interaction. The Effects of Mono-and Disaccharides on the Solution Structure of Amp, Damp, Atp, Gmp, Dgmp, and Gtp Studied by Ftir Difference Spectroscopy.* Journal of Inorganic Biochemistry, 1997. **65**(2): p. 123-131.
360. W.F. Wolkers, H. Oldenhof, F. Tablin, and J.H. Crowe, *Preservation of Dried Liposomes in the Presence of Sugar and Phosphate.* Biochimica et Biophysica Acta (BBA) - Biomembranes, 2004. **1661**(2): p. 125-134.
361. H. Takeuchi, M. Matsuno, S.A. Overman, and G.J. Thomas, *Raman Linear Intensity Difference of Flow-Oriented Macromolecules: Orientation of the Indole Ring of Tryptophan-26 in Filamentous Virus Fd.* Journal of the American Chemical Society, 1996. **118**(14): p. 3498-3507.
362. H. Tajmir-Riahi, M. Bertrand, and T. Theophanides, *Synthesis, Structure, Proton-Nuclear Magnetic Resonance, and Fourier Transform Infrared Spectroscopy of Several Transition and Nontransition Metal-Adenosine-5-Triphosphate Complexes.* Canadian Journal of Chemistry, 1986. **64**(5): p. 960-966.
363. R. Savoie, J.-J. Jutier, L. Prizant, and A.L. Beauchamp, *Raman and Infrared Spectra of Methylmercury Complexes of Adenine.* Spectrochimica Acta Part A: Molecular Spectroscopy, 1982. **38**(5): p. 561-568.
364. Y.Q. Gao, W. Yang, and M. Karplus, *A Structure-Based Model for the Synthesis and Hydrolysis of ATP by F 1-Atpase.* Cell, 2005. **123**(2): p. 195-205.
365. Y. Marcus, *Thermodynamics of Solvation of Ions. Part 5.—Gibbs Free Energy of Hydration at 298.15 K.* Journal of the Chemical Society, Faraday Transactions, 1991. **87**(18): p. 2995-2999.
366. H.W. Jomaa and J.B. Schlenoff, *Salt-Induced Polyelectrolyte Interdiffusion in Multilayered Films: A Neutron Reflectivity Study.* Macromolecules, 2005. **38**(20): p. 8473-8480.
367. T.R. Farhat and J.B. Schlenoff, *Doping-Controlled Ion Diffusion in Polyelectrolyte Multilayers: Mass Transport in Reluctant Exchangers.* Journal of the American Chemical Society, 2003. **125**(15): p. 4627-4636.
368. J. Dai, A.W. Jensen, D.K. Mohanty, J. Erndt, and M.L. Bruening, *Controlling the Permeability of Multilayered Polyelectrolyte Films through Derivatization, Cross-Linking, and Hydrolysis.* Langmuir, 2001. **17**(3): p. 931-937.
369. C. Gao, E. Donath, S. Moya, V. Dudnik, and H. Möhwald, *Elasticity of Hollow Polyelectrolyte Capsules Prepared by the Layer-by-Layer Technique.* The European Physical Journal E, 2001. **5**(1): p. 21-27.
370. I. Ohmine and T. Tanaka, *Salt Effects on the Phase Transition of Ionic Gels.* The Journal of Chemical Physics, 1982. **77**(11): p. 5725-5729.
371. E.Y. Kramarenko, A.R. Khokhlov, and K. Yoshikawa, *Collapse of Polyelectrolyte Macromolecules Revisited.* Macromolecules, 1997. **30**(11): p. 3383-3388.
372. J. Ricka and T. Tanaka, *Swelling of Ionic Gels: Quantitative Performance of the Donnan Theory.* Macromolecules, 1984. **17**(12): p. 2916-2921.
373. A. Katchalsky, S. Lifson, and H. Heisenberg, *Polym Sci 1951, 7, 571.* Direct Link: Abstract PDF (143K) References Web of Science® Times Cited. **98**.
374. A. Katchalsky and I. Michaeli, *Polyelectrolyte Gels in Salt Solutions.* Journal of Polymer Science, 1955. **15**(79): p. 69-86.
375. P.J. Flory and J. Rehner Jr, *Statistical Mechanics of Cross-Linked Polymer Networks Ii. Swelling.* The Journal of Chemical Physics, 1943. **11**(11): p. 521-526.
376. P.J. Flory and J. Rehner Jr, *Statistical Mechanics of Cross-Linked Polymer Networks I. Rubberlike Elasticity.* The Journal of Chemical Physics, 1943. **11**(11): p. 512-520.

377. P.J. Flory, *Principles of Polymer Chemistry*. 1953: Cornell University Press.
378. O. Mermut and C.J. Barrett, *Stable Sensor Layers Self-Assembled onto Surfaces Using Azobenzene-Containing Polyelectrolytes.* Analyst, 2001. **126**(11): p. 1861-1865.
379. J.-L. Barrat and J.-F. Joanny, *Theory of Polyelectrolyte Solutions.* Advances in Chemical Physics, Polymeric Systems, 1997: p. 1.
380. K.E. Uhrich, S.M. Cannizzaro, R.S. Langer, and K.M. Shakesheff, *Polymeric Systems for Controlled Drug Release.* Chemical Reviews, 1999. **99**(11): p. 3181-3198.
381. L. Pauling, *Atomic Radii and Interatomic Distances in Metals.* Journal of the American Chemical Society, 1947. **69**(3): p. 542-553.
382. T. Fujieda, K. Ohta, N. Wakabayashi, and S. Higuchi, *H-Aggregation of Methyl Orange at the Interface between the Water Phase and Oil Phase in a Water-in-Oil Microemulsion.* Journal of Colloid and Interface Science, 1997. **185**(2): p. 332-334.
383. R.T. Buwalda and J.B. Engberts, *Aggregation of Dicationic Surfactants with Methyl Orange in Aqueous Solution.* Langmuir, 2001. **17**(4): p. 1054-1059.
384. K.C. Wood, J.Q. Boedicker, D.M. Lynn, and P.T. Hammond, *Tunable Drug Release from Hydrolytically Degradable Layer-by-Layer Thin Films.* Langmuir, 2005. **21**(4): p. 1603-1609.
385. H. Sato, R. Okuda, A. Sugiyama, M. Hamatsu, and J.-i. Anzai, *Loading and Release of Methyl Orange in Layer-by-Layer Assembled Polyelectrolyte Films.* Materials Science and Engineering: C, 2009. **29**(3): p. 1057-1060.
386. B. Jiang and B. Li, *Tunable Drug Loading and Release from Polypeptide Multilayer Nanofilms.* International Journal of Nanomedicine, 2009. **4**: p. 37.
387. S.E. Burke and C.J. Barrett, *Acid-Base Equilibria of Weak Polyelectrolytes in Multilayer Thin Films.* Langmuir, 2003. **19**(8): p. 3297-3303.
388. M. McCormick, R.N. Smith, R. Graf, C.J. Barrett, L. Reven, and H.W. Spiess, *Nmr Studies of the Effect of Adsorbed Water on Polyelectrolyte Multilayer Films in the Solid State.* Macromolecules, 2003. **36**(10): p. 3616-3625.
389. N. Kato, P. Schuetz, A. Fery, and F. Caruso, *Thin Multilayer Films of Weak Polyelectrolytes on Colloid Particles.* Macromolecules, 2002. **35**(26): p. 9780-9787.
390. S. Bharadwaj, R. Montazeri, and D.T. Haynie, *Direct Determination of the Thermodynamics of Polyelectrolyte Complexation and Implications Thereof for Electrostatic Layer-by-Layer Assembly of Multilayer Films.* Langmuir, 2006. **22**(14): p. 6093-6101.
391. P. Nazaran, V. Bosio, W. Jaeger, D. Anghel, and R. v. Klitzing, *Lateral Mobility of Polyelectrolyte Chains in Multilayers.* The Journal of Physical Chemistry B, 2007. **111**(29): p. 8572-8581.
392. B.E. Lacher, *Pharmaceutical Calculations for the Pharmacy Technician*. 2008: Lippincott Williams and Wilkins.
393. H. Hackenberg and M. Klingenberg, *Molecular Weight and Hydrodynamic Parameters of the Adenosine 5'-Diphosphate-Adenosine 5'-Triphosphate Carrier in Triton X-100.* Biochemistry, 1980. **19**(3): p. 548-555.
394. F. Gröhn, *Electrostatic Self-Assembly as Route to Supramolecular Structures.* Macromolecular Chemistry and Physics, 2008. **209**(22): p. 2295-2301.
395. F. Gröhn, *Soft Matter Nanoparticles with Various Shapes and Functionalities Can Form through Electrostatic Self-Assembly.* Soft Matter, 2010. **6**(18): p. 4296-4302.
396. Y. Kitajyo, Y. Nawa, M. Tamaki, H. Tani, K. Takahashi, H. Kaga, T. Satoh, and T. Kakuchi, *A Unimolecular Nanocapsule: Encapsulation Property of Amphiphilic Polymer Based on Hyperbranched Polythreitol.* Polymer, 2007. **48**(16): p. 4683-4690.
397. W. Norde and C.E. Giacomelli, *BSA Structural Changes During Homomolecular Exchange between the Adsorbed and the Dissolved States.* Journal of Biotechnology, 2000. **79**(3): p. 259-268.
398. M.A. Skorobogatiy and A. Kabashin, *Plasmon Excitation by the Gaussian-Like Core Mode of a Photonic Crystal Waveguide.* Optics Express, 2006. **14**(18): p. 8419-8424.

399. C. Herzinger, B. Johs, W. McGahan, J. Woollam, and W. Paulson, *Ellipsometric Determination of Optical Constants for Silicon and Thermally Grown Silicon Dioxide Via a Multi-Sample, Multi-Wavelength, Multi-Angle Investigation.* Journal of Applied Physics, 1998. **83**(6): p. 3323-3336.
400. M. Mueller, *Handbook of Polyelectrolytes and Their Applications*. 2002, American Scientific Publishers: Stephenson Ranch, CA.
401. M. Mueller, T. Rieser, K. Lunkwitz, and J. Meier-Haack, *Polyelectrolyte Complex Layers: A Promising Concept for Anti-Fouling Coatings Verified by in-Situ Atr-Ftir Spectroscopy.* Macromolecular Rapid Communications, 1999. **20**(12): p. 607-611.
402. J.C. Lindon, G.E. Tranter, and D. Koppenaal, *Online Encyclopedia of Spectroscopy and Spectrometry: 3 Volume Set*. 2010: Academic Press.
403. D. Calloway, *Beer-Lambert Law.* Journal of Chemical Education, 1997. **74**(7): p. 744.

8. APPENDIX

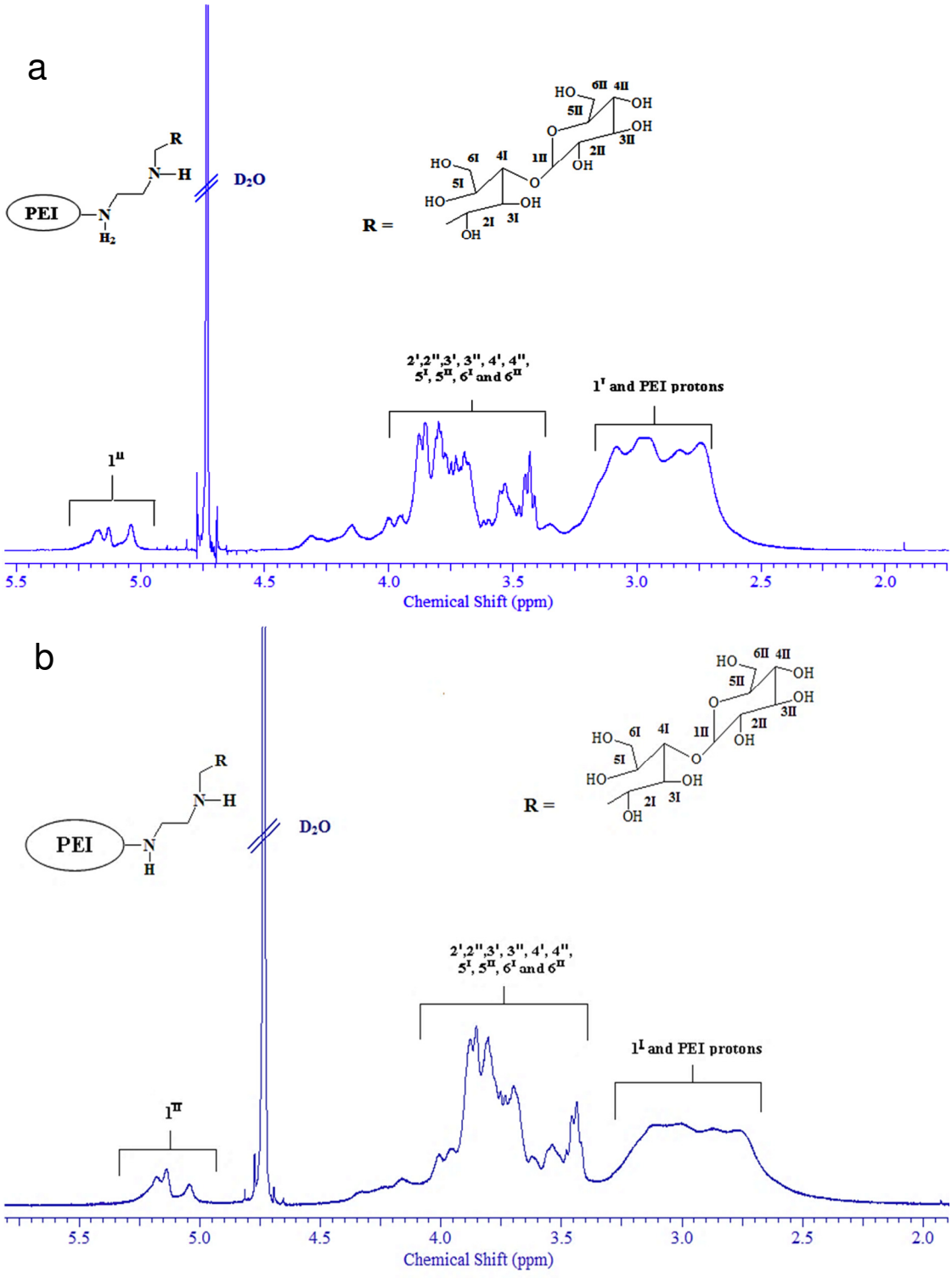

Figure 8-1. ^{1}H NMR spectra of PEI-Mal-B in D_2O obtained from educt ratio 1:0.5 (R= reductively attached maltose unit).

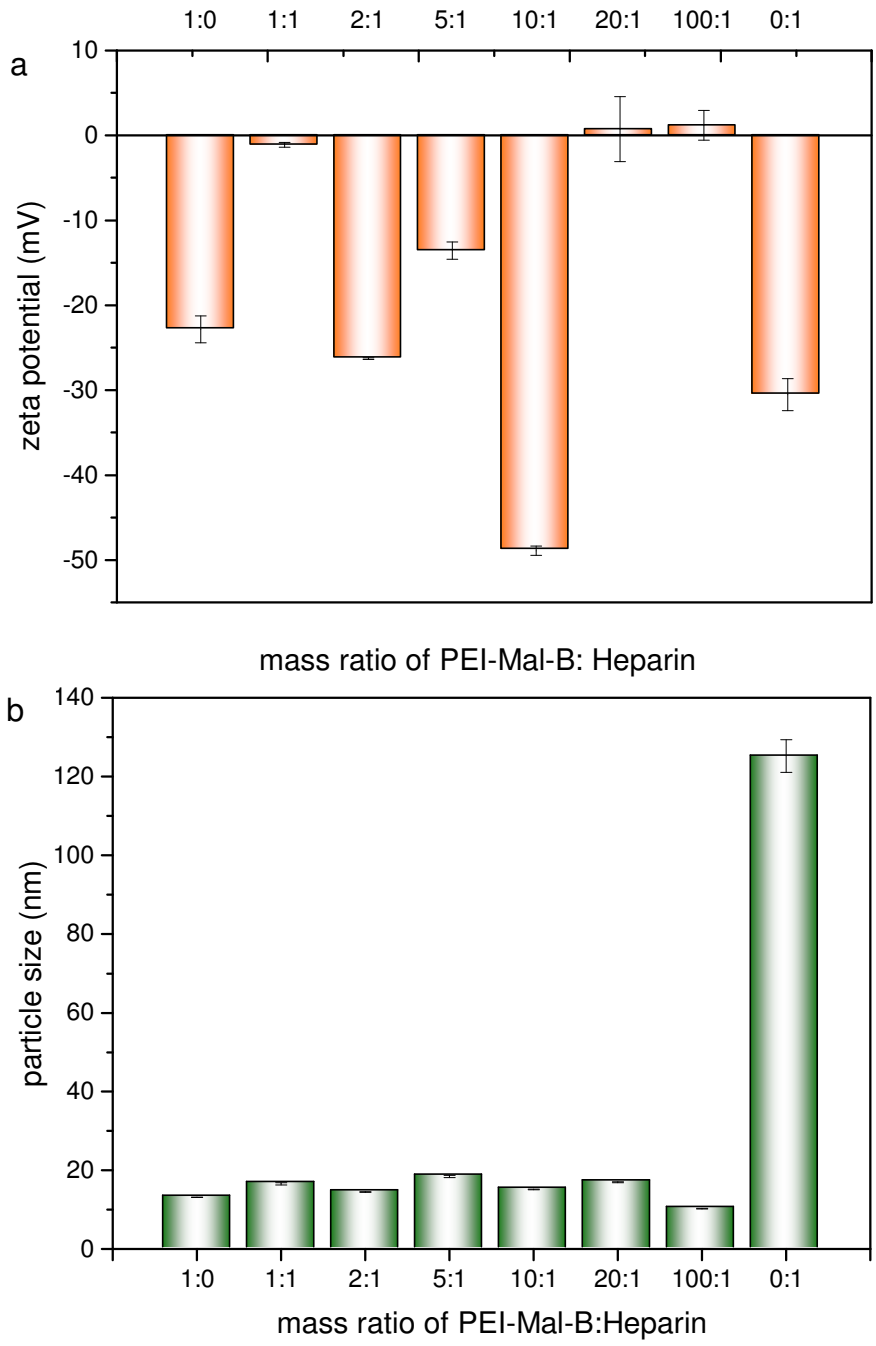

Figure 8-2. DLS and zetapotential measurements showing (**a**) zetapotential (mV) (**b**) particle size for different mass ratio for the complex PEI-Mal-B and HE-Na^+

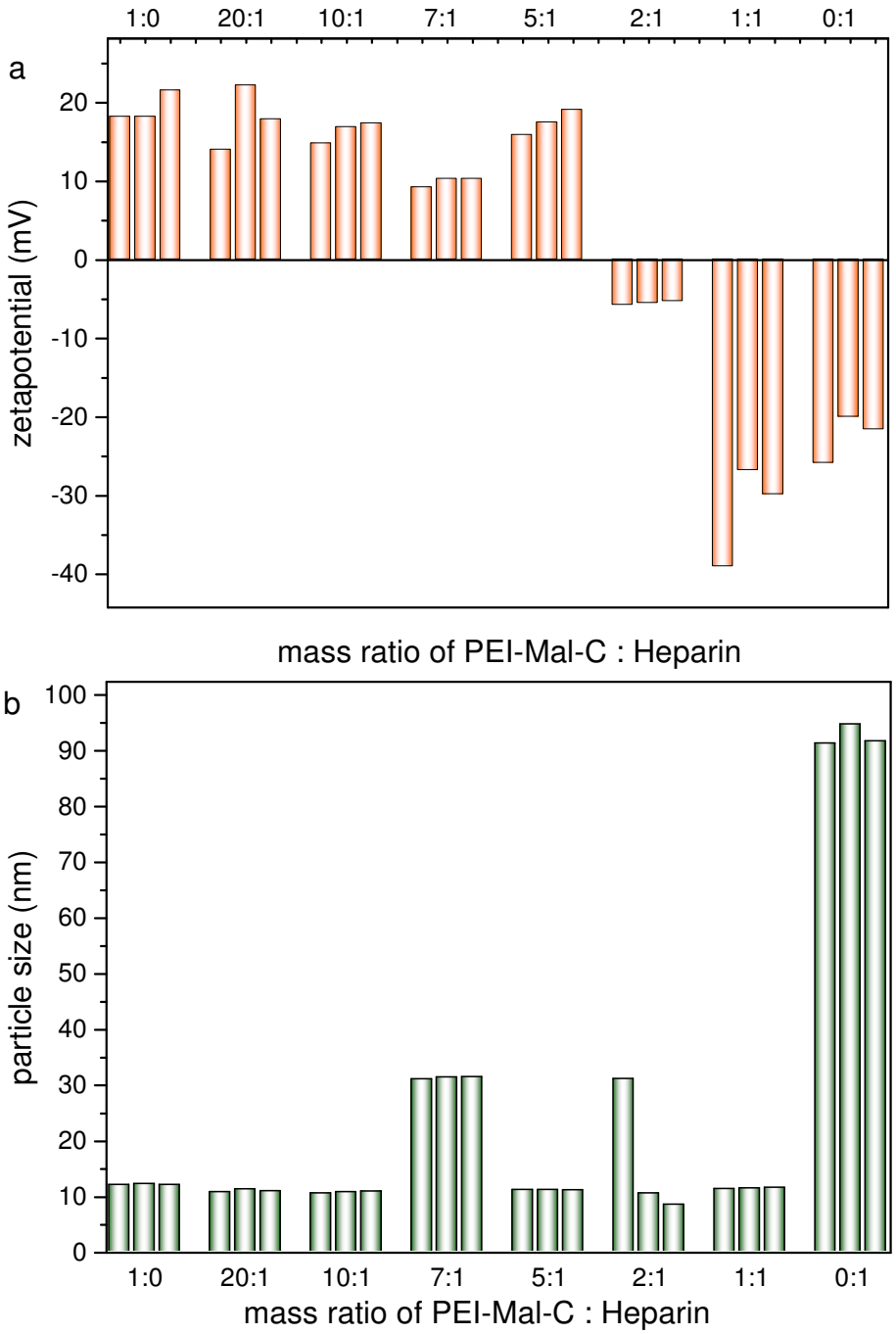

Figure 8-3. DLS and zetapotential measurements showing (**a**) zetapotential (mV) (**b**) particle size for different mass ratio for the complex PEI-Mal-C and HE-Na^+

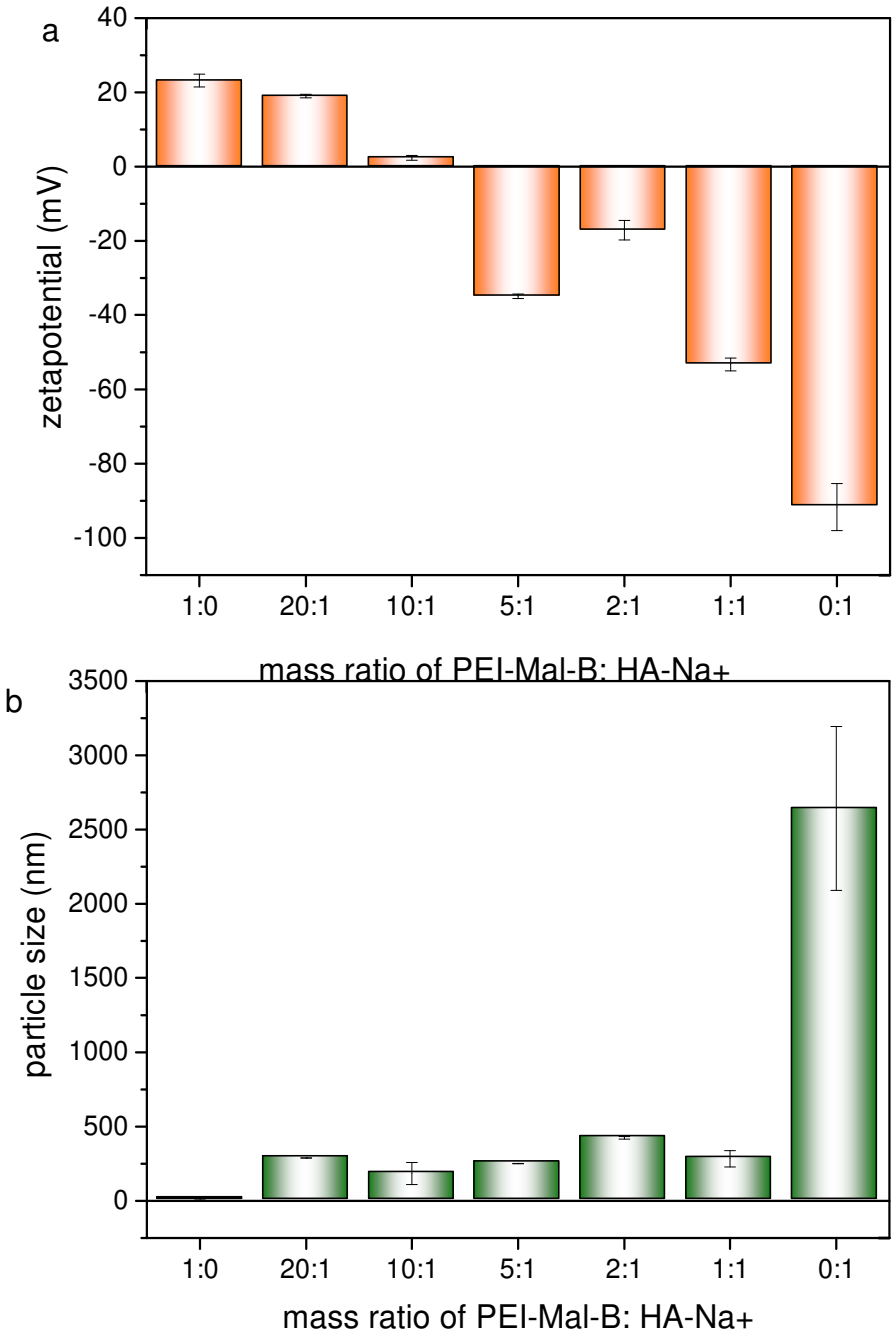

Figure 8-4. DLS and zetapotential measurements showing (**a**) zetapotential (mV) (**b**) particle size for different mass ratio for the complex PEI-Mal-B and HA-Na^+

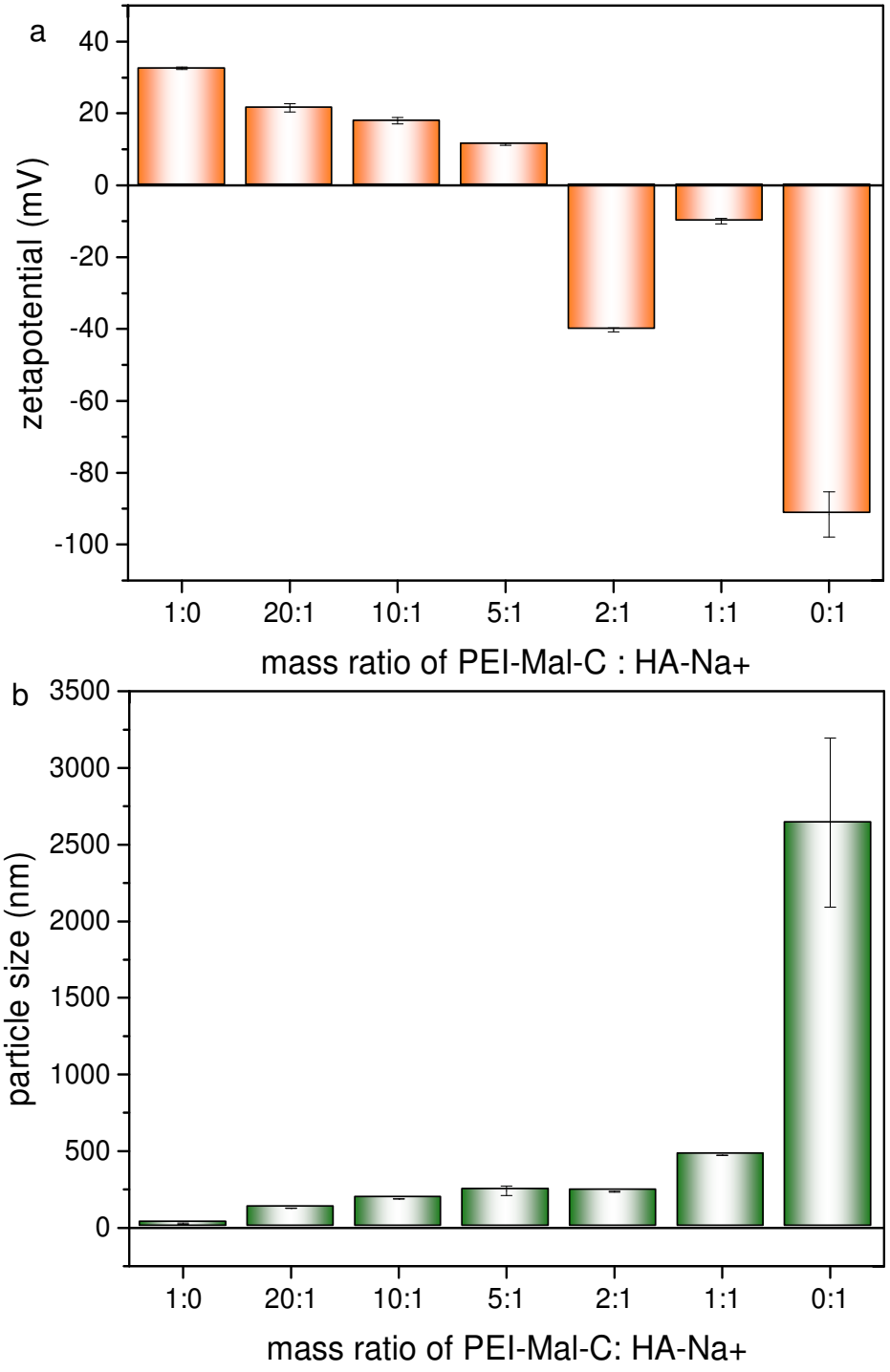

Figure 8-5. DLS and zetapotential measurements showing (**a**) zetapotential (mV) (**b**) particle size for different mass ratio for the complex PEI-Mal-C and HA-Na^+

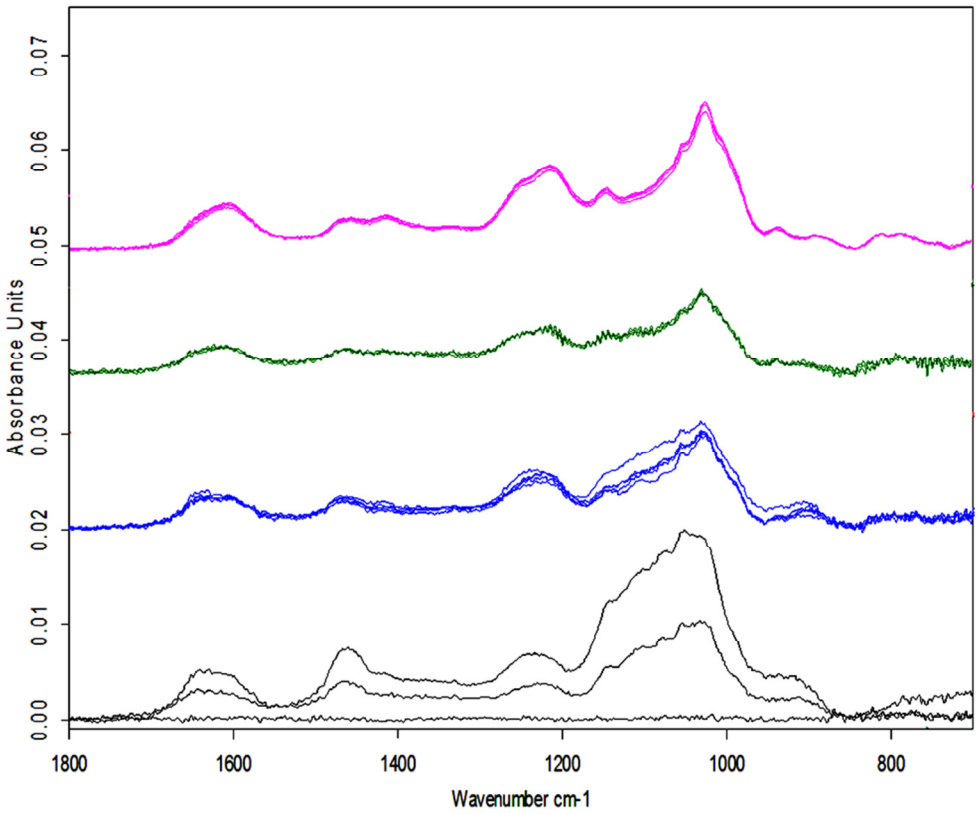

Figure 8-6. ATR-FTIR measurements for PEM and PEC of PEI-Mal-B and HE-Na^+ compare the loaded amount, stability and PE release for PEM of 20 bilayers (PEM-20) system with systems of casted polyelectrolyte complexes (PEC) with different mass ratios. PEM: (PEI(HE-Na^+/PEI-Mal-B)$_{20}$) [pink spectrum] and PEC with different mass ratio; 20:1 [green spectrum], 12:1 [blue spectrum] and 1:1 [black spectrum]. Series of release in Millipore-water for 0, 5, 60 and 1440 min have been measured. Experiments have been done on the surface Germanium interreflection elements (GE-IREs). Surface activation was done by using plasma cleaner for 20 min. The Experiments have been done in Dr. Martin Müller's laboratory.

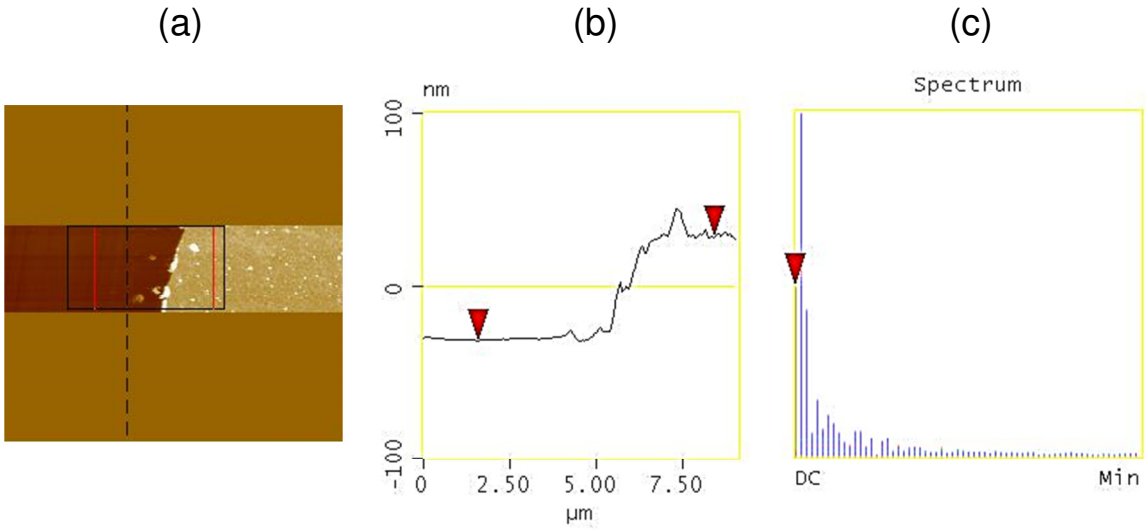

Figure 8-7. AFM thickness measurements are obtained by scratching. The scratch is made by hand with a razor blade to remove all the polyelectrolyte multilayer film from an area. These scratches are represented by dark valleys in the AFM height images in (**a**). The image in (**a**), precoating PEI-25k (2mg mL^{-1}) and pH11 prepared in Millipore water. Activated silica wafer is immersed in PEI-25k solution for 20 hours. A dark brown border encloses the area where the average cross section was taken. The average cross sections are shown in (**b**). Thickness measurements are made at several points and three samples. Examples are indicated by red arrows. The high peaks adjacent to the scratched area in (**b**) represent the buildup of the precoating displaced during scratching. The vertical high is measured in a value of 58 nm. These appear as bright areas in (**a**). (**c**) Spectrum of AFM for the presented scratch.

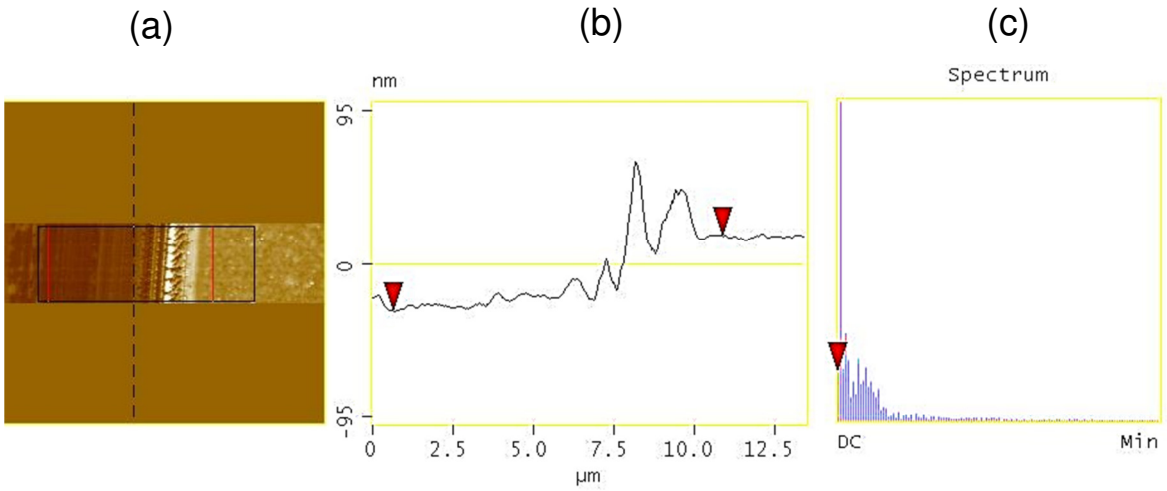

Figure 8-8. AFM thickness measurements are obtained by scratching. The scratch is made by hand with a razor blade to remove all the polyelectrolyte multilayer film from an area. These scratches are represented by dark valleys in the AFM height images in (**a**). The image in (**a**), precoating PEI-25k (2mg mL^{-1}) and pH 9.5 adjusted with HCl (0.5M). Activated silica wafer is immersed in PEI-25k solution for 20 hours. A dark brown border encloses the area where the average cross section was taken. The average cross sections are shown in (**b**). Thickness measurements are made at several points and three samples. Examples are indicated by red arrows. The high peaks adjacent to the scratched area in (**b**) represent the buildup of the precoating displaced during scratching. The vertical high is measured in a value of 31 nm. These appear as bright areas in (**a**). (**c**) Spectrum of AFM for the presented scratch.

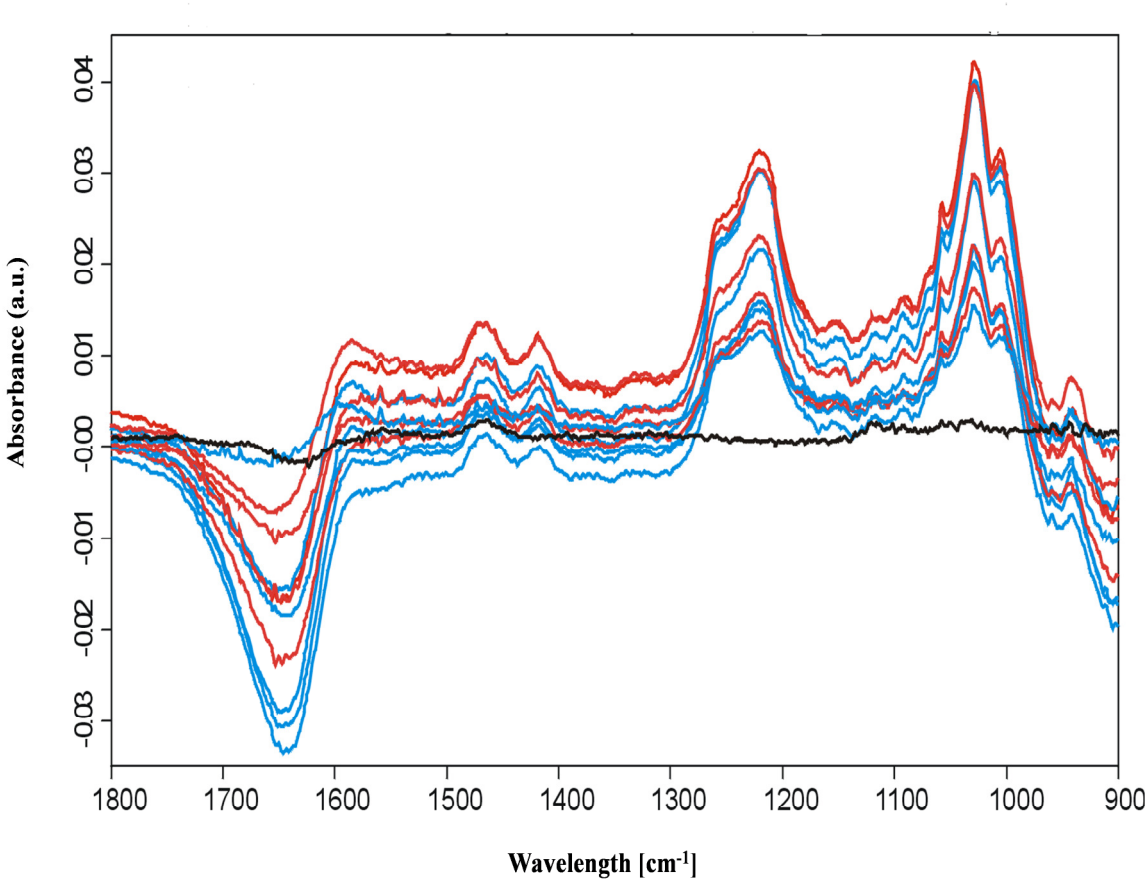

Figure 8-9. ATR-FTIR spectra on the consecutive build-up of PEMs of 10 bilayers (PEI(HE-Na^+/PEI-Mal-C)$_{10}$) fabricated with Approach C. The building up has been performed in a closed in-situ ATR- flow cell system on the surface of silicon internal reflection element (Si-IRE) using peristaltic pump at a flow rate of 5mL min^{-1} for a defined number of adsorption steps. Every adsorption step takes 20 min and every rinsing step (Millipore water) 1 min.

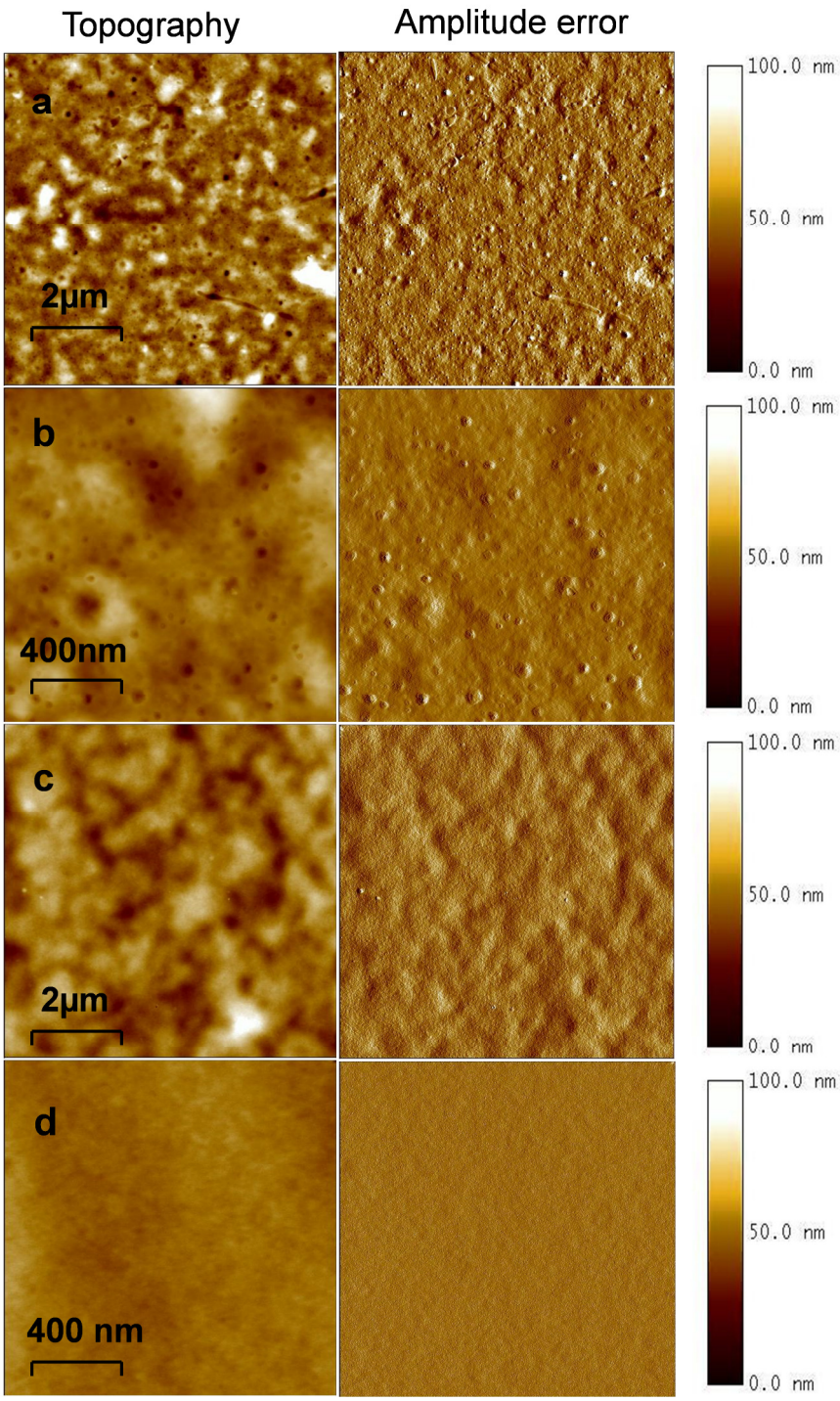

Figure 8-10. AFM topography and amplitude error of PEM (PEI(HE-Na^+/PEI-Mal-B)$_n$) with 10 and 50 bilayers fabricated with Approach **A** . (**a**) and (**b**): (PEI(HE-Na^+/PEI-Mal-B)$_{10}$) with film thickness of ~ 92 nm. (**c**) and (**d**) (PEI(HE-Na^+/PEI-Mal-B)$_{50}$) with film thickness of ~165 nm. The root mean square (rms) value for surface roughness is 14 nm for (**a**) and (**b**), and 6 nm for (**c**) and (**d**). Substrate is Si wafer with additional layer of SiO_2 of thickness 27 nm measured by the mean of ellipsometry.

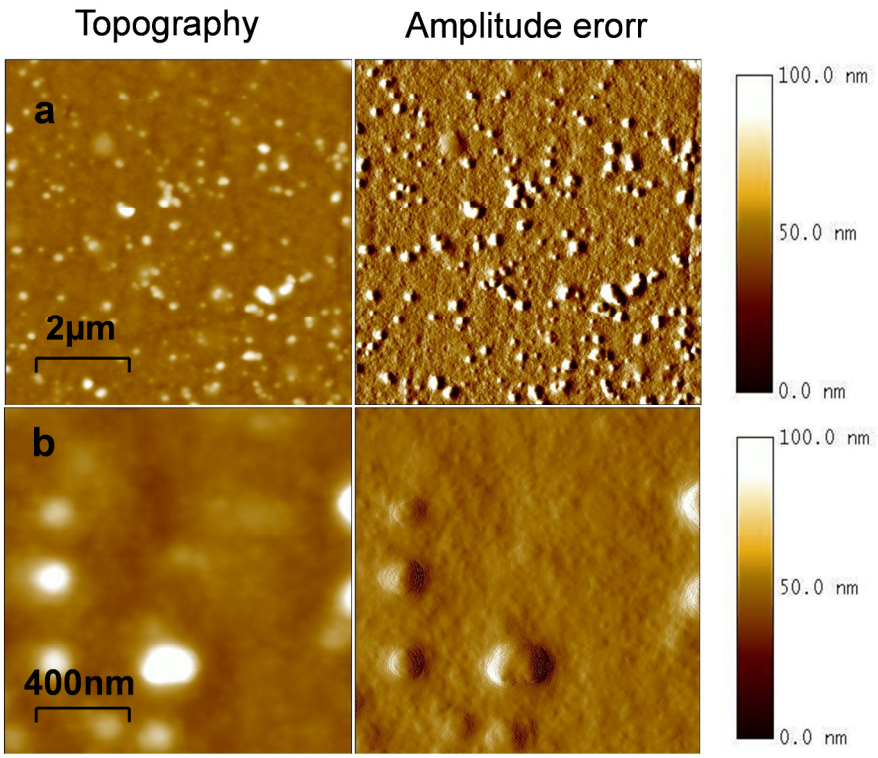

Figure 8-11. AFM topography and amplitude error of PEM (PEI(HE-Na^+/PEI-Mal-B)$_n$) with 10 bilayers fabricated with Approach **A** . (**a**) and (**b**): (PEI/(HE-Na^+/PEI-Mal-B)$_{10}$), having islands on the surface of order of 200nm. The root mean square (rms) value for surface roughness is 22 nm for (**a**) and (**b**). PEM has built-up on a surface of Si-IRE.

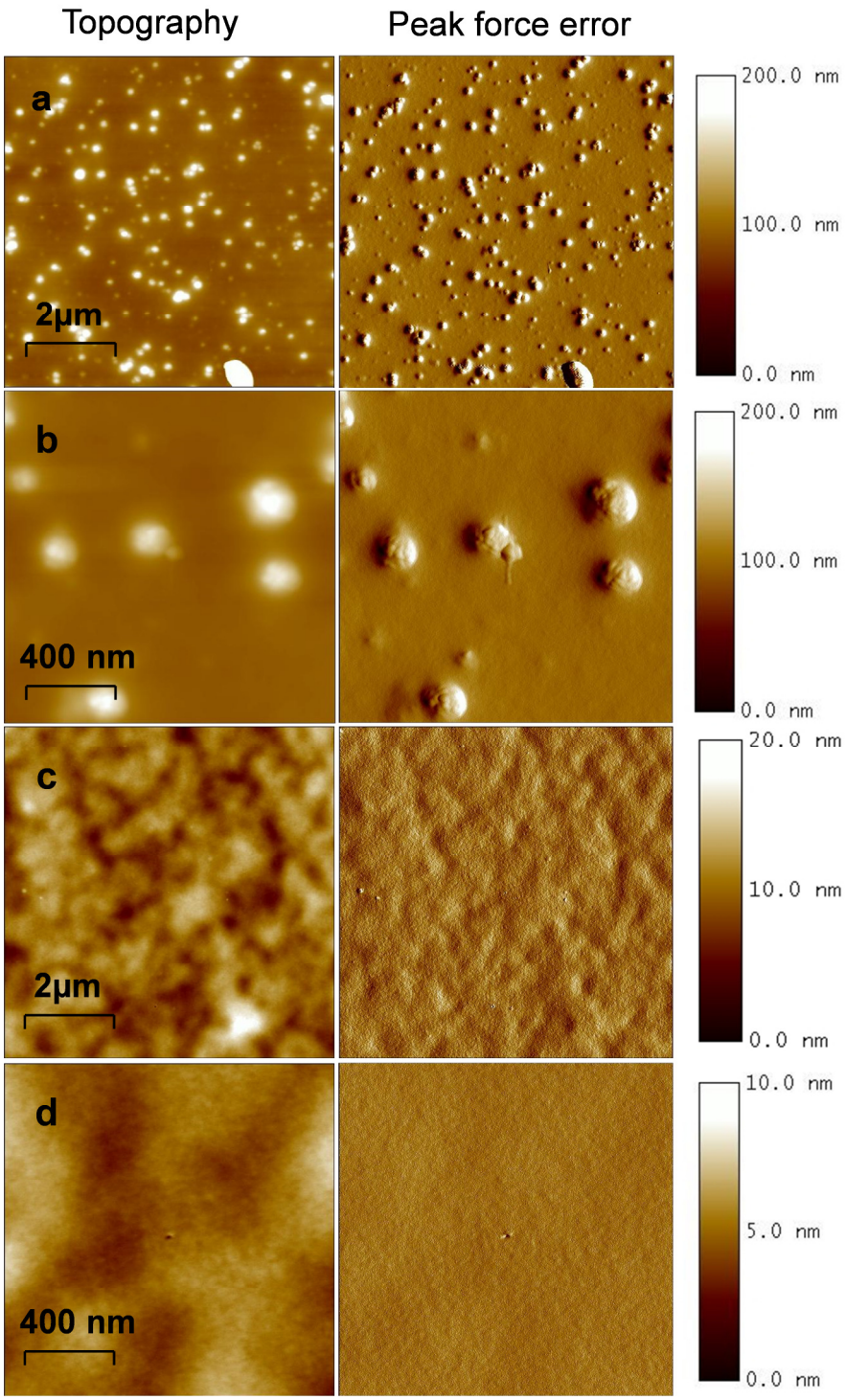

Figure 8-12. AFM topography and peak force error of PEM (PEI(HE-Na^+/PEI-Mal-C)$_n$) with 10 and 50 bilayers fabricated with Approach **A** . (**a**) and (**b**): (PEI(HE-Na^+/PEI-Mal-C)$_{10}$) with film thickness of ~ 130nm, having islands on the surface of order of 500 nm. (**c**) and (**d**) (PEI(HE-Na^+/PEI-Mal-C)$_{50}$) with film thickness of ~1291 nm. The root mean square (rms) value for surface roughness is 28nm for (**a**) and (**b**), and 2nm for (**c**) and (**d**). Substrate is Si wafer with additional layer of SiO_2 of thickness 27 nm measured by the mean of ellipsometry.

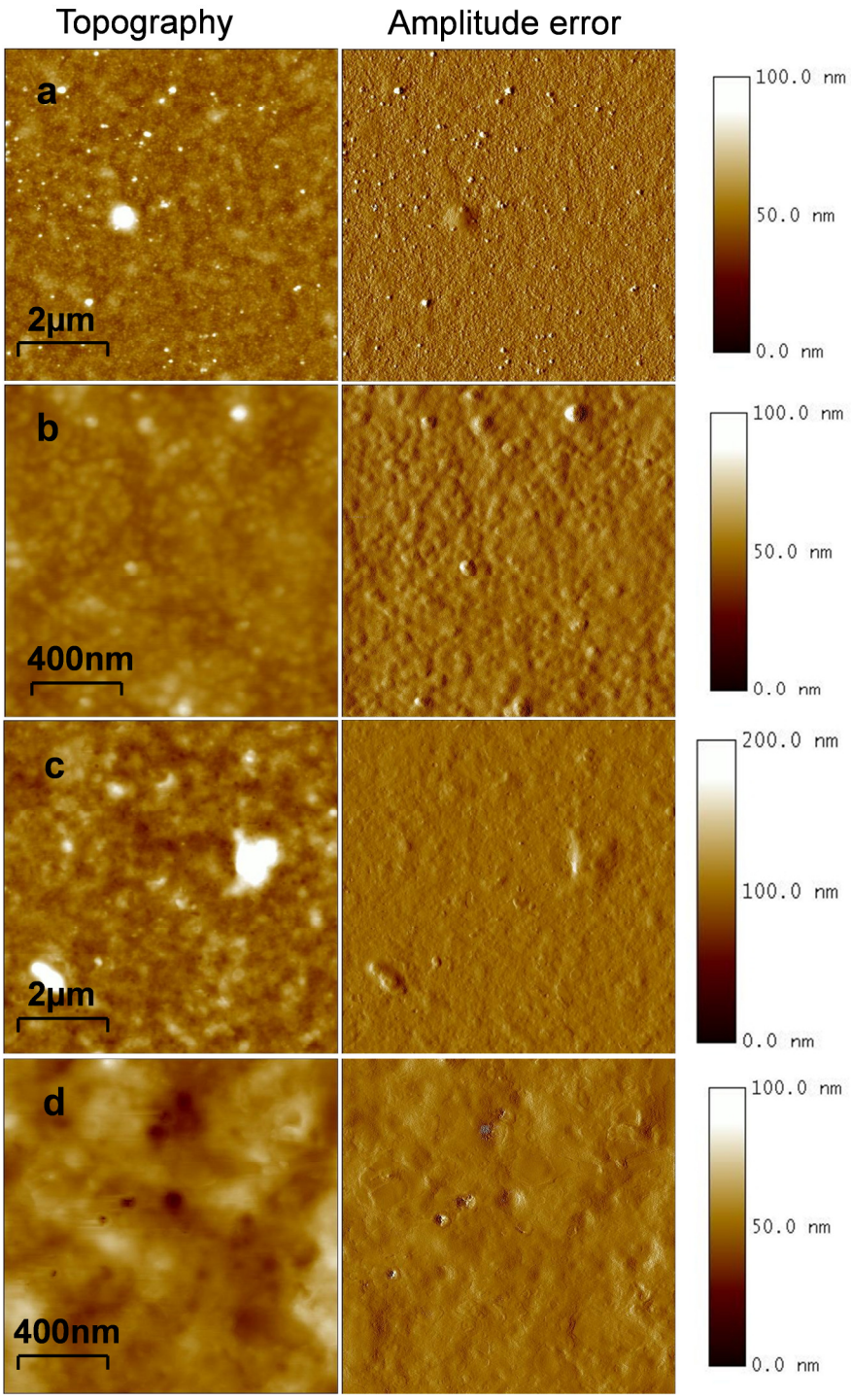

Figure 8-13. AFM topography and amplitude error of PEM (PEI(HE-Na^+/PEI-Mal-B)$_n$) with 10 and 50 bilayers fabricated with Approach **B** . (**a**) and (**b**): (PEI(HE-Na^+/PEI-Mal-B)$_{10}$) with film thickness of ~ 52 nm. (**c**) and (**d**) (PEI(HE-Na^+/PEI-Mal-B)$_{50}$) with film thickness of ~139 nm. The root mean square (rms) value for surface roughness is 20 nm for (**a**) and (**b**), and 7nm for (**c**) and (**d**). Substrate is Si wafer with additional layer of SiO_2 of thickness 27 nm measured by the mean of ellipsometry.

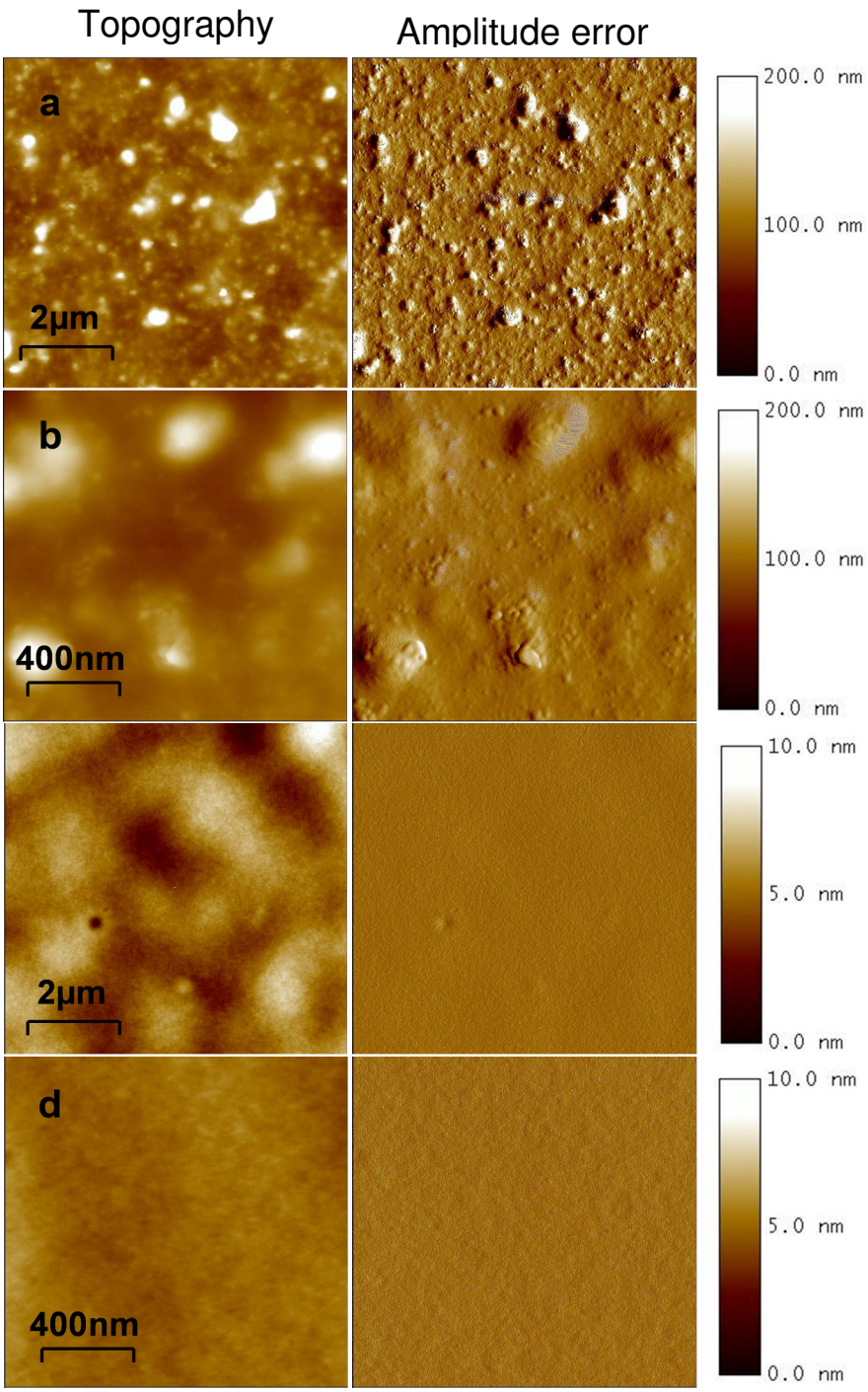

Figure 8-14. AFM topography and amplitude error of PEM (PEI(HE-Na+/PEI-Mal-C)$_n$) with 10 and 50 bilayers fabricated with Approach **B** . (**a**) and (**b**): (PEI(HE-Na$^+$/PEI-Mal-C)$_{10}$) with film thickness of ~ 42 nm. (**c**) and (**d**) (PEI(HE-Na+/PEI-Mal-C)$_{50}$) with film thickness of ~1149 nm. The root mean square (rms) value for surface roughness is 32 nm for (**a**) and (**b**), and 1nm for (**c**) and (**d**). Substrate is Si wafer with additional layer of SiO_2 of thickness 27 nm measured by the mean of ellipsometry.

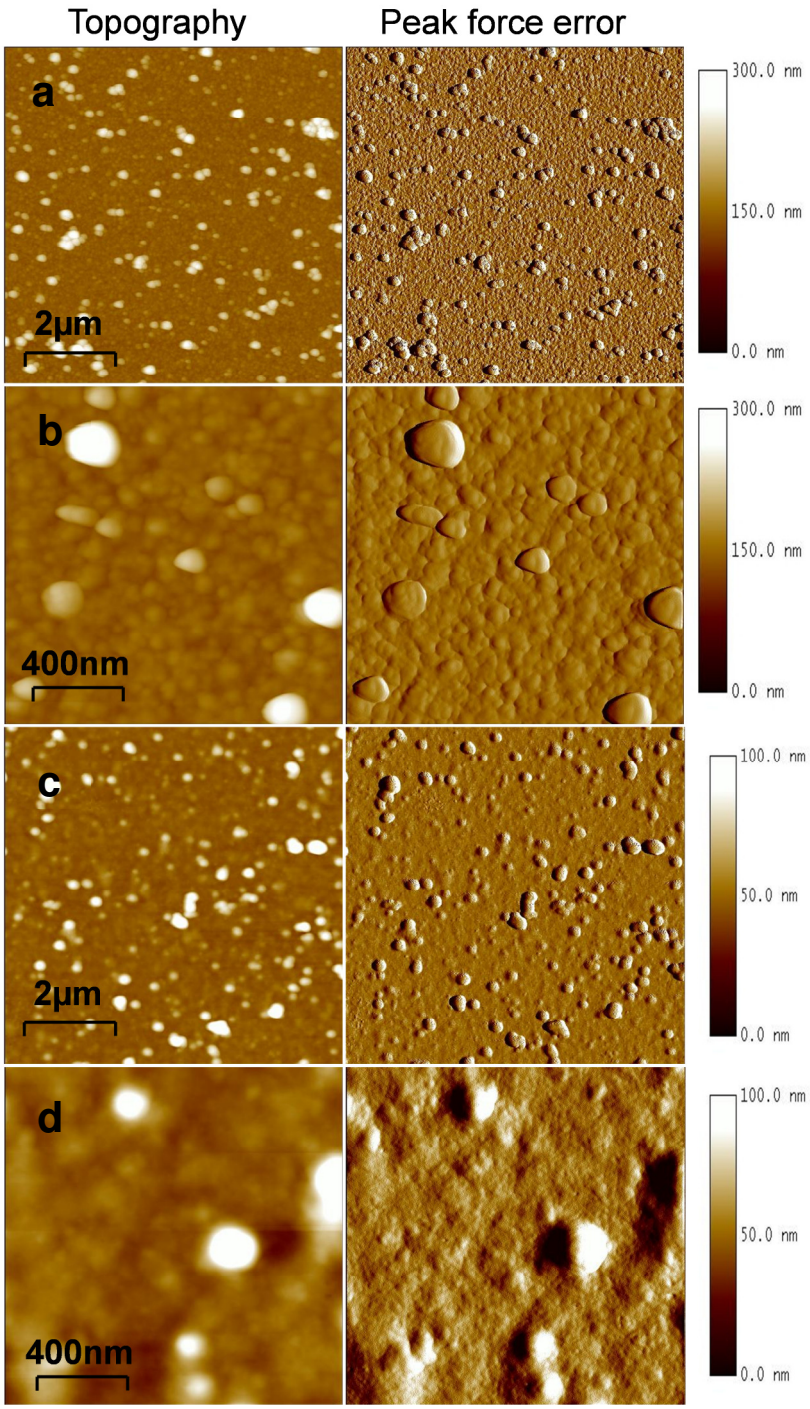

Figure 8-15. AFM topography and peak force error of PEM (PEI(HE-Na^+/PEI-Mal-B)$_n$) with 10 and 50 bilayers fabricated with Approach **C** . (**a**) and (**b**): (PEI(HE-Na^+/PEI-Mal-B)$_{10}$) with film thickness of ~ 102 nm. (**c**) and (**d**) (PEI(HE-Na^+/PEI-Mal-B)$_{50}$) with film thickness of ~ 175 nm. The root mean square (rms) value for surface roughness is 36 nm for (**a**) and (**b**), and 27nm for (**c**) and (**d**). Substrate is Si wafer with additional layer of SiO_2 of thickness 27 nm measured by the mean of ellipsometry.

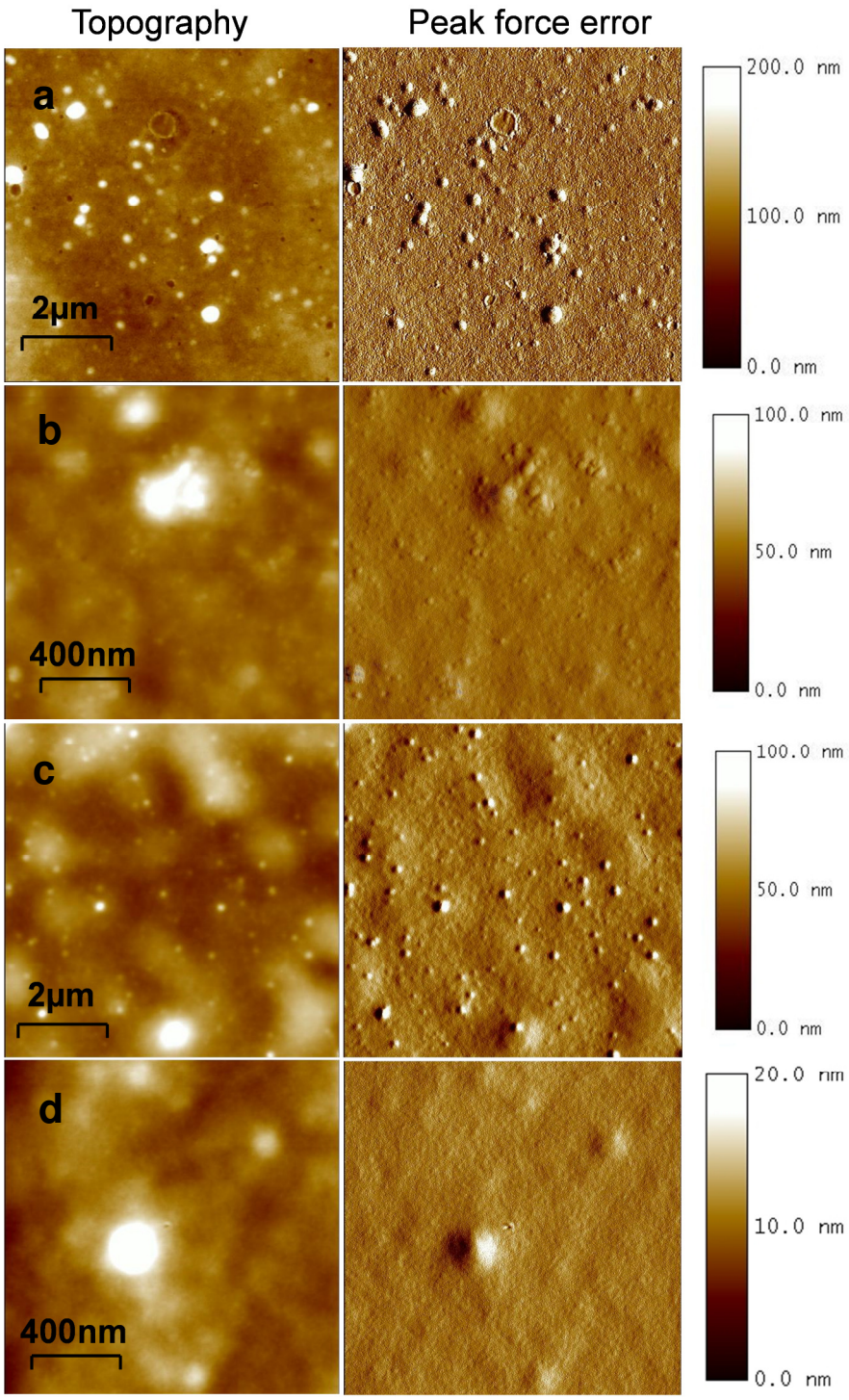

Figure 8-16. AFM topography and peak force error of PEM (PEI(HE-Na^+/PEI-Mal-C)$_n$) with 10 and 50 bilayers fabricated with Approach **C** . (**a**) and (**b**): (PEI(HE-Na^+/PEI-Mal-C)$_{10}$) with film thickness of ~ 98 nm. (**c**) and (**d**) (PEI(HE-Na^+/PEI-Mal-C)$_{50}$) with film thickness of ~185 nm. The root mean square (rms) value for surface roughness is 18 nm for (**a**) and (**b**), and 10 nm for (**c**) and (**d**). Substrate is Si wafer with additional layer of SiO_2 of thickness 27 nm measured by the mean of ellipsometry.

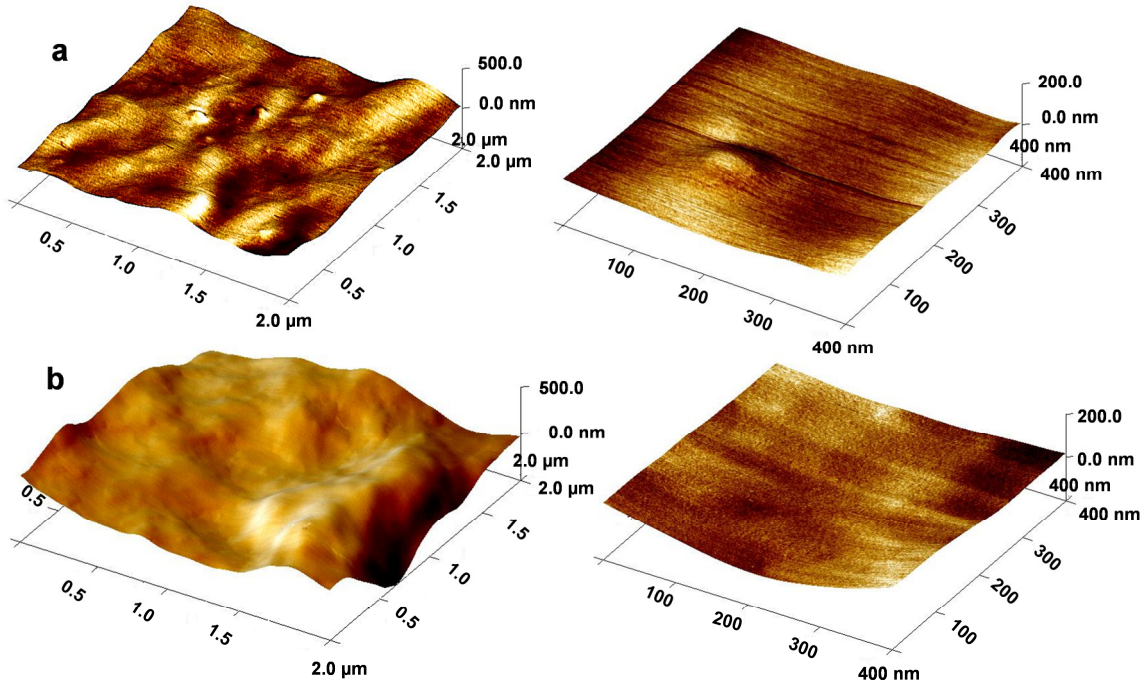

Figure 8-17. AFM topography of PEM $(PEI(HA\text{-}Na^{+}/PEI\text{-}Mal\text{-}C)_{n})$ with 10 and 25 bilayers fabricated with Approach **A**. (**a**): $(PEI(HA\text{-}Na^{+}/PEI\text{-}Mal\text{-}C)_{10})$ with film thickness of ~ 565 nm. (**b**): $(PEI(HA\text{-}Na^{+}/PEI\text{-}Mal\text{-}C)_{25})$ with film thickness of ~1440 nm. The root mean square (rms) value for surface roughness is 18 nm for (**a**), and 1 nm for (**b**). Substrate is Si wafer with additional layer of SiO_2 of thickness 27 nm measured by the mean of ellipsometry.

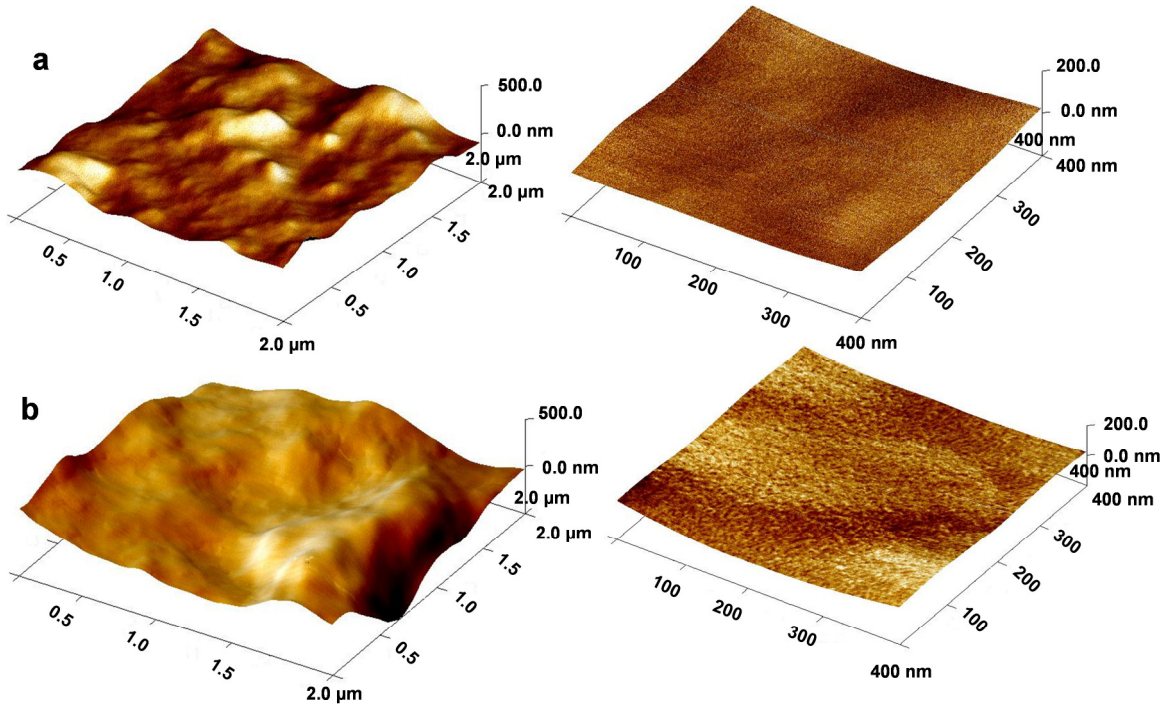

Figure 8-18. AFM topography of PEM (PEI(HA-Na^+/PEI-Mal-C)$_n$) with 10 and 25 bilayers fabricated with Approach **B**. (**a**): (PEI(HA-Na^+/PEI-Mal-C)$_{10}$) with film thickness of ~ 565 nm. (**b**): (PEI(HA-Na^+/PEI-Mal-C)$_{25}$) with film thickness of ~1427 nm. The root mean square (rms) value for surface roughness is 20 nm for (**a**), and 5 nm for (**b**). Substrate is Si wafer with additional layer of SiO_2 of thickness 27 nm measured by the mean of ellipsometry.

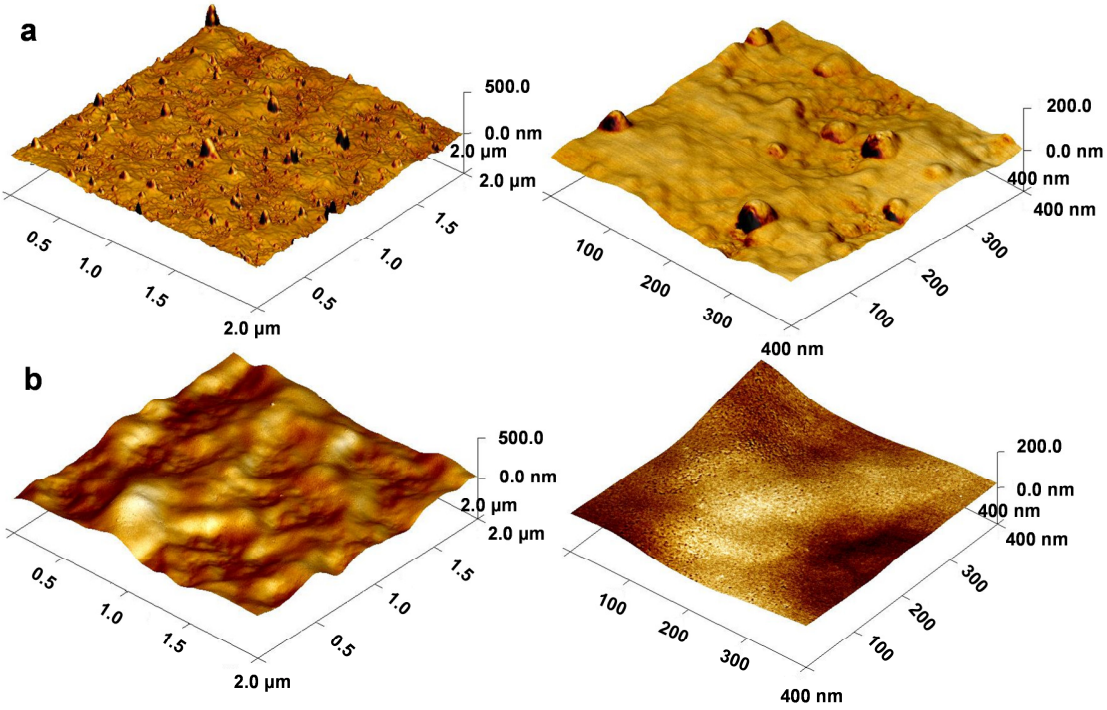

Figure 8-19. AFM topography of PEM (PEI(HA-Na^+/PEI-Mal-C)$_n$) with 10 and 25 bilayers fabricated with Approach **C**. (**a**): (PEI(HA-Na^+/PEI-Mal-C)$_{10}$) with film thickness of ~ 223 nm. (**b**): (PEI(HA-Na^+/PEI-Mal-C)$_{25}$) with film thickness of ~479 nm. The root mean square (rms) value for surface roughness is 30 nm for (**a**), and 10 nm for (**b**). Substrate is Si wafer with additional layer of SiO_2 of thickness 27 nm measured by the mean of ellipsometry.

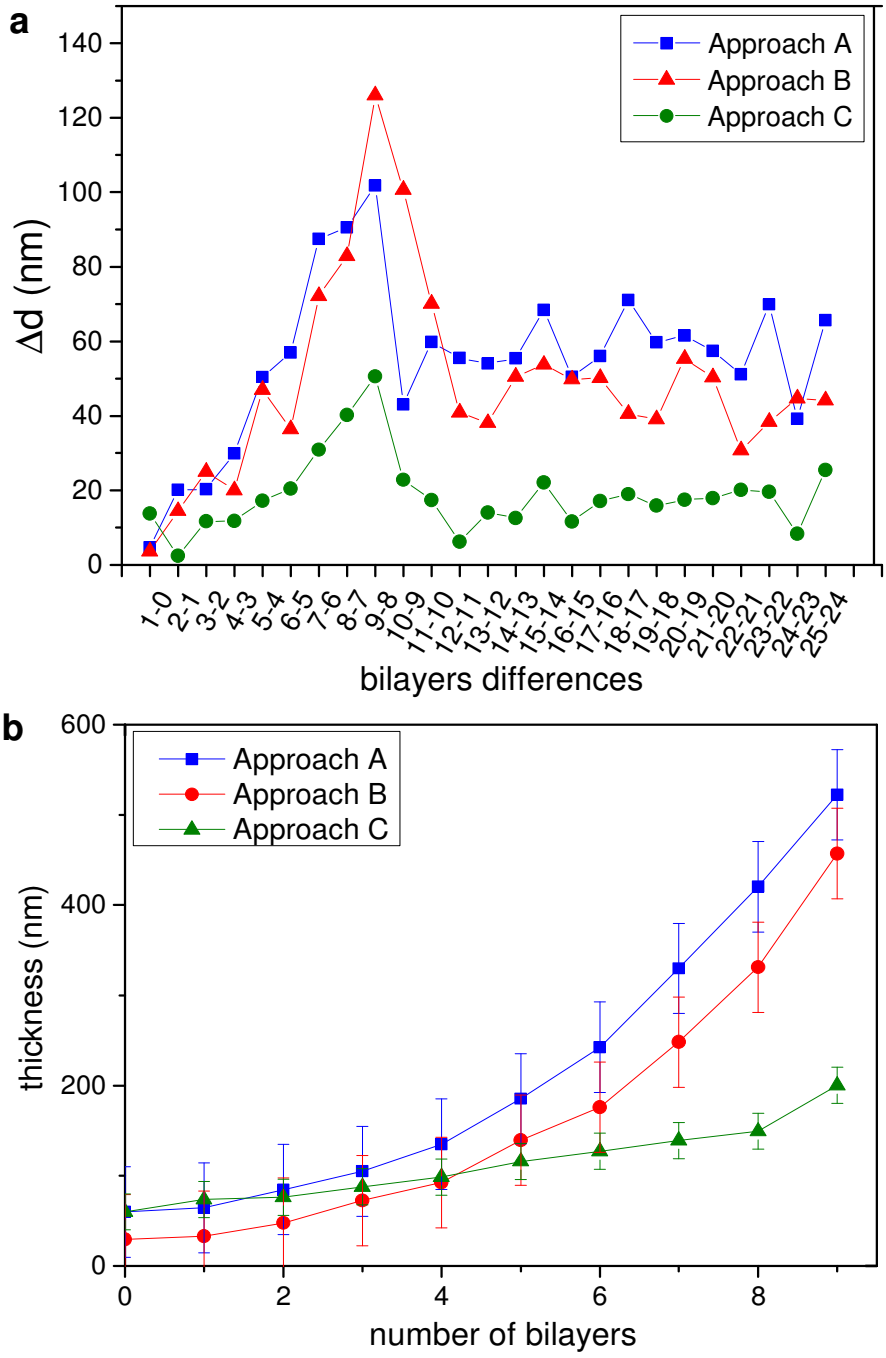

Figure 8-20. Figure represents (**a**) PEM (PEI(HA-Na^+/PEI-Mal-C)$_{25}$) thickness differences Δd (nm) versus bilayers differences (**b**) Zooming –in for the PEM thickness progression versus number of adsorbed bilayers during the fabrication of final PEM (PEI(HA-Na^+/PEI-Mal)$_9$) with 9 bilayers of PEI-Mal-C fabricated by approaches A-C.

Appendix

Table 8-1. Table presents dry and swollen thicknesses for weak/strong system PEM (PEI(HE-Na^+/PEI-Mal-C)$_{50}$) and weak/weak system PEM (PEI(HA-Na^+/PEI-Mal-C)$_{25}$). Dry state thickness: $d_{initial\ dry}$ (nm), swollen thickness at 0 hour: $d_{swollen}$ initial, swollen thickness at 96 hour: $d_{swollen}$ final, percentage degree of swelling for 0 hour and 96 hours: SD% [a)] and final dry PEM thickness after being immersed in PBS for 96 hours: $d_{final\ dry}$ are presented. PEM has swollen in PBS (PO_4^{3-} (0.01M) + NaCl (137 mM)+ KCl (2.7 mM)). The experiment has been repeated for three times. Dry and swollen thicknesses have been monitored at λ = 632.8 nm by ellipsometry.

Weak/strong system PEM (PEI(HE-Na^+/PEI-Mal-C)$_{50}$)						
	Dry state	**Swollen State**		**SD%**		Dry state
Approach	$d_{initial}$ **dry** **[nm]**	$d_{swollen\ initial}$ **[nm]**	$d_{swollen\ final}$ **[nm]**	**0h**	**96h**	d_{final} **dry** **[nm]**
A	1291	3501	2655	171	106	849
B	1149	4002	2702	248	135	991
C	185	309	310	67	68	180
Weak/weak system PEM (PEI(HA-Na^+/PEI-Mal-C)$_{25}$)						
A	1440	2160	2067	50	44	1282
B	1427	2146	2053	50	44	1256
C	479	720	730	50	52	480

[a)] Degree of swelling % = 100× (d $_{swollen\ state}$ − d $_{Dry\ state}$)/ (d $_{Dry\ state}$)

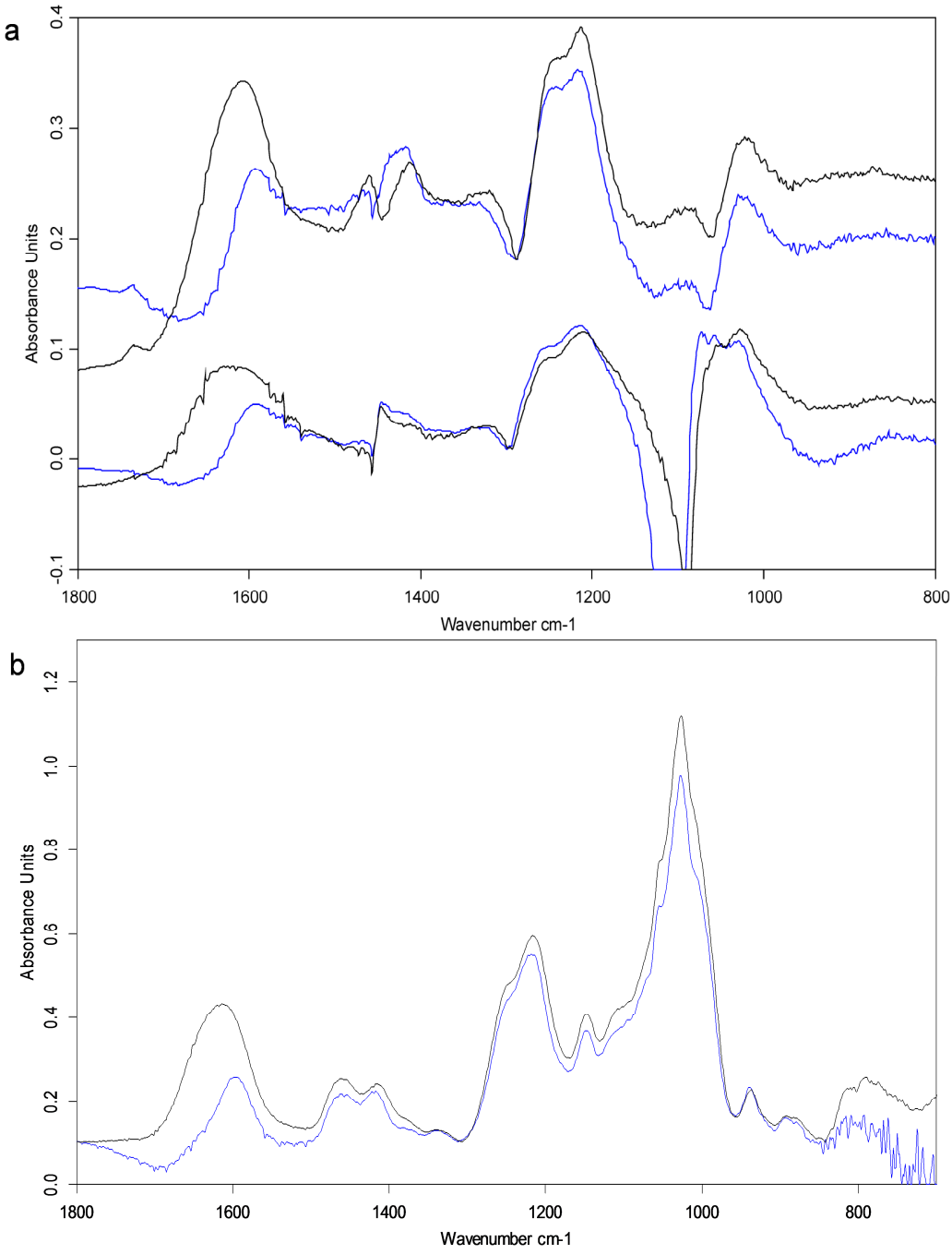

Figure 8-21. In-situ ATR-FTIR spectra of polyelectrolyte multilayers PEM (PEI(HE-Na^+/PEI-Mal)$_{20}$) with 20 bilayers: (**a**) Approach A the upper panel is related to PEM with PEI-Mal-B, while the lower is to PEM with PEI-Mal-C (**b**) Approach C for PEM with PEI-Mal-C, showing ATR-FTIR spectra in dry (black lines) and wet state after swelling (blue lines-soaked in PBS at pH 7.4). The PEM was directly build-up on ATR-FTIR internal reflection crystal. PBS concentration: PO_4^{3-} (0.01M) + NaCl (137 mM)+ KCl (2.7 mM)

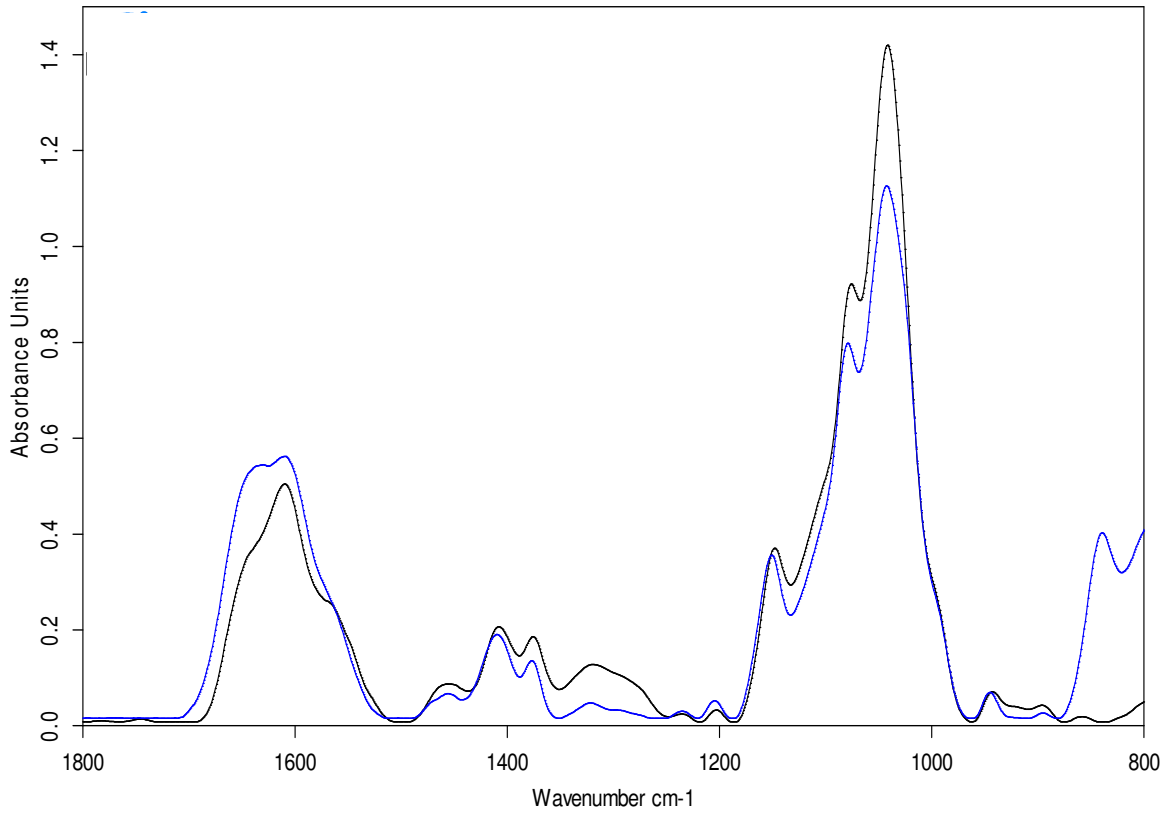

Figure 8-22. In-situ ATR-FTIR spectra of polyelectrolyte multilayers PEM (PEI(HA-Na^+/PEI-Mal)$_{20}$) with 20 bilayers for Approach C, showing ATR-FTIR spectra in dry (black lines) and wet state after swelling (blue lines-soaked in PBS at pH 7.4). The PEM was directly built-up on ATR-FTIR internal reflection crystal. PBS concentration: PO_4^{3-} (0.01M) + NaCl (137 mM)+ KCl (2.7 mM)

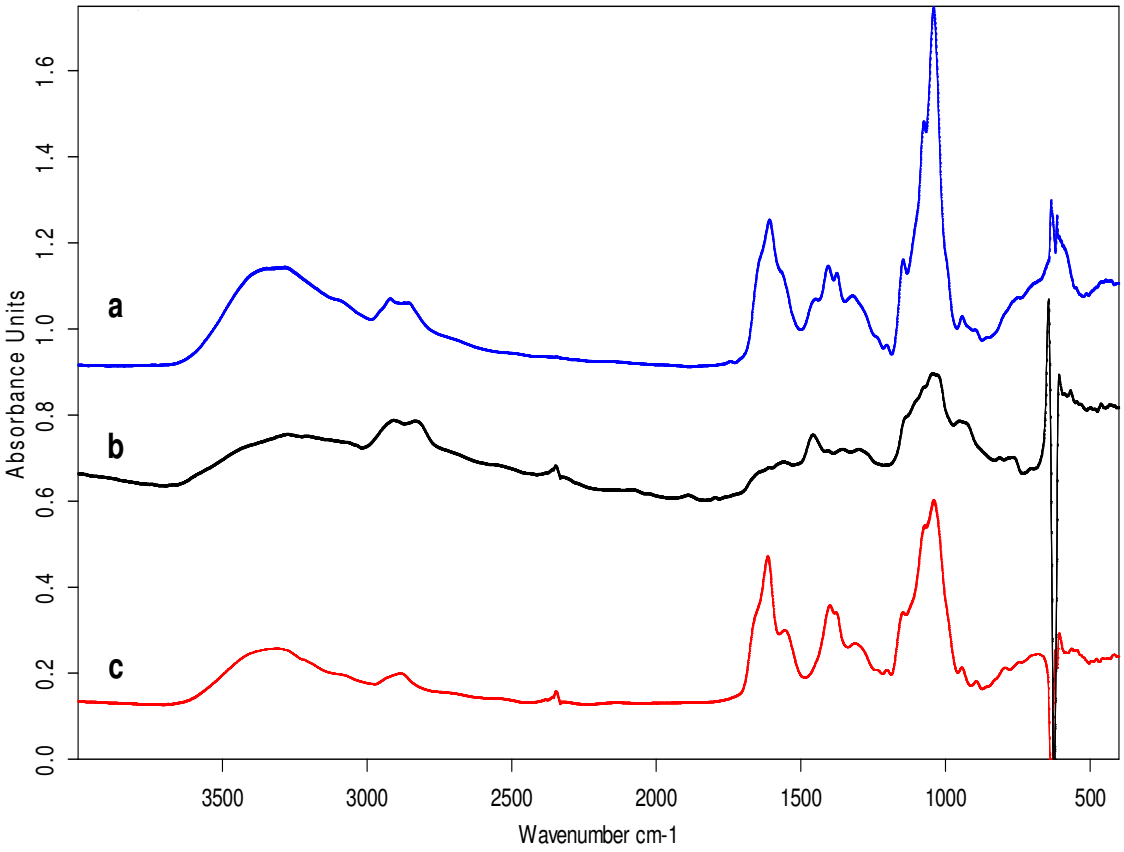

Figure 8-23. In-situ ATR-FTIR spectra : (**a**) casting model for HA-Na^+ solution of 50ml of concentration 0.5 mg mL^{-1} (**b**) casting model for PEI-Mal-C solution of 50ml of concentration 0.5 mg mg^{-1} (**c**) free loaded PEM (PEI(HA-Na^+/PEI-Mal)$_{20}$) with 20 bilayers for Approach C, showing ATR-FTIR spectra in dry (black lines) and wet state after swelling (blue lines-soaked in PBS at pH 7.4). All of the spectra were directly built-up on Ge-IRE.

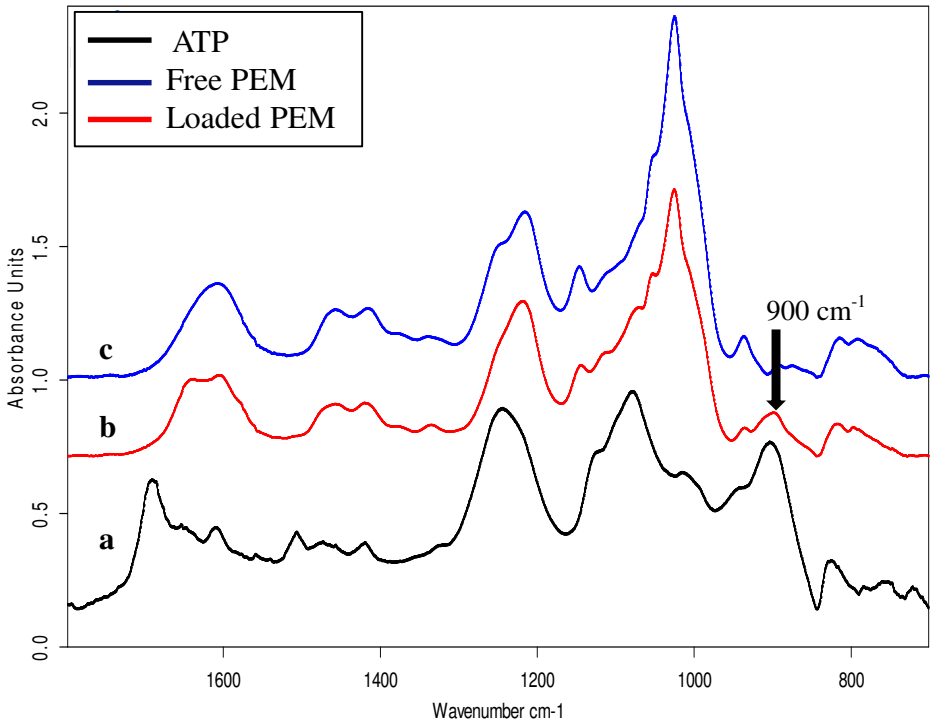

Figure 8-24. ATR-FTIR spectra for (**a**) ATP, (**b**) loaded PEM (PEI(HE-Na^+/PEI-Mal-C)$_{20}$) with ATP as a model drug and (**c**) free PEM (PEI(HE-Na^+/PEI-Mal-C)$_{20}$). ATP concentration in all cases was 0.5 mg mL^{-1}

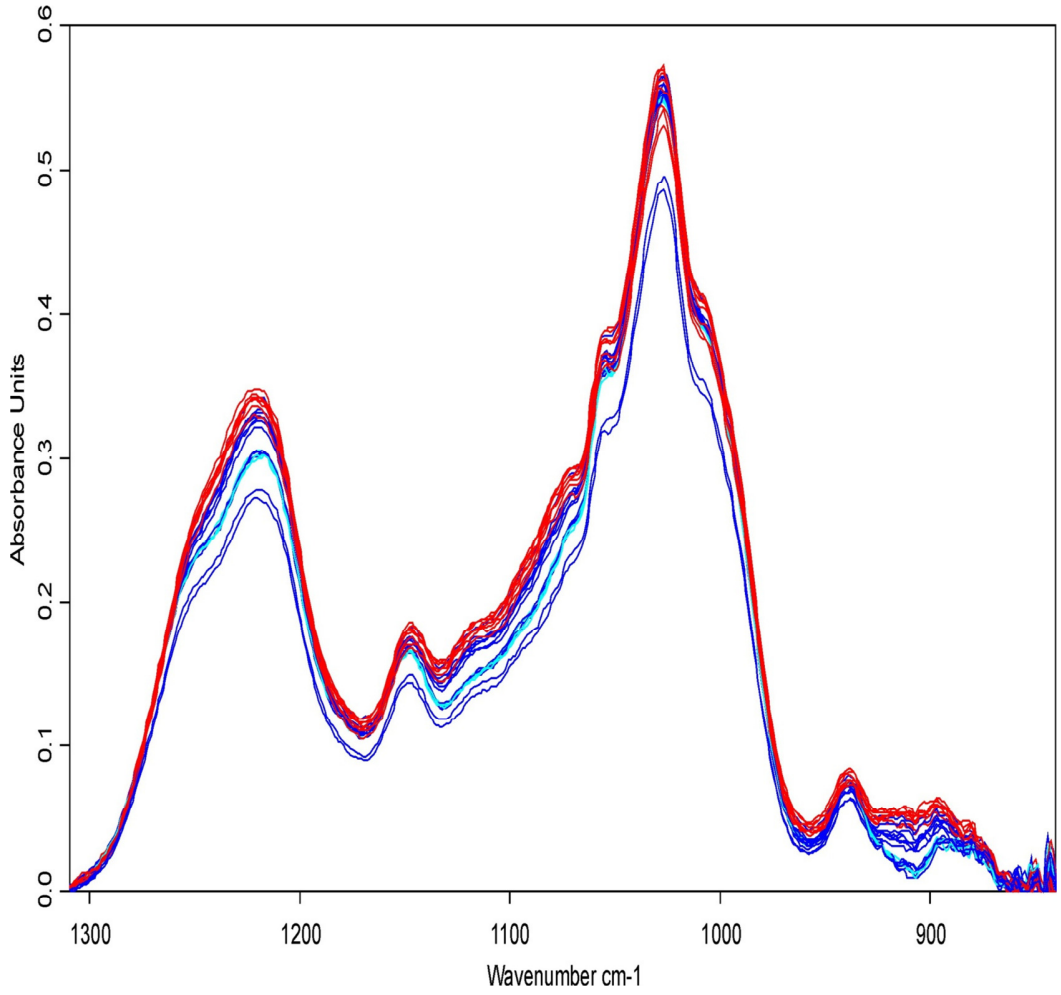

Figure 8-25. In-situ ATR-FTIR measurements for cyclic upload and release of ATP molecule for PEM (PEI(HE-Na^+/PEI-Mal-C)$_{20}$) PEM was subjected to Millipore water as a swelling medium followed by ATP addition then the rinsing steps which have been divided into two mediums (**i**) Millipore-water followed by the final rinsing step with (**ii**) NaCl (0.1M) solution (pH 6). The uptake and the release were done as an in-situ measurements using closed loop mode at a flow rate of 5mL min^{-1}, cycle was measured for ~4 hour.

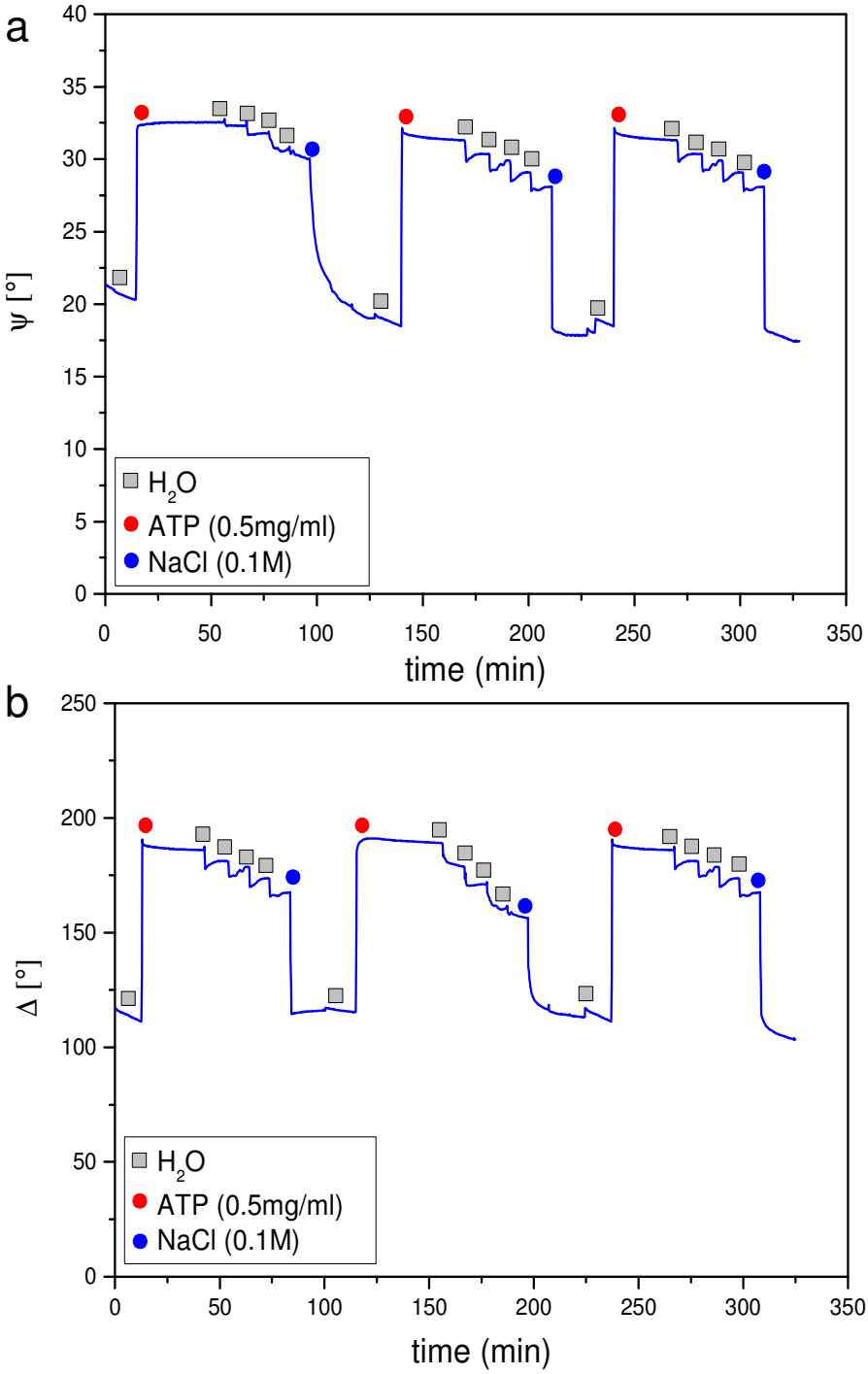

Figure 8-26. Dynamic scan of the experimental ellipsometric parameters, (**a**) phase difference (Δ) (**b**) amplitude ratio for cyclic upload and release of PEM (PEI(HE-Na^+/PEI-Mal-C)$_{20}$), swollen and rinsed via Millipore-water (e.g. for λ = 632.8 nm), ATP (c= 0.5 mg mL^{-1}) .

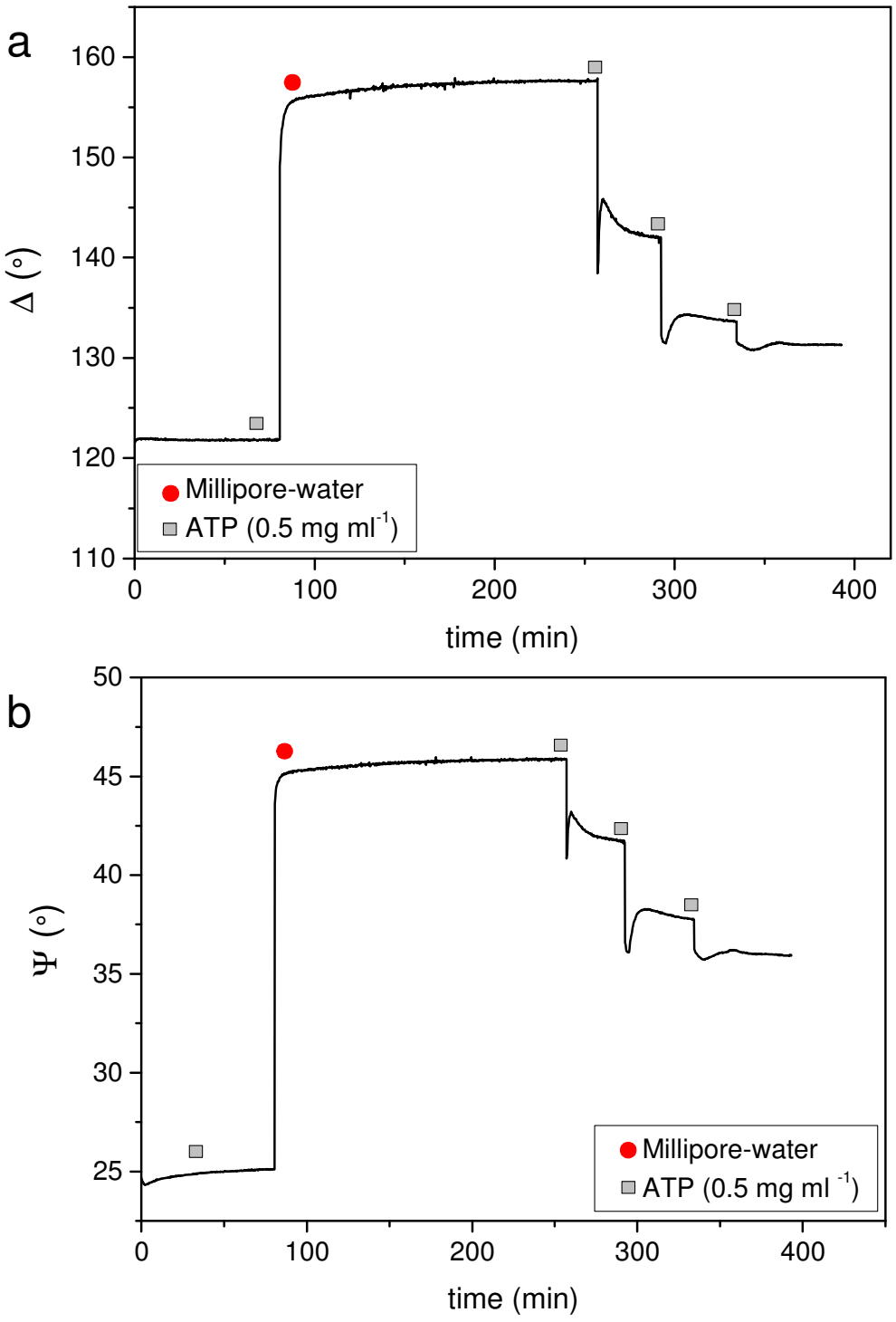

Figure 8-27. Dynamic scan of the experimental ellipsometric parameters, (**a**) phase difference (Δ) (**b**) amplitude ratio (ψ) for PEM (PEI(HE-Na^+/PEI-Mal-C)$_{20}$), swollen and rinsed in Millipore water (e.g. for λ = 632.8 nm), ATP (c= 0.5 mg mL^{-1}) .

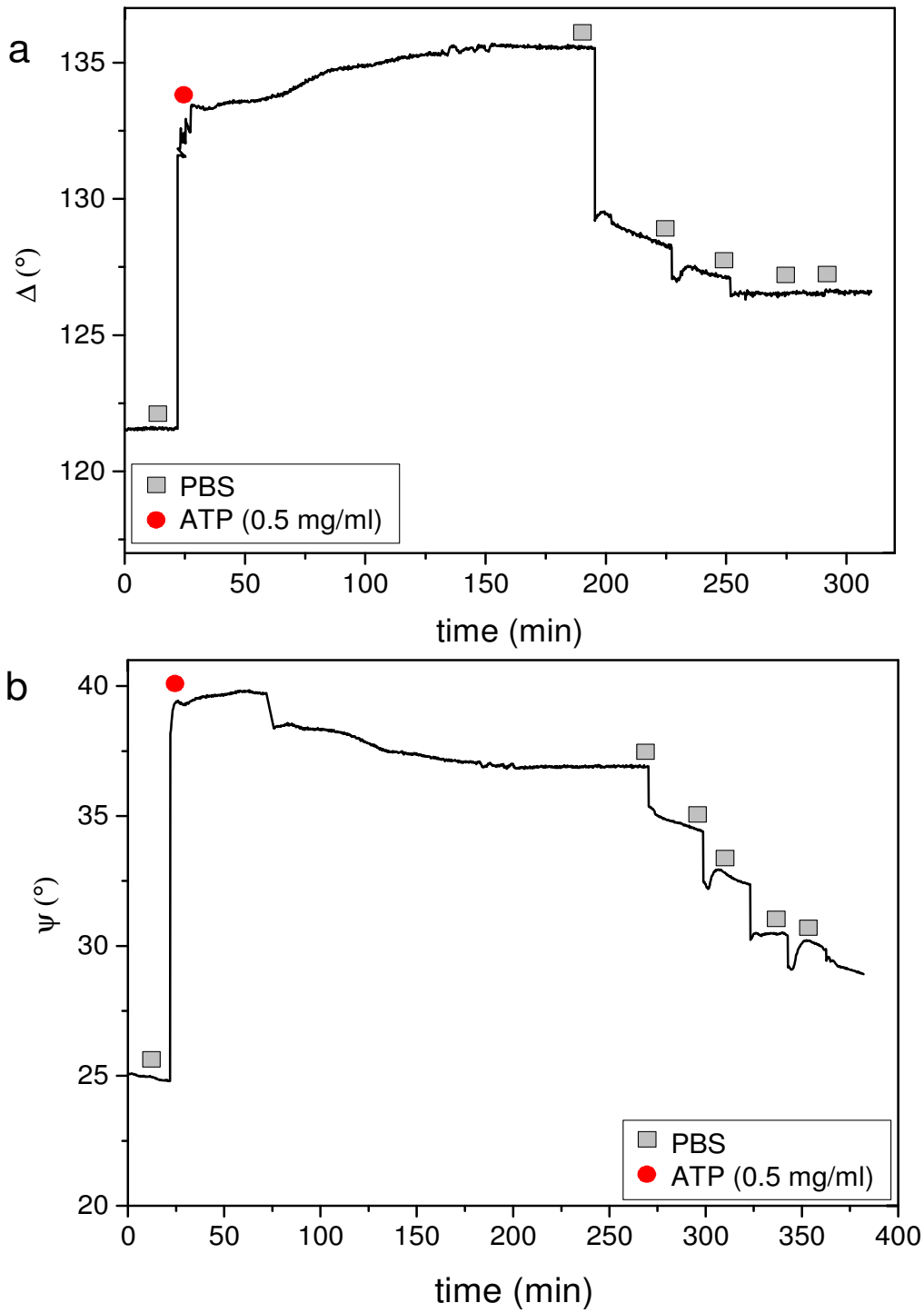

Figure 8-28. Dynamic scan of the experimental ellipsometric parameters, (**a**) phase difference (Δ) (**b**) amplitude ratio (ψ) for PEM (PEI(HE-Na^+/PEI-Mal-C)$_{20}$), swollen and rinsed via PBS (e.g. for λ = 632.8 nm), ATP (c= 0.5 mg mL^{-1}) . PBS buffer saline is of concentration PO_4^{3-} (0.01M) + NaCl (137 mM)+ KCl (2.7 mM) and pH7.4.

Appendix

Table 8-2. PEM of (PEI(HE-Na^+/PEI-Mal-C)$_{20}$), thickness after the addition of ATP[b]; thickness *d* (nm) and refractive index *n* at λ = 632.8 nm from ellipsometry, PEM was swollen and rinsed in Millipore-water. The experiment has been repeated for three times.

Conditions	PEM 1		PEM 2		PEM 3	
	d (nm)	*n*	*d (nm)*	*n*	*d (nm)*	*n*
Dry state	206	1.537	195	1.535	220	1.537
Swelling [a]	434	1.467	419	1.401	461	1.398
ATP [b]	472	1.468	464	1.488	476	1.388
Rinse 1 [c]	478	1.463	460	1.408	473	1.400
Rinse 2 [c]	459	1.465	449	1.406	465	1.386
Rinse 3 [c]	454	1.465	442	1.413	464	1.345

[a, c] Swelling and rinsing in Millipore-water, respectively

[b] ATP addition

Table 8-3. PEM of (PEI(HE-Na^+/PEI-Mal-C)$_{20}$), thickness after the addition of ATP[b]; thickness *d* (nm) and refractive index *n* at λ = 632.8 nm from ellipsometry, PEM was swollen and rinsed in PBS. The experiment has been repeated for three times. PBS buffer saline is of concentration PO_4^{3-} (0.01M) + NaCl (137 mM)+ KCl (2.7 mM) and pH7.4.

Conditions	PEM 1		PEM 2		PEM 3	
	d (nm)	*n*	*d (nm)*	*n*	*d (nm)*	*n*
Dry state	223	1.504	201	1.512	218	1.525
Swelling [a]	397	1.466	400	1.462	401	1.460
ATP [b]	541	1.441	539	1.445	535	1.444
Rinse 1 [c]	527	1.453	524	1.449	524	1.452
Rinse 2 [c]	525	1.462	529	1.460	524	1.459
Rinse 3 [c]	529	1.464	515	1.462	529	1.463
Rinse 4 [c]	429	1.469	504	1.464	506	1.469
Rinse 5 [c]	410	1.466	199	1.465	500	1.461

[a, c] Swelling and rinsing in PBS, respectively

[b] ATP addition

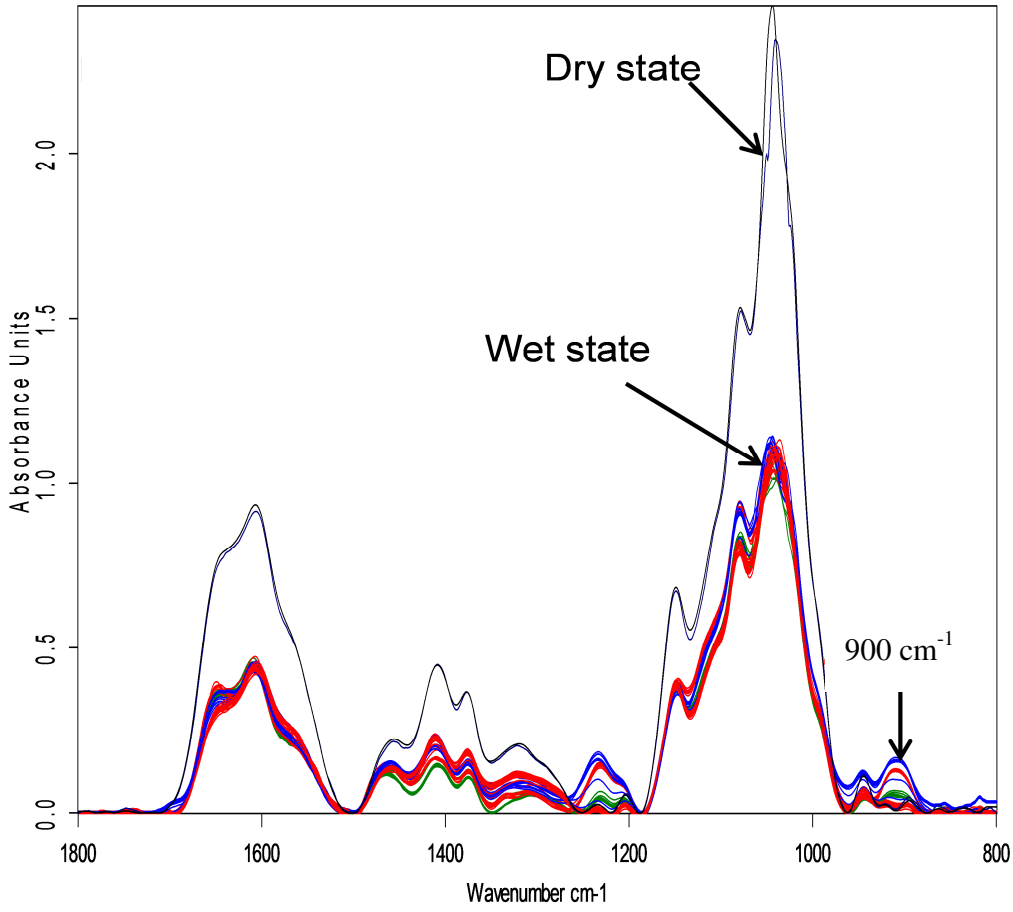

Figure 8-29. In-situ ATR-FTIR measurements for cyclic upload and release of ATP molecule for PEM (PEI(HA-Na^+/PEI-Mal-C)$_{20}$) PEM was subjected to Millipore water as a swelling medium followed by ATP addition then the rinsing steps which have already divided into two mediums Millipore-water followed by the final rinsing step with HEPES buffer (0.05)+ NaCl (0.1M) solution (pH 9). The uptake and the release were done as an in-situ measurements using closed loop mode at a flow rate of 5ml/min, cycle was measured for ~4 hour.

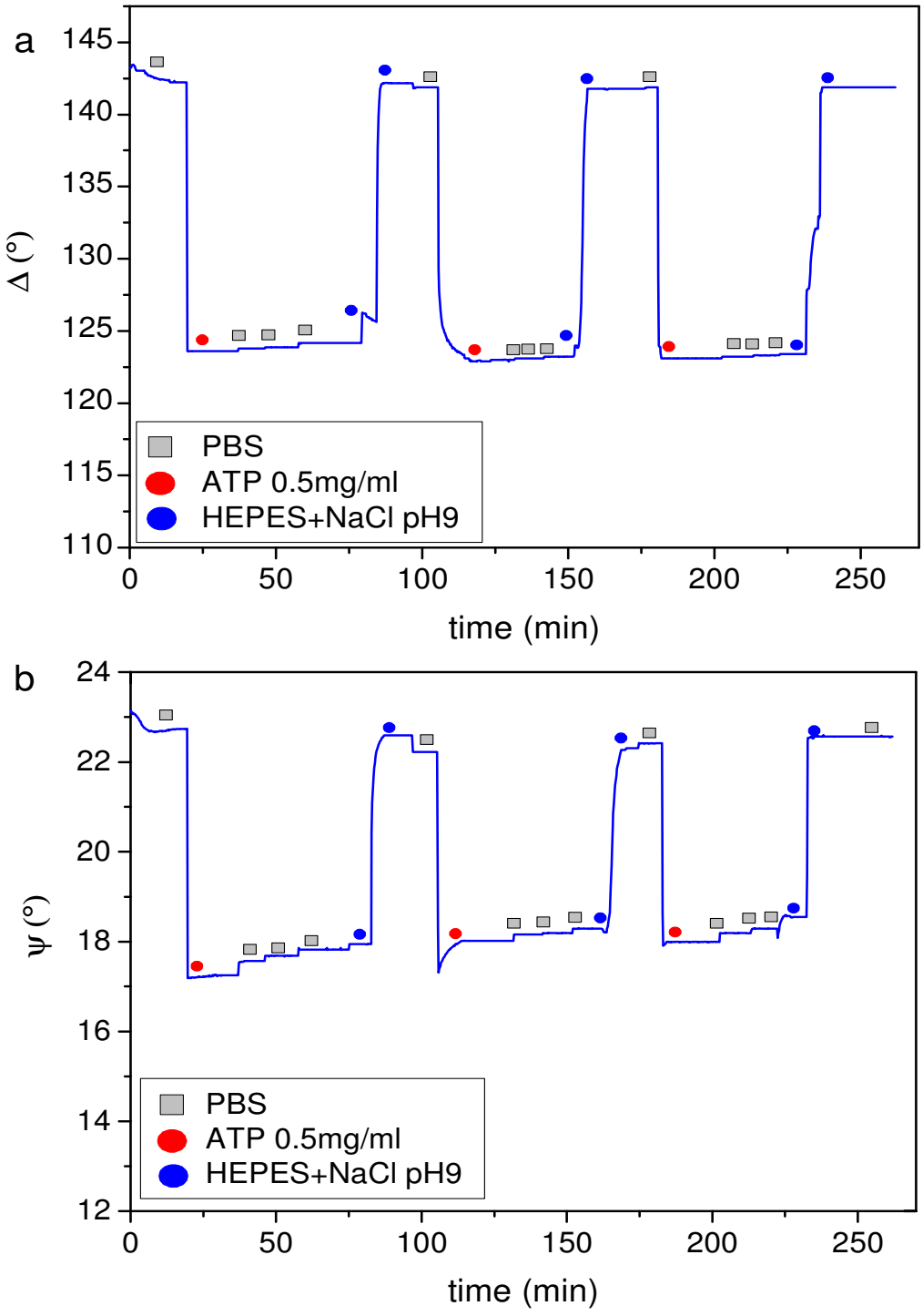

Figure 8-30. Dynamic scan of cyclic upload and release, (**a**) phase difference (Δ) (**b**) amplitude ratio (ψ) for PEM (PEI(HA-Na^{+}/PEI-Mal-C)$_{20}$), swollen and rinsed via PBS (e.g. for λ = 632.8 nm), ATP (c= 0.5 mg mL^{-1}) . PBS buffer saline is of concentration PO_4^{3-} (0.01M) + NaCl (137 mM)+ KCl (2.7 mM) and pH7.4.

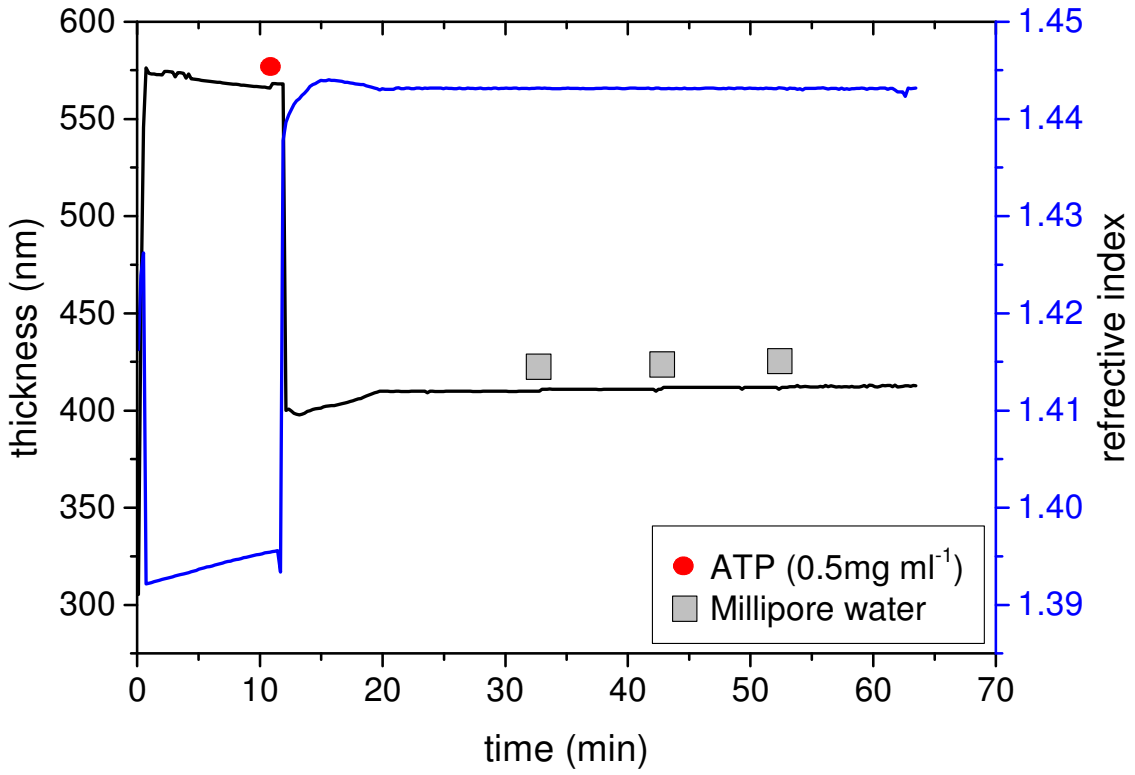

Figure 8-31. Thickness traced by ellipsometry for PEM (PEI(HA-Na^+/PEI-Mal-C)$_{20}$), swollen and rinsed via Millipore-water (e.g. for λ = 632.8 nm), ATP (c = 0.5 mg mL^{-1}).

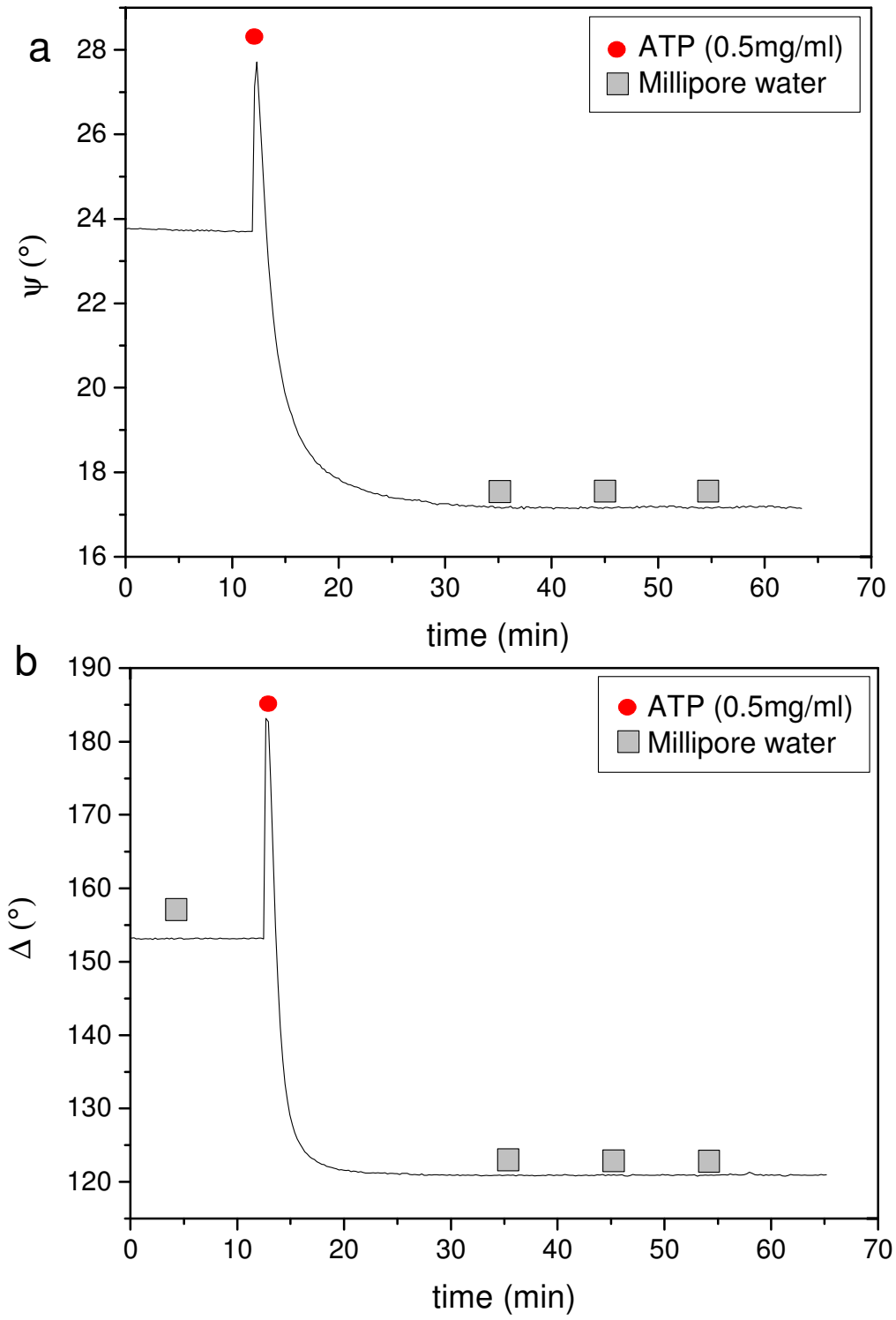

Figure 8-32. Dynamic scan of the experimental ellipsometric parameters, (**a**) amplitude ratio (ψ) (**b**) phase difference (Δ) for PEM (PEI(HA-Na+/PEI-Mal-C)$_{20}$), swollen and rinsed via Millipore-water (e.g. for λ = 632.8 nm), ATP (0.5 mg mL^{-1}) .

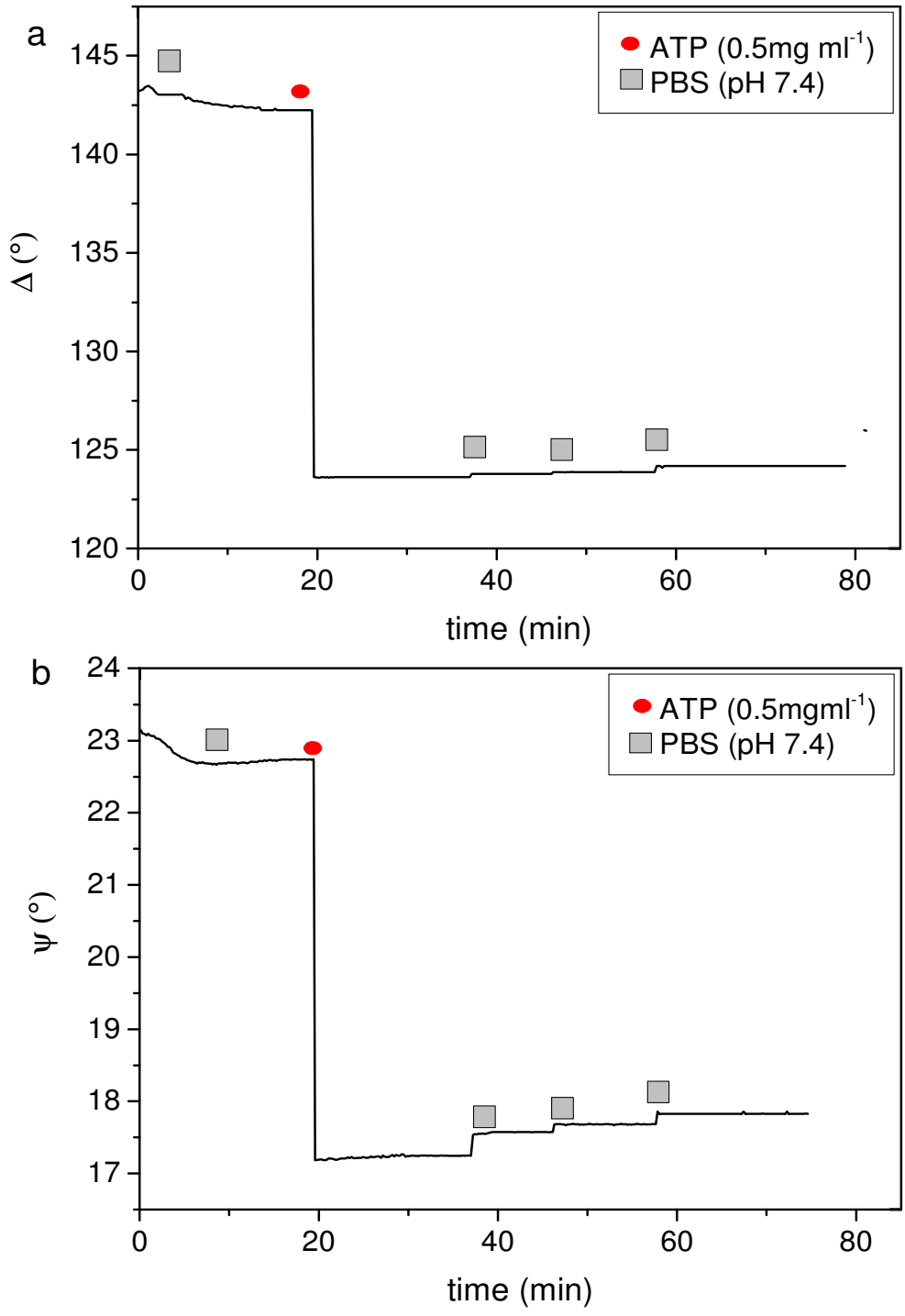

Figure 8-33. Dynamic scan of the experimental ellipsometric parameters, (**a**) phase difference (Δ) (**b**) amplitude ratio (ψ) for PEM (PEI(HA-Na+/PEI-Mal-C)$_{20}$), swollen and rinsed via PBS (e.g. for λ = 632.8 nm), ATP (c= 0.5 mg mL^{-1}) . PBS buffer saline is of concentration PO_4^{3-} (0.01M) + NaCl (137 mM)+ KCl (2.7 mM) and pH7.4.

Appendix

Table 8-4. PEM of (PEI(HA-Na^+/PEI-Mal-C)$_{20}$), thickness after the addition of ATP[b]; thickness *d* (nm) and refractive index *n* at λ = 632.8 nm from ellipsometry, PEM was swollen and rinsed in Millipore-water. The experiment has been repeated for three times

Conditions	PEM 1		PEM 2		PEM 3	
	d (nm)	*n*	*d (nm)*	*n*	*d (nm)*	*n*
Dry state	300	1.553	306	1.535	302	1.551
Swelling [a]	558	1.438	545	1.434	544	1.440
ATP [b]	410	1.443	403	1.447	409	1.444
Rinse 1 [c]	411	1.443	404	1.447	410	1.443
Rinse 2 [c]	412	1.442	404	1.446	410	1.443
Rinse 3 [c]	412	1.442	405	1.446	411	1.443

[a, c] Swelling and rinsing in Millipore-water, respectively

[b] ATP addition

Table 8-5. PEM of (PEI(HA-Na^+/PEI-Mal-C)$_{20}$), thickness after the addition of ATP[b]; thickness *d* (nm) and refractive index *n* at λ = 632.8 nm from ellipsometry, PEM was swollen and rinsed in PBS. The experiment has been repeated for three times. PBS buffer saline is of concentration PO_4^{3-} (0.01M) + NaCl (137 mM)+ KCl (2.7 mM) and pH7.4.

Conditions	PEM 1		PEM 2		PEM 3	
	d (nm)	*n*	*d (nm)*	*n*	*d (nm)*	*n*
Dry state	300	1.504	304	1.560	303	1.545
Swelling [a]	568	1.443	570	1.446	563	1.447
ATP [b]	382	1.465	393	1.468	398	1.464
Rinse 1 [c]	383	1.463	394	1.463	398	1.464
Rinse 2 [c]	384	1.464	394	1.465	399	1.463
Rinse 3 [c]	384	1.465	395	1.461	398	1.460

[a, c] Swelling and rinsing in PBS, respectively

[b] ATP addition

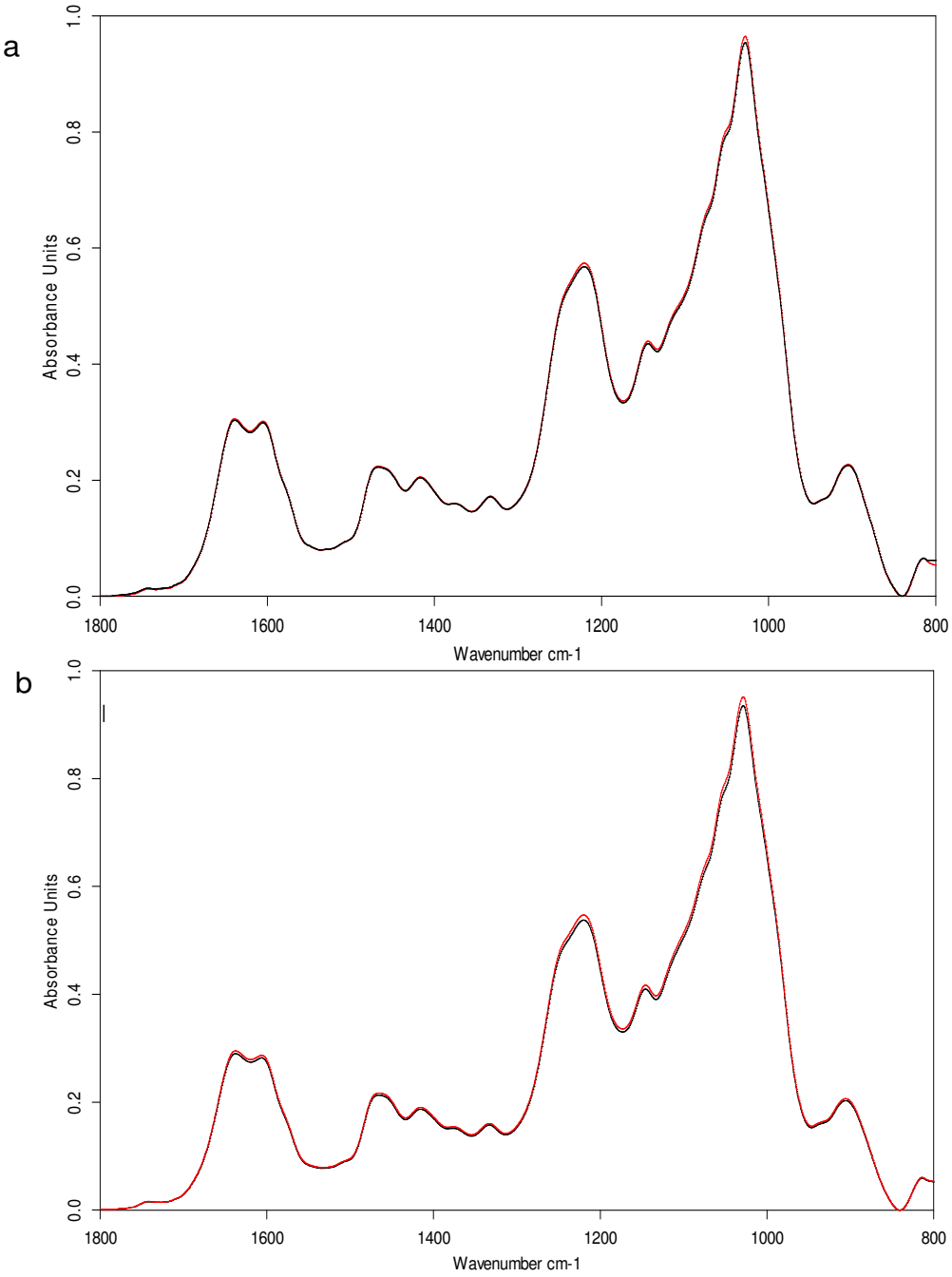

Figure 8-34. Preloading and release experiments traced by single beam –ATR-FTIR held in open holder for PEM (PEI(HE-Na^+/PEI-Mal-C/ATP)$_{20}$). ATP was of concentration (0.3 mg mL^{-1}), the release step has been done in (**a**) Millipore-water (**b**) HEPES of concentration 0.01 M. The black spectrum was for the initial PEM while the red one was after been soaked in the released medium for 1 day. The prepared PEM shows high stability toward uncharged medium.

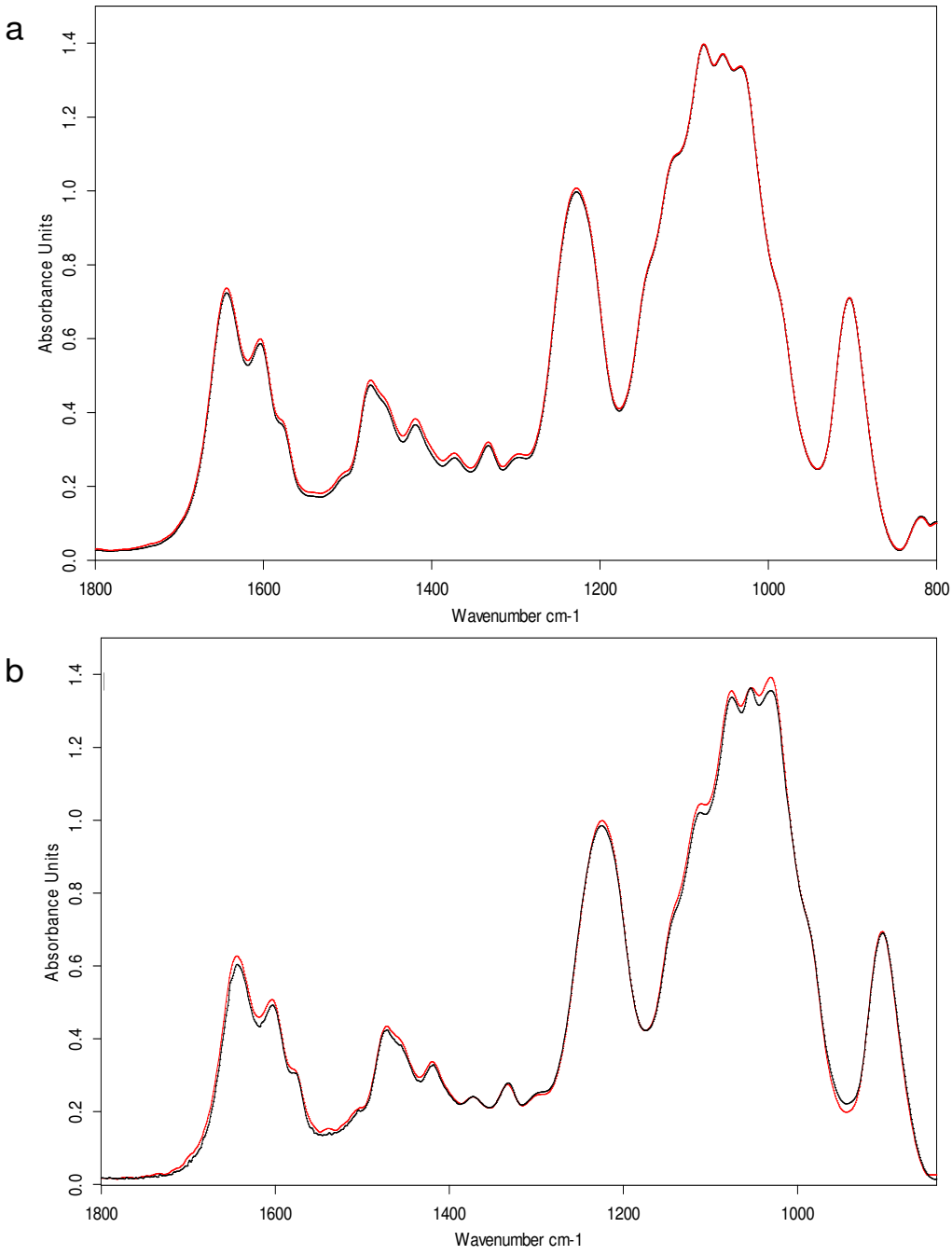

Figure 8-35. Preloading and release experiments traced by single beam –ATR-FTIR held in open holder for PEM (PEI(HE-Na^{+}/PEI-Mal-C/ATP)$_{20}$). ATP was of concentration (0.5 mg mL^{-1}), the release step has been done in (**a**) Millipore-water (**b**) HEPES of concentration 0.01 M. The black spectrum was for the initial PEM while the red one was after been soaked in the released medium for 1 day. The prepared PEM shows high stability toward uncharged medium.

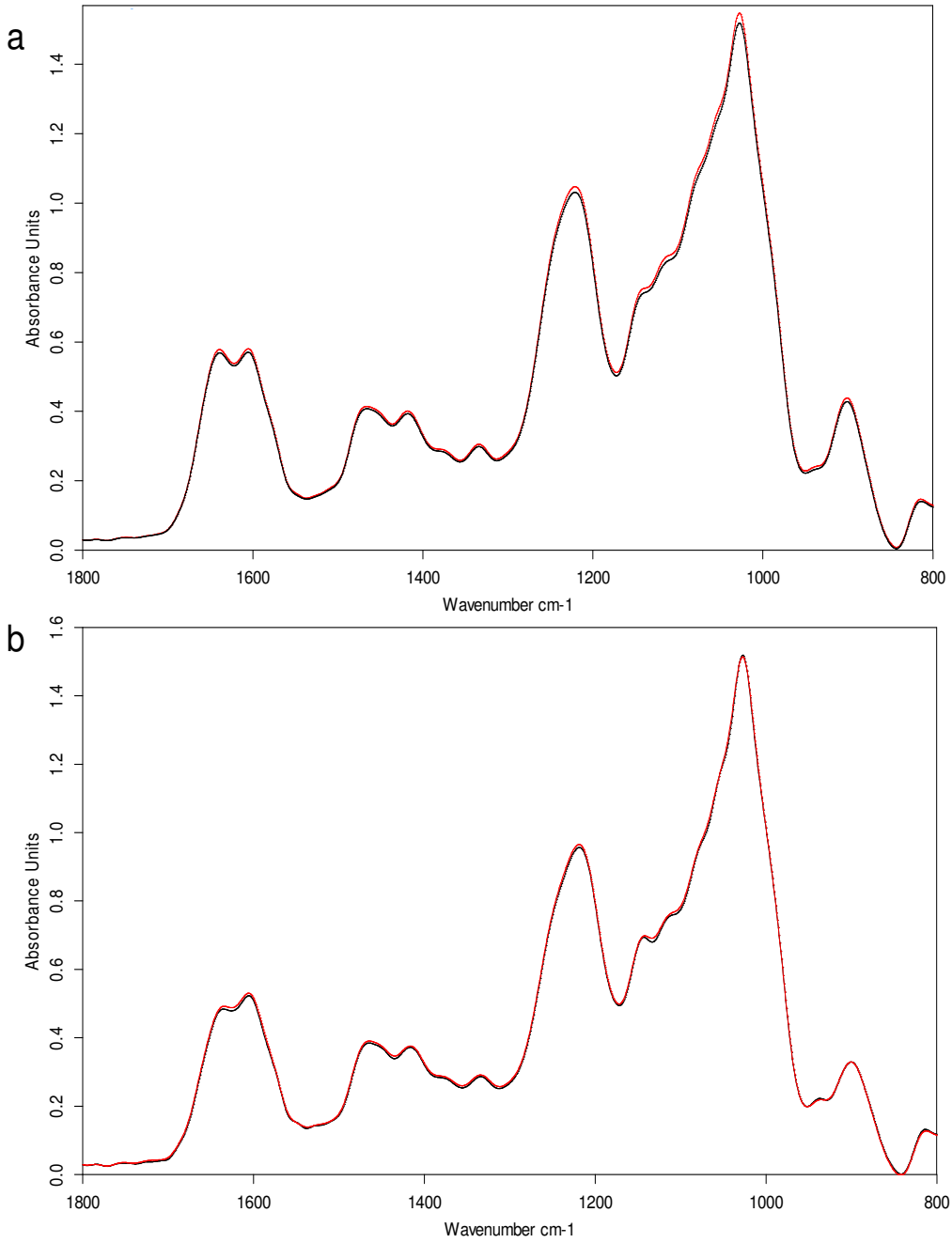

Figure 8-36. Preloading and release experiments traced by single beam –ATR-FTIR held in open holder for PEM (PEI(HE-Na^{+}/PEI-Mal-C/ATP)$_{20}$). ATP was of concentration (0.6 mg mL^{-1}), the release step has been done in (**a**) Millipore-water (**b**) HEPES of concentration 0.01 M. The black spectrum was for the initial PEM while the red one was after been soaked in the released medium for 1 day. The prepared PEM shows high stability toward uncharged medium.

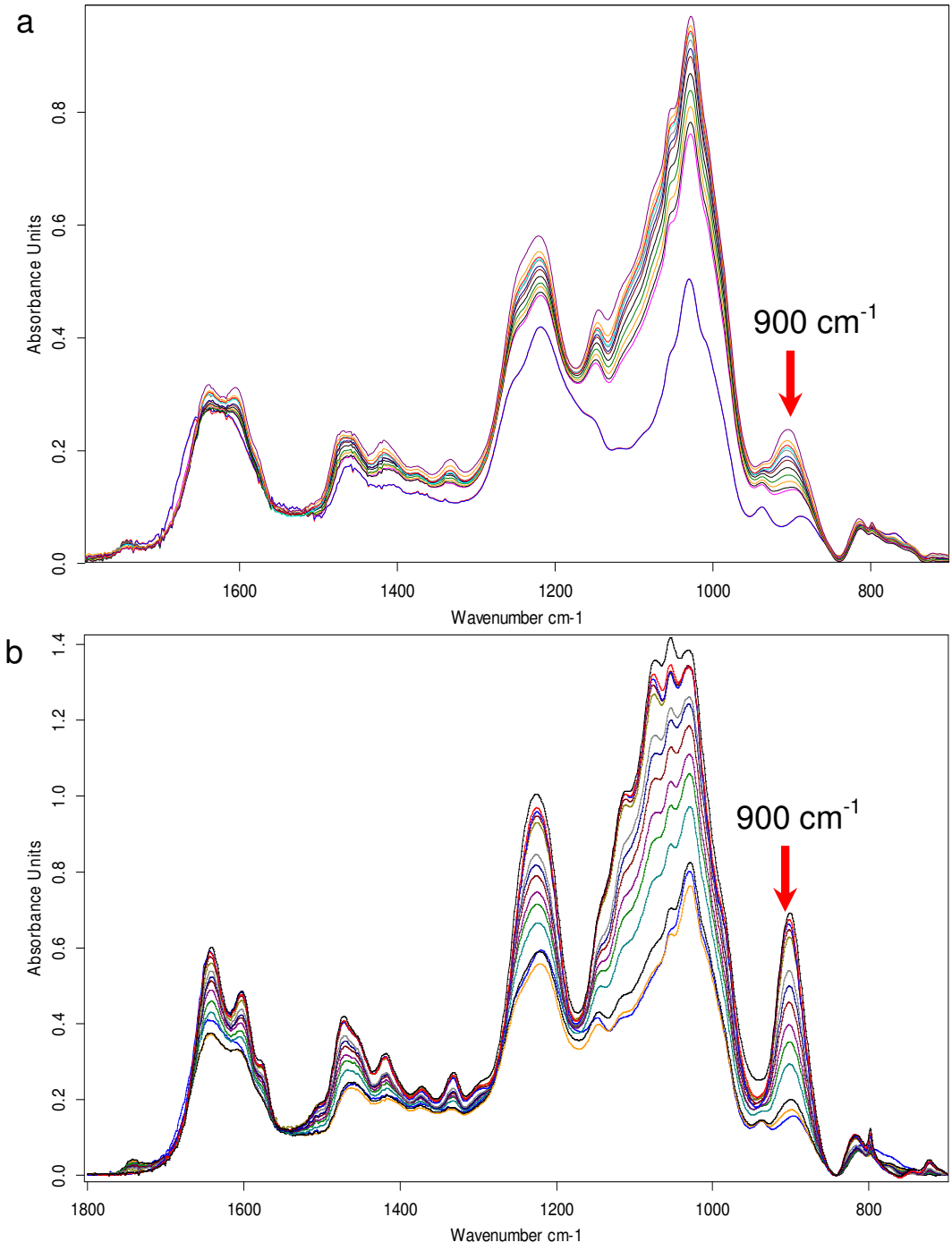

Figure 8-37. Preloading and release experiments traced by single beam –ATR-FTIR held in open holder for PEM (PEI(HE-Na^+/PEI-Mal-C/ATP)$_{20}$). ATP was of concentration (**a**) 0.3mg mL^{-1} (**b**) 0.5 mg mL^{-1}, the release step has been done in HEBES buffer (0.01M) and NaCl (0.1M) medium mixed with ratio (1:1), one of ATP identified and isolated band at wavelength 900 cm^{-1}, the band at which all of integration calculation has been done.

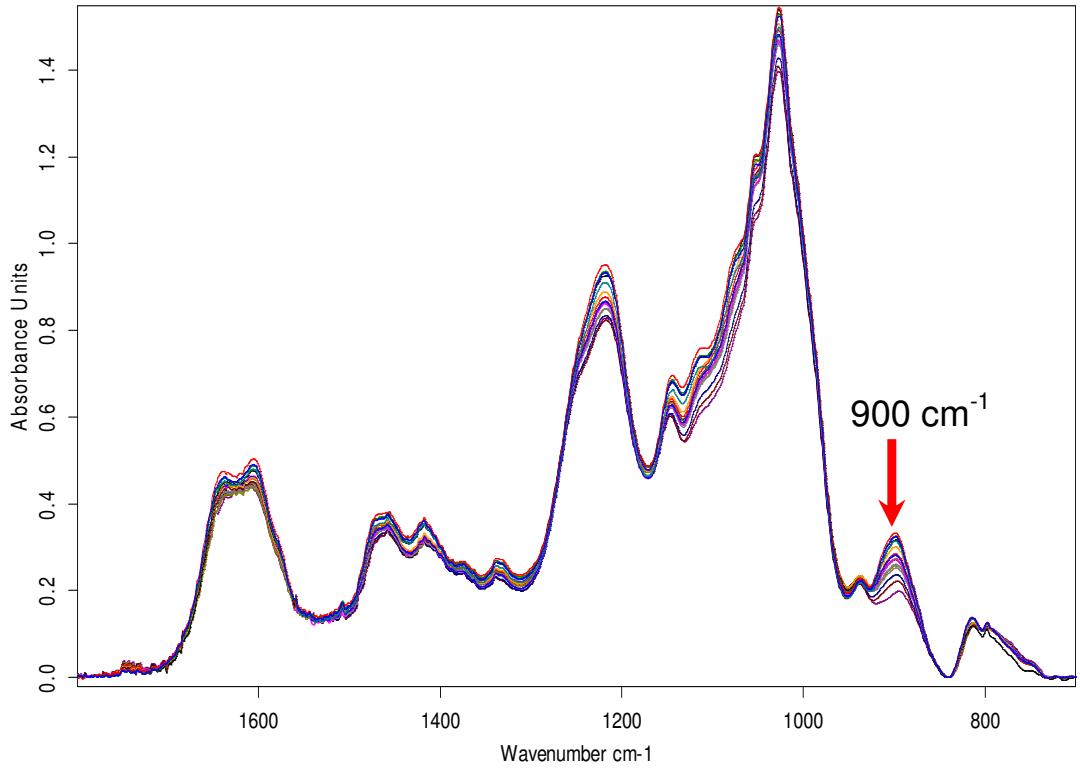

Figure 8-38. Preloading and release experiments traced by single beam –ATR-FTIR held in open holder for PEM (PEI(HE-Na^{+}/PEI-Mal-C/ATP)$_{20}$). ATP was of concentration (0.6 mg mL^{-1}), the release step has been done in HEBES (0.01M) buffer and NaCl (0.1M) medium mixed with ratio (1:1), one of ATP identified and isolated band at wavelength 900 cm^{-1}, the band at which all of integration calculation has been done.

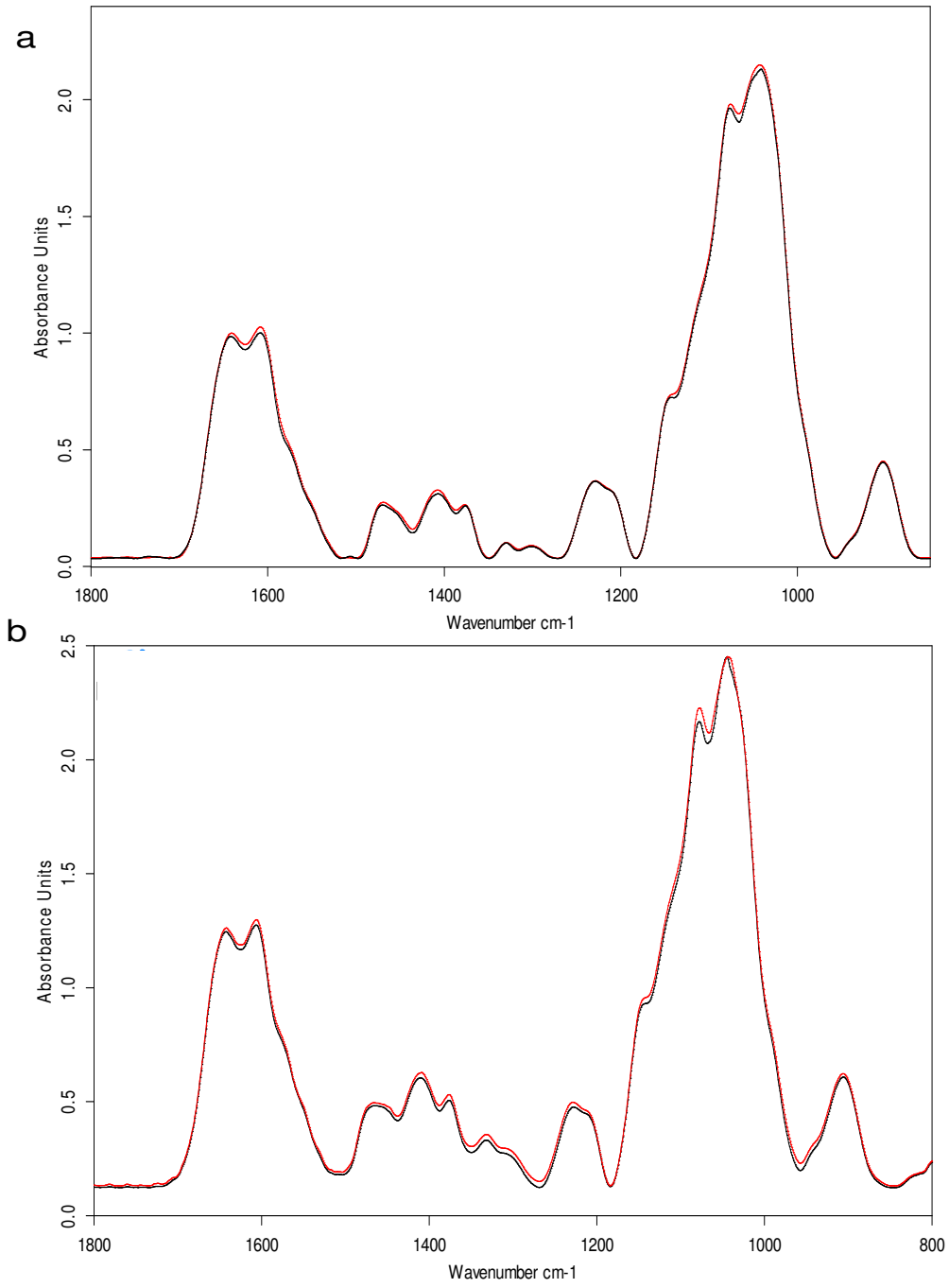

Figure 8-39. Preloading and release experiments traced by single beam –ATR-FTIR held in open holder for PEM (PEI(HA-Na^+/PEI-Mal-C/ATP)$_{20}$). ATP was of concentration (0.2 mg mL^{-1}), the release step has been done in (**a**) Millipore-water (**b**) HEPES of concentration 0.05 M. The black spectrum was for the initial PEM while the red one was after been soaked in the released medium for 1 day. The prepared PEM shows high stability toward uncharged medium.

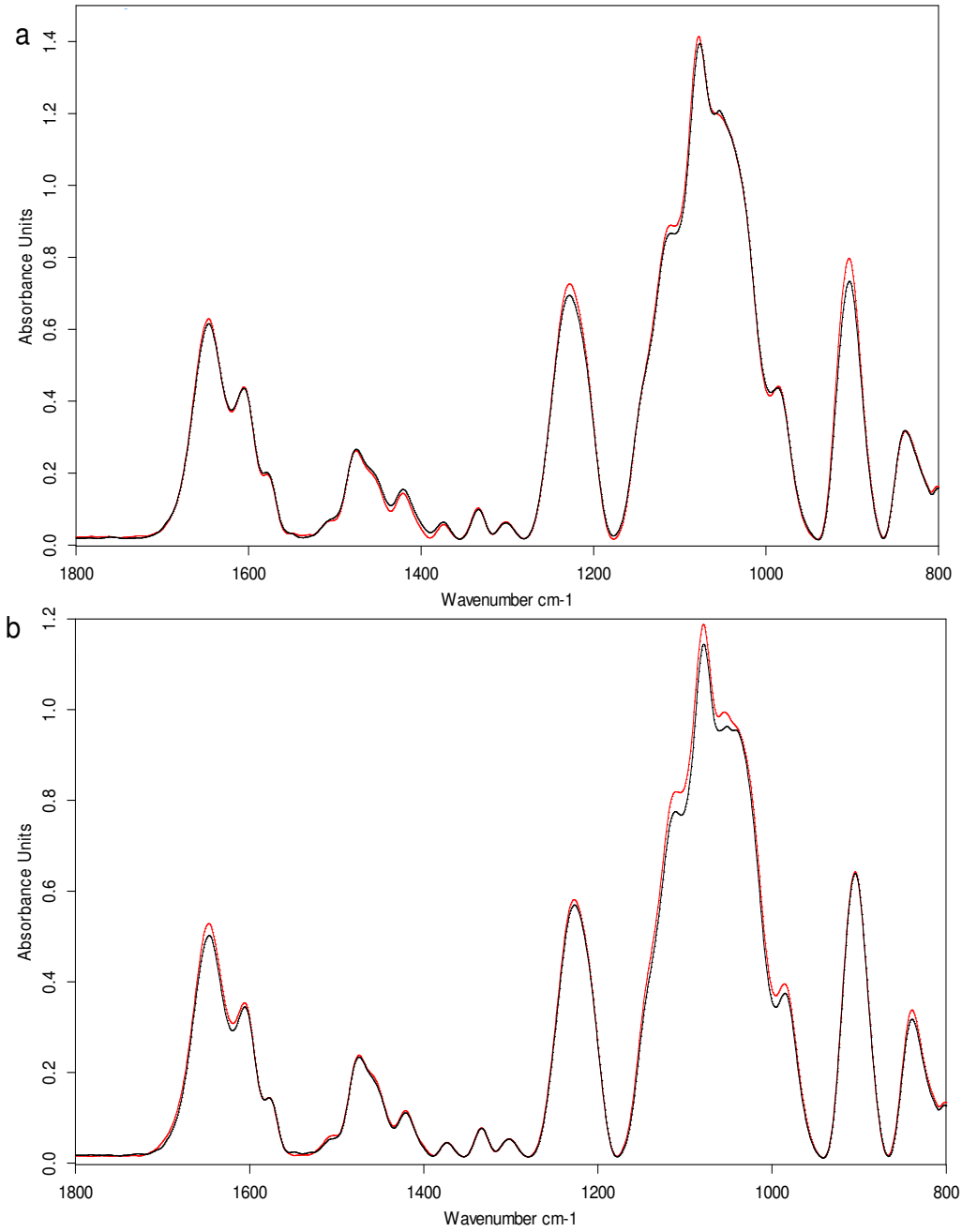

Figure 8-40. Preloading and release experiments traced by single beam –ATR-FTIR held in open holder for PEM (PEI(HA-Na^+/PEI-Mal-C/ATP)$_{20}$). ATP was of concentration (0.3 mg mL^{-1}), the release step has been done in (**a**) Millipore-water (**b**) HEPES of concentration 0.05 M. The black spectrum was for the initial PEM while the red one was after been soaked in the released medium for 1 day. The prepared PEM shows high stability toward non-charged medium.

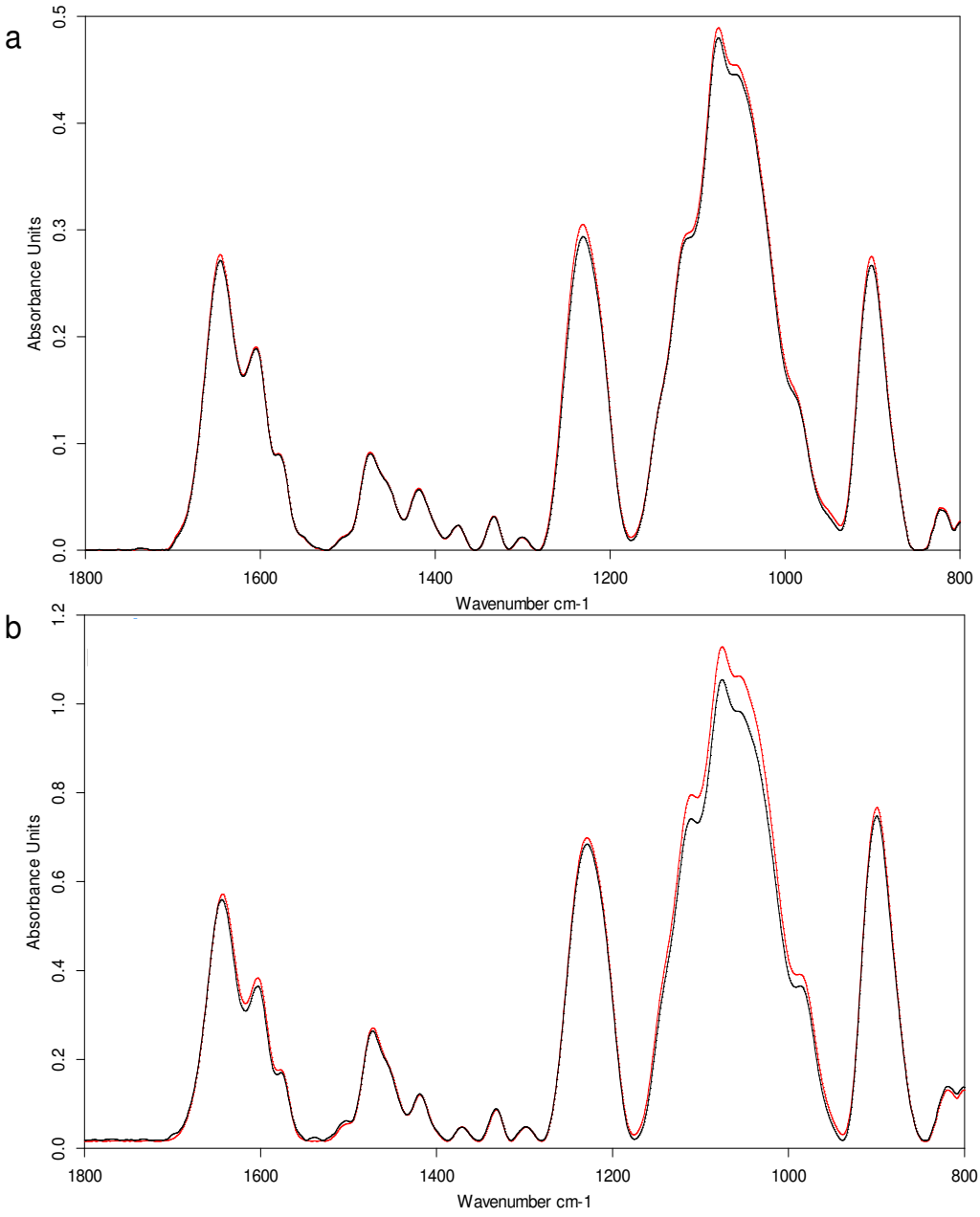

Figure 8-41. Preloading and release experiments traced by single beam –ATR-FTIR held in open holder for PEM (PEI(HA-Na^+/PEI-Mal-C/ATP)$_{20}$). ATP was of concentration (0.5 mg mL^{-1}), the release step has been done in (**a**) Millipore-water (**b**) HEPES of concentration 0.05 M. The black spectrum was for the initial PEM while the red one was after been soaked in the released medium for 1 day. The prepared PEM shows high stability toward non-charged medium.

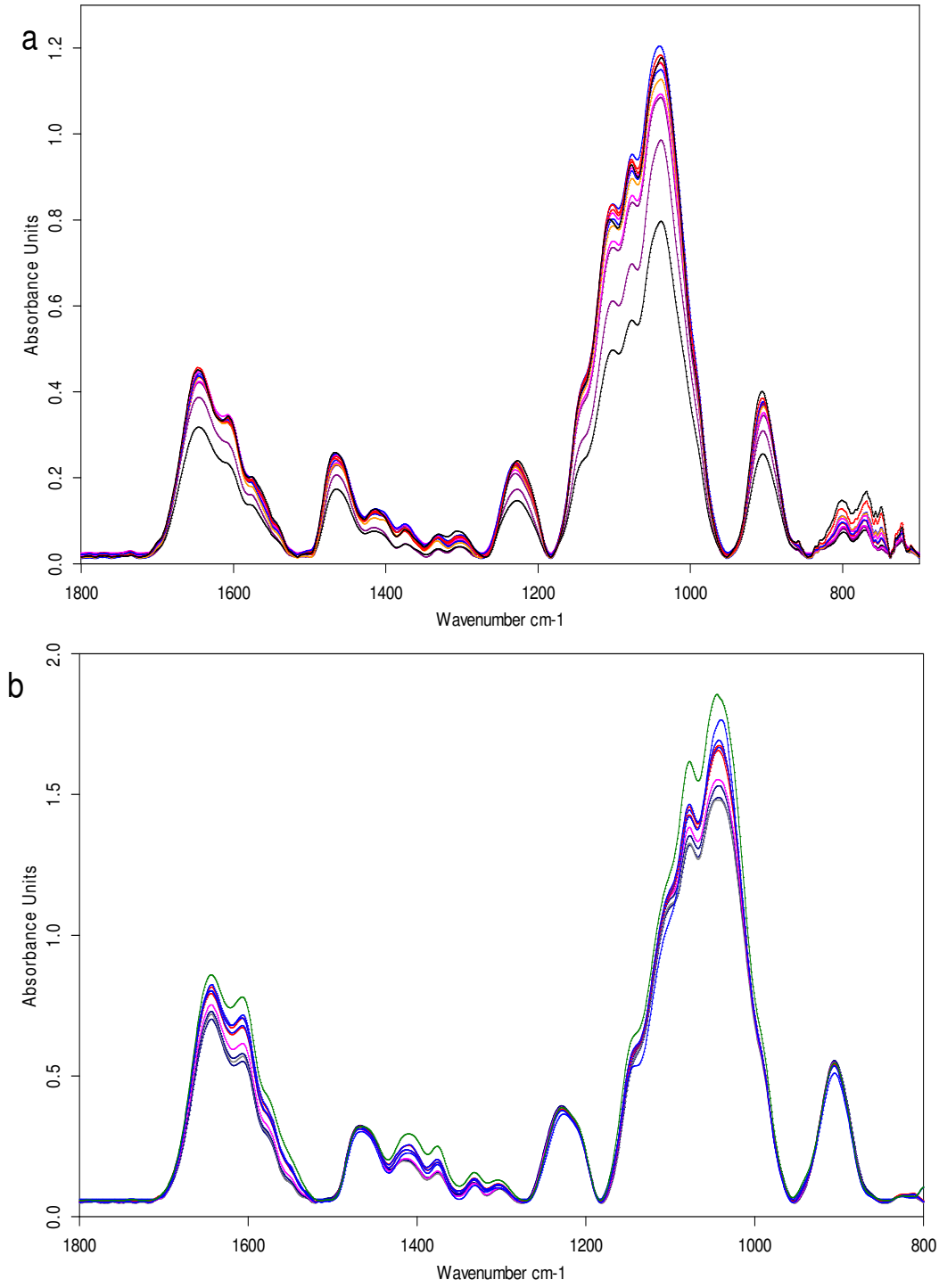

Figure 8-42. Release study using single beam ATR-FTIR in open holder, PEM (PEI(HA-Na^+/PEI-Mal-C)$_{20}$) prepared via Approach C complexed with ATP of concentration(0.2 mg mL^{-1}) , the release study was done in HEPES buffer (0.05M) and NaCl (0.1M) mixed with ratio 1:1 for 3 days (**a**) pH 9 (**b**) pH 7.4, pH was adjusted using NaOH 0.1M.

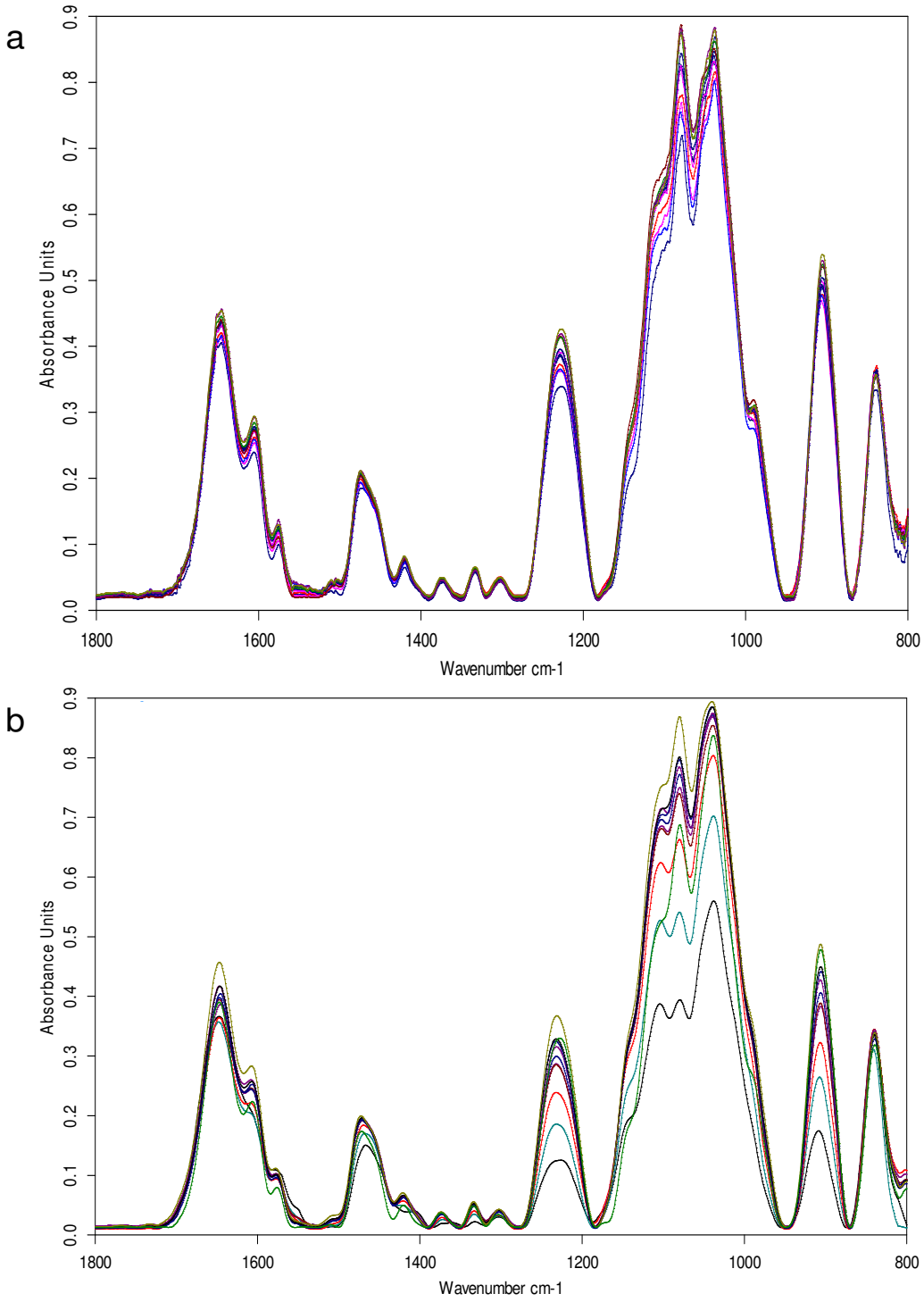

Figure 8-43. Release study using single beam ATR-FTIR in open holder, PEM (PEI(HA-Na^+/PEI-Mal-C)$_{20}$) prepared via Approach C complexed with ATP of concentration (0.3 mg mL^{-1}) , the release study was done in HEPES buffer (0.05M) and NaCl (0.1M) mixed with ratio 1:1 for 3 days (**a**) pH 7.4 (**b**) pH 9, pH was adjusted using NaOH 0.1M.

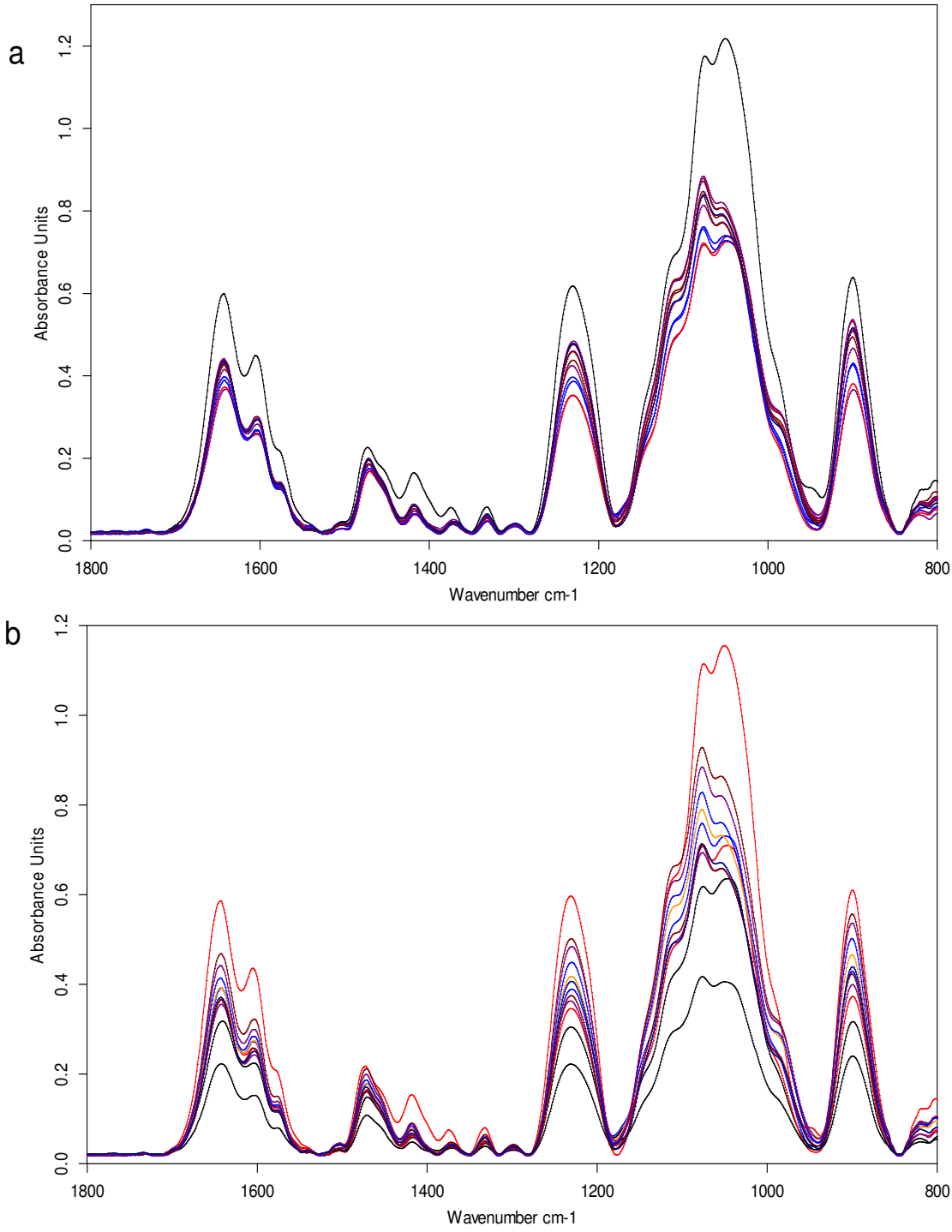

Figure 8-44. Release study using single beam ATR-FTIR in open holder, PEM (PEI(HA-Na^+/PEI-Mal-C)$_{20}$) prepared via Approach C complexed with ATP of concentration (0.5 mg mL^{-1}) , the release study was done in HEPES buffer (0.05M) and NaCl (0.1M) mixed with ratio 1:1 for 3 days (**a**) pH 7.4 (**b**) pH 9, pH was adjusted using NaOH 0.1M.

Appendix

Table 8-6. PEM of (PEI(HE-Na^+/PEI-Mal-C/ATP)$_{20}$); ATP 0.5 mg mL^{-1}, thickness *d*(nm) and refractive index *n* at λ = 632.8 nm from ellipsometry, PEM was swollen and rinsed in (**i**) Millipore-water (**ii**) pure HEPES buffer pH 7.4 (0.01M) (**iii**) PBS (PO_4^{3-} (0.01M) + NaCl (137 mM)+ KCl (2.7 mM) (**iv**) HEPES (0.01) +NaCl (0.1M) pH 7.4 . All release experiments were performed at least in duplicate.

Submersion medium	Strat dry thickness (0 min)		Start swelling thickness (0 min)		End swelling thickness (1 day)		End dry thickness (1 day)	
	d [nm]	*n*	*d* [nm]	*n*	*d* [nm]	*n*	*d* [nm]	*n*
Millipore water	210	1.551	1670	1.456	1708	1.415	229	1.550
Pure HEPES (0.01 M)	204	1.553	1325	1.454	1277	1.452	300	1.552
PBS (pH 7.4)	206	1.547	1536	1.408	1459	1.396	195	1.531
HEPES+NaCl (pH7.4)	206	1.552	1325	1.497	554	1.459	150	1.461

Table 8-7. PEM of (PEI(HA-Na^+/PEI-Mal-C/ATP)$_{20}$); thickness *d* (nm) and refractive index *n* at λ = 632.8 nm from ellipsometry, PEM was swollen and rinsed in (**i**) Millipore-water (**ii**) pure HEPES buffer pH 7.4 (0.05M) (**iii**) PBS (PO_4^{3-} (0.01M) + NaCl (137 mM)+ KCl (2.7 mM)) (**iv**) HEPES (0.05) +NaCl (0.1M) pH 9.

Submersion medium	Strat dry thickness (0 min)		Start swelling thickness (0 min)		End swelling thickness (1 day)		End dry thickness (1 day)	
	d [nm]	*n*	*d* [nm]	*n*	*d* [nm]	*n*	*d* [nm]	*n*
Millipore water [a]	300	1.541	503	1.445	501	1.443	229	1.540
Pure HEPES (0.05 M) [a]	303	1.560	525	1.443	526	1.441	300	1.559
PBS (pH 7.4) [a]	301	1.553	560	1.434	505	1.424	245	1.531
HEPES+NaCl (pH9) [a]	300	1.551	512	1.435	422	1.420	170	1.472
HEPES+NaCl (pH9) [b]	302	1.552	562	1.431	387	1.415	150	1.461

[a] ATP 0.3 mg mL^{-1}
[b] ATP 0.5 mg mL^{-1}

Publications and Contributions to Academic Conferences

PUBLICATIONS

- B.Torger, D. Vehlow, B. Urban, S. Salem, D. Appelhans, M. Müller, *Cast adhesive polyelectrolyte complex particle films of unmodified or maltose-modified poly(ethyleneimine) and cellulose sulphate: fabrication, film stability and retarded release of zoledronate*. Biointerphaces , 2013. 8 (1): p. 25-36

- S. Salem, M. Müller, B. Torger, A. Janke, K.-J. Eichhorn, B Voit, D. Appelhans, *Glycopolymer polyelectrolyte multilayers composed of heparin and maltose-modified poly(ethyleneimine) as a strong/weak polyelectrolyte system for future drug delivery coatings: Influence of pH and sugar architecture on growth of multilayers and multilayer swelling and stability*. Macromolecular Chemistry and Physics, 2015. 216 (2): p.182-195

CONTRIBUTIONS TO ACADEMIC CONFERENCES

- S.Salem , M. Müller, B. Torger, A. Janke, K.- J. Eichhorn, B. Voit , D. Appelhans, *Glycopolymer polyelectrolyte multilayers composed of heparin and maltose-modified poly(ethyleneimine) as a strong/weak polyelectrolyte system* – poster presentation at POLYSOLVAT-10, 22-25 September 2014, Salerno- Italy.

VERSICHERUNG

Hiermit versichere ich, dass ich die vorliegende Arbeit ohne unzulässige Hilfe Dritter und ohne Benutzung anderer als der angegebenen Hilfsmittel angefertigt habe; die aus fremden Quellen direkt oder indirekt übernommenen Gedanken sind als solche kenntlich gemacht. Die Arbeit wurde bisher weder im Inland noch im Ausland in gleicher oder ähnlicher Form einer anderen Prüfungsbehörde vorgelegt.

Die vorliegende Dissertation wurde in der Zeit vom Dezember 2011 bis April 2015 am Leibniz-Institut für Polymerforschung Dresden e.V. unter der Leitung von Frau Prof. Dr. Brigitte Voit angefertigt.

Frühere Promotionsverfahren haben nicht stattgefunden.

Ich erkenne die Promotionsordnung der Fakultät Mathematik und Naturwissenschaften der Technischen Universität Dresden vom 23. Februar 2011 in vollem Umfang an.

Dresden, den 15.07.2015